The University Of Sheffield.

Oncolytic Virotherapy Targeting Tim-3 Expressing Macrophages in Breast Cancer

Secil Demiral

Registration number: 190245670

A thesis submitted in partial fulfilment of the requirements for the degree of Doctor of Philosophy

The University of Sheffield

Faculty of Medicine and Population Health

Division of Clinical Medicine

31st of January 2024

Acknowledgement

I would like to express my deepest gratitude to my supervisor, Prof Munitta Muthana, for providing me with the opportunity to pursue my PhD under her guidance. Her unwavering positive energy and extensive academic knowledge were instrumental in helping me navigate and successfully complete this challenging process. Munitta holds a special place at the top of my unforgettable list of life experiences. I also extend my thanks to my second supervisor, Prof Craig Murdoch, whose consistent support and diverse problem-solving approaches were invaluable throughout our academic journey.

I owe a debt of gratitude to the State of the Republic of Turkiye as a financial support played a crucial role in making this doctoral project possible, covering my living expenses during this period.

A heartfelt appreciation goes out to the exceptional team I had the privilege to work with. Faith Howard and Natalie Winder, destined for great positions in academia, have been both academic mentors and cherished friends. I am grateful for their contributions. Special thanks to my other teammates, Hawari Bin Mansor, Zijian Gao, and Brindley Hapuarachchi, for making our collaborative efforts enjoyable and standing by my side. I want to express my gratitude to our master project students, Zoi Papasavva and Soumya Rupangudi, whose projects I managed. Their experimental assistance and wonderful friendship enhanced the overall experience.

I also appreciate Profs Penelope Ottewell and Claire Lewis for generously allowing us to use human breast cancer tissue and data and Richard Allen for sharing his data with us. Thanks to Luke Tattersall for sharing insights into migration and invasion experiments. I extend my appreciation to the dedicated technicians—Sue Justice, Kay Hopkinson, Maggie Glover, Richard Allen, Sue Clark, Ameera Jailani, Paris Avgoustou—for their invaluable support in conducting the experiments.

Lastly, I owe a debt of gratitude to my precious family including Mehmet, Zubeyde, Melike, Seda, Yilmaz, Merve. My parents and oldest sister, through their sacrifices, have been unwavering supporters throughout my educational journey. To my youngest sister, Merve, my indescribable companion, I am endlessly thankful for her wonderful companionship.

Publications

1. Iscaro, A., Jones, C., Forbes, N., Mughal, A., Howard, F. N., Janabi, H. A., **Demiral, S.**, Perrie, Y., Essand, M., Weglarz, A., Cruz, L. J., Lewis, C. E., & Muthana, M. (2022). Targeting circulating monocytes with CCL2-loaded liposomes armed with an oncolytic adenovirus. *Nanomedicine: nanotechnology, biology, and medicine*, *40*, 102506. https://doi.org/10.1016/j.nano.2021.102506

2. Gao, Z., Mansor, M. H., Winder, N., **Demiral, S**., Maclnnes, J., Zhao, X., & Muthana, M. (2023). Microfluidic-Assisted ZIF-Silk-Polydopamine Nanoparticles as Promising Drug Carriers for Breast Cancer Therapy. *Pharmaceutics*, *15*(7), 1811. https://doi.org/10.3390/pharmaceutics15071811

Poster/oral presentations

1. Poster presentation; The 15th Annual International Oncolytic Virotherapy Conference 2023, Canada.

2. Poster presentation; 17th University of Sheffield Medical School Research Meeting 2022,

Sheffield, UK.

3. Oral Presentation; PGR Symposium Day 2023, University of Sheffield, Sheffield, UK.

4. Oral Presentation; PGR Symposium Day 2020, University of Sheffield, Sheffield, UK.

TABLE OF CONTENTS

TABLE OF FIGURES

TABLE OF TABLES

LIST OF ABBREVIATIONS

Abbreviation	Description
Ab	Antibody
BC	Breast Cancer
CAFs	Cancer associated fibroblasts
CARs	Chimeric antigen receptors
CEACAM-1	Carcinoembryonic antigen-related cell adhesion molecule 1
ChT	Chemotherapy
CSF-1	Colony stimulating factor
CSF1R	Colony stimulating factor receptor
CCR2	Chemokine (C-C motif) receptor 2
CTLA-4	cytotoxic T-lymphocyte-associated protein 4
CXCL1	(C-X-C motif) ligand 1
DAMPs	Damage-associated molecular patterns
DC	Dendritic Cells
DCR	Disease control rate
DMEM	Dulbecco's Modified Eagle Medium
DMEM/F-12	Dulbecco's Modified Eagle's Medium/Nutrient Mixture F-12 Ham
DMSO	Dimethyl sulfoxide
E1	Early region 1
ER	Oestrogen receptor
ET	Endocrine therapy
FBS	Foetal Bovine Serum
FDA	The United States Food and Drug Administration
FSC-A	Forward scatter-area
Gal-9	Galectin-9
GM-CSF	granulocyte macrophage colony-stimulating factor
H&E	Haematoxylin and Eosin
HAVCR2	Hepatitis A virus cellular receptor 2
HCC	Hepatocellular carcinoma
HER2	Human epidermal growth factor receptor 2
HMGB1	High mobility group box-1 protein
HEVs	Human enteroviruses
HSV	Herpes Simplex Virus
HVEM	Herpes virus entry mediator
ICAM-1	Intercellular adhesion molecule-1
ICD	immunogenic cell death
ICI	Immune Checkpoint Inhibitor

IE	Immediate-early
ICP	Infected cell protein
IFNs	interferons
IT	Intratumoural
IP	Intra Peritoneal
IV	Intravenous
MDSCs	Myeloid-derived suppressor cells
MHC	major histocompatibility complex
MitC	Mitomycin C
MMP	Matrix metalloproteinase
MOI	Multiplicity of infection
MV	measles virus
M1	Classically activated macrophages
M2	Alternatively activated macrophages
NDV	Newcastle disease virus
NK cells	Natural Killer cells
OCT	Optımal cutting temperature
oHSV	oncolytic HSV
ORR	Objective response rate
OS	Overall survival
OV	Oncolytic Virus
OVT	Oncolytic Virotherapy
PAMPs	Pathogen-associated Molecular Patterns
PBMC	Peripheral blood mononuclear cells
PBS	Phosphate buffered saline
PD1	Programmed cell death 1
PDL1	Programmed death-ligand 1
PFA	Paraformaldehyde
pfu	Plaque-forming Units
PR	Progesterone receptor
PTHrP	Parathyroid hormone-related peptide
PtdSer	Phosphatidylserine
RANKL	Nuclear factor kappa-B ligand
siRNA	Small interfering RNA
SSC-A	Side scatter-area
SEM	standard error of the mean
TAAs	Tumour associated antigens
TAMs	Tumour associated macrophages
TANs	Tumour associated neutrophils
TCR	T cell receptor
TCM	Tumour conditioned medium
Th	T helper cells

TGFβ	Transforming growth factor beta
TILs	Tumour infiltrating Lymphocytes
Tim-3	T-Cell Immunoglobulin and mucin domain-3
TLRs	Toll-like receptors
TME	Tumour Microenvironment
TNBC	Triple Negative Breast Cancer
TNF	tumour necrosis factor
Treg	Regulatory T cells
T-VEC	Talimogene laherparepvec
VEGF	Vascular endothelial growth factor

Abstract

Background: Cancer immunotherapy with Immune Checkpoint Inhibitors (ICIs) has demonstrated significant clinical success, but not so much in the treatment of immunologically 'cold' tumours including Breast cancer (BC). One compelling solution is offered by oncolytic viruses (OVs) which induce direct cancer cell killing whilst activating anti-tumour immunity, resulting in turning "cold" mammary tumours "hot,". This works, in part, by reprogramming the tumour microenvironment leading to recruitment of T cells and re-education of tumour-associated macrophages (TAMs). We hypothesise that targeting a new immune checkpoint 'Tim-3' in combination with OVs will induce anti-tumour immunity in BC.

Methods: We investigated the antitumour effects of 3 types of oncolytic herpes simplex virus-1 (oHSV-1) in combination with anti-Tim-3 antibody. Cell survival, migration and invasion following treatment with this combination was also assessed in 3 different BC cell lines (MCF-7, MDA-MB-231, SKBR-3). The optimal combinations were then investigated in two mouse models of mammary carcinoma (4T1 and E0771). Biodistribution and antitumour properties were assessed post-mortem.

Results: Blocking Tim-3 resulted in a significant decrease in cell viability in all 3 BC cell lines with synergistic effects when used in combination with oHSVs. Moreover, blocking Tim-3 with and without OV statistically reduced cell invasion and migration in MCF-7 and SKBR-3 BC cell lines. These effects were not seen in the aggressive MDA-MB-231 cells. Preliminary data from in vivo studies suggests that combination therapy reduced tumour volume and increased overall survival time compared to the individual treatments with clear reductions in tumour necrosis and a significant reduction in pulmonary and liver metastasis compared to untreated tumour-bearing mice.

Conclusion: Inhibiting TIM-3 with OV shows potential for enhancing antitumor responses in vitro and in vivo. This approach could be a promising immunotherapy strategy, particularly if tailored to specific breast cancer subtypes. Future studies should focus on optimising treatment regimens and delivery methods. While these results are encouraging, careful consideration of efficacy across different cancer subtypes and potential side effects is necessary as research progresses towards clinical application.

CHAPTER 1

GENERAL INTRODUCTION

1.0 Introduction

1.1. Breast Cancer

Breast cancer (BC) is the fourth most common cause of cancer-related deaths in the UK, accounting for 7% of all cancer-related deaths. Chemotherapy, radiotherapy and surgical methods are used for the treatment of most patients **Table 1.1.**, but despite this in the UK approximately 11,500 die every year due to BC ("BC statistics | Cancer Research UK," n.d.). BC has been linked to obesity, lack of physical exercise, drinking alcohol, hormone replacement therapy during menopause, ionizing radiation, early age at first menstruation and having children late or not at all (Guo et al., 2020; Hurvitz et al., 2013; Jia et al., 2022). BCs are very heterogeneous and can be classified into several subtypes based on distinct gene expression profiles (Perou et al., 2000). These include ER+/- (oestrogen receptor), PR+/- (progesterone receptor) and HER2+/- (ERBB2 receptor) based on their expression (Yeo and Guan, 2017). More effective treatments are needed for patients with advanced BC, particular triple negative BC (TNBC), where none of the receptors are present, this accounts for 15-20% of all BCs and is characterised by its aggressiveness including relapse and metastasis behaviour (Keenan and Tolaney, 2020).

Breast cancer frequently metastasizes to organs including bones, liver, lungs, and brain (Shao and Varamini, 2022). Bone is the most common site, with a metastasis incidence of approximately 73% (Suva et al.,2011). While the exact reason for this preference for bone is still under investigation, certain signalling pathways and molecular expressions might play a role in attracting and promoting the migration of breast cancer cells to the bone (Xu and Tang, 2023; Wang et al., 2023). The chemokine CXCL12, secreted by osteoblasts, plays a crucial role in directing the migration of osteogenic precursors towards the bone marrow microenvironment. This chemotactic response is mediated by the interaction of CXCL12 with its receptor, CXCR4, expressed on the surface of osteogenic precursors.

Moreover, metastatic BC cells overexpress CXCR4 indicating that BC prone to metastases to bone more than other organs (Muller et al.,2001). The receptor activator of nuclear factor kappa-B ligand (RANKL) binds to its receptor, RANK, on osteoclasts (bone-resorbing cells). This interaction stimulates osteoclast activity, leading to the breakdown of bone matrix and triggering bone metastasis feed forward cycle (Jackson et al.,2013). Interestingly, breast cancer cells can secrete parathyroid hormone-related peptide (PTHrP), which can further induce the overexpression of RANKL by bone cells (Jackson et al.,2013). Studies have shown that PTHrP expression is often higher in bone-metastatic breast cancer cells compared to those in the primary tumour or other metastatic sites (Martin,2002; Southby et al.,1990; Powell et al.,1991). Furthermore, inhibiting RANKL in breast cancer patients with bone metastasis has been shown to significantly reduce bone turnover markers (indicating decreased bone breakdown), highlighting the important role of this pathway (Body et al.,2006; Lipton et al.,2007; Lipton et al.,2008).

Table 1.1. Breast Cancer treatment in clinic (Gennari et al.,2021; Loibl et al.,2023)

Early Breast Cancer		
Subtypes	**Preferred Therapies**	**Drugs of therapies**
Hormone receptor positive (HR+)	Adjuvant endocrine therapy	Tamoxifen or aromatase inhibitor
Premenopausal patients receiving ovarian function suppression	Adjuvant bisphosphonates	pamidronate, ibandronic acid, sodium clodronate and zoledronic acid
HR+/HER2-	Adjuvant therapy with or without chemotherapy (ChT), primary surgery, systemic treatment	Abemaciclib or Olaparib
HER2+	Neoadjuvant therapy, surgery with or without radiotherapy, systemic treatment	Paclitaxel, trastuzumab, pertuzumab

TNBC	Neoadjuvant therapy, surgery with or without radiotherapy, systemic treatment	Taxane-carboplatine with or without doxorubicin-cyclophosphamide, Olaparib, pembrolizumab, capecitabine
Metastatic Breast Cancer		
ER+/HER2-	Endocrine therapy (ET) with or without ChT	Everolimus–exemestane or Everolimus–fulvestant or Fulvestrant+ CDK4/6 inhibitor or fulvestrant–alpelisib or PARP inhibitor
HER2+	1st-line treatment with or without ChT	Trastuzumab– pertuzumab with/without ET or Docetaxel/ paclitaxel+ trastuzumab+ pertuzumab with/without ET
	2nd-line treatment in active brain metastatic patients with or without ChT	stereotactic radiotherapy or whole brain radiotherapy or Tucatinib+capecitabine+ trastuzumab/ Trastuzumab+deruxtecan
	2nd-line treatment in no/stable/unknown brain metastatic patients with or without ChT	Trastuzumab+deruxtecan or ado-trastuzumab emtansine(T-DM1)
	3rd -line treatment in active brain metastatic patients with or without ChT	Tucatinib+capecitabine+trastuzumab or Trastuzumab+deruxtecan
	3rd -line treatment in no/stable/unknown brain metastatic patients with or without ChT	Tucatinib+capecitabine+trastuzumab or Trastuzumab+deruxtecan or T-DM1 or Lapatinib+trastuzumab or Trastuzumab/ Margetuximab/ Neratinib + eribulin/capecitabine/vinorelbine

TNBC	Immunotherapy with ChT+Trop-2-directed antibody and topoisomerase inhibitor in PD-L1+	Atezolizumab+nab-paclitaxel or Pembrolizumab+ eribulin/capecitabine/vinorelbine followed by Sacituzumab govitecan
	ChT + Trop-2-directed antibody and topoisomerase inhibitor with or without PARP inhibitor in germline BRCA1/2 mutation	Platinum preferred over taxane or Olaparib/niraparib/rucaparib preferred over eribulin/capecitabine/vinorelbine followed by Sacituzumab govitecan
	ChT+ Trop-2-directed antibody and topoisomerase inhibitor with or without mAb/ nucleoside metabolic inhibitor in PD-L1-	Anthracycline+taxane based combination or taxane+bevacizumab or capecitabine+bevacizumab or taxane/ anthracycline monotherapy with opposite agent used at progression followed by Sacituzumab govitecan

TNBC is sensitive to chemotherapy but the overall patient outcome in response to therapy is worse than for other BCs, and TNBC is still one of the most fatal diseases for women. Therefore, new treatments are urgently needed for this patient group. Immunotherapy is an oncologic treatment modality that uses the way to strengthen the host immune system to treat cancer (Marin-Acevedo et al., 2018). Immunotherapy has recently exploded for the clinical treatment of some cancer types. The first generation of antibody-based immunotherapy, immune-checkpoint blockade (ICB), provided significant clinical benefit for a small group of patients with persistent/durable responses. ICB works by blocking/inhibiting receptor and/or ligand interactions of molecules such as cytotoxic T-lymphocyte) associated antigen 4 (CTLA-4) and programmed death 1 (PD-1), which attenuate T cell activation or function (Binnewies et al., 2018).

Initially BC was not thought of as an immunogenic disease with fewer immunogenic tumour antigens (Kwa and Adams, 2018), as a result BC has not been considered suitable for immunotherapy with ICB. However, recent investigations have provided evidence of a large numbers of tumour-infiltrating lymphocytes (TILs) in the tumour microenvironment (TME) a subset of BC patient tumours and that in TNBC there is higher expression levels of PD-L1 and more TILs (Ono et al., 2012; Stanton and Disis, 2016). In addition, the number of TILs in the TME can be a prognostic and predictive marker in standard therapies whereby high numbers of TILs correlate with improved patient complete responses to chemotherapy in TNBC, which demonstrates that the immune system plays an active role in the subgroup of BC (Li et al., 2018; Ono et al., 2012). Together this suggests that immunotherapy is emerging as a novel promising option for TNBC.

1.1.2. Tumour microenvironment in Breast Cancer

Tumour cells exhibit crosstalk with surrounding stromal cells and immune cells, including T-lymphocytes, neutrophils, macrophages, fibroblasts, dendritic cells, epithelial cells, and adipocytes. This well-structured network comprises both structural components, such as lymphatic and blood vessels, and soluble factors, such as chemokines, growth factors, and cytokines (Bejarano et al., 2021). This intricate network plays a crucial role in tumour formation, progression, metastasis **(Figure 1.1.)**, recurrence, and therapeutic resistance (Zhang et al., 2019).

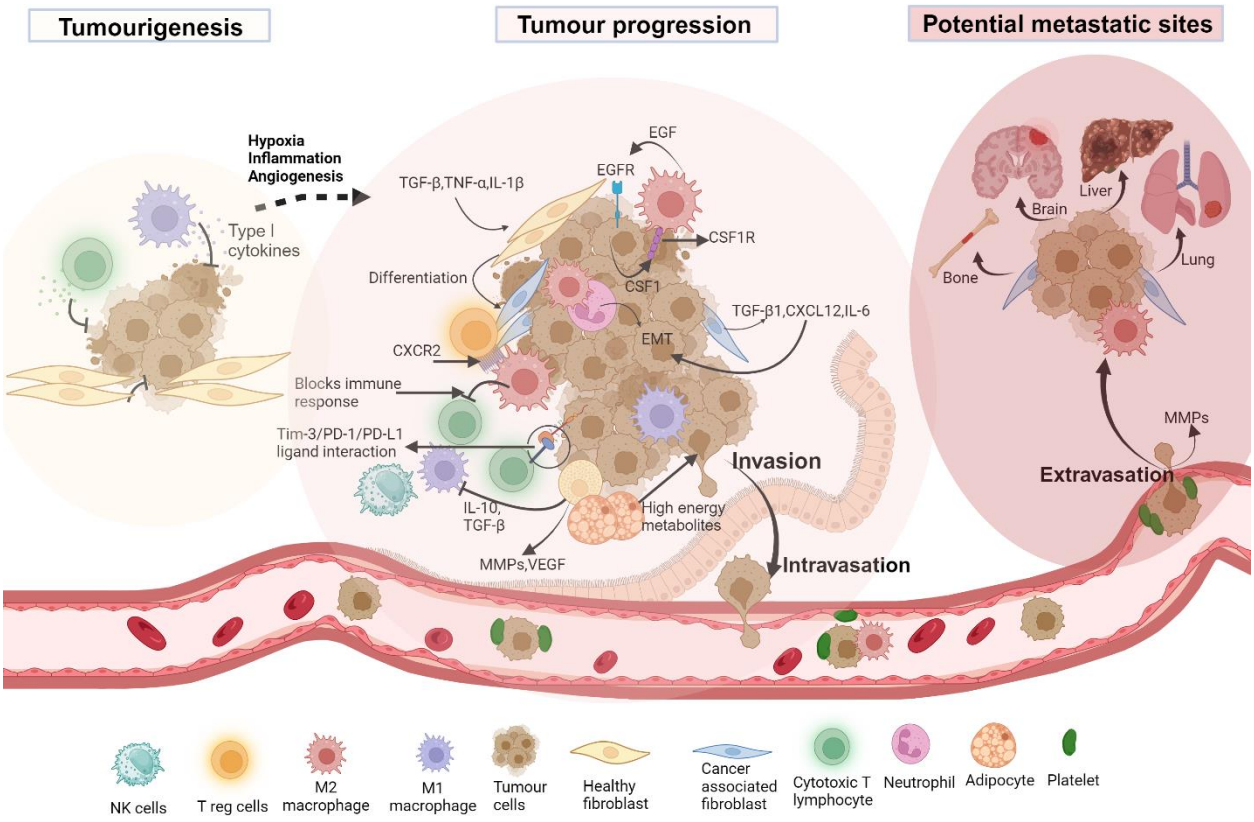

Figure 1.1. The Breast Cancer tumour microenvironment in primary sites. *Initially, BC cells face growth-suppressive signals from the immune system, regulated by cytotoxic T lymphocytes, M1 macrophages, and fibroblasts. However, these cells have evolved mechanisms to override these inhibitory signals and establish a pro-tumorigenic environment. Critically, cytokines (TGF-β, IL-1β and TNF-α) released from the inflammatory process modulate the differentiation of normal fibroblasts into cancer-associated fibroblasts (CAFs). These CAFs secrete factors (TGF-β, CXCL12, IL-6) that promote epithelial-mesenchymal transition (EMT), tumour growth, and progression. Neutrophils and adipocytes also play a role in tumour progression by inducing EMT/secreting high energy metabolites. Tumour-associated macrophages (TAMs), primarily M2 macrophages, actively support tumour growth and invasion by secreting pro-tumorigenic cytokines and growth factors. TAMs recruit immune-suppressive cells through (CXCL5-CXCR2, TGF-β), such as Tregs and MDSCs, that disrupt immune surveillance and inhibit cytotoxic T lymphocytes, M1 macrophages, and natural killer cells. BC cells evade immune surveillance by overexpressing the PD-L1/Tim-3/PD-1 ligand, further hindering immune cell activation. These orchestrated events in the primary tumour allow BC cells to acquire a motile and invasive phenotype, facilitating intravasation into the bloodstream through secreted MMPs, VEGF. In the bloodstream, BC cells interact with platelets and M2 macrophages for survival and protection. Platelets escort tumour cells to secondary sites, where they extravasate and infiltrate surrounding tissues. The preferred site of metastasis is often influenced by the subtype of BC. Figure was created using Biorender and adapted from (Terceiro et al., 2021).*

Aspects of BC, tumour-infiltrating lymphocytes (TILs) are present at lower densities compared to other cancer types, suggesting a possible antitumor immune response (Jenkins et al., 2021). A systematic review of HER2+ and TNBC patients revealed that at least 50% of these tumours exhibit TIL infiltration (Stanton et al., 2016). Moreover, lower TIL infiltration has been correlated with favourable prognostic indicators, smaller tumour size, and lower grade (Kohrt et al., 2005).

NK cells in TME play a role in tumour cell lysis and elimination through crosstalk with tumour cells and immune cells (Malmberg et al., 2017) and further contribute to the elimination of metastatic cells in the BC-TME (López-Soto et al., 2017). A study in HER2+ BC patients treated with trastuzumab (Herceptin) and chemotherapy of Anthracyclines + Taxanes showed a better pathological reaction and disease-free survival were achieved in HER2-positive patients [discovery cohort (*n* = 113) patients with higher NK cell infiltration and that tumour-infiltrating NK cells are a potential biomarker with excellent predictive value for response to treatment with Herceptin (Muntasell et al., 2019).

Cancer-associated fibroblasts (CAFs) in the TME contribute to the development of an immunosuppressive microenvironment by remodelling the extracellular matrix (ECM), thereby enhancing tumour cell proliferation and invasion (Fan and He, 2022). Notably, CAFs modulate IL-6 and IL-8, activating the NF-κB/STAT-3 pathway, as confirmed by HIF1α upregulation in BC. Consequently, NF-κB activation upregulates the transcription of multidrug resistance-associated protein-2/BC resistance protein, potentially leading to reduced drug sensitivity and resistance to chemotherapy (Lan et al., 2021). A meta-analysis of 15 studies involving 3680 BC patients reported a significant correlation between fibroblast infiltration and decreased overall survival (OS) and disease-free survival (Hu et al., 2018). Additionally, researchers isolated CAFs and normal fibroblasts from 6 human breast carcinoma patients and co-cultured them with BC cells. They observed that tumour growth in BC cells co-cultured with CAFs was enhanced, along with increased vascularization, compared to BC cells co-cultured with normal fibroblasts.

They also found upregulation of SDF-1 levels, indicating enhanced tumour angiogenesis (Orimo et al., 2005). This suggests that using CAFs from patients could improve the culture of primary BC tissue and this may improve in vitro models.

Macrophages are white blood cells derived from myeloid precursors and play an important role in tissue development, homeostasis and immune surveillance (Gabrilovich et al., 2012). Macrophages are classified as either classically activated macrophages (M1) or alternatively activated (M2) in terms of polarised subsets. M1 activation is triggered byTh1-derived cytokines such as IFNγ, GM-CSF or toll-like receptor (TLR) agonism (Chávez-Galán et al., 2015; N. Wang et al., 2014). This leads to the increased expression of surface molecules including major histocompatibility complex II (MHC II) and costimulatory molecules (CD80 and CD86) together this activates T cell priming. M1 macrophages have microbicidal and tumouricidal properties and are involved in the recruitment of Th1 cells. This occurs via chemokine gradients and involves chemokine (C-X-C motif) ligand 9 (CXCL9) and chemokine (C-X-C motif) ligand 10 (CXCL10). Importantly M1 macrophages secrete proinflammatory cytokines as tumour necrosis factor alpha (TNFα) and interleukins (IL)-1β, IL6, IL12, and IL23 (Biswas and Mantovani, 2010; Genard et al., 2017). However, on the other side, Th2-derived cytokines such as IL4, IL10, IL13, transforming growth factor beta (TGFβ), prostaglandin E2 (PGE2) or colony stimulating factor 1 (CSF1 or M-CSF) are promoters for M2 polarised cells (Hamilton, 2008; Quatromoni and Eruslanov, 2012). M2 macrophages lose their antigen presenting capabilities and are involved immune modulation (Gabrilovich et al., 2012). They have opposite effects to M1 macrophages, they produce adrenomedullin and VEGFs leading to angiogenesis, and express immunosuppressive molecules such as IL10, programmed death ligand 1 (PD-L1) and TGFβ (Chen et al., 2011; Mosser and Edwards, 2008). M2 macrophages promote the recruitment of Treg, tissue repair and remodelling and have a role in tumour progression (Mantovani et al., 2013).

Many cell types can be found in the TME including cells involved in innate immunity such as macrophages, neutrophils, mast cells, myeloid derived suppressor cells, dendritic cells, and natural killer cells. In addition, cells involved in adaptive immunity like T and B cells as well as cancer cells and their surrounding stroma (here fibroblasts, endothelial cells, pericytes, and mesenchymal cells can be found) (De Visser et al., 2006). Macrophages can form one of the major components of immune cell infiltrate in the TME as TAM. TAMs mostly promote tumour growth, angiogenesis, invasion, and metastasis (Condeelis and Pollard, 2006). Lin et al., demonstrated that a mutation in the CSF-1 that codes the macrophage growth factor, dramatically reduced tumour progression as assessed by tumour morphology and lung metastasis (Lin et al., 2001). Moreover, CSF1 is an important regulator of TAM polarisation into an M2 phenotype (Hamilton, 2008). In line with this, a study targeting chemokine (C–C motif) receptor 2 (CCR2) or colony-stimulating factor 1 receptor (CSF1R) showed improved chemotherapeutic efficacy, inhibiting metastasis, and increasing anti-tumour T-cell responses in pancreatic tumours (Mitchem et al., 2013). This suggested that by targeting TAMS via CCR2 or CSF1R resistance to chemotherapies can be overcome.

Together these studies suggest a role for immune cells in the BC TME and indication that immunotherapy could work in this patient group. However, this highly depends on the subtype. Below is a review on cancer immunity and current applications of immunotherapy in this disease.

1.2. Immunotherapy for Breast Cancer

In 1908, Paul Ehrlich argued that immunity plays an important role in eliminating cancer before it is reflected in clinical findings. However, it was William Coley who paved the way for immunotherapy for the treatment of cancer and is known as the father of cancer immunotherapy (Rusch et al., 2018). He conducted the first systematic studies showing positive outcomes of the exposure of cancer patients to bacterial products like Bacillus Calmette-Guerin for some solid tumours, for instance bladder cancer, in 1890.

However, it was not until the 1970s and 1980s that immunotherapy began to take off. Interleukin-2 (IL-2) or lectin-activated lymphocytes were shown to target tumour cells *in vitro* (Kantarjian et al., 1997). It was also discovered that interferon-α (IFN-α) had antitumour function in hairy cell leukaemia, melanoma, renal cell carcinoma (RCC), and other solid tumours in the same period. IFNα2 became the first human immunotherapeutic approved by the FDA for cancer (Kantarjian et al., 1997). Meanwhile, IL-2 was described as a T-cell growth factor in 1976 and was subsequently approved by the FDA in 1998 for the treatment of metastatic melanoma (Kirkwood et al., 2012).

The concept of cancer immune surveillance was proposed by Burnet and Thomas in 1970, he proposed that tumour antigens are recognized by the immune system and cause a cytotoxic response therefore protecting the host from developing cancer (Burnet, 1970). Three essential phases have been proposed in immune surveillance: elimination, equilibrium and escape, which are referred to as the 'three E's'. This involves the interaction of a number of immune cells and cytokines secreted by these cells which play a critical role in pursuing each of these phases (Dunn et al., 2004) (**Figure 1.2.**).

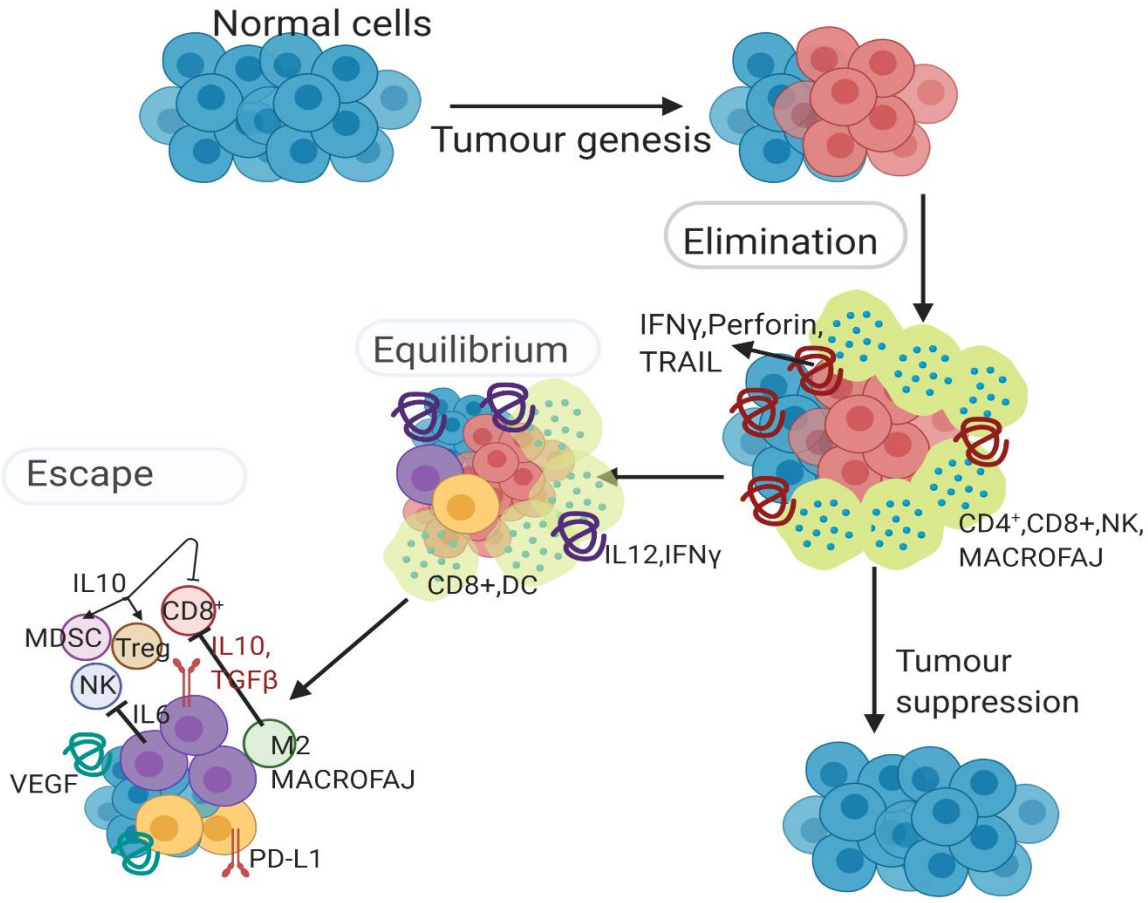

Figure 1.2. Cancer Immuno-editing. *Elimination phase: antitumor effector cells and molecules are recruited to the place where tumour antigens are, and immune attack is stimulated. Equilibrium phase: Cancer cells, which can exceed the elimination phase, are prevented from growing by immunological mechanisms. Regulation of tumour immunogenicity occurs and immune selection pressure on tumour cells creates new tumour cell genetic variants. Escape phase: Variations in the balance phase allow this phase to pass. This phase, secretion of immune suppressor cytokines, recruitment of immune suppressor cells, tumour cell PD-L1 upregulation, and tumour cells are no longer recognized by immunity (Figure was created using Biorender and Adapted from (Tower et al., 2019)).*

In the relationship between cancer and the immune system, the immune system acts bilaterally and can control / prohibit and shape/amplify cancer by immune- regulation. Tumour cells can initially be eliminated by immune cells like natural killer cells (NK cells) and T cells (TCs) and the increased release of pro-immune humoral factors (e.g. interferons) in the tumour microenvironment (Domschke et al., 2016). As the tumour progresses, it can change, immune selection produces tumour cell variants that lose major histocompatibility complex class I and II antigens and reduces the amounts of tumour antigens in the equilibrium phase despite the presence of an adaptive immune response. Furthermore, tumour-derived soluble factors help the tumour cells escape from immune surveillance, allowing progression and metastatic spread (Kim et al., 2007). In 2011 a review by Hanahan and Weinberg proposed the idea of "avoiding immune destruction" as an emerging hallmark of cancer (Hanahan and Weinberg, 2011) and in 2022, avoiding immune destruction was included among the core hallmarks of cancer (Hanahan, 2022).

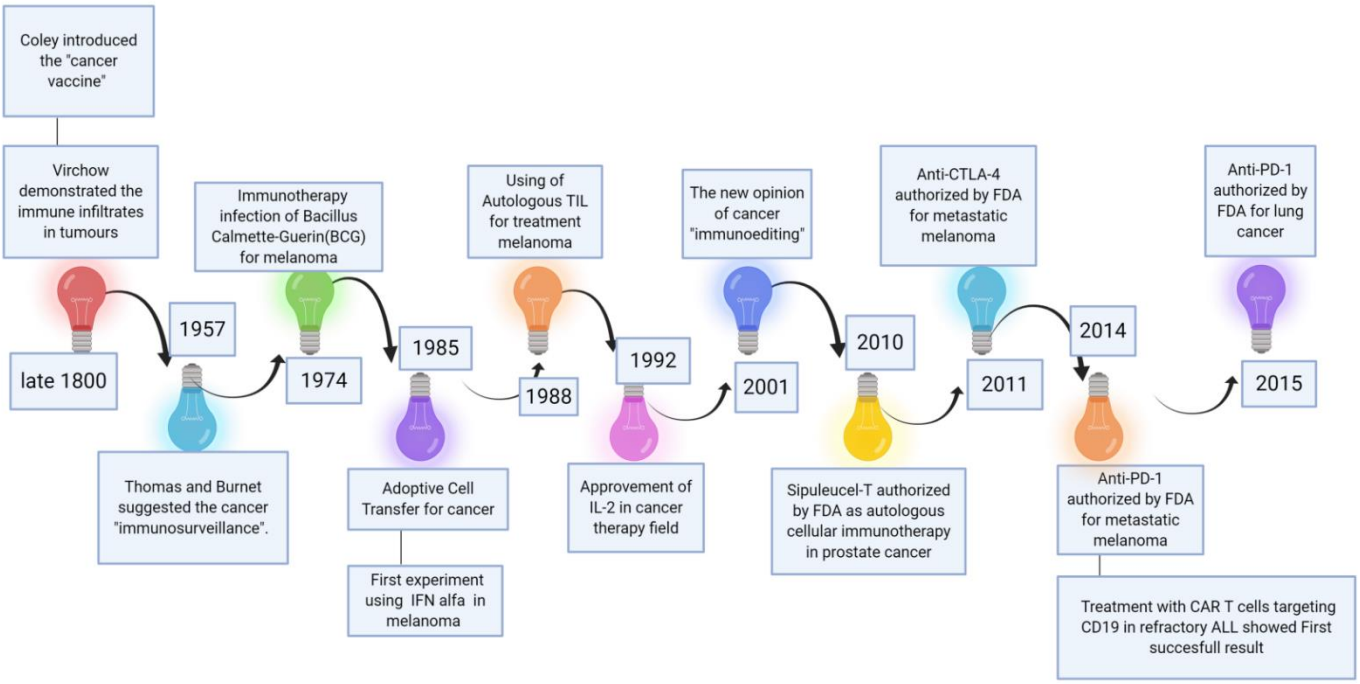

Figure 1.3. Historical advancement of cancer immunotherapy. (Figure was created using Biorender)

Since Burnet and Thomas's concept of cancer immune surveillance the role of immune system in the process of cancer including prevention, advancement, and expansion has been extensively studied and in recent years immunotherapy has emerged a powerful method in the treatment of cancer (Chen and Mellman, 2013) **(Figure 1.3.).** It is now recognised that the immune system is able to recognise tumour antigens and respond by generating an antigen specific cytotoxic CD8+ T cell response (Boon et al., 1994).

However, the antigen specific T cell response will eventually fail for two main reasons. Firstly, via the process of elimination of tumour cells that express antigens recognised by T cells **(Figure 1.2.)**, this process is called cancer immune editing (Mittal et al., 2014; Schreiber et al., 2011). Secondly the tumour microenvironment becomes hostile and immune suppressive, and the tumour cells secrete signals (e.g. via the production of immune-suppressive mediators such as inhibitory cytokines) that inhibit or block the activated anti-tumoral T cells, these are called immune checkpoint pathways (Baitsch et al., 2012; Chen and Mellman, 2013).

Immunotherapy aims to enhance or restore the immune system's ability to fight diseases like cancer, and to do this successfully it needs to increase the quality or quantity of immune effector cells (e.g. cytotoxic T cells), expose additional protective tumour antigens (i.e. antigen spread), and/or inhibit cancer-induced immunosuppressive mechanisms (Shore, 2015). Notably, cancer immunotherapy has exploded in the last 15 years and is now used in addition to the more conventional cancer treatments like surgery, hormonal therapy, radiotherapy and chemotherapy for some cancer types (Liu et al., 2022; Rouzbahani et al., 2018). Chemotherapy and radiotherapy are the fundamentals of cancer treatment, however because of the various limitations such as systemic toxicities, lack of specificity for malignant cells, recurrence of drug-resistant tumours, and the inability to target and treat micro-metastasis or subclinical disease, immunotherapy is an attractive alternative (Sanghera and Sanghera, 2019; Su et al., 2023). However, it is clear that multiple combination therapies are needed for cancer as single drug therapies are not sufficient and this is likely to be the case for immunotherapy too (Rouzbahani et al., 2018).

So far, cancer immunotherapy has involved the use of recombinant cytokines (e.g., IFN alpha) antibody therapies that bind to and inhibit the function of proteins expressed by cancer cells. An example of these are the checkpoint inhibitors (e.g., PD-L1, CTLA-4).

Other cancer immunotherapies include vaccines and T cell infusions. The latter (adaptive T-cell therapy) based on chimeric antigen receptors (CARs) have provided advancement in immunotherapy with very promising results (Naran et al., 2018). The approach of CAR T cell therapy harnesses the method of genetically producing T cells with CARs *in vitro* and re-injecting the patient's CAR T cells which are intended to recognize tumour antigens (Liu et al., 2022; Shukla and Steinmetz, 2016). In a study by Schuster *et al.,* 2017, autologous T cells that express a CD19-directed CAR (CTL019) were used to treat 28 patients with diffuse large B-cell lymphoma (14 patients) and follicular lymphoma (14 patients). They reported that a complete remission was observed in 6 of the first group and 10 of the second group and was able to maintain this response for an average of 28.6 months in 86% and 89% of these patients, respectively (Schuster et al., 2017).

In a study, researchers designed ICAM1-specific CAR-T cells to test antitumor activity on TNBC *in vitro* and in NSG mouse xenograft model bearing subcutaneous MDA-MB-231-luc tumour. Firstly, in vitro data showed effectively killing of ICAM1-positive TNBC cells and reducing tumour size in mice treated with ICAM1-specific CAR-T cells. Furthermore, the treated mice serum samples showed 3- to 16-fold increase in the concentration of cytokines (IL-2, IL-6, TNF-α, and IFN-γ) and considerable prolonged survival (Wei et al., 2020).

A recent preclinical study designed a CaCO3 biomineralized silk fibroin hydrogel DC vaccine by embedding membrane proteins from murine mammary carcinoma 4T1 cell-DC fusion cells (FP) within the hydrogel. In vitro, they treated 4T1 cells with 4T1 cytomembrane protein (CP), DC cytomembrane protein (DP), and FP to assess cell viability, T cell activity, and macrophage polarisation. Compared to controls and groups receiving CP or DP, FP treatment promoted DC maturation with 1.5-fold higher IL-12 and TNF-α secretion, and enhanced CTL activity (21.8% vs. 19.2% and 20.8% in CP and DP groups).

Notably, FP-treated T cells exhibited lower viability (60.6% compared to 81.6% and 83.9% in CP and DP groups, respectively). FP treatment also impacted macrophage polarization, downregulating CD206 (M2 marker) and upregulating CD80 (M1 marker). This shift was accompanied by 1.7-fold and 2.8-fold increases in IL-12 and TNF-α, respectively, compared to controls. In vivo, BALB/c mice transplanted with 4T1 cells and treated with FP displayed the most significant tumour inhibition. Deep tumour tissues showed elevated levels of apoptotic cells, CD4+ and CD8+ T cells, with FP-treated mice having the highest CD8+ population (15.3%) and enhanced IL-6 and IFN-γ secretion compared to CP and DP groups. Notably, FP treatment also increased mature DC levels (20.9% vs. 12.9%, 16.5%, and 5.02% in CP, DP, and control groups, respectively). Compared to controls, M2 macrophages were reduced to a quarter, while M1 macrophages were over 2.5 times higher. Importantly, two FP-treated mice showed no lung metastases, and others had minimal and localized nodules. No cancer cells were found in in the liver, kidney, spleen and heart in any group at the end of the study. These findings suggest that this novel immunotherapy effectively remodels the TME, hinders metastasis, and inhibits tumour growth (Huo et al., 2022).

Checkpoint blockade therapies, on the other hand work by inhibiting pathways that keep the duration and strength of the immune system in check. The recent approval of two checkpoint blockade therapies targeting the receptors cytotoxic t-lymphocyte-associated protein 4 (CTLA-4) and programmed cell death protein 1 (PD-1) have come off the back of several successful clinical trials where treatment with checkpoint blockade inhibitors has resulted in striking T cell function restoration in melanoma, renal cell carcinoma and lung cancer (Shukla and Steinmetz, 2016). Checkpoint blockade therapies will be discussed in more detail in the next section.

1.2.2. Immune checkpoints

The immune system maintains homeostasis by regulating immune cell activation, ensuring appropriate responses to both infection and cancer (Huang et al., 2019). This balanced state allows the immune system to ignore harmless self-antigens, a process known as immune tolerance, while effectively recognizing and eliminating harmful non-self-antigens (Pardoll, 2012a). Various lymphoid and myeloid cell types contribute to this delicate balance, with T cells playing a crucial role in maintaining the finely tuned equilibrium between proinflammatory and anti-inflammatory responses (Marin-Acevedo et al., 2021).

T cells identify self- versus non-self-molecules through a network of costimulatory and co-inhibitory receptors, also known as immune checkpoints, that govern T cell activation (Karachaliou et al., 2015). Activation of T cells involve the engagement of T cell receptors (TCRs) with MHC molecules, the binding of costimulatory receptors to their ligands, and the receipt of cytokines from antigen-presenting cells (APCs). This activation pathway triggers feedback signals that induce co-inhibitory receptors, preventing excessive T cell activation and maintaining self-tolerance (Huang et al., 2019). For instance, ligation of CD28 and ICOS promotes T cell activation, while CTLA-4, PD-1, and TIM-3 inhibit T cell activation (Karachaliou et al., 2015).

However, genetic and epigenetic variations can disrupt this balance, contributing to autoimmune diseases and cancer. In cancer, co-stimulatory receptors regulating T cell activation are often not overexpressed, while co-inhibitory receptors regulating T cell inhibition are frequently upregulated, potentially compromising the anti-inflammatory response (Sakowska et al., 2022). To overcome immune tolerance to cancer and awaken the immune system, immune checkpoint inhibitor blockades are employed, specifically targeting CTLA-4, PD-1, BTLA, and TIM-3 (**Table 1.1.)**. These blockades have demonstrated FDA approval for the treatment of various cancers.

Table 1.1. List of approved ICIs by FDA *(Wei et al., 2018)*

Disease	**IC blockade drug**	**Target IC**	**FDA approval year**
Melanoma	Ipilimumab	CTLA-4	2011
Melanoma	Nivolumab	PD1	2014
Melanoma	Pembrolizumab	PD1	2014
Non–small cell lung cancer	Nivolumab	PD1	2015
Non–small cell lung cancer	Pembrolizumab	PD1	2015
Melanoma (BRAF wild type)	Ipilimumab + nivolumab	CTLA-4 and PD1	2015
Melanoma (adjuvant)	Ipilimumab	CTLA-4	2015
Renal cell carcinoma	Nivolumab	PD1	2015
Hodgkin lymphoma	Nivolumab	PD1	2016
Urothelial carcinoma	Atezolizumab	PD-L1	2016
Head and neck squamous cell carcinoma	Nivolumab	PD1	2016
Head and neck squamous cell carcinoma	Pembrolizumab	PD1	2016
Melanoma (any BRAF status)	Ipilimumab + nivolumab	CTLA-4 and PD1	2016

Non–small cell lung cancer	Atezolizumab	PD-L1	2016
Hodgkin lymphoma	Pembrolizumab	PD1	2017
Merkel cell carcinoma	Avelumab	PD-L1	2017
Urothelial carcinoma	Avelumab	PD-L1	2017
Urothelial carcinoma	Durvalumab	PD-L1	2017
Urothelial carcinoma	Nivolumab	PD1	2017
Urothelial carcinoma	Pembrolizumab	PD1	2017
MSI-high or MMR-deficient solid tumors of any histology	Pembrolizumab	PD1	2017
MSI-high, MMR-deficient metastatic colorectal cancer	Nivolumab	PD1	2017
Pediatric melanoma	Ipilimumab	CTLA-4	2017
Hepatocellular carcinoma	Nivolumab	PD1	2017
Gastric and gastroesophageal carcinoma	Pembrolizumab	PD1	2017
Non–small cell lung cancer	Durvalumab	PD-L1	2018
Renal cell carcinoma	Ipilimumab + nivolumab	CTLA-4 and PD1	2018

CTLA-4, expressed on T cells, B cells, and monocyte-derived dendritic cells (Laurent et al., 2010), was the first immune checkpoint receptor studied in clinical trials as a potential downregulator of T cell activation (Berg and Zavazava, 2008). Several publications have demonstrated durable responses and prolonged overall survival (OS) in patients treated with CTLA-4 checkpoint blockade therapies (Lisi et al., 2022). The recent approval of two checkpoint blockade therapies targeting the receptors cytotoxic t-lymphocyte-associated protein 4 (CTLA-4) and programmed cell death protein 1 (PD-1) have come off the back of several successful clinical trials where treatment with checkpoint blockade inhibitors has resulted in striking T cell function restoration in melanoma, renal cell carcinoma and lung cancer(Shukla and Steinmetz, 2016). In a clinical study conducted by Topalian et al., 2014, Nivolumab an antibody targeting the receptors PD-1 was administered to 107 patients with melanoma. The mean survival time of treated patients was 16.8 months longer with 31% of patients experiencing an objective tumour regression (Topalian et al., 2014).

Whilst the number of approved immunotherapeutic drugs have increased over recent years a key challenge in their use is overcoming the serious immune-related adverse effects including pneumonitis, pancreatitis, and colitis, which are relatively infrequent but can limit therapeutic options for some patients (Riley et al., 2019). This has raised considerable worry for care providers and costs for health care. In a study with 915 patients who were given anti PD-L1, it was noted that pneumonitis developed in 43 patients from 9 days to 19,2 months and 5 of these patients died (Naidoo et al., 2017). Understanding how to manage or reduced these adverse effects is key to improving efficacy of these drugs. One way of overcoming such effects is by improving drug delivery systems through the use of advanced biomaterials like nanoparticles or cell delivery (e.g. T cells to deliver therapies) this could improve the potency of immunotherapies while reducing unwanted toxic side effects (Timin et al., 2018).

More research is needed into understanding toxicity to ICIs so these drugs can be given to patients safely. A better understanding of the immunosuppressive TME including neoantigens, epigenetic modifications and the microbiome is needed. Also new strategies to overcome or reverse these effects. Another consideration for the use of these drugs is overcoming resistance which is seen for conventional cancer treatments.

The discovery of novel immune checkpoints like Tim-3 holds promise for expanding the immunotherapy arsenal and potentially reducing associated toxicities. Unlike CTLA-4 and PD-1, which are broadly expressed on activated T cells, Tim-3 expression appears limited to terminally differentiated T cells producing interferon-gamma (IFNγ). Additionally, Tim-3 expression in intratumoural regulatory T cells (Tregs) is more restricted compared to the widespread expression of CTLA-4 on Tregs (Wolf et al.,2020). This suggests Tim-3 targeting might have a more favourable safety profile compared to current immune checkpoint inhibitors (ICIs). Supporting this notion, studies have shown that CTLA-4 and PD-1 deficient mice develop spontaneous autoimmunity, whereas Tim-3 deficient mice remain healthy (Wolf et al.,2020). Furthermore, clinical trials with Tim-3 inhibitors, as discussed in **section 1.2.6**, indicate a well-tolerated safety profile. These findings, coupled with its specific expression pattern, make Tim-3 a compelling target for further investigation in this PhD project.

1.2.2. TIM-3

1.2.3. Structure Of Tim-3

T-Cell Immunoglobulin and mucin domain-3 (Tim-3) or hepatitis A virus cellular receptor 2 (HAVCR2) belongs to the TIM gene family (He et al., 2018) which consists of 8 members (TIM-1–8) in the mouse genome and 3 members (TIM-1, TIM-3, and TIM-4) in the human genome (Z. Li et al., 2013).

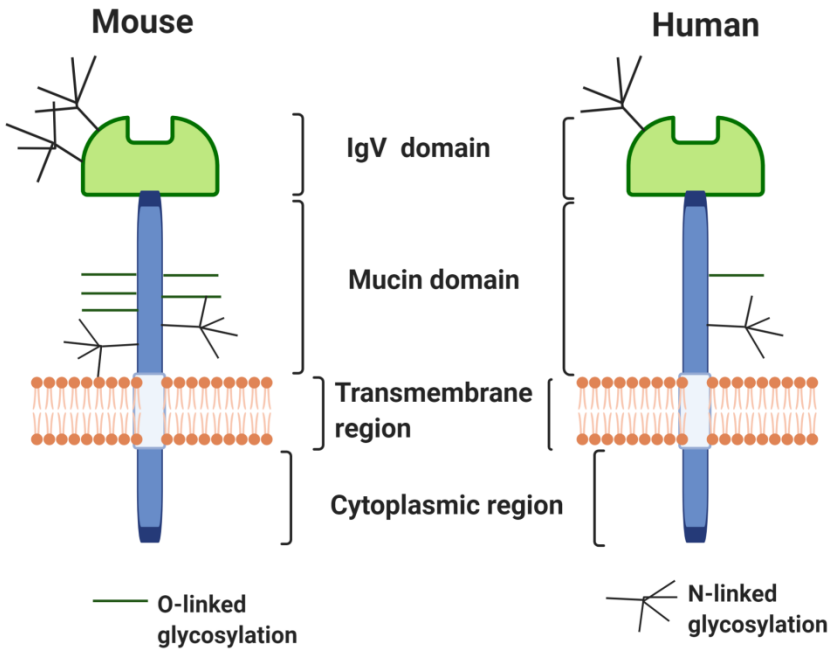

Figure 1.4. Human and mouse T cell immunoglobulin domain and mucin domain-3 (TIM-3) protein structures. *TIM-3 consists of an N-terminal immunoglobulin (Ig) V domain followed by a mucin domain, transmembrane region, and a cytoplasmic region. The IgV and mucin domains contain O- and N-linked glycosylation sites (Jinushi and Yoneda, 2013).*

As shown in **Figure 1.4.**, Tim-3 is a type-I cell-surface glycoprotein and consists of signal peptides, extracellular Ig V domains, mucin-like and transmembrane domains with an intracellular cytoplasmic tail. Tim-3 was first identified by Monney at al. as selectively expressed on the surface of lymphocytes including CD4+T helper type 1 (Th1) and CD8+T cytotoxic type 1 (Tc1) cells (Monney et al., 2002a). Further work has now identified it presence on T cells, DCs, macrophages, NK cells, cancer stem cells (Freeman et al., 2010; Gleason et al., 2012; Nagahara et al., 2008; Y. Zhang et al., 2012). Upregulated Tim-3 on NK cells lead to rising on perforin, granzyme B, IFN-γ, and TNF-α production and when Tim-3 was cross-linked on NK cells this caused suppressed NK cell-mediated cytotoxicity(Jiang et al., 2022; Ndhlovu et al., 2012). Moreover, upregulation Tim-3 on NK cells were related to the stage of the disease and poor prognosis in human lung adenocarcinoma, advanced melanoma, and hepatitis B virus-related hepatocellular carcinoma (Da Silva et al., 2014; Xu et al., 2015; Yu et al., 2021). Tim-3 on phagocytic cells like DCs and macrophages mediates clearance of apoptotic cells and in the presence of anti-Tim-3 antibodies phagocytosis of apoptotic cells is inhibited, suggesting cross-presentation of apoptotic material is associated with peripheral tolerance (Chiba et al., 2012; Nakayama et al., 2009).

Tim-3 was shown to be incorporated in the regulation of macrophage activity and may take a role as an inhibitor of macrophage activation. One study showed that viral infection led to rapid Tim-3 expression on macrophages and that blockade of the Tim-3 pathway led to a reduction in expression of the co-stimulatory molecule CD80 (Frisancho-Kiss et al., 2006). Furthermore, in other studies it was suggested that Tim-3 expression regulates the ability of macrophages to counter lipopolysaccharide induced pulmonary epithelial barrier dysfunction, this was assessed by monitoring cell monolayer permeability following co-culture of lipopolysaccharide (LPS) injured musculus lung epithelial cells (MLE 12) with M1 or M2 macrophages. Co-culture of LPS treated epithelial MLE 12 cells with M1-like macrophages diminished cell migration and furthered permeability, whereas co culture with M2 macrophages induced the opposite effect.

However, when they used Tim 3 small interfering RNA (siRNA) and anti-mouse Tim 3 antibody to both knockdown and block endogenous Tim 3, this removed the barrier protection supplied by M2 macrophages, highlighting a role for Tim 3 in maintaining macrophage M2 polarization which is important in the macrophage mediated barrier repair process (Zhang et al., 2011).

1.2.4. Ligands and Roles

Tim-3 binds to specific ligands depending on the cell types including galectin-9 (Gal-9), phosphatidylserine (PtdSer), high mobility group box-1 protein (HMGB1), and carcinoembryonic antigen-related cell adhesion molecule 1 (CEACAM-1), these are illustrated in **Figure 1.5**.

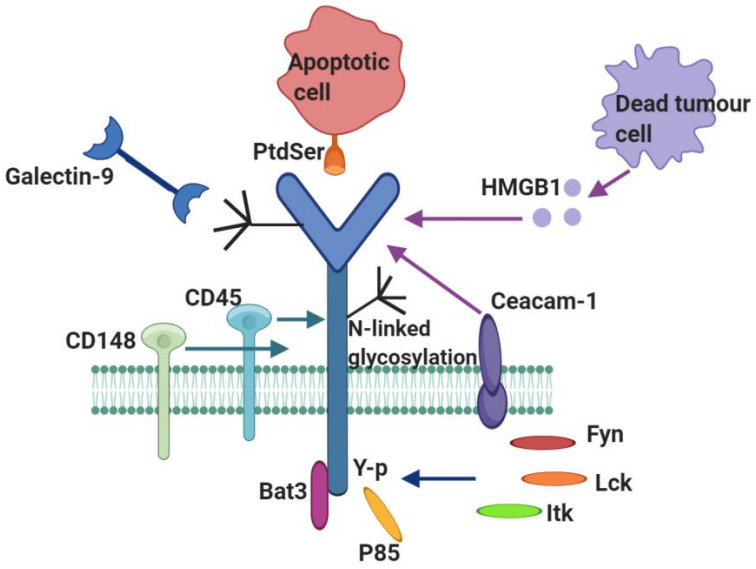

Figure 1.5. T cell immunoglobulin and mucin domain 3 (Tim-3), its ligands, and signalling adaptor proteins. *Four ligands—namely, galectin-9 (Gal-9), phosphatidylserine (PtdSer), high mobility group protein B1 (HMGB1), and carcinoembryonic antigen cell adhesion molecule 1 (Ceacam-1)—have been identified to bind to the variable immunoglobulin (IgV) domain of TIM-3. (Du et al., 2017)**.*

Galectin-9 and HMGB1 are soluble ligands, while Ceacam-1 and PtdSer belong to surface ligands. Galectin-9 specifically recognizes the structure of N-linked sugar chains in the Tim-3 IgV domain and also has the highest affinity as compared with interactions of the Tim-3 IgV domain and other galectins. Interaction between them may mediate effector T cell apoptosis (Zhu et al., 2005) and increased Tim-3-mediated IFN-γ production in NK cell (Gleason et al., 2012).

In DCs, HMGB1 plays a critical role in the transport of nucleic acids into endosomal vesicles and Tim-3 binds to HMGB1 to block the transport of nucleic acids into endosomes, thereby suppressing pattern recognition receptor-mediated innate immune responses to tumour-derived nucleic acids (Chiba et al., 2012). Ceacam1-Tim-3 interaction is thought to inhibit effector T cell function and is required for maintaining T cell tolerance (Huang et al., 2015; Y. Zhang et al., 2017). Huang et al, show that Tim-3 is co-expressed and forms a heterodimer with CEACAM1. In a mouse adoptive transfer colitis model, CEACAM1-deficient T cells are highly inflammatory with marked a reduction of cell surface Tim-3 expression which is restored by T-cell-specific CEACAM1 expression. This suggests that TIM-3 is required for its ability to mediate T-cell inhibition, and this interaction has a crucial role in regulating autoimmunity (Huang et al., 2015).

Finally, PtdSer is established as a ligand for TIM-1 and TIM-4 receptors, exposed on the surfaces of apoptotic cells. However, recent studies identified TIM-3 as a receptor for PtdSer proteins and the interaction of PtdSer with Tim-3 has been shown to play a role in the phagocytosis of apoptotic bodies on fibroblastic (3T3) cells (DeKruyff et al., 2010).

1.2.5. Tim-3 function In Immune System

Early studies suggested Tim-3 is involved in the induction of autoimmune diseases. A study by Monney *et al*., demonstrated that during the development of experimental autoimmune encephalomyelitis (EAE), a Th1-dependent autoimmune disease in mice, Tim-3 expression levels on CD4+ and CD8+ T cells, significantly increased. However, administration of Tim-3 antibodies resulted in disease progression and more severe clinical symptoms, and this was accompanied by an increase in the number of macrophages and their activation. Thus, in this study, Tim-3 blocking has been shown to negatively regulate the immune response in autoimmune disease and suggested this may be via regulating macrophages (Monney et al., 2002a). These data provided the first indication that Tim-3 may function as a T cell inhibitory receptor.

Furthermore, a study conducted to identify galectin-9 has reported that the interaction between Tim-3 and galectin-9 induces TH1 cell death and eliminates IFN-γ-producing TH1 cells. As a result, they suggested that the Tim-3–galectin-9 pathway may have evolved to control the population expansion and tolerance of T helper 1 cells in the immune compartment and to prevent prolonged inflammation in target tissues (Zhu et al., 2005).

A further study in Tim-3-deficient mice treated with a fusion protein of both Tim-3 isoforms (Tim-3–Ig) showed that it induced hyperproliferation of Th1 cells and release of Th1 cytokines ex vivo as well as abrogated tolerance induction (Sabatos et al., 2003a). These results suggested that the interaction of Tim-3 with Tim-3 ligand prevents effector T helper cells during a normal immune response and may be crucial for the induction of peripheral tolerance.

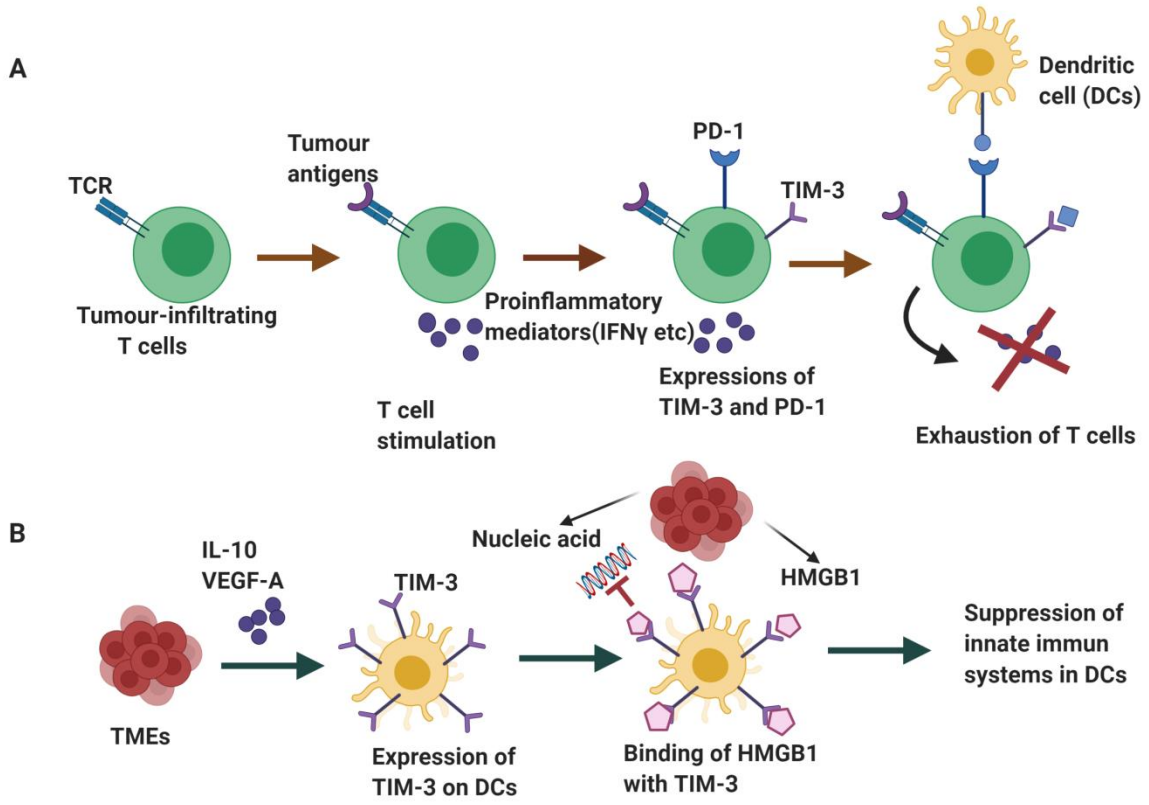

Figure 1.6. Role of T cell immunoglobulin domain and mucin domain-3 (Tim-3) in cancer immunosuppression*. **(A)** Exhaustion of T cells by Tim-3 and programmed cell death protein 1 (PD-1). Tumour-infiltrating T cells secrete interferon-γ (IFNγ) upon binding of tumour antigens by T cell receptors (TCR). However, Tim-3 and PD-1 are upregulated on tumour-infiltrating T cells upon chronic exposure to antigenic stimuli and interact with galectin-9 (Gal9) and programmed cell death 1 ligand 1 (PD-L1) expressed on tumours or tumour-infiltrating stromal cells. These interactions impair the effector activities of tumour-infiltrating T cells, leading to cancer immunosuppression. **(B)** Immunosuppression of dendritic cells (DCs) by TIM-3. TIM-3 expression on DCs is induced via stimulation by interleukin (IL) 10 and vascular endothelial growth factor A (VEGF-A), which are mainly secreted from tumour microenvironments (TMEs). Tim-3 on DCs binds high mobility group box 1 (HMGB1) from inflammatory TMEs, and negatively regulates the HMGB1-mediated recruitment of TMR-derived nucleic acids, thereby suppressing the innate immune systems. As a result, Tim-3 on DCs enables tumours to acquire immunosuppressive capabilities (Jinushi and Yoneda, 2013)***.**

Recent studies have also identified that Tim-3 acts as a regulator of the dysfunctional or exhausted CD8+T-cell in advancement of chronic diseases, including chronic viral infections and cancer (Fourcade et al., 2010; Gleason et al., 2012; Golden-Mason et al., 2009; Jin et al., 2010; Sakuishi et al., 2010a). In a study conducted by Fourcade et al., melanoma patients who had received a melanoma vaccine led to the induction of tumour antigen-specific CD8+ T cell responses that could be detected ex vivo. Most of the vaccine-induced CD8+ T cells upregulated checkpoint inhibitor PD-1 and some also upregulated Tim-3 expression. Interestingly, inhibiting PD-1 and Tim-3 enhanced the expansion and cytokine production of vaccine-induced CD8+ T cells in vitro supporting the use of PD-1 and Tim-3 blockades with cancer vaccines to stimulate improved anti-tumour T cell responses and ultimately increase the chance of clinical responses in patients with advanced melanoma (Fourcade et al., 2010).

Additionally, in a study that investigated the role of Tim-3 in HIV viral infection, 31 HIV infected, and 9 uninfected cases showed Tim-3 expression was up-regulated on HIV-1–specific CD8+ T cells. Tim-3–expressing T cells failed to produce cytokines or proliferate in response to antigen. Blocking the Tim-3 signalling pathway restored proliferation and enhanced cytokine production in HIV-1–specific T cells (Jones et al., 2008).

A recent study also identified a correlation between Tim-3 on T cells with clinical-virological features in 320 treatment-naïve chronic hepatitis B (CHB) patients. Peripheral blood mononuclear cells (PBMCs) were isolated from fresh blood of patients using Ficoll density gradients and stained with markers for CD8 and CD4 T cells and Tim-3. They found that Tim-3 positive T cells in these patients was linked to virology, liver inflammation and liver fibrosis, suggesting that Tim-3 may play an important role in the disease process and that Tim-3 should be considered in determination of antiviral treatment in the future (Gu et al., 2020). A limitation of this study is that they did not look at other inhibitory molecules, for example it would have been useful to also investigate PD1 or CTLA-4.

Interestingly, another study echoes these findings by demonstrating Tim-3 upregulation in CHB patients' serum, with correlations observed for the degree of inflammation and fibrosis. This further strengthens the notion of Tim-3 as a potential candidate for both therapeutic targeting and prognostic serum marker development in CHB (Wu et al., 2022).

Collectively, these studies demonstrate that Tim-3 has an inhibitory role and is an immune check point receptor that should be considered when treating patients.

1.2.6. Tim-3 in Cancer

As mentioned above the past decade has been an explosion in the development of immune checkpoint inhibitors (ICIs) (Yi et al., 2018), chimeric antigen receptor T cell (Yu et al., 2017)and bispecific antibodies (Han et al., 2017). Despite some ICIs showing compelling clinical effectiveness in certain tumour types like melanoma, success in other cancers and also resistance in the majority of patients, needs to be overcome. As a result, the overall efficacy of immune checkpoint therapy remains unsatisfactory. Therefore, exploring additional immune checkpoint molecules is important and Tim-3 has been identified as a potential checkpoint target. In cancer patients, we know that TIM-3 is upregulated on tumour antigen-specific CD8+ T cells, CD8+ TIL and CD4+TIM-3+ TIL (Baitsch et al., 2011; Fourcade et al., 2010; Gao et al., 2012a).

Tim-3 is also expressed on TAMs in a variety of tumours, including hepatocellular carcinoma, lung cancer, clear cell renal cell carcinoma, osteosarcoma, Langerhans cell sarcoma, and neoplasms derived from histiocytic and dendritic cells (Dannenmann et al., 2013; Han et al., 2016; J. Li et al., 2013). In a study conducted by Sakuishi 3 cancer types were investigated in mouse models including CT26 colon carcinoma, 4T1 mammary adenocarcinoma and B16F10 melanoma. One of observations is that the CD8+ tumour infiltrating T lymphocyte (TIL) subsets that co-express the checkpoint inhibitors Tim-3 and PD-1 comprise the dominant T cell population (~50%) in tumours.

Moreover, they examined cytokine production of CD8+ TILs (IL-2, TNF, and IFN-γ) and found that the Tim-3+PD-1+ TILs showed impairment in production of these cytokines compared with the Tim-3−PD-1+ TILs and Tim-3−PD-1− TILs. Finally, treatment with a combination of anti–Tim-3 and anti–PD-L1 antibodies was reported to effectively restore anti-tumour immune responses compared to the single treatments (Sakuishi et al., 2010a).

A further study in non-small cell lung cancer (NSCLC) patients (n=51) found high Tim-3 expression on very little expression on T cells from patients' peripheral blood. Interestingly, they reported that approximately 70% of Tim-3+CD4+ TILs expressed forkhead box P3 (FOXP3) and about 60% of FOXP3+ TILs were TIM-3+. FOXP3 expression on CD4 T cells is associated with T regs. An increase in T regs in tumours and in the circulation of cancer patients has been linked to pathogenesis and cancer progression. In addition, they carried out mouse studies using the B16 melanoma model, where they found that about 50% of the Foxp3+CD4+ TILs expressed Tim-3 and these were mainly restricted to the tumours of the mice. Negligible levels of Tim-3 on CD4 T cells were identified in other organs like the spleen or lymph nodes regardless of expression of FoxP3. Thus, they suggested a new role of Tim-3 in the tumour microenvironment via its predominant expression in regulatory CD4+FoxP3 T cells in both human and mouse tumours (Gao et al., 2012a).

Of interest to this PhD is also the role of Tim-3 in TAMs. Macrophages are the most well-characterized type of tumour-infiltrating immune cell and TAMs are a subpopulation of macrophages in TME. In line with this, a study conducted by Yan et al., investigated the role of Tim-3 in TAMs in patients with HCC. They investigated Tim-3 expression on tumour infiltrating macrophages freshly isolated from surgically resected tumour tissue and also the adjacent tissues where no tumour was evident as well as the patients' monocytes in circulation. Tim-3 expression was highly expressed in both circulating monocytes and TAMs and this expression in monocytes/TAMs correlated with more aggressive tumours and poor patient survival in HCC. As a comparison they also investigated the effects of Tim-3 knockdown on macrophages in a BALB/c mouse model of HCC and in in vitro in cell lines. Tim-3 knockdown was carried out using a number of techniques including neutralising antibody, small interfering RNA or short hairpin RNA-expressing lentivirus.

Tim-3 blockade in macrophages significantly reduced the alternative activation of macrophages and suppressed HCC tumour cell growth, both in vitro and in vivo. This suggest that Tim-3 plays an important role in the tumour microenvironment-induced activation and protumoural effects of TAMs in HCC and therapeutically blocking Tim-3 may offer an opportunity in HCC therapy (Yan et al., 2015).

Furthermore, in a study by Cheng et al., of 42 sections from BC patients, Tim-3 staining was positive in 18 out of 42 sample when semi quantitative scoring was used based on the distribution and the intensity of immunohistochemistry staining. When they evaluated the high immunoreactivity of Tim-3, it was found to be significantly correlated with clinical stage and metastasis. In terms of overall survival (OS) at the end of the 5 years follow up period, 5 patients died in the Tim-3 positive group while only 1 in Tim-3 negative group, so the 5-year survival rate was 72.2% vs 95.8% respectively. In vitro studies were also performed and the presence of Tim-3 protein in a number 3 breast cell lines was confirmed by western blotting. Tim-3 knockdown in siRNA transfected MCF-7 cells significantly inhibited cell proliferation while overexpression of Tim-3 following infection of MDA-MB-231 cells with a recombinant adenovirus vector containing a fragment of Tim-3 cDNA significantly promoted cell proliferation. Based on these data, they suggested that Tim-3 can play role in the proliferation, migration, and invasion of BC cells(Cheng et al., 2018). Further study in 3,992 BC specimens reported that TIM-3 immunohistochemical scoring of TIM-3+ intra-epithelial expression significantly improved BC-specific survival in early BC patients (Burugu et al., 2018).

Like this study, 109 TNBC patients` TIL were evaluated by H&E staining and high TIM-3 expression showed significantly correlation with younger patients, high levels of TILs and tumour stage addition to significantly better disease-free survival and longer overall survival (Byun et al., 2018). Notably, 49 clinical trials of anti-Tim-3 antibody alone/combination therapy have been documented and 7 of these were completed (“Search of: Tim-3 combination - List Results - ClinicalTrials.gov,” n.d.)**(Table 1.2.)**.

Table 1.2. Examples of Anti-Tim-3 mAbs alone or combination clinical trials in cancer *(Cai et al., 2023).*

Clinical trial ID	**Phase**	**Start date**	**Status**	**Cancer type (population, N)**	**Interventions and Combination**	**Target**
NCT05738980	Not Applicable	Feb 1, 2023	Recruiting	HCC, *N* = 88	Auto-anti-TIM-3-blocked RAK cells	TIM-3
NCT03489343	I	May 24, 2018	Completed	Advanced Solid Tumor or Lymphomas, *N* = 24	Sym023	TIM-3
NCT04623892	I	Dec 01, 2020	Unknown	Advanced Solid Tumors, *N* = 50	TQB2618	TIM-3
NCT04823624	II	Sep 2021	Unknown	Lower Risk MDS, *N* = 20	MBG453	TIM-3
NCT03652077	I	Sep 24, 2018	Completed	Select Advanced Malignancies, *N* = 40	INCAGN02390	TIM-3
NCT05020912	II	Dec 13, 2021	Completed	HR/vHR MDS, *N* = 20	MBG453 + azacytidine + venetoclax	TIM-3
NCT03946670	II	Jun 4, 2019	Active, not recruiting	IM/H/VH-MDS, *N* = 127	MBG453 + HMAs	TIM-3
NCT04623216	I/II	Sep 14, 2021	Recruiting	AML/AML MRD + post-aHSCT, *N* = 59	MBG453 + Azacitidine	TIM-3
NCT04878432	II	Mar 17, 2022	Recruiting	IM/H/VH-MDS, *N* = 90	MBG453 + HMA	TIM-3

Clinical trial ID	Phase	Start date	Status	Cancer type (population, N)	Interventions and Combination	Target
NCT04266301	III	Jun 8, 2020	Active, not	IM/H/VH-MDS, CMML-2, *N* = 530	MBG453 + Azacitidine	TIM-3
NCT04443751	I	Sep 10, 2020	Recruiting	R/R-AML, HR-MDS, *N* = 42	SHR-1702	TIM-3
NCT04150029	II	Sep 1, 2020	recruiting	ND-AML, *N* = 86	MBG453 + HMA + Venetoclax	TIM-3
NCT04812548	II	May 31, 2021	Not yet recruiting	HR-MDS, *N* = 76	MBG453 + HMA + Venetoclax	TIM-3
CTR20201781	III	Aug 6, 2020	recruiting	HR-MDS, CMML-2, *N* = 100	MBG453 + Azacitidine	TIM-3
NCT03680508	II	Dec 19, 2019	Recruiting	HCC, *N* = 42	TSR-022 + TSR-042	TIM-3, PD-1
NCT03311412	I	Nov 20, 2017	Completed	Advanced Solid Tumor or Lymphomas, *N* = 89	Sym023 ± Sym021	TIM-3, PD-1
NCT03099109	Ia/Ib	Apr 12, 2017	Active, not recruiting	advanced relapsed/refractory solid tumors, *N* = 275	LY3300054 ± LY3321367	TIM-3, PD-L1
NCT02608268	I-Ib/II	Nov 23, 2015	Terminated	Advanced Malignancies, *N* = 252	PDR001 ± MBG453	TIM-3, PD-1

Clinical trial ID	**Phase**	**Start date**	**Status**	**Cancer type (population, N)**	**Interventions and Combination**	**Target**
NCT02817633	I	Jul 8, 2016	Recruiting	Advanced Solid Tumors, *N* = 475	TSR-042 ± TSR-022	TIM-3, PD-1
NCT04641871	I	Oct 12, 2020	Active, not recruiting	BTC, ESCC, *N* = 148	Sym021 + Sym023 + irinotecan	TIM-3, PD-1
NCT05645315	Ib	Apr 28, 2022	Recruiting	Advanced Solid Tumors, *N* = 127	TQB2618 + TQB2450	TIM-3, PD-L1
NCT05563480	II	Oct 27, 2022	Recruiting	R/M NPC, *N* = 90	TQB2618 + Penpulimab	TIM-3, PD-1
NCT03066648	Ib	Jul 6, 2017	Active, not recruiting	AML/HR-MDS, *N* = 241	PDR001± MBG453 with HMA	TIM-3, PD-1
NCT05834543	Ib	May 2023	Not yet recruiting	Advanced ESCC, *N* = 75	TQB2618 + Penpulimab + Chemotherapy	TIM-3, PD-1
NCT05451407	I	Aug 9, 2022	Not yet recruiting	Advanced Melanoma, *N* = 50	TQB2618 + Toripalimab	TIM-3, PD-1
NCT04139902	II	Jun 12, 2020	Recruiting	operable melanoma, *N* = 56	TSR-022 ± TSR-042	TIM-3, PD-1
NCT05400876	Ib	Jun 9, 2022	Recruiting	R/R Lymphoma, *N* = 92	TQB2618 + Penpulimab	TIM-3, PD-1

Clinical trial ID	Phase	Start date	Status	Cancer type (population, N)	Interventions and Combination	Target
NCT03940352	I	Jun 24, 2019	Active, not recruiting	AML, HR-MDS, *N* = 52	MBG453 + HDM201	TIM-3, p53-MDM2
NCT05783921	I/II	Mar 2023	Not yet recruiting	R/M-HNSCCs, *N* = 60	TQB2618 + Penpulimab + Chemotherapy	TIM-3, PD-1
NCT03961971	I	Feb 18, 2020	Active, not recruiting	Recurrent GBM, *N* = 16	MBG453 + Spartalizumab + Stereotactic radiosurgery SRS	TIM-3, PD-1
NCT05367401	I/II	Dec 20, 2024	Not yet recruiting	Unfit ND-AML/HR-MDS/R/R-AML, *N* = 63	MBG453 + Magrolimab + Azacitidine	TIM-3, CD47
NCT04370704	I/II	Jul 27, 2020	Recruiting	Melanoma, *N* = 146	INCAGN02385 INCAGN02390 + I NCMGA00012	TIM-3, PD-1, LAG-3
NCT04810611	I	Jun 18, 2021	Recruiting	LR-MDS, *N* = 90	MBG453 ± NIS793 ± Canakinumab	TIM-3, TGF-β, IL-1β
NCT03744468	I/II	Nov 13, 2018	Recruiting	Advanced Solid Tumors, *N* = 358	BGB-A425 + Tislelizumab + LBL-007	TIM-3, PD-1, LAG-3

Clinical trial ID	Phase	Start date	Status	Cancer type (population, N)	Interventions and Combination	Target
NCT04586244	II	Jan 14, 2022	Recruiting	Urothelial Carcinoma, *N* = 45	INCAGN02390 + INCAGN02385 + Retifanlimab	TIM-3, LAG-3, PD-1
NCT05287113	II	Nov 14, 2022	Recruiting	PD-L1-Positive R/M-HNSCCs, *N* = 162	Retifanlimab + INCAGN02385 + INCAGN02390	TIM-3, LAG-3, PD-1
NCT03307785	I	Oct 12, 2017	Active, not recruiting	Advanced or Metastatic Cancer, *N* = 58	TSR-022 + TSR-042 + Niraparib + Chemotherapy	TIM-3, PD-L1, PARP1/2
NCT04810611	I	Jun 18, 2021	Recruiting	LR-MDS, *N* = 90	MBG453 ± NIS793 ± Canakinumab	TIM-3, TGF-β, IL-1β

The NCT03652077/INCAGN02390 clinical trial enrolled 40 patients with locally advanced or metastatic breast (15%), lung (13%), and colorectal (10%) solid tumours that failed other available therapies. The study was completed and reported that the anti-TIM-3 antibodies were well-tolerated. ("ESMO Congress 2022 | OncologyPRO," n.d.).

Subsequently, a combination therapy of anti-Tim-3 (LY3321367) and anti-PD-1/-L1 (LY3300054) was conducted in 82 patients with Microsatellite Instability–High/Mismatch Repair–Deficient Tumours. The patients were divided into three groups: 40 who had not received prior anti-PD-1/-L1 therapy for anti-PD-1/-L1 monotherapy, 20 who had not received prior anti-PD-1/-L1 therapy for combination therapy with Tim-3, and 22 who had been treated with anti-PD-1/-L1 and had relapsed for combination treatment. Monotherapy provided a 71% one-year overall survival rate, 60% disease control rate (DCR), and 33% objective response rate (ORR), while combination therapy yielded a 45% ORR, 70% DCR, and 64% one-year OS in those with no prior anti-PD-1/-L1 treatment. However, data from those treated with anti-PD-1/-L1 and relapsed reported poor anti-tumour response with a 4.5% ORR and 32% DCR. The monotherapy/combination treatment results in patients who had not received prior anti-PD-1/-L1 therapy indicate considerable clinical activity, durable responses, and promising survival rates, even slightly more in the combination group. These results suggest further investigation into the role of TIM-3 in PD-1/PD-L1 inhibition-related primary and acquired resistance (Hollebecque et al., 2021).

Overall, these clinical trials indicate a safety and well-tolerated profile of targeting TIM-3, promising improved immune activity. However there still needs to be a lot more investigation into understanding the mechanisms of the immune suppressive function of TIM-3 and this is also the case for understanding its role in BC and the different subtypes of this disease. So far many of these trials are phase I where patients have failed most treatments. It would be great to see more Tim-3 trials in patients at phase III or in patients who are not end of life or have not responded to other therapies so that efficacy studies can take place.

In summary, ICIs have opened up new avenues for treating cancers with the possibility for durable response and extension of survival improving in some malignancies but not all. BC in particular has not benefited fully from ICIs, largely because of the cold TME. Potential therapeutic strategies to improve clinical benefit in BC are needed to overcome resistance to the potentially life saving drugs.

A compelling solution is offered by oncolytic viruses (OVs). This immunotherapy offers specific and effective targeting resulting in the destruction of cancer cells. OVs are superior relative to other immunotherapeutic approaches as they rely on its specificity against tumour cells and not healthy cells, therefore preventing many of the unwanted side effects seen with other cancer drugs. In addition, OVs are less dependent on specific receptor expression patterns and the resultant mutational or transcriptional resistance that may occur with other drugs (Howells et al., 2017a). Importantly, OVs not only kill cancer cells they can also activate anti-tumour immunity and will be the focus of this PhD.

1.3. Immunotherapy based on Oncolytic viruses

Viruses have attracted attention in tumour destruction since the end of the 19th century when they were first recognised (Kelly and Russell, 2007). It was noted that cancer patients suffering from viral infections (e.g. measles) led to tumour remission as early as the mid-1800s (before viruses were identified), but it was not until the mid-20th century, that attenuated viral strains could be used for cancer treatment (Reale et al., 2019).

In early clinical studies human viruses such as hepatitis, Epstein-Barr, adenovirus and rabies yielded no clear data with regards to their use as oncolytics and none of them provided a solution to the problem of human infection with these viruses. On the one hand, animal viruses have been investigated which are both non-pathogenic and replicating however these showed poor results in human cancer cells (Sokolowski et al., 2015a). Safety concerns related to the virus and insufficient infrastructure for virus modification postponed the development of oncolytic virotherapy (Reale et al., 2019). Finally, the emergence of genetic engineering towards the end of the twentieth century enabled engineered forms of the viruses to be developed which are both attenuated types and also lacked some genes that are required to replicate in normal cells (Sokolowski et al., 2015a). Now OVs are selectively targeted, can kill cancer cells, and replicate without damaging normal tissue (Ma et al., 2018a) (**Figure 1.7.**).

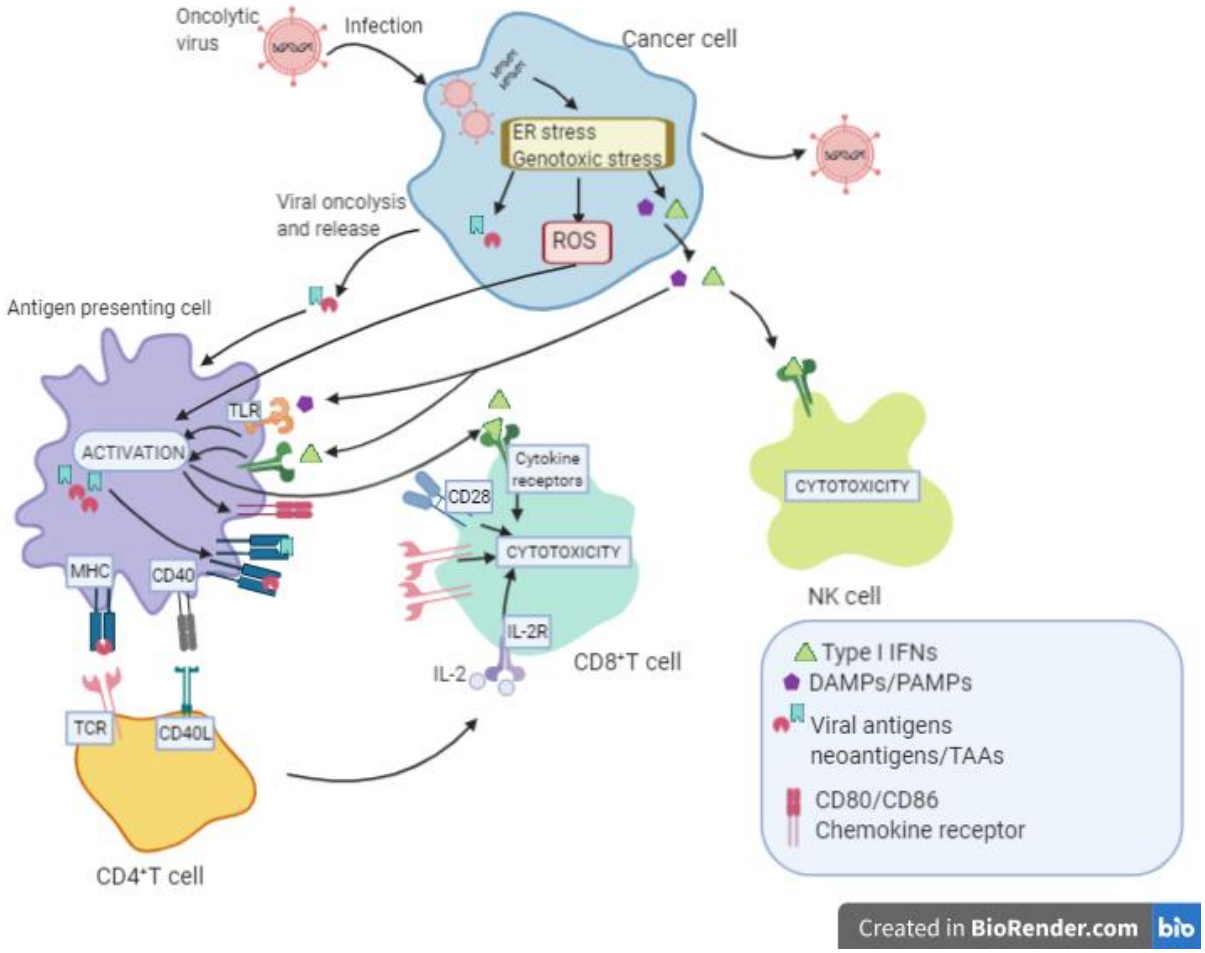

Figure 1.7. Mechanisms of action OVs inducing anti-tumour immunity (Adapted from *(Kaufman et al., 2015)**).*** *Oncolytic viruses directly kill tumour cells through immunogenic cell death, which results in the release of soluble tumour-associated antigens, viral pathogen-associated molecular patterns (PAMPs) and cell-derived damage-associated molecular patterns (DAMPs). These molecules recruit and activate immune cells (antigen presenting cells, $CD8^+$ T cells, and natural killer (NK) cells). Viral-mediated release of type I interferons and chemokines results in increased levels of antigen processing and presentation factors, including the expression of MHC class I molecules, and in recruitment of tumour-specific $CD8^+$ T cells. These cytotoxic CD8+ T lymphocytes (CTLs) recognize and kill tumour cells.*

Furthermore, unlike other immunotherapies, which depend on the presence of a specific ligand and lack tumour specificity, OVs have neoplastic cell specificity and wide immune stimulatory tolerance. They owe these characteristics to their ability to utilise malignant signals and also using response of the host adaptive immune system, which can clearly discriminate between target and non-target cells (Raja et al., 2018a). Thanks to the specificity of OVs to tumour cells, the fact that they do not harm normal cells during the treatment process provides a significant advantage to this method (Howells et al., 2017b).

OVs, on the other hand, can also facilitate the infection and killing of cells, which are not protected by the immune system, by aiming to exploit the tumour tolerogenic mechanism (Raja et al., 2018a). For example, E1 (early region 1) viral genes allow adenoviruses to proliferate in normal cells and provide specificity for mutation. The products of the E1a and E1b genes prohibit the apoptosis inhibiting p53 (tumour protein 53) and stop the cell cycle by inhibiting Rb (Retinoblastoma tumour suppressor). Adenoviruses that have mutations or deletion in these genes can often replicate by infecting tumour cells that do not have p53 and Rb function and can lead to response formation (Russell and Peng, 2007).

Another advantageous property is that after lysing the tumour cells, they generate an immune response to both viral and tumour antigens. Thus, their ability to produce permanent immunity has created an exciting field of research in the fight against cancer. OV can also be modified to include genes for the purpose of enhancing the efficiency of administration, also numerous anti-cancer genes such as rat cytochrome P450 (CYP2B1) (Chase et al., 1998), Granulocyte-macrophage colony-stimulating factor (GM-CSF) (Malhotra et al., 2007) have been used**.** Therefore, OV are a valuable candidate for this purpose and a promising platform for treating cancer (Howells et al., 2017b). The last 20 years have been a period of intense interest in oncolytic virus-mediated cancer treatment, and with the continued study of new virus candidates, 157 have been enrolled and 53 of which was completed in this field so far ("Search of: Oncolytic virus | Completed Studies - List Results - ClinicalTrials.gov," n.d.) (**Table 1.3.**).

Table1.3. Some current and completed trials using OV (Adapted from** (Carter et al., 2021; Goradel et al., 2021; Raja et al., 2018b)* **.

Virus	**Strain**	**Tumour**	**Phase**
Herpes SimplexVirus	Talimogene Laherparepvec (T-Vec)	Breast	I/II
		Melanoma,Sarcoma	II
		Pancreatic (PaC)	I
	TBI-1401(HF10)	Superficial Solid Tumours,PaC	I
		Melanoma	II
	G207	Glioma	Ib/II
	HSV-1716	Mesothelioma	I/II
		Bone,Sarcomas,Neuroblastomas	I
	OrienX010	Melanoma	Ic
	OncoVEX^{GM-CSF}	metastatic solid tumours	I
	ONCR-177	Melanoma and other solid tumours	I
	OH2	Gastrointestinal tumoUrs and other solid tumours	I/II
	RP1	Cutaneous squamous cell carcinoma	I/IB
	RP2	Advanced Solid Tumour	I
Adenovirus	LOAd703	Pancreatic	I/II
	CG0070	Bladder	II
	ColoAd1(Enadenotucirev)	Colorectal, NSCLC, Bladder, and Renal Cell	I
		Colorectal, Bladder, and Epithelial	I/II
		Ovarian	I
	ONCOS-102	Advanced Solid Tumour	I
		Melanoma	I
	DNX-2401	Brain	II

Adenovirus	VCN-01	Advanced Solid Tumours	I
		Pancreatic	I
	Ad-MAGEA3 and MG1-MAGEA3	NSCLC	I/II
		Advanced Solid Tumours	I/II
	NSC-CRAd-Survivin-pk7	Glioma	I
	Ad5yCD/mutTKSR39rep-hIL12	Prostate	I
	Ad5yCD/mutTKSR39repADP	NSCLC	I
	OBP-301	Solid tumours,Esophagel,HCC	I
	AdVince	Neuroendocrine tumours	I/IIa
	EnAd	Ovarian cancer	I
	CGTG-102	Solid tumours	I
	CGTG-602	Advanced metastatic tumours	I
	Ad5-D24-GMCSF	Advanced solid tumours	I
	Ad5-RGD-D24, Ad5-RGD-D24-GMCSF	Solid tumours	I
	ICOVIR-7	Advanced metastatic solid tumours	I
	Telomelysin	Solid tumours	I
	ONYX-015	Advanced solid tumours	I

Table 1.3. Continued

Measles virus	MV-NIS	Breast and Head and Neck	I
		Ovarian	I/II
		Nerve Sheath	I
		Mesothelioma	I
		Multiple Myeloma	I/II
Vaccinia	GL-ONC1	Advanced Solid Tumors	I
		Head and Neck	I
		Advanced Solid Tumors	Ib
		Ovarian	I
	PexastimogeneDevacirepvec (Pexa-Vec)	Hepatocellular	III
		Colorectal	I/IIa
		Advanced Solid Tumors	I
		Blue Cell	I
		Melanoma, Lung, Renal Cell, Head and Neck	I
	TG6002	CNS cancers	I/II
	JX-929/vvDD	Advanced solid tumours	I
Reovirus	REOLYSIN	Colorectal	I
		Bladder	Ib
		Pancreatic	Ib
		Multiple Myeloma	I
		Plasma Cell Cytoma	Ib
		Ovarian and Peritoneal	II
Coxsackievirus	CVA21(CAVATAK)	Melanoma	II
		NSCLC	I
Parvovirus	H-1PV(ParvOryx)	Glioblastoma Multiforme	I/IIa
Polio/Rhinovirus	PVSRIPO	Glioma	I

VSV	VSV-IFNβ-NIS	Solid tumours	I
Newcastle Disease Virus	PV701	Advanced solid tumours	I

Although the number of viruses is more than 3000, not all of them have oncolytic potential. The required properties that OV must have are non-pathogenicity, cancer cell specificity and killing, genetic modification e.g. for expression of attenuating or arming genes (Russell and Peng, 2018a). Most OV are modified for two purposes: enhance tumour tropism and reduce virulence for non-neoplastic host cells. Modifications may allow for the stimulation of a pro-inflammatory environment by accelerating antigen presentation, followed by resistance to the escape of malignant cells from immunity (Raja et al., 2018a). In the field of oncolytic virotherapy, the first successful phase III results were obtained with thalimogene laherparepvec (T-VEC) originating from the herpes simplex virus-type 1 (HSV). This has been approved by the FDA for the treatment of advanced metastatic melanoma in 2015 (Aurelian, 2016). There are still large numbers of viral strains that are currently being studied for immuno-oncology and these are at different experimental stages, and so far, probably the best studied are herpes viruses, therefore it is no surprise that this is one of the first approved viruses for patient use. Although virus development studies are still ongoing, it is reported that at least 8 OV have progressed to phase I-II-III clinical trials as of 2016 and 78 clinical trials were documented for 2017 (Raja et al., 2018a).

1.4. Oncolytic viruses

1.4.1. Adenoviruses

Isolation of adenoviruses was first carried out in 1953 (Singh et al., 2012) and is one of the first viruses to be tested in patients (Lawler et al., 2017). Although there is limited efficacy in therapeutic single applications of adenoviruses, promising results have been seen with combinations with other treatments and genetic modifications of the adenovirus. The ability of these viruses to infect the various types of cells and their ability to be genetically modified makes them desirable in this field (Goldufsky et al., 2013).

In 1996, the first genetically engineered adenovirus-derived oncolytic virus, ONYX-015, was introduced to clinical trials (Bischoff et al., 1996). As such, there was a deletion in the E1B gene for selective proliferation in p53-deprived cells, this was given the name H101. Subsequently, it was recorded as the first approved OV in the world and results obtained from phase III clinical trials using a combination of chemotherapy and H101 were very promising (Choi et al., 2016).

In a study with the combination of H101 and transhepatic arterial chemoembolization (TACE) for unresectable hepatocellular carcinoma (HCC), 87 patients were given TACE and 88 patients were given TACE in combination with H101. In the combination groups: 25 patients demonstrated complete responses, 28 partial responses; stable disease in 23 patients and progression of 11 patients' disease was reported. In the other group, complete response was in 13 patients, partial response was in 19 patients, stability was in 34 patients; progress was seen in 22 patients. It was also reported that there was a significant difference in overall survival (OS) and progress-free survival (PGS) values of these two groups. It was stated that there were 12.8 and 10.49 months for the combination group and 11.6 and 9.72 months for the other group, respectively (Lin et al., 2015). H101 has been approved in China for the treatment of head and neck cancer (Old et al., 2016).

There are a number of clinical trials with oncolytic adenoviruses for the treatment of glioma, ovarian cancer, pancreatic cancer, prostate cancer and colorectal cancer (Singh et al., 2012) and also DNX-2401 (Lang et al., 2018), CG0070 (Packiam et al., 2018), and OBP-301 (Khan et al., 2019).

One of these, OBP-301 has been engineered so that the human telomerase reverse transcriptase (hTERT) promoter element drives expression of E1A and E1B genes linked with an internal ribosome entry site (IRES)(Watanabe et al., 2006) in human prostate cancer cells (LNCaP, PC3, DU145). In mouse models they observed remarkable reduction in tumour size up until 20 days and also about a 50% reduction in tumour volume in the contralateral distant tumour on day 20 in LNCaP (Huang et al., 2008).

1.4.2. Vaccinia viruses

Vaccinia viruses belong to the class of human pathogens and are associated with skin reactions like eczema. It has the characteristics of a large genome, dispensable genes, wide host range, cytoplasmic replication, and vector stability that enable it to be a good candidate OV (Goldufsky et al., 2013).

PexaVec (JX-594) is an oncolytic vaccinia virus of the Wyeth vaccinia vaccine strain origin, which has been tested in more than 300 patients and various tumour types (Lawler et al., 2017). This virus expresses human granulocyte-macrophage colony-stimulating factor (GM-CSF) as well as the degraded/mutant thymidine kinase (TK) locus to enhance tumour specificity(Choi et al., 2016; Fountzilas et al., 2017). GMCSF is known to regulate the differentiation of granulocytes and monocytes, to stimulate the proliferation and function of antigen-presenting cells (APCs), and to enhance natural killer (NK) cell function (Grossardt et al., 2013). HSV-1 TK converts deoxythymidine to deoxythymidine 5'-phosphate (dTMP) and phosphorylates deoxycytidine and nucleoside analogues which is needed for viral DNA synthesis. TK deletion/mutation prevents replication of virus in nondividing cells (Peters and Rabkin, 2015). Pexavec phase I-II clinical studies have yielded an acceptable safety profile and overall well tolerated in hepatocellular carcinoma (Breitbach et al., 2015) and colorectal cancer patients (Park et al., 2015).

Furthermore, GL-ONC1 (GLV-1h68) that expresses luciferin is an inactivated vaccinia virus (Buijs et al., 2015) and in a phase 1 study GL-ONC1 was administered into the peritoneal cavity of 9 patients with advance peritoneal cancer. The virus was well tolerated and infected the tumour cells very well with efficient viral replication as well as tumour cell killing (Lauer et al., 2018).

1.4.3. Reoviruses

Reoviruses are viruses that can easily enter human cells (Lawler et al., 2017), have benign characteristics in humans, cause slight symptoms of respiratory and gastrointestinal disorders (Cripe et al., 2009), as well as naturally stimulate the innate and adaptive immune system (Lawler et al., 2017).These viruses are naturally oncolytic in their original form without being genetically modified (Cripe et al., 2009) and available efficacy data in various types of cancers has been demonstrated in preclinical and clinical studies (Goldufsky et al., 2013). In a study, researchers reported that reovirus directly activates human DC, and that infected DC can in turn elicit NK and T cell-mediated innate anti-tumour activity (Errington et al., 2008).

A study was conducted with Reolysin to treat 21 patients with metastatic melanoma. They reported that reovirus treatment was well tolerated and also observed progression-free survival of 45 days and a median overall survival of 168 days (Galanis et al., 2012). Reoviruses are commercially available and Reolysin was FDA approved in 2015 for use in the treatment of malignant glioma (Lawler et al., 2017).

1.4.4. Coxsackie viruses

Human enteroviruses (HEVs) are small, nonenveloped RNA viruses that belong to the *Picornaviridae* family. There are 4 HEV species (HEV-A to -D) based on their molecular and antigenic properties (Fields et al., 2007). HEVs are linked to a number of diseases including mild upper respiratory tract infections to severe illnesses such as meningitis, encephalitis, myocarditis, acute flaccid paralysis, and hand-foot-and-mouth disease(Xiang et al., 2012).

Oncolytic CVA21 is manufactured by Viralytics (Sydney, NSW, Australia) as CAVATAK™ using the wild type of Kuykendall strain. It interacts with tumour cells via the intercellular adhesion molecule-1 (ICAM-1), receptor-based mechanism of attachment and cell internalisation. This receptor is overexpressed in many cancer cell types compared to non-cancer cells and is upregulated in melanoma, breast, colon, endometrial, head and neck, pancreatic, and lung cancers as well as in multiple myeloma and malignant glioma (Lin et al., 2018).

A number of clinical trials demonstrating the safety and efficacy of an oncolytic coxsackie virus called CAVATAK (CVA 21) have been documented in the UK and elsewhere for a number of different cancers (Choi et al., 2016). A phase I/II study in patients with non-muscle invasive bladder (NMIBC) cancer was carried out. Patients received neo-adjuvant CVA21 or low dose mitomycin-C prior to the routine surgical removal of the tumour. The combination of CVA21 with mitomycin-C was shown to increase expression of ICAM-1 on the cell surface thus enhancing the binding of the virus to cancer cells. All patients tolerated intravenous CVA21 treatment with viral replication and signs of viral-induced tumour inflammation in the analysed surgically removed tumours. The observed tumour targeting, and viral replication indicates the potential of local and systemic anti-tumour immunity with CVA21 (Pandha et al., 2016).

1.4.5. Newcastle Disease Viruses

Newcastle disease viruses (NDV) belong to the class of bird viruses (Buijs et al., 2015) but do not have pathogenicity in humans (Buijs et al., 2015; Fountzilas et al., 2017). It has oncolytic ability in its original form(Lawler et al., 2017)and has also been studied in various human tumours cell lines and mouse tumour models (Fountzilas et al., 2017). Pre-clinical studies in mice, rats and humans have administered high doses of NDV, but no serious side effects were detected, and its use was reported as safe (Pecora et al., 2002). On the other hand, there is an environmental issue with NVD and the concern that it may affect bird species (Buijs et al., 2014).

Early phase 1 studies in 79 advanced solid cancers patients demonstrated safety following intravenous administration of PV701**.** This virus exploits the IFN antiviral responses that is common in tumour cells. This results in a growth advantage but also lead to impaired antiviral defences, rendering cancer cells especially sensitive to infection by PV701. Progression-free survival ranged from 4 to 31 months, and it was suggested that PV701 warranted further study as an OV for cancer treatment (Pecora et al., 2002).

1.4.6. Herpes Simplex Virus (HSV)

This PhD thesis will involve working with HSV. This is an enveloped, double chain, neurotropic DNA virus belonging to the Alpha Herpesviridae subfamily of the Herpesviridae family (Sanchala et al., 2017). It has two subtypes: HSV-1 and HSV-2 (Sanchala et al., 2017) and it contains a genome of at least 120 kb that encodes 90 or more genes (Ma et al., 2018b). These genes can be grouped as essential or non-essential genes depending on their ability to replicate in tissue culture.

For instance, the essential genes are required for virus growth so viral mutants without these genes cannot replicate without the help of an engineered cell line. The non-essential genes are needed for host cell interaction with the virus, this includes genes that enable the escape of the virus from the immune system this is important for infection in vivo but these genes are not needed for growth in tissue culture medium (Manservigi et al., 2010). In the field of oncolytic viruses, HSV is attractive as a recombinant vector because:

- HSV is very infectious.
- HSV has a large repertoire of receptors, HS, PILRα, HVEM, and nectin-1 and 2 which can be found on many cell types.
- Ability to improve cancer cell targeting by modification of fusion glycoproteins in enveloped structure.
- Potential to infect multiple types of cells as well as non-dividing cells.
- The 90 known viral genes for nonessential growth in tissue culture can be removed to create genomic space for exogenous transgenes
- Recombinant HSV vectors can be easily produced to high titres without wild type contaminants.

HSV-1 is a neurotropic virus that consists of a number of important adaptations to the nervous system. Interestingly, these can be modified in the design of new gene therapy vectors which could have implications in neurological applications (Frampton et al., 2005).

HSV-1 dsDNA arranged as long and short unique segments (UL and US) flanked by inverted repeated sequences (TRL/IRL and IRS/TRS, respectively). The repeated regions of the viral genome contain two immediate-early (IE) genes [infected cell protein (ICP) 4 and ICP0], a late (L) gene (ICP34.5) and the latency associated transcripts (LAT) that are each present in two copies (Manservigi et al., 2010) (**Figure 1.8.**).

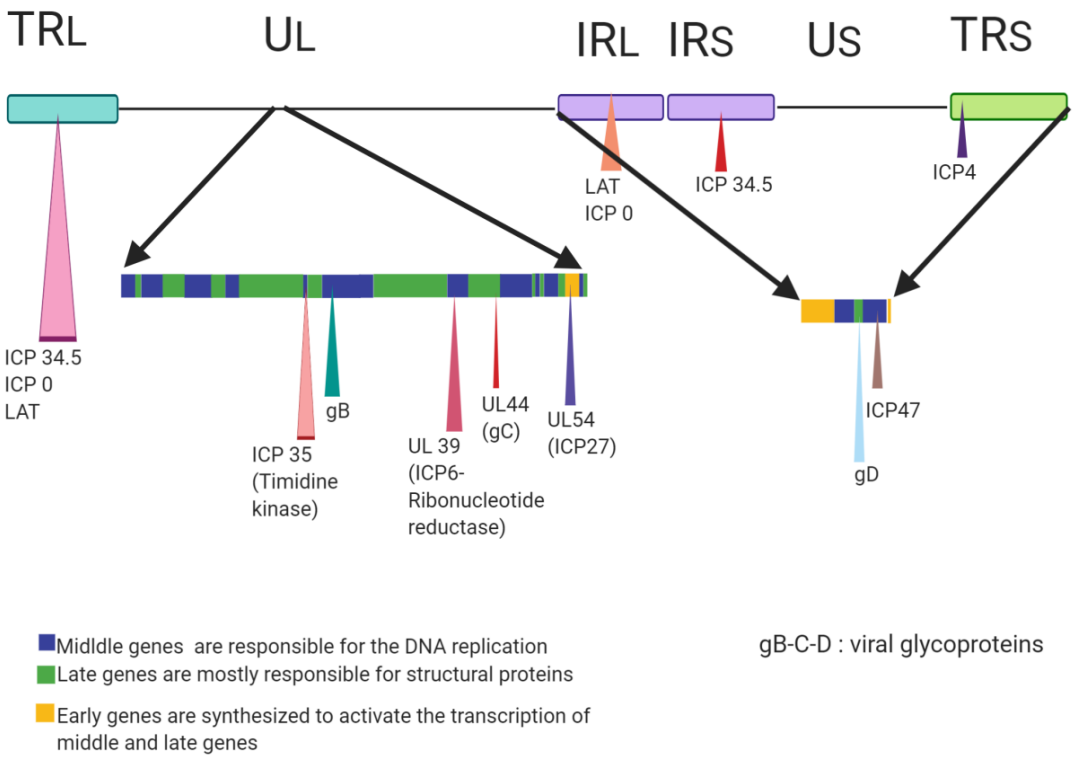

Figure 1.8. Map of HSV-1 genome and some genes encoding protein. (Adapted from https://viralzone.expasy.org/5756)

HSV-1 has been the most studied oncolytic virus and is classified into 3 groups depending on its functions: amplicons, conditionally replicating vector, and vector deprived replicating. The genome of several vectors has been constructed in which the IE genes, expressing ICP 0, 4, 22, 27, and 47, have been deleted in various combinations (Krisky et al., 1998; Samaniego et al., 1997). Subsequently, eliminating the pathogenicity inherent in the wild-type virus, has been a major goal of vector deprived replicating construction (Burton et al., 2002). Non-essential genes have been deleted in conditionally replicating viruses and still have the ability to infect, replicate, lyse tumour cells. The last vectors, amplicons are vectors intended to produce HSV-1-like particles and use bacterial plasmids to locate transgene frames and viral genes encoding production signals (Sanchala et al., 2017).

1.4.6.1. Position of HSV in oncolytic virotherapy

The HSV-1 story began with the observation that HSV-dlspTK virus is capable of destroying human glioblastoma cells both in cell culture and in nude mice (Martuza et al., 1991). Detailed studies have been conducted with many strains of oHSVs such as JS-1, G207, 1716, OncoVEX, NV1020, HF10, G47Δ (Bommareddy et al., 2018). The first OV generated by genetic engineering technology was G207 (Mineta et al., 1995). Although studies of phase I clinical trials resulted in the virus being well tolerated even at high doses (Markert et al., 2009, 2000), it did not reach phase II because of lack clinical efficacy (Zhang, 2015). G47Δ was shown to enhance the anti-tumour efficacy with the additional safety characteristics of G207 (Fukuhara et al., 2005; Todo et al., 2001). G47Δ showed efficacy in some solid tumour models tested in vivo, such as hepatocellular carcinoma (J. Wang et al., 2014), schwannoma (Prabhakar et al., 2007), prostate cancer (Fukuhara et al., 2005), nasopharyngeal carcinoma (Wang et al., 2011).

NV1020 was tested for liver metastasis from colorectal cancer in phase II trials and they reported that NV1020 stabilized liver metastases with minimal toxicity (Geevarghese et al., 2010). As mentioned above T-VEC originated from strain JS-1 and encodes human granulocyte-macrophage colony stimulating factor (GM-CSF) (Kohlhapp and Kaufman, 2016). T-VEC appeared in 2003 and was approved by the FDA in 2015 (Conry et al., 2018). T-VEC is currently being investigated in a number of clinical trials in combination with inhibitors of immune checkpoints: like pembrolizumab and atezolizumab (Clinic et al., 2019). 34 such clinical trials have taken place and 4 of them were completed (“Search of: herpes simplex oncolytic virus - List Results - ClinicalTrials.gov,” n.d.).

1.4.6.2. Genetic engineering of oHSVs

The use of HSV as an OV can be accomplished by single viral gene deletion, multiple gene deletion approach, and also by modifications to the function of these genes (Sokolowski et al., 2015b) some of these oHSV-1 constructs are described below **(Figure 1.9.).** Single gene deletions restrict HSV replication in dividing cells examples of this are: TK (thymidine kinase), UL39, and ICP 34.5 (Manservigi et al., 2010). HSV-1s that have TK deleted restrict replication in non- dividing cells and have a safer profile than the original virus (Peters and Rabkin, 2015). HSV-1 Dlsptk is the first oncolytic form of TK deleted HSV-1 and contains the mutation in the UL 23 gene encoding the TK gene (Ma et al., 2018b). A study with this virus reported that dlsptk selectively killed U87 glioblastoma cells and increased the survival of in nude mice with intracranial U87 gliomas. Consequently, it validated the hypothesis that mutations in viral nucleotide metabolism could endow HSV-1 with tumour selectivity (Martuza et al., 1991). Another deletion is the UL39 gene which encodes ICP6 and is the subunit of the broad viral ribonucleotide reductase (RR) (Peters and Rabkin, 2015; Shen and Nemunaitis, 2006). The RR unit plays a role in viral replication in non-dividing cells (Peters and Rabkin, 2015). ICP-eliminated recombinant HSV-1, hrR3, replication ability in normal cells is quite weak and effectively replicates in dividing cancer cells like tumour cells (Shen and Nemunaitis, 2006; Sokolowski et al., 2015b).

Furthermore, the absence of ICP (infected cell protein) prevents normal cell damage and provides temperature sensitivity, hypersensitivity to DNA replication inhibitors and antiviral nucleoside analogs (Peters and Rabkin, 2015). ICP34.5 is encoded by the γ34.5 gene located in the repeat long (RL) regions of the HSV-1 genome and is present in two copies (Kanai et al., 2016). This is an important neurovirulence gene central to counteracting many of the effector pathways of the IFN host response (Wilcox and Longnecker, 2016). R3616 HSV-1, in which both copies of this gene were deleted are known to be the most neurologically attenuated HSVs so less able to replicate in the brain but still able to replicate efficiently in tumour cells. ICP34.5 deleted HSV-1s are safe and demonstrate antitumor responses in human (Manservigi et al., 2010).

In the G207 strain both copies of the gamma 34.5 gene were deleted and the *E.coli* lacZ gene was inserted into the UL39 gene encoding ICP6 ("Department of Neurosurgery, The University of Tokyo, Tokyo, Japan," 2008). The aim of this design was originally for peripheral nervous system tumours and brain tumours such as meningiomas, malignant gliomas (Lou, 2003). These regulations ensure the G207 strain had reduced neurovascular activity, heat sensitivity, replication competence in tumour cells, possess histochemical marker and infection can be controlled with TK-converted prodrugs (e.g ganciclovir) (Shen and Nemunaitis, 2006).

Another multi-gene deletion product, NV1020 design was generated by plaque purification of a construct designated R7020. R7020 consisted of deletion of two regions of the HSV-1 strain, the internal repeat of the UL56 gene and a region from the UL24 gene (including the gene for TK) (Cadoz *et al.,* 1992). The R7020 strain was still replication competent but not as pathogenic in animals. Because the endogenous TK gene was inactivated by deleting the UL24/TK region from HSV-1, a functional HSV-1 TK gene was inserted into the NV1020 virus genome. This allows the NV1020 infection to be stopped with prodrugs like acylclovir (Sokolowski et al., 2015b).

NV1020 was evaluated for safety, pharmacokinetics and antitumor efficacy in a multicentre phase I/II study in patients with advanced metastatic colorectal cancer (mCRC) to the liver. The phase I patients were first administered with 3×10^6, 1×10^7, 3×10^7, and 1×10^8 plaque-forming units (PFU)/dose to determine the optimal biological dose for phase II. Phase I recruited 13 patients and phase II recruited 19 patients. Mild–moderate febrile reactions were noted after patients received each NV1020 infusion and grade 3/4 virus-related toxicity only occurred in in 2 patients. After NV1020 treatment stable disease was noted in 50% of patients. The authors concluded that NV1020 was able to stabilise liver metastases with minimal toxicity (Geevarghese et al., 2010).

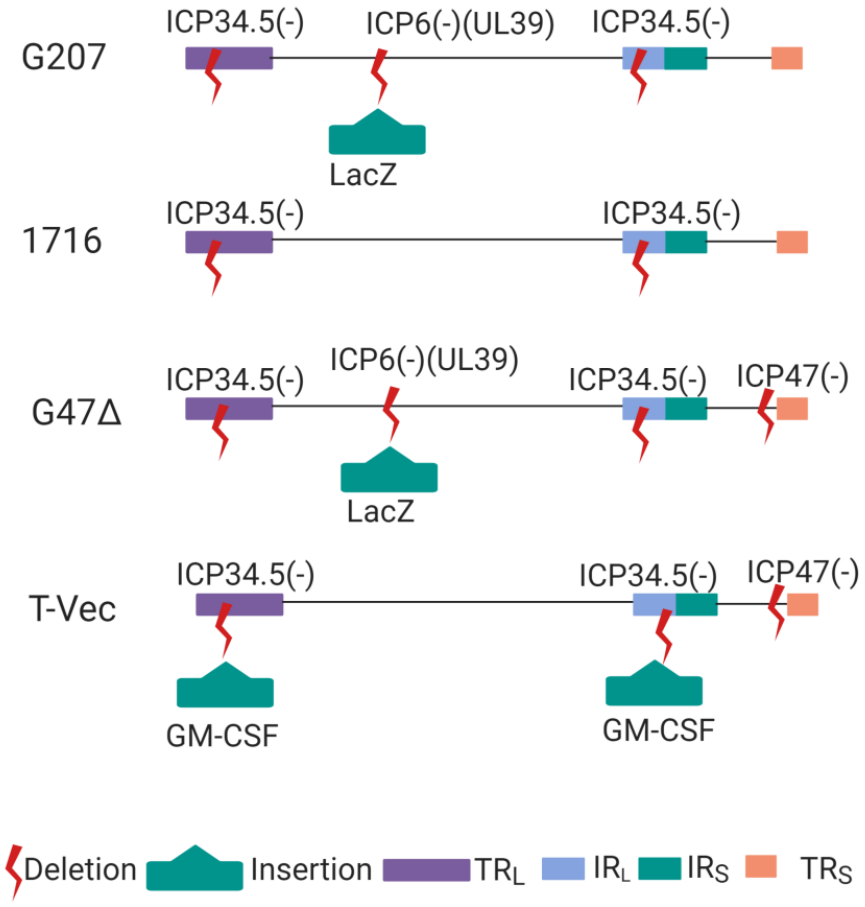

Figure 1.9. oHSV constructs already reported in the literature.

1.4.6.3. Armed oHSVs

As mentioned above the use of OVs in the fight against cancer has accelerated with T-VEC (Kahramanian et al., 2019), however, new oHSVs armed with additional genes are being developed (Peters and Rabkin, 2015; Shen and Nemunaitis, 2006). These armed oHSVs have been engineered to increase tumour cytotoxicity, induce specific immune responses that change the tumour microenvironment and the addition of reporter genes within the virus enabled visual monitoring to determine distribution (Peters and Rabkin, 2015).

1.4.6.3.1. Reporter Genes

Being able to follow the oHSV application *in vivo* is made possible by adding reporter sequences. One of these is achieved by inserting the Escherichia coli LacZ gene into the ICP6 gene, this has been done in G207and G47Δ which is a 3rd generation vector derived from G207. β-galactosidase (β-gal) encoded by this gene breaks down X-gal substrate leading to a colour change that can be tracked. For example, the distribution of G47Δ has been successfully tracked in brain tumours of mice with metastatic BC following intracarotid arterial delivery of the virus using X-gal staining (Liu et al., 2005). It is also possible to assess distribution of the virus with reporter genes using bioluminescence or fluorescent imaging by inserting the luciferase or green fluorescent protein gene. In a study with NV1066 carrying a transgene for enhanced green fluorescent protein (GFP) in 110 types of cancer cells from 16 different primary organs was reported that using it revealed microscopic tumour deposits unrecognized by conventional laparoscopy/thoracoscopy (Adusumilli et al., 2006).

1.4.6.3.2. Cytotoxic Transgenes/Prodrug Conversion

One of the methods to increase the effectiveness of oHSVs may be to equip HSV with transgenes, which will also provide toxicity to non-infected tumour cells. Developing HSV, which expresses prodrug-activating enzyme genes, is a common approach (Peters and Rabkin, 2015). These enzymes convert the inactive prodrug forms into an active form (Kahramanian et al., 2019). HSV-1yCD and M012 are armed HSV-1s that express cytosine deaminase (CD), thus converting 5-fluorocytosine (5-FC) to 5-fluorouracil (5-FU) (Guffey et al., 2007; Nakamura et al., 2001). CD is an enzyme found in bacteria, fungi and viruses, but not in humans. The conversion of 5-FC to the highly toxic chemotherapy 5-fluorouracil (5-FU) causes RNA disruption and blocks DNA synthesis by covalently binding thymidylate synthetase. 5-FU is a potent radiosensitizer and has been used as a single agent or in combination with other drugs for the treatment of a variety of solid cancer including malignant glioma (Wilson and Osenblum, 1983). However, it has major limitations if delivered secondary to the toxic effects it causes. Therefore, using OV to deliver to express CD could overcome these problems. Guffey et al., produced a conditionally replication-competent HSV engineered to express CD so that after administration of the 5-FC prodrug 5-FU can be produced to kill malignant glioma cells. They reported that intratumoural administration of M012 into glioma flank tumours in combination with 5-FC significantly reduced tumour growth (Guffey et al., 2007).

Another example is rRp450 this contains rat cytochrome P450 (CYP2B1) so that cyclophosphamide (CPA) can be converted into the toxic phosphoramide mustard form (Kahramanian et al., 2019). In a study with rat hepatocellular carcinoma (HCC) (McA RH7777), human HCC (Hep-3B, Hep-G2, and SK-Hep), and mouse HCC (Hep 1-6) cell lines, it was reported that the rRp450 virus was oncolytic at MOI 0.1 whereas the human cell line SK-Hep needed a higher MOI 1-10. In addition, when ganciclovir and cyclophosphamide were given together cytotoxic effects were observed in all HCC cell lines, while reduced cytotoxicity was observed in combination with ganciclovir. The reason for the decrease is thought to be the prevention of viral and cellular DNA synthesis by ganciclovir (Pawlik et al., 2000).

In another oHSV-1 design, MGH2, UL39 and ICP34.5 genes have been deleted, and CYP2B1 and secreted human intestinal carboxylesterase (shiCE) have been inserted (Manservigi et al., 2010). Of the inserted genes, shiCE plays a role in activation of the topoisomerase 1 inhibitor Irinotecan, and MGH2 administration exhibited an increase in tumour cell death and chemo sensitisation, as well as viral replication in glioma cells (Tyminski et al., 2005).

1.4.6.3.3. Immune Modulation of HSV

There are also studies to equip oHSVs with various genes for immune modulation, including IL-12, IL-15, IL-18, tumour necrosis factor alpha, fms-like tyrosine kinase 3 ligand (Sokolowski et al., 2015b), IL-4, IL-10, GM-CSF, CD80 (B7.1) (Manservigi et al., 2010). According to the results of a study carried out with the R8306 and R8308 HSV vectors, where IL-4 and IL-10 were inserted and the ICP 34.5 gene was deleted; it was reported that R8306 administration significantly prolongs survival in mice with glioma and that R8308 administration prolongs mouse survival. In addition, these results for IL-4 were associated with striking infiltration of the tumour with macrophages, CD4 + and CD8 + T cells (Andreansky et al., 1998).

IL-12 is known to induce Th1 pro-inflammatory antitumor immune response by directly affecting Natural Killer (NK) cells, NK T cells, and T effector cells (Kahramanian et al., 2019). The designs powered by IL-12 were studied in squamous cell carcinoma, metastatic prostate cancer; in glioblastoma and malignant peripheral nerve sheath tumours; in brain tumours, respectively using NV1042,G47Δ-mIL12,M002 (Peters and Rabkin, 2015). Vectors expressing IL-12 showed significantly more antitumor activity than others, and also through tumour specific cytotoxic T-lymphocytes stimulation and tumour angiogenesis inhibition (Shen and Nemunaitis, 2006).

Another transgene used for immune regulation is human immunostimulant GMCSF. GMCSF has the ability to recruit dendritic cells and macrophages and to initiate their differentiation and functionality. Several HSV-1 studies encoding GMCSF were conducted, and some were also continued in clinical trials (Campadelli-Fiume et al., 2011).

In a study conducted by Liu, both copies of the ICP 34.5 gene and the ICP 47 gene were deleted, and GMCSF inserted, the strain JS1 was used. ICP34.5 deletion provides tumour-specific replication and expression of the US11 gene. This expression also increased tumour replication because it prevents PKR phosphorylation. ICP 47 deletion resulted in increased expression of class I MHC, as its presence inhibited antigen presentation. GMCSF insertion, together with the above effects, increase tumour shrinkage in a mouse lymphoma model and the virus provided protection against tumour cell challenge for at least 6 months (Liu et al., 2003). Moreover, this design, under the name OncoVex, showed good tolerance and significant biological effects in phase I breast, head & neck and melanoma solid tumours (Shen and Nemunaitis, 2006). Phase II showed promising results in unresectable malignant melanoma (Manservigi et al., 2010). Phase III studies were performed in 436 unresectable melanoma patients between 2009 and 2011 and a durable response lasting at least 6 months in 16.3% of patients. Subsequently, in 2015, US marketing approval was obtained for this virus (Russell and Peng, 2017).

1.4.6.4. Tumour microenvironment Modulation by oHSV

The tumour mass formed by the proliferation of cancer cells includes other cell types including cancer-associated fibroblasts (CAFs), vascular endothelial cells (ECs) and various resident or migratory immune cell subsets e.g. NKs, T cells, dendritic cells (DCs). The extra cellular matrix that attaches them together with these cells and establishes the organization network is called the tumour ecosystem or the tumour microenvironment (TME) (Achard et al., 2018). In the invasion and proliferation of tumours, regulatory T cells (Tregs), cancer-associated fibroblasts (CAFs) and dendritic cells (DCs) have been reported to play a role in disease progression. The most leaky cells from immune suppressor cells are tumour-associated macrophages (TAMs), tumour-associated neutrophils (TANs) and myeloid-derived suppressor cells (MDSCs). The data supporting the imperative role of TME in tumour formation, progression, metastasis, recurrence and drug resistance are increasing (Zhang et al., 2019). The majority of tumours exhibits a profile with weak lymphatic system, high collagen density, and wide interstitial pressure.

Poor blood flow causes a decrease in injection dosage, while dense matrix prevents the passage of large molecules. In addition, although the expression of angiogenic molecules is abundant, leakage, expansion; and random binding with a wide variety of abnormal structures are seen in the vascular system. OV that targets the TME have been developed. In study by Zhang et al., an oHSV with the antiangiogenic peptide angiostatin in the ICP locus (G47Δ-mAngio) was tested in human U87 glioma athymic mice. It was observed that the intratumoral VEGF level reduced significantly during the first 3 days of treatment (W. Zhang et al., 2012).

Another HSV vector 'RAMBO' expresses vasculostatin (Vstat120) under the IE4 / 5 promoter, and this molecule is the secreted extracellular fragment of the brain-specific angiogenesis inhibitor 1 (BAI1). In addition, both copies of the γ34.5 genes are deleted, and green fluorescent protein inserted at the UL39 locus. In a study, RAMBO was reported to inhibit endothelial cell migration and tube formation *in vitro* and *in vivo* it was reported to inhibit angiogenesis in glioma cells (Hardcastle et al., 2010). The same team improved the design of RAMBO 34.5ENVE (viral ICP34.5 expressed by Nestin promotor and Vstat120 expressing) using rQnestin34.5. This OV design increased antitumour effects compared to RAMBO; both *in vivo* and *invitro* it was shown to improve glioma-specific killing and anti-angiogenesis effects (Yoo et al., 2012).

Other antiangiogenic HSVs are HSV-endo expressing endostatin; T-TSP-1177 with thrombospondin-1 and matrix metalloproteinase (MMP) -9 inhibitor; G47 sıra-PF4 with platelet factor-4. Chondroitinase ABC (Chase-ABC) is a bacterial enzyme type and increases interstitial diffusion without disrupting the extracellular matrix structure (Peters and Rabkin, 2015). OV-expressing Chase-ABC (OV-Chase), driven by the HSV-1 IE4 / 5 promoter within the backbone of the double attenuated rHsvQ, was developed by Dmitrieva to find a solution to tackling the tumour extracellular matrix. In their study with this design, the migration of glioma cells did not increase, and longer average survival was detected. Consequently, they concluded that degradation of glioma extracellular matrix with OV-Chase enhanced OV spread and antitumor efficacy (Dmitrieva et al., 2011).

In an opposite approach, there is an example of working with the tissue inhibitors of MMPs (TIMP). This protein class inhibits MMP activity and in particular TIMP-3 is capable of inhibiting all known MMPs. They designed rQT3 oHSV expressing TIMP-3 using rHSVQ1 and reported an increase in antitumour activity and a decrease in tumour neovascularisation (Mahller et al., 2008).

1.4. Methods of delivery of OVs in the body

One of the challenges of oncolytic virotherapy is the route of delivery and the challenge associated with this. Many of the viruses used are one's humans have been exposed to throughout life, so the challenge is to prevent these from being sequestered by the mononuclear phagocytic system and thus cleared before they reach the tumour. The amount of virus set to infect tumour cells is determined by the effectiveness of the OV route of administration including inhalation, intrapleural, intraportal, limb perfusion, intracranial, intratumoural, intraperitoneal, and intravenous (IV) (Harrington et al., 2019) and there are positive aspects and limitations to achieve this (Maroun et al., 2017). However, most preferred are local (intratumoural/IT) or regional (such as intraperitoneal or intracranial) approaches (Harrington et al., 2019) and indeed the viruses that have been approved in patients are mainly via delivery directly into the tumour. This avoids the virus being neutralised by pre-existing antibodies or being cleared by the mononuclear phagocytic system.

1.5.1. Intratumoural (IT)

IT injection is a popular OV deliver approach with its ability to cope with some challenges in the process. Provides direct injection of the oncolytic virus into the tumour, eliminating systemic dilution in the blood, anti-target immunity and retention in non-targeted areas (Harrington et al., 2019). However, on the other hand, although IT provides a high concentration of OV exposure, it may not be able to reach metastases in distant regions due to the absence of secondary viremia (Harrington et al., 2019; Maroun et al., 2017).

Secondary viremia, after viral infection, offers spreading to remote areas. For instance, this method is utilised for T-Vec administration and regression of untreated lesions and failure to detect viremia suggests that it may be related to the immune system rather than oncolytic activity. Finally, it is easier to obtain the amount of viral concentration that will initiate the oncolytic process by the IT application, compared to IV (Maroun et al., 2017).

1.5.2. Intravenous (IV)

In the intravenous delivery method, OVs have access to not only the site of administration but also the surrounding metastases (Harrington et al., 2019; Maroun et al., 2017). In addition to this aspect, it has become a clinically preferred method with its ease and reliability (Harrington et al., 2019). Nevertheless, applications have resulted in limited achievements. This is because the virus is exposed to dilution in the blood, eliminated through neutralizing antibodies (nAbs), retained in non-targeted tissues, and unable to extravasate in tumour vessel networks (Harrington et al., 2019; Maroun et al., 2017). IV administration requires a 1000-fold increase in concertation in order to achieve results seen with IT, but applying this concentration amount can induce toxicities, meanwhile difficulties also exist in producing this amount of virus.

1.5.3. Other Delivery Methods

Intraperitoneal virus application is directly injected with the tumour at the site of injection, which is similar to the IT method, with a higher risk of exposure to neutralization (Maroun et al., 2017). Intraperitoneal delivery can render possible the reaching of the virus to larger compartment and provide lower toxicity compared with the intravenous route. Thus, alike intravenous administration, it may present poor distribution and more rapid viral clearance (Harrington et al., 2019). However, a study with hrR3 was compared ip and iv deliveries in immunocompetent mice bearing colon carcinoma peritoneal metastases. They reported that tumour burden was more effectively reduced and median survival was approximately twice following i.p. compared with i.v. administration (Kulu et al., 2009).

Another method belongs to the isolated limb perfusion surgical technique class and is used in the treatment of locally progressive or recurrent sarcomas. It uses high-pressure perfusion, relative hyperthermia and intra-arterial tumour necrosis factor administration to promote extravasation of the OV while allowing for recirculation (Harrington et al., 2019). A study with oncolytic vaccinia virus (GLV-1h68) in an animal model of extremity soft tissue sarcoma, it was reported that virus was unable to prevent metastatic disease in our model. They mentioned that future work will be directed at combining oncolytic virotherapy with other immunomodulatory adjuvant therapies (Wilkinson et al., 2016).

Additionally, a method is intracranial delivery for glioma, astrocytoma and neuroblastoma tumours, which attempts to cross the blood-brain barrier to allow injection of oncolytic virus into the tumour. For lung and liver tumours, however, aerosol delivery with dry powder and sprayed forms of viruses is possible. While it's ability maintaining safety, stability and immunogenicity come to the fore, unpredictable satisfactory concentration, difficulties in formulating, and risk of systemic exposure are disadvantages of this method (Harrington et al., 2019).

1.5. Clinical advancements and challenges of oncolytic virus in the clinic

Rigvir was the first approved OV which does not have genetic modification and first registered in Latvia in 2004 for melanoma treatment (Doniną et al., 2015a). Rigvir is an OV belonging to the *Picornaviridae* family, *Enterovirus* genus, ECHO (Enteric Cytopathogenic Human Orphan) group, type 7(Alberts et al., 2018). In a retrospective study with Rigvir in79 substage IB, IIA, IIB and IIC melanoma patients. They reported that Rigvir administration after surgery; substage IIA–IIC patients had a 4.39-fold lower mortality and substage IIB–IIC patients had a 6.57-fold lower mortality compared with the control group, and no reverse side effects (Doniną et al., 2015b). Oncorine (formerly ONYX-015) was the first approved OV for clinical administration in China, as well as in the world as the first recombinant OV. It was approved for patients with head and neck cancer in combination with chemotherapy in 2005 (Liang, 2018).

However, it is the only approved adenovirus for cancer therapy, and only when given in combination with chemotherapy (Russell and Peng, 2018b) .T-VEC is a recombinant human herpes simplex virus type 1 (HSV1) deleted for both copies of the HSV1 gamma34.5 and viral ICP47, which accelerates the expression of US11, and encodes 2 copies of GM-CSF (Liu et al., 2003). It was approved for the treatment of non-resectable metastatic melanoma by the FDA in 2015 and later in the EU for locally advanced or metastatic cutaneous melanoma (Russell and Peng, 2018b). Systemic administration of OVs is important for accessing hard to reach and metastatic tumours (Seymour and Fisher, 2016). Ensuring that OVs reach the targeted tumour without being affected by immune attack and other physiological barriers is necessary to make the treatment successful. Rapid neutralization can be encountered in the delivery process, with a non-specific binding to anti-viral cytokines, immunoglobulin M, macrophages and complements.

Moreover, poor viral leakage from the tumour vascular network leads to reduced efficacy through immunity, which leads to reduced effectiveness (Ferguson et al., 2012; Marchini et al., 2016). In addition, other difficulties in terms of physical obstacles may be attributed to the passage of the endothelial tissue of injection, dense extracellular matrix, interstitial hypertension that reduces viral leakage, high permeability of tumour vessels, and abnormal forms of lymphatic networks. Because of these obstacles, it is not easy to be sure of the dosage that will provide the effective result reaching the tumour. Finally, solid tumours can secrete chemokines and cytokines such as interleukin (IL)-10, transforming growth factor b (TGF-b), and arginase-1. This causes suppression of the immune cell population and serves to recruit immunosuppressive cells, including T-regulatory cells, myeloid derived suppressor cells, tumour-associated macrophages (TAMs), tumour-associated fibroblasts, and neutrophils.

Inhibitory signals and immune checkpoint receptors, such as PD-1, CTLA-4, TIM-3, and LAG-3, are upregulated in TILs, contributing to an immunosuppressive tumour environment. Moreover, the abnormal organization and structure of the tumour vasculature can disrupt blood supply. Localized hypoxia and low-pH microenvironment might inhibit tumour cell apoptosis, promote angiogenesis, upregulate tumour growth factors, and make tumour cells more resistant to standard therapeutic methods such as radiotherapy, cytotoxic drugs, and immunotherapy.

Therefore, the immunosuppressive tumour microenvironment (TME) can be a critical obstacle and prevents the virus from reaching, infiltrating and maintaining the target (Zheng et al., 2019). Taken together, Oncolytic viruses can reshape the immunosuppressive tumour microenvironment by increasing T cell infiltration and modulate checkpoint inhibitor expression, which may make tumours more sensitive to immune checkpoint inhibitors (ICIs) in cancer. Moreover, the combination of OVs and ICIs can be effective in treating patients presenting immunologically 'cold` TME profile.

1.8. Conclusion

Cancer immunotherapy has produced excellent results in the clinic in recent years. Yet despite the success of checkpoint inhibition strategies targeting CTLA-4 and PD-1 receptors, there a still many cancer patients that have not yet benefited from this novel approach. As described above Tim-3 has been shown to mediate immune tolerance in mouse models of infectious diseases, autoimmune diseases and in cancer. Thus, targeting Tim-3 is now becoming a promising approach for cancer immunotherapy. Tim-3 inhibitors are currently being developed such as MBG453 (NCT02608268), LY3321367 (NCT03099109), TSR-022 (NCT02817633) and these are currently being tested in advanced cancers in phase I or II clinical trials. For example, MBG453 is a high-affinity, humanised, anti-Tim-3 IgG4 antibody being developed for treatment of patients with myelodysplastic syndrome (hr-mds) and acute myeloid leukemia (AML) (Brunner et al., 2020). Since Tim-3 is expressed on immune cells as well as leukemic stem cells and blasts, but not on normal hematopoietic stem cells, this makes it a promising target in MDS/AML. Although still in its early phase this antibody in combination with standard therapies for these diseases including decitabine (Dec) or azacitidine (Aza) was safe and well tolerated with encouraging response rates and emerging durability. So far, these clinical studies have been used in combination with chemotherapies or with anti- PD-1/L1 mAbs and early data have shown that this combination is broadly safe and well tolerated. The aim of this PhD is targeting the immune checkpoint 'Tim-3' in combination with OVs.

1.9. Hypothesis and aims

The overall hypothesis of this project is that the immune checkpoint 'Tim-3' in combination with OVs will induce anti-tumour immunity in BC by releasing the brake on immune checkpoints.

Specific Aims of the project are:

1. To determine Tim-3 expression on immune cells and human and mouse BC cancer cells and patient derived-tissue (Chapter 3).
2. To assess the effects of combining anti-Tim-3 with OV in BC cell lines including cancer hallmarks e.g invasion and metastasis in vitro (Chapter 4).
3. To administer anti-Tim-3 with OV therapy in mouse mammary carcinoma models to evaluate the impacts on survival, tumour growth, tumour necrosis, organ metastasis and anti-tumour immunity (Chapter 5).

Together this will provide an opportunity to reprogramme the TME to be more immunogenic (hot) in BC and if successful pave the way for this treatment combination in this patient group.

CHAPTER 2

MATERIALS AND METHODS

2.1 Materials

Table 2.1. List of Reagents

Reagents	**Supplier**	**Location**
4 mM L-Glutamine (200mm in 0.85% sodium chloride solution)	Lonzo, BioWhittaker Ltd	Wokingham, UK
Agarose	Sigma-Aldrich	Suffolk, UK
Alamar Blue	Thermo Fisher Scientific	Loughborough, UK
Bovine serum albumin (1%)	Sigma-Aldrich	Suffolk, UK
Crystal Violet (0.5%)	Sigma-Aldrich	Suffolk, UK
Dimethyl sulfoxide	Sigma-Aldrich	Suffolk, UK
Dulbecco's Modified Eagle Medium	Gibco	Loughborough, UK
Dulbecco's Modified Eagle Medium F-12	Gibco	Loughborough, UK
Eosin stain	Sigma-Aldrich	Suffolk, UK
Foetal Bovine Serum (10%)	Biosera	East Sussex, UK
Formaldehyde or paraformaldehyde (4%)	Merk Millipore	Hertfordshire, UK
Haematoxylin stain	Sigma-Aldrich	Suffolk, UK
HSV1716	Virttu	Glasgow, UK

HSV1716-GFP	Virttu	Glasgow, UK
Isoflurane	Teva UK Ltd	Castleford, UK
Matrigel Matrix	Sigma-Aldrich	Suffolk, UK
OCT Compound	Agar Scientific	Essex, UK
Penicillin Streptomycin (1%)	Lonzo, BioWhittaker Ltd	Wokingham, UK
Phosphate buffered saline	Lonzo, BioWhittaker Ltd	Wokingham, UK
Propan-2-ol	Merk Millipore	Hertfordshire, UK
Roswell Park Memorial Institute medium	Gibco	Loughborough, UK
Sodium dodecyl sulphate (2%)	Sigma-Aldrich	Suffolk, UK
Sodium dodecyl sulphate solution (2%)	VWR	Atlanta, USA
Trypan Blue (0.4%)	Sigma-Aldrich	Suffolk, UK
Trypsin/EDTA	Lonzo, BioWhittaker Ltd	Wokingham, UK
Xylene	Sigma-Aldrich	Suffolk, UK

2.2 Methods

2.2.1. Cell Culture

2.2.1.1. Preparation of cells

Cell culture medium, Dulbecco's Modified Eagle Medium (DMEM), and DMEM Ham's F-12 or RPMI 1640 containing 2 mM glutamine were both supplemented with 10% Foetal Bovine Serum (FBS) and 1%100 IU/mL Penicillin and 100ug/mL Streptomycin (PS).

2.2.1.2. Culturing of human and mouse BC cells

BC MDA MB-231, MCF-7, 4T-1 and E0771 cell lines were cultured in DMEM complete medium while SKBR-3 cell line was cultured in RPMI complete medium in a humidified atmosphere of 5% CO2 (Heraeus incubator, Loughborough, UK) at 37°C. The cells were exposed to trypsin (0.05%) for passaging once they had reached ~80-90% cell confluency. (**Table 2.2.**)

Table 2.2. List of Cell lines

Cell line	Cell type	Origin
MCF-7	ER+ human breast cancer	The cells were isolated from a 69-year-old woman's pleural effusion who had metastatic illness. ATCC (Middlesex, UK)
MDA-MB-231 cells	Triple negative human breast cancer	Derived from a 51-year-old Caucasian female and obtained directly from a metastatic location by multiple infusion at ATCC (Middlesex, UK).
SK-BR-3 cells	Human metastatic breast cancer (HER2+)	Derived from a 43-year-old White, Caucasian female was obtained directly from the metastatic location by multiple infusion. The patient had previously been treated with radiation, steroids, cytoxan, and 5-fluorouracil from ATCC (Middlesex, UK).
4T1 cells	Triple negative mouse breast cancer	They were obtained from a mouse model with features similar to stage IV human breast cancer. ATCC (Middlesex, UK).
E0771 (parental)	ER+, PR+,HER2-	This cell line, syngeneic in nature, originates from the spontaneous development of breast cancer in C57BL/6 mice.
Vero cells	Healthy monkey kidney cells	Derived from the kidney tissue of an African green monkey, extensively employed in mammalian tissue culture. Kindly presented by Virttu Biologics Ltd (Glasgow, Scotland).

2.2.1.3. Vero cells

Vero is a kidney cell line derived from a healthy adult African Green monkey. These cells exhibit remarkably receptive features in case of infection and replication with viruses such as reovirus and HSV-1. This cell line is commonly used for oncolytic HSV-1 expansion *in vitro*. HSV-1 does not have the essential replication genes, such as RL1, which are provided by the cell line (Carew et al., 2001; Nakamori et al., 2003; Leddon et al., 2015). Vero cells were cultured to 80% confluency with DMEM/F-12 complete medium and passaged when required.

2.2.1.4. Cell counting

Detached cells from culture flasks were transferred to a benchtop centrifuge (SANYO, London, UK) and centrifuged at 179 g for 5 minutes. For re-suspension, pellets were diluted in ratios of 1:10 or 1:100 mixed with trypan blue exclusion dye (0.4%) following by placement into a counting slide. The amount of live cells/mL was calculated with an automated cell counter, T20TM (Bio-Rad, Hertfordshire, UK).

2.2.1.5. Freezing down cells

Counted cells based on protocol 2.2.1.4 were re-suspended in freezing medium containing 90% FBS +10% Dimethyl sulfoxide at a concentration of 2 million cells/ml. Cells were aliquoted at 1ml per cryotubes in a NALGENE cryo 1 freezing container (Thermo Fisher Scientific Inc, Loughborough, UK) filled with propan-2-ol and stored at -80°C until the following day. Cryotubes were retrieved and for long term storage placed in liquid nitrogen.

2.2.1.6. Cell cultivation

Cells were cultured in T75 Tissue culture flasks. Upon reaching 70-80% confluency MCF-7 and MDA-MB-231 cells were plated into 96 well plates at the optimum density (**Table 2.3.**) and incubated for a further 2 days. For plaque assays Vero cells were plated into 12 well plates and incubated for 24 h before carrying out experiments.

Table 2.3. Cell lines and their optimal seeding densities

Cell line	**Seeding density**	**Plate size**
MDA-MB-231	3.2 x 10^3 (per 100 µL)	96 well plate
MCF-7	3.2 x 10^3 (per 100 µL)	96 well plate
SKBR-3	3.2 x 10^3 (per 100 µL)	96 well plate
Vero	2.0 x 10^5 (per 1 mL)	12 well plate

2.2.2. Propagation and purification of HSV1 virus

For virus propagation Vero cells were transferred into larger T175 flasks and grown to 70% confluency before infecting with the HSV1 at a multiplicity of infection (MOI) of 0.01-0.05. Infected cells were incubated for 72-96 hours until most have lifted of the wells. Following that, entire infected supernatant in the T175 flasks or 50 ml cryo PP tubes were moved to -80^{o}C freezer overnight. After thawing, the cells were centrifuged in 50 ml falcon tubes at 1613 g to remove cell debris and then supernatants were next transferred to fresh 50 ml falcon tubes. These supernatants were centrifuged at 18000 g for 2 hours.

Meanwhile, buffer was prepared to resuspend in DPBS containing 10% glycerol. After centrifugation 3-5 ml DPBS containing 10% glycerol buffer was added to each falcon and then transferred to -80 ^{o}C freezer in cryovials (Protocol from Joe Connor, from Virtuu Biologics).

2.2.2.1. Plaque assay

Vero cells (2x10^5 per well) were seeded into 12 well plate in 1ml of cell culture medium and incubated overnight to reach confluency. To determine the viral concentration, HSV-1716, HSV E17 RL1del7, and V17RL1del2 were defrosted on ice and were diluted serially in PBS. Diluted virus (0.1ml) was distributed dropwise to ensure the whole monolayer was covered, then incubated for a period of 2 hours. Next, the viral inoculum was removed, and the agarose overlay was prepared. This is consisted of a sterile solution of 4% agarose in distilled which was autoclaved at 120^{o}C for 20 minutes. Medium following equilibration in a water bath at 65^{o}C was added to make up a 1:10 dilution of agarose:medium. Following which 2 ml of this agarose/medium mixture was added to each well. Mixture was waited for agar solidifying in 15 minutes at room temperature and after that incubation at 37^{o}C for a further 72 hours. For fixation, 37% PFA was diluted to 4% in DPBS to the cells in a volume of 1 ml and incubated for an hour. Fixation was terminated by removing agarose plugs and washing with PBS. For staining, crystal violet solution was added in a volume of 1ml and after 5 minutes, rinsed with cold tap water and dried with a paper towel. The number of plaques were counted per well and viral titre was determined as described by Baer and Kehn-Hall (Baer and Kehn-Hall, 2014).

The formula is:

Number of white circle/ (well dilution factor*added virus volume(ml)) = X pfu/ml

2.2.3. Cell viability assay using Alamar blue

Alamar blue is a commercial assay for assessing cell death and is none toxic to cells, which was used to determine the cytotoxic effects of HSV-1716, HSV E17 RL1 del7, and HSV V17 RL1 del2 on BC cell lines. This assay based on resazurin which is dissolved in water and a highly fluorescent compound. Moreover, resorufin entry to cell causes to reduction of this compound. Thus, through the incubation viable cells will continuously convert resazurin into resorufin, resulting in a greater fluorescent intensity (Rampersad, 2012).

Firstly, in this assay, cells were seeded into 96 well plates and were treated with OV (HSV-1716 or HSV E17 RL1 del7 or HSV V17 RL1 del2) next day. Alamar blue reagent was pipetted into each well in a volume of 10µl (10%) and incubated for 4 hours (1-4 hours is the sufficient time scale to convert the resazurin into resorufin) which were applied at 1^{st},2^{nd},5^{th}, and 7^{th} post infection days The cells were analysed on a fluorescent plate reader at excitation peak 570nm and emission peak 585nm. After removing reagent and washing with PBS, 100µl of complete medium was added. This plate can be used at every post infection day. The aim of this time scale was to assess the acute effects of HSV-1716, HSV E17 RL1 del7, and HSV V17 RL1 del2, and its ability to self-replicate overtime without repeat administration. Viruses were gradually thawed on ice and administered to plates for infection using a serial dilution of multiplicity of infection (MOI 30, 10, 3, 1, 0.3, 0.1 and 0.03). The following calculation was used to determine the correct volume of stock virus (1x10^8 PFU/ml) to add to the cell lines.

1x10^8PFU/ml=1x10^5PFU/µl1x10^5PFU/µlx10=1x10^6PFU/10µl

1x10^6 PFU/10 µl x 5= 5x10^6 PFU /50 µl

Prior to the virus administration, the medium of the cells to be infected with the virus was removed and washed with PBS. Then, 100µl of serum free DMEM was added to ensure cellular senescence and prevent non-viral induced gene or cytokine production. Exposure was for 2 hours to enable sufficient infection time.

At the end of 2 hours, complete DMEM medium was replaced with serum free medium. Cell viability was calculated using GraphPad Prism 9. Each experiment was repeated n=3 times to determine reproducibility. The same plates were also used for the Crystal violet staining (**2.2.1.6.**).

2.2.3.1. Crystal Violet assay to determine cell death

Crystal Violet staining was used to assess cell death. After completion of the alamar blue assay, alamar blue reagent was removed and wells were washed in PBS (100ul). Formaldehyde (4%) was added to the cells in a volume of 100µl for 15 min at room temperature. The formaldehyde was removed, and cells were washed with PBS. Then 50µl of crystal violet (0.5%) was added for 20 minutes at room temperature in the dark. Cells were then washed with tap water and the plates were left to air dry overnight. Finally, the fixed cells were solubilised with 100µl of 2% w/v SDS for a further 20 minutes on an orbital shaker. A Keliado plate reader (optical density 570nm) was used to measure the stain.

2.2.3.2. IC50 evaluation

The oncolytic effect of three oncolytic HSV-1 viruses (HSV-1716, HSV-E17RL1del7, HSV-V17RL1del2) was assessed in 3 BC cell lines. HSV-E17RL1del7, HSV-V17RL1del2 were provided by Dr Joe Conner and are genetic variants of HSV-1716 that have not yet been investigated. IC50 values were determined by Alamar blue assay on 1 st,2nd,5th, and 7th day post infection. The concentration of virus used was MOI 30, 10, 3, 1, 0.3, 0.1, 0.03, this range has been determined by HSV-1716 on MDA-MB-231. In this experiment the IC50 for infected cells was measured generating from MOIs values (**See Appendix 7.3. for raw data**). This determines the concentration of a virus that causes death of half the number of total cells (**Table 2.4**.). Therefore, it could be used to compare their effectiveness and determine concentrations for other experiments.

Table 2.4. Viruses' MOIs values of cell lines based on IC50 results

	HSV-1716	HSV-E17	HSV-V17
MCF-7	MOI-1	MOI-3	MOI-10
MDA-MB-231	MOI-3	MOI-30/10	MOI-30
SKBR-3	MOI-1	MOI-10	MOI-10

2.2.4. Flow cytometry analysis

2.2.4.1. Sample preparation and tagged with antibodies

Cells were washed twice with a cold Flow cytometry buffer (2% FCS in DPBS) and $5x10^5$ cells were dispensed into 1.5 mL eppendorf tubes followed by centrifuge. Once removed supernatant, 1 uL of Zombie UV dye and 5 uL of antibodies (**Table 2.6.**) were added top on the cells. They were kept on ice covering aluminium foil and left it for 1 h. Following 500 uL cold Flow cytometry buffer was added to top on the cells and centrifuged at 90 g for 5 mins to wash, which was repeated twice. Finally, 300 uL of flow cytometry buffer was added and transferred to flow cytometry tubes, and The BD LSR II flow cytometer was used to quantify fluorochrome listed in **Table 2.5.** labelled cells. Samples were examined using the BD FACSCalibur Flow Cytometer. For each sample 10,000 live events (equivalent to 10,000 cells) were collected and just before analysis Zombie UV dead (1 ul) was added to exclude dead cells. This is dye is only taken in by dead cells with compromised membranes. As this is an amine reactive fluorescent dye only dead cells with abundant exposure of amines will bind to the dye. Cells were gated based on size (FSC) and granularity (SSC) to exclude any cellular debris and live cells of interest were selected. For our studies these are monocytes or lymphocytes or tumour cells. Fluorescent quadrant plots were created from this gated population containing only live cells and from this any information on cells positively stained with tagged antibodies was based collected based on changes in forward scatter (FSC-H) and side scatter (SSC-H). The analysis of the gated events was carried out using soft BD FACSDiva™ Software ware.

Table 2.5. List of human antibodies for Flow cytometry experiment

Antibodies	Volume/cell number	Fluorochrome	Laser	Supplier
CD4	2 ul/5x10^5	BV421	Violet Laser (405 nm)	Biolegend
CD8	2 ul/5x10^5	AF700	Red Laser (633 nm)	Biolegend
CD14	2 ul/5x10^5	AF488	Blue Laser (488 nm)	Biolegend
CD80	2 ul/5x10^5	PECY5.5	Blue(488nm) Green(532nm)/Yellow Green (561 nm)	Biolegend
CD86	2 ul/5x10^5	BV421	Violet Laser (405 nm)	Biolegend
CD163	2 ul/5x10^5	AF647	Red Laser (633 nm)	Biolegend
HLA-DR	2 ul/5x10^5	BV421	Violet Laser (405 nm)	Biolegend
Tim-3	8 ul/5x10^5	PE	Blue(488nm) Green(532nm)/Yellow-Green (561 nm)	Biolegend
Zombie UV dead	1 ul/5x10^5	UV	Ultraviolet (355 nm)	Biolegend

2.2.5. PBMC isolation from human blood

Human platelet-depleted waste buffy coats were supplied by the Sheffield Blood Transfusion Service. This was carried out under ethics SMBRER139.

Firstly, whole blood (20 ml) was mixed with 30ml of cold PBS and 30ml of blood/PBS mix was pipetted into a tube containing 20ml of Ficoll-Paque slowly to avoid mixing. After this was centrifuged for 40 minutes at 351 g with no brakes on the machine.

This resulted in 4 layers (Plasma, PBMCs, Ficoll-hypaque and red blood cells); 2 nd "creamy" layer was transferred into a 50 ml falcon tube by filling the tube up to the 50ml mark line with PBS. Once one more centrifuge was done for 10 mins at 351 g, the supernatant was removed and diluted in PBS again to the 50ml mark to resuspend the pellet. Following that cells were counted and seeded at 7 x 10^7 cells/ml in 10ml of IMDM + dGlutamine in a T75 flask and incubated for 2 hours. Then the medium including the non-adherent lymphocytes was removed and replaced with a fresh IMDM complete medium.

2.2.5.1. Culturing of primary MDM

Following the above protocol, attached monocytes were cultured to lead fully mature monocyte derived macrophages (MDM) for a further 7 days in IMDM complete medium replenishing every few days.

2.2.5.2. Differentiation of MDMs into TAMs

Tumour-conditioned supernatant of MDA-MB-231 cell line was collected after 72 h culture and centrifuged at 179 g for 5 mins to remove any cells. At the day 7, IMDM on the MDM was replaced with MDA-MB-231 supernatant to promote tumour conditioning to differentiate MDM into TAMs for 24 h.

2.2.5.3. Harvesting of MDM

MDM were enzymatically detached by adding 3 ml of trypsin/EDTA solution incubating for 15-20 min (37C at 5% CO2). Flasks were tapped and 9 ml of medium was added, after that cells were gently scraped and collected in falcon tubes then centrifuged at 351 g for 10 min.

2.2.5.4. Co-culturing of fresh PBMC and tumour conditioned medium

Fresh PBMC were isolated from human whole blood as mentioned in **2.2.5**. Tumour conditioned medium (TCM) was collected from confluent MDA-MB-231 cell lines and centrifuged at 5 min 179 g to remove death MDA-MB-231 cells. Fresh PBMC and TCM were then mixed as ratio of 10^6 PBMC/ml with 1 mL TCM incubating 24 h at cell culture incubator.

2.2.8. Migration assay (Wound healing assay)

In this assay, SKBR-3, MDA-MB-231, MCF-7 cells were seeded into 48 well plates at 1.2 x 10^6 cells/mL. SKBR-3 cells were cultured in complete RPMI 1640 medium, for MDA-MB-231, 2 x 10^5 cells/mL and 6 x LMCF-7 cells were cultured in complete DMEM medium at 37˚C and 5% CO_2. After they formed a confluent monolayer, the media was replaced with serum-free RPMI or DMEM for starvation and left in the incubator for a further 48 h. The medium was removed and serum-free RPMI/DMEM containing 5 mg/mL Mitomycin C (2 mg/mL for MCF-7) medium was added to each well and the plate was incubated in the incubator for 2 h. After creating a scratch down the middle of each well using a 10 µl pipette tip the cells in the wells were washed twice with phosphate buffered saline (PBS). Cells were then treated, and Skbr-3 cells imaged at 0, 24, 48 and 72 h, MCF-7 was imaged at 0, 6, 18, 24 hours and MDA-MB-231 cells were imaged at 0, 18, 24 h after treatment using the EVOS microscope at 10x magnification.

2.2.9. Invasion assay

2 x 10^6 cells/mL of SKBR-3 cells, 10^6 cells/mL of MDA-MB-231, and 2 x10^6 cells/mL of MCF-7 cells were exposed to serum-free RPMI/DMEM containing 5 mg/mL Mitomycin C (2 mg/mL for MCF-7) and incubated for 2 h at 37°C. Flouroblock Transwells were washed with serum-free medium and 32 mL of 1 mg/ml Matrigel was added to the centre of the transwells followed by 2 h incubation. After, cells were centrifuged, and the supernatant was removed. Cells and treatment solutions were mixed in 1.5 ml eppendorf tubes and then added to the centre of the transwells.

FBS containing medium was added into the bottom of the wells as a recruitment agent. After 24 h incubation (48 hours for SKBR-3), wells were washed with DPBS twice and stained with 100 mL of DPBS 5 mM/mL Calcein-AM followed by 45 min incubation. Wells then were washed twice with DPBS and imaged by EVOS microscope at 4x magnification.

Table 2.6. The dosages of treatments

	HSV-1716	HSV-E17	HSV-V17	anti-Tim-3	IGg antibody
MCF-7	MOI-1	MOI-3	MOI-10	5mg/ml	5mg/ml
MDA-MB-231	MOI-3	MOI-30/10	MOI-30	5mg/ml	5mg/ml
SKBR-3	MOI-1	MOI-10	MOI-10	5mg/ml	5mg/ml

2.2.10. Immunofluorescence (IF) staining analysis

2.2.10.1. IF staining for paraffin wax embedded tumour tissue samples

Immunofluorescence assay was carried out to stain markers of CD-3, -4, -8,-31,-163 and Tim-3 in paraffin wax embedded human breast tumour tissues slides. At the first step, slides were dewaxed for 10 mins in xylene 1, 5 min in xylene 2 and rehydrated through alcohol gradients (100%, 95%, 90% and 70%) for 5,3,3,3 mins respectively then rinsed in tap water for 5 min. Then, antigen retrieval was performed using Dako 1:10 retrieval solution (S1699) in distilled water utilising a hot water bath at 80oC for 20 minutes. After retrieval, slides were cooled for 20 minutes at room temperature and rinsed 5 minutes under tap water. Cooled slides were washed with PBST Buffer 1x 1 min and 2 x 5 min followed by drawing a barrier around tissue with a wax pen to not allow it to dry out. Blocking the samples was performed by adding 2% BSA in PBST, covering black /foil lid through 1 hour at room temperature. Then BSA was tipped off without washing followed by dropping conjugated/unconjugated antibodies **(Table 2.7.)** diluted in BSA blocker on tissue samples for 2 hours or overnight at 4 degrees.

Next step, they were washed with PBST for 1 x 1 min, and then 2 x 5 mins. For unconjugated antibodies, secondary antibody diluted in BSA blocker was dropped on the slide followed by 2 hours incubation. Finally, samples were mounted using Vectashield Mountant containing DAPI and then the edges of the coverslip were sealed using clear nail varnish and stored in a grey tray in a fridge covered with foil to take images in following days.

Table 2.7. List of Immunofluorescence staining experiment antibodies

Primary Ab	Dilution	Conjugate	Secondary Ab	Supplier
CD3	1:100	AF647	NA	BIOLEGEND
CD4	1:100	AF488	NA	BIOLEGEND
CD8	1:100	AF488	NA	BIOLEGEND
CD31	1:100	AF700	NA	BIOLEGEND
CD163	1:100	FITC	NA	BIOLEGEND
Tim-3	1:10	Unconjugated	AF594	BIOLEGEND

2.2.11. *Preclinical model*

2.2.11.1. Mouse model of primary BC

All animal work was carried out under the approved guidelines of UK Animals (Scientific Procedures) Act, 1986 and the University of Sheffield Research Ethics Committee. This work was carried out under Home Office project licence PP1099883 (Prof. Munitta Muthana) and the animal handling and procedures were performed by personal licence holders Dr. Faith Howard, me (I02143396) and another Ph.D. student, Muhamad Hawari Bin Mansor.

A total of 80 mice including 40 BALB/c and C57BL/6 were divided into 8 cages with 5 mice in each cage. Both strains were allowed to acclimate for a week in the biological services unit (BSU) before implantation with BC cells grown in vitro in the tissue culture facility. Mice were anaesthetised via Inhalant isoflurane (IsoFlo) followed by injecting $1x10^5$ 4T-1-Luc/EO771-Luc cells/mice into the nipple of BALB/c and C57BL/6 mice using an insulin syringe in 20ul PBS containing 50 % matrigel/50 % PBS. Tumour progression was monitored every 2 days by manual measurement, alongside daily animal weighing using the following equation:

$$\text{Tumour volume (mm3)} = \frac{W^2 \times L}{2}$$

They received their first treatment when tumour size reached 100 mm3 and the mice were given the following treatments;

1. **Control mice:** Injected IV with PBS in a volume 0.1 ml.

2. **Isotype mice:** Injected intratumorally with isotype antibody (200 ug/mice) in a volume 0.1 ml.

3. **anti-Tim-3 mice:** Injected intratumorally with anti-Tim-3 antibody (200 ug/mice) in a volume 0.1 ml.

4. **HSV-1716 mice:** Injected IV with HSV-1716 (10^5 pfu/mice for Balb/c and 10^6 pfu/mice for C57bl/6) in a volume 0.1 ml.

5. **Combination mice:** Injected IV with HSV-1716 (10^5 pfu/mice for Balb/c and 10^6 pfu/mice for C57BL/6) in a volume 0.1 ml and intratumorally with anti-Tim-3 antibody (200 ug/mice) in a volume 0.1 ml.

Three doses were given in each treatment group on consecutive days regime to Balb/c while C57BL/6 were given once a week. HSV treatment was given via IV while antibodies were received intratumorally. (**Figure 2.1.**).

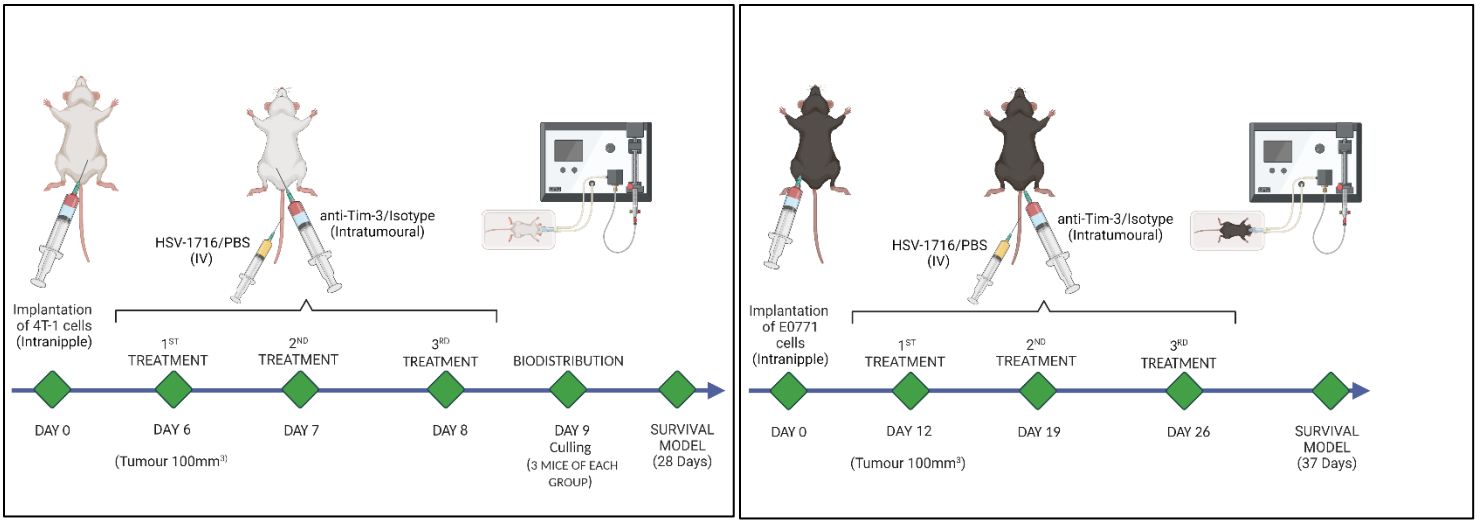

Figure 2.1. Schematic diagram to demonstrate the in vivo study design and treatment regimens for both mice strain.

Treatments were conducted in the same manner for both strains except for treatment days scale. Randomly selected 3 mice of each treatment group were culled for biodistribution study after 24 hours of final treatment by cervical dislocation. Blood and organs (kidneys, spleen, brain, lung and liver) and tumours were extracted for post-mortem analysis studies. Left mice were allowed to reach their overall humane endpoints including ulceration of tumours, neurological deficit (mobility issues, head tilting, extreme sensitivity and seizures), weight loss prior to culling, extraction of blood/organs/tumours same as biodistribution study for survival model.

2.2.11.2. Mice tumour/organs storing for post-mortem analysis

Excised half of all mice organs, half of biodistribution study tumours and half of survival study tumours were placed into a cryobuffer (90 % FCS with 10 % DMSO) and frozen at -80^{o}C for flow cytometry. The remaining half of the survival study tumours were embedded into optimal cutting temperature (OCT) by freezing down at -80^{o}C and then sectioned (10µM thick) for Haematoxylin and Eosin staining using a cryostat. The remaining half of organs and half of biodistribution study tumours were fixed in formaldehyde (4%) for 48 h before processed into paraffin wax. Paraffin wax embedding and sectioning (4 µm) was provided by the University of Sheffield, histology laboratory service (Ms Maggie Glover).

Murine blood samples were allowed to coagulate at room temperature and centrifuged at 12000 g for 5 min, after which serum kept at -80°C for clinical biochemistry or cytometric bead arrays.

2.2.11.3. Dissociation of frozen tumours/organs

Frozen tumour samples washed 3 times with ice-cold DPBS containing 2% FCS (Flow Cytometry buffer). Samples were then incubated in 5 ml enzymatic dissociation solution comprising 0.2 mg/mL collagenase, 2 mg/mL dispase, and 1.25 mg/mL DNase I in serum-free IMDM for 30 min using a rotator at warm temperature. Subsequently, 10 % FBS was added to neutralise the enzymes in the medium followed by passing through a 40-70 mm nylon filter. After centrifuging at 4500 g for 5 min, cells were washed three times in 500 µL Flow Cytometry buffer for flow cytometry as mentioned in section **2.2.4.1** with antibodies listed in **Table 2.8**.

Table 2.8. List of Flow cytometry experiment antibodies

Marker	**Clone**	**Fluorescent tag**	**Species**	**Supplier**
CD8	53-6.7	Super Bright 645	Mouse	Thermo fisher
F4-80	BM8.1	APC-Cy7	Mouse	Cytek Biosciences
CD3	17A2	FITC	Mouse	Cytek Biosciences
CD45	30-F11	BUV395	Mouse	Thermo fisher
CD4	RM4-5	PerCP-Cy5.5	Mouse	Cytek Biosciences
CD161 (NK1.1)	PK136	APC	Mouse	Cytek Biosciences
CD19	1D3	BV480	Mouse	Thermo fisher
CD366 (Tim-3)	RMT3-23	PE	Mouse	Cytek Biosciences
CD274 (PD-L1)	MIH5	BUV737	Mouse	Thermo fisher
Viability		GhostDyeUV450	Mouse	Cytek Biosciences
Glycoprotein B (HSV-1&HSV-2)		Qdot 800	Mouse	Thermo fisher

2.2.11.4. Haematoxylin and Eosin staining

Cryosectioned slides were removed from -20°C and incubated at room temperature for 1 h and then fixed in ice cold 50:50 acetone methanol for 20 min. Following washed x 2 in PBS, slides were placed in Gill's Haematoxylin solution for 30 seconds prior to rinse in tap water till water ran clear. Sections were then rested in 70% and 90% ethanol for 3 minutes each to dehydrate, after which, they were placed in Eosin stain for 15 seconds followed by washing in 100% alcohol. Sections were then removed to the hood for mounting step by placing in xylene twice for 5 min each. Excess xylene was removed by wiping off and one drop of DPX added. Slides were cover-slipped keeping at room temperature then scanned using a Pannoramic slide scanner and analysed using QuPath software.

2.2.11.5. Necrosis assessment

Mouse tumour samples were immediately embedded in OCT following removal from mice and then stored in -80°C until these were cryosectioned. H&E staining was performed on triplicate sections from each tumour sample, and images were captured using Panoramic slide scanner as described in previous section. Necrotic areas, characterized by cytoplasmic swelling, plasma membrane damage and organelle breakdown (Festjens et al., 2006), appeared as light pink patches (no cells, no haematoxylin) in H&E-stained images. The percentage of necrotic area was calculated by comparing the necrotic area to the total tumour area using QuPath software.

2.2.11.6. Metastasis assessment

Mouse organs were embedded in paraffin wax and stored at room temperature. H&E staining was performed on triplicate sections from each organ sample, and images were captured using Panoramic slide scanner as mentioned in **section 2.2.11.4.** Liver and lung sections were used for this analysis because of their relevance to BC metastasis. The metastasis quantification was performed by counting 10 or more tightly packed haematoxylin-stained cells using QuPath software. Training to spot metastasis was provided and corroborated by Prof. Muthana.

2.2.11.7. Statistical analysis

All statistical analysis was performed within GraphPad prism Version 9 (GraphPad Inc,San Diego,CA, USA). Quantification of IHC staining was performed using QuPath version 0.4.0 (GitHub, Inc. California, USA. All data was presented as mean and SD or SEM, with a minimum of n=3, unless stated otherwise within the figure legend. The P values are shown as; *=P ≤ 0.05, **=P ≤ 0.01, ***=P ≤ 0.001 and ****=P ≤0.0001. Cell viability assays used to determine dose response were analysed using a Two-Way Anova, to determine the differences seen between variables. The chapter for *in vivo* study used a One-way Anova to analyse *ex vivo* IHC staining. A Two-Way Anova was used to assess observations of humane endpoints and animal weight fluctuations. Animal weights were assessed using a last observation carried forward. For analysis of the overall survival, Kaplan-Meier survival analysis using a Log-rank (Mantel-Cox) test was performed, comparing each treatment group against the control.

Chapter 3
Tim-3 expression on the surface of cells

3.1. Introduction

The immune system protects against foreign pathogens, which is orchestrated by T cells (Fife and Bluestone, 2008). T cells have two main signalling pathways for complete functionality including binding of the antigenic peptide/major histocompatibility complex (MHC) on the surface of antigen-presenting cells (APCs) with the T cell receptor (TCR); and the antigen-independent co-signalling molecules called immune checkpoints (ICs) (Wang et al., 2022). Binding with the TCR triggers an immune response while immune checkpoints manage that response. In health, ICs are responsible for preventing excessive immune responses to prevent tissue damage and providing self-tolerance to pathogenic infections (Pardoll, 2012b; Waldman et al., 2020). In the case of cancer, the immune system can exhibit a profile of self-tolerance to the cancer cells. ICs are one of the pathways that provide this profile by downregulating the immune system creating immune escape of tumour antigens (**Figure 3.1**.) (Topalian et al., 2016). Thus, blocking of ICs could enable recognition of tumour antigens.

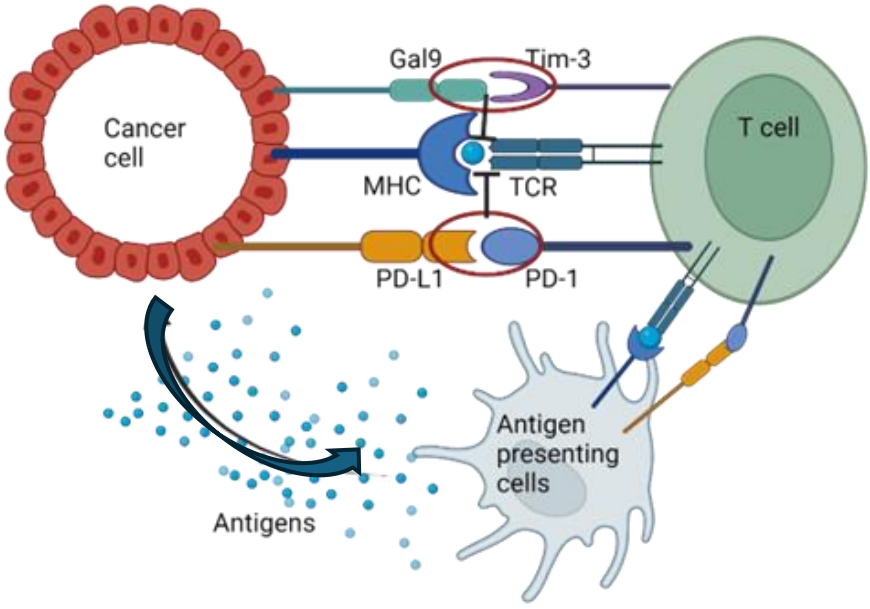

Figure 3.1. Mechanisms of cancer cell mediated immune escape*. Antigen presenting cells absorb antigens released by cancer cells and present them to T cells to promote T cells activation and high expression of PD-1/Tim-3. Upon T cell activation, the PD-1/Tim-3 receptor binds to PD-L1/Gal-9 expressed on the surface of cancer cells and suppresses the immune response (**Adapted from** (Su et al., 2020)).*

Discovery of the programmed death molecule-1 (PD-1) and cytotoxic T-lymphocyte antigen-4 (CTLA-4) was awarded the 2018 Nobel Prize in Physiology or Medicine to Tasuku Honjo and James Allison. This paved the way for additional research demonstrating that PD-1 and CTLA-4 pathways suppress T cell activation and that blocking these molecules via immune checkpoint inhibitors (ICIs) could overcome suppression leading to immune activation to tumours (Topalian et al., 2012; Weber et al., 2008). By now, the number of ICIs and their applications has expanded and includes VISTA, TIGIT and Tim-3 (Wang et al., 2022)**.** Tim-3 is not as widely investigated but is of interest as the mRNA expression levels in breast tumour cell lines are elevated (Sauer et al., 2023).

To obtain a more global view the Human Protein Atlas was used and from this an upregulated profile was observed in 62 different human BC cell lines including MCF-7, MDA-MB-231, and SKBR-3 **(Figure 3.2.)** when analysed by the Oncomine database (Tu et al., 2020). The transcript per million (y-axis) was greatest in HCC-1500 (ER+, HER2-) cells and MDA-MB-415 (ER+, HER2-) cells at 1,1 nTPM and 1 nTPM, respectively. It has also been suggested that Tim-3 over expression on breast tumour cells contributes to disease progression (Zhang *et al.*, 2017; Cheng *et al.*, 2018; Cong *et al.*, 2021). A study involving 150 invasive ductal BC (IDC) patients documented their age, primary tumour size, axillary lymph node metastasis, TNM stage, World Health Organization (WHO) grade, Ki-67 level, molecular classification, and lesion location. Tumour tissue specimens were extracted from all patients, and normal breast tissue or benign lesion samples were also obtained from a distance of 3.0-5.0 cm from the tumour. H&E, Tim-3 and CD8+ cytotoxic T cells (CTL) staining revealed that the total Tim-3 expression in tumour tissue was 98%, compared to 13% in normal breast tissue. Similarly, 90% of the CTLs were Tim-3+ CD8+ in tumour tissue samples, while only 23% were present in normal breast tissue samples. Notably, clinicopathological characteristics, including lymph node metastasis and TNM stage, were significantly correlated with the expression of Tim-3 on tumour cells and the median expression level of Tim-3 on CTL (H. Zhang et al., 2017).

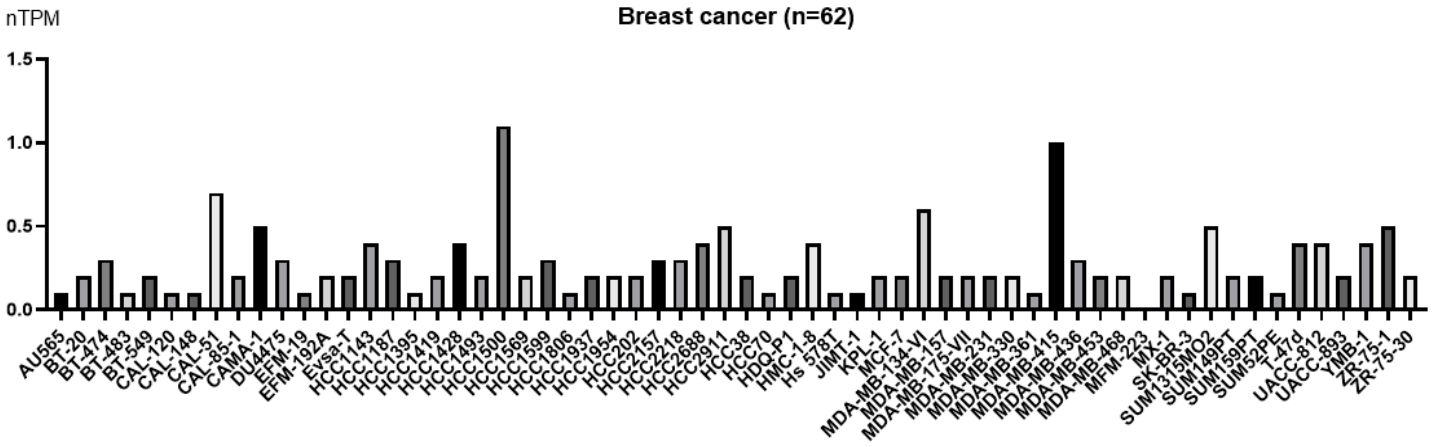

Figure 3.2. RNA expression data as normalized transcript million (nTPM) values of Tim-3 in BC cell lines. *This data was obtained by using the search terms Tim-3 or HAVCR2 and selecting the RNA cell line database section on the the website Human Protein Atlas (https://www.proteinatlas.org/).*

The overall hypothesis of this project is that targeting the immune checkpoint molecule 'Tim-3' in combination with OVs will reprogram the TME to be more immunogenic (hot), leading to the recruitment of T cells and induce anti-tumour immunity in BC by releasing the brake on immune checkpoints. In this chapter, the aim was to demonstrate the expression of Tim-3 on a panel of BC cell lines and patient tissue sections. These cell lines and tissue section are derived from different BC subtypes allowing us to obtain a broader view of Tim-3 expression. Expression of Tim-3 on human peripheral blood mononuclear cells was also examined as these cells play important roles in the tumour microenvironment.

The specific objectives were to determine;

- Abundance of Tim-3 on human BC cell lines using flow cytometry
- Abundance of Tim-3 on human peripheral blood mononuclear cells (PBMC) using flow cytometry.
- Levels of and cellular distribution of Tim-3 on paraffin wax embedded human breast tumour tissue via immunofluorescence staining

3.2. Tim-3 is expressed on human BC cells

Tim-3 expression on the surface of human BC cells lines was assessed by flow cytometry. A panel of BC cell lines including MDA-MB-231, MCF-7, SKBR-3 were stained with anti-human-Tim-3 antibody as described in section **2.2.4.1** and analysed on BD LSR II Flow Cytometer. The viability dye Zombie UV was added to exclude dead cells and tumour cells were identified based on their side scatter-area (SSC-A) and forward scatter-area (FSC-A) profiles. Using these scatter plots, viable tumour cells were gated to identify the Tim-3 positive cells **(Figure 3.3A)**.

The data showed that cell surface expressions of Tim-3 was 10.6% on MCF-7, 14.4% on MDA-MB-231, and 11.5% on SKBR-3 cells **(Figure 3.3-3.5)**. However, it was not possible to create a graph showing the median percentage positive expression of Tim-3 due to reproducibility issues with the antibodies. These experiments were repeated 8-10 times, but the staining was unpredictable. Furthermore, the results showed that Tim-3+ cells were smaller in size but still viable compared to the remaining tumour cell population. This may be because the cells are undergoing apoptosis (Bortner and Cidlowski, 2003). As a result, an alternative anti-Tim-3 antibody was purchased and investigated along with cell death in chapter 4. This data goes against previous publications showing that this antibody works in flow cytometric applications. However, this antibody has been used successfully to stain immune cells such as T cells (Monney et al., 2002b; Sabatos et al., 2003b). It could be that these tumour cells do not highly express Tim-3 of the cell surface and western blots would have useful to look at intracellular expression. For instance, a study using western blot reported successfully the Tim-3 expression in MCF-7 and MDA-MB-231 cell lines (Cheng et al., 2018).

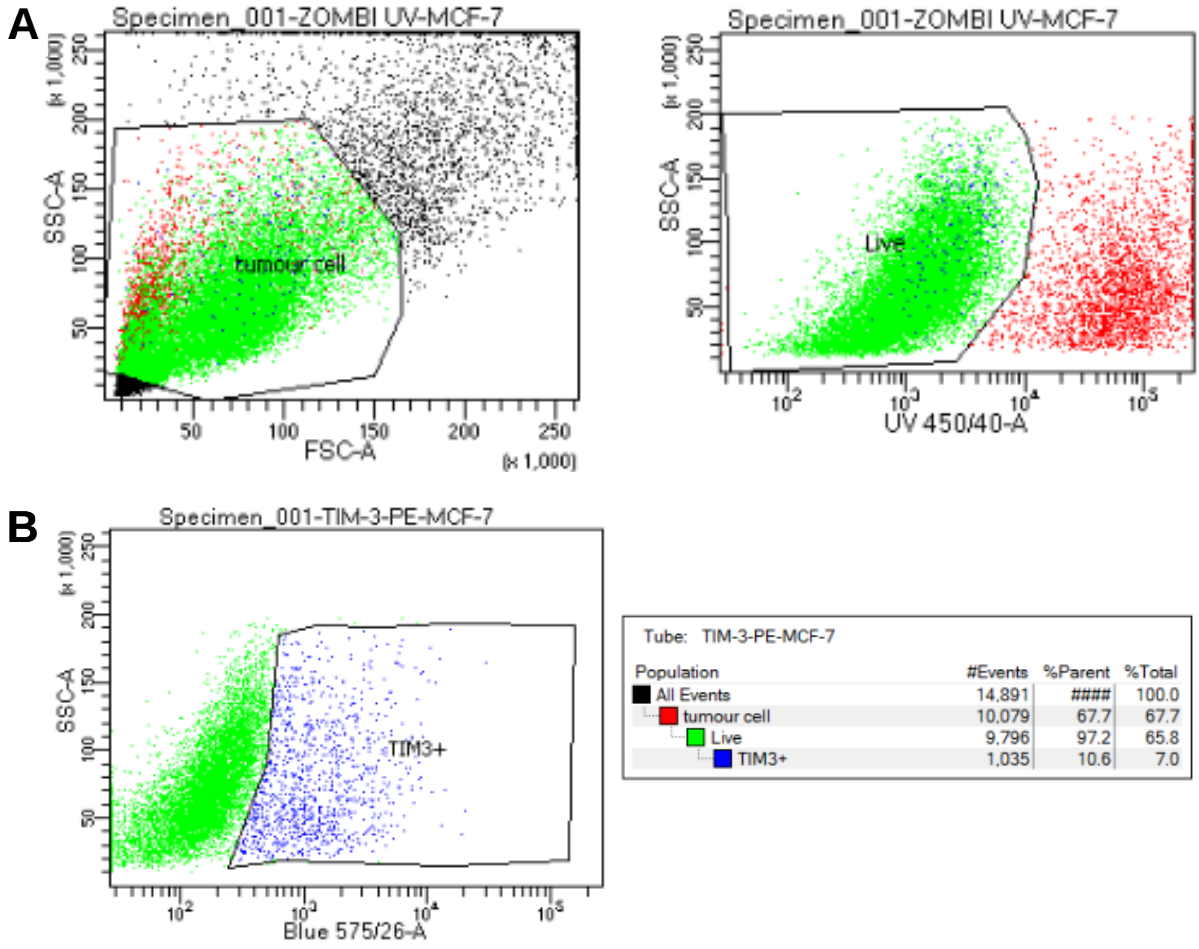

Figure 3.3. Representative Tim-3 expression on MCF-7 human BC cells using Flow cytometry. A. *Upper left-hand dot plot was used to draw a gate around tumour cell population excluding cellular debris based on tumour cell side scatter-area (SSC-A) and forward scatter-area (FSC-A) profiles. Upper right-hand dot plot shows cells selected based on zombie UV uptake and used to draw a gate around alive tumour cell.* ***B.*** *Tim-3+cells were shown from gated alive cells. Data indicates the percentage of cells stained with 7 ul of anti-Tim-3 in half a million cells of n=1 experiment.*

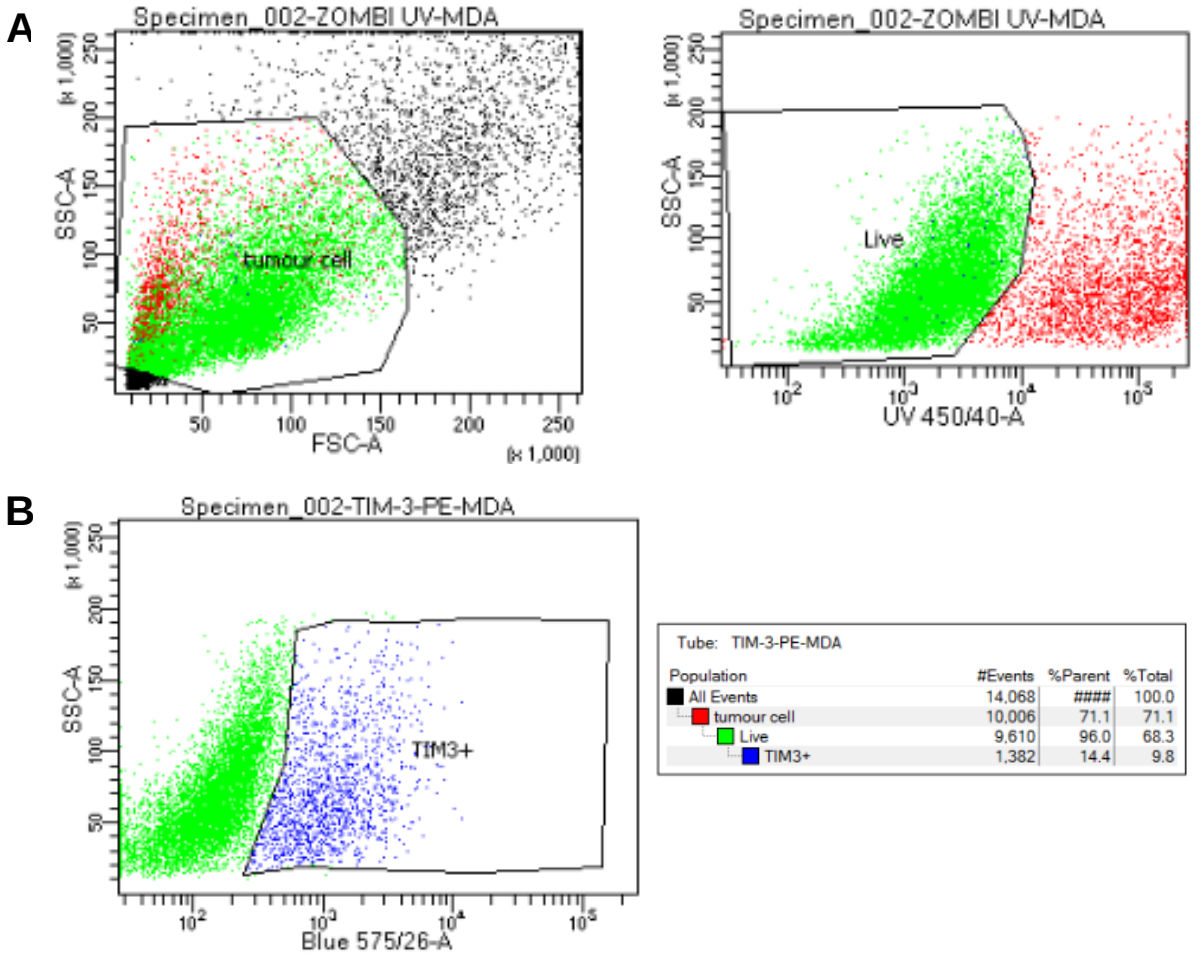

Figure 3.4. Representative Tim-3 expression on MDA-MB-231 human BC cells using Flow cytometry. ***A.*** *Upper left-hand dot plot was used to draw a gate around tumour cell population excluding cellular debris based on tumour cell side scatter-area (SSC-A) and forward scatter-area (FSC-A) profiles. Upper right-hand dot plot shows cells selected based on zombie UV uptake and used to draw a gate around alive tumour cell.* ***B.*** *Tim-3+cells were shown from gated alive cells. Data indicates the percentage of cells stained with 7 ul of anti-Tim-3 in half a million cells of n=1 experiment.*

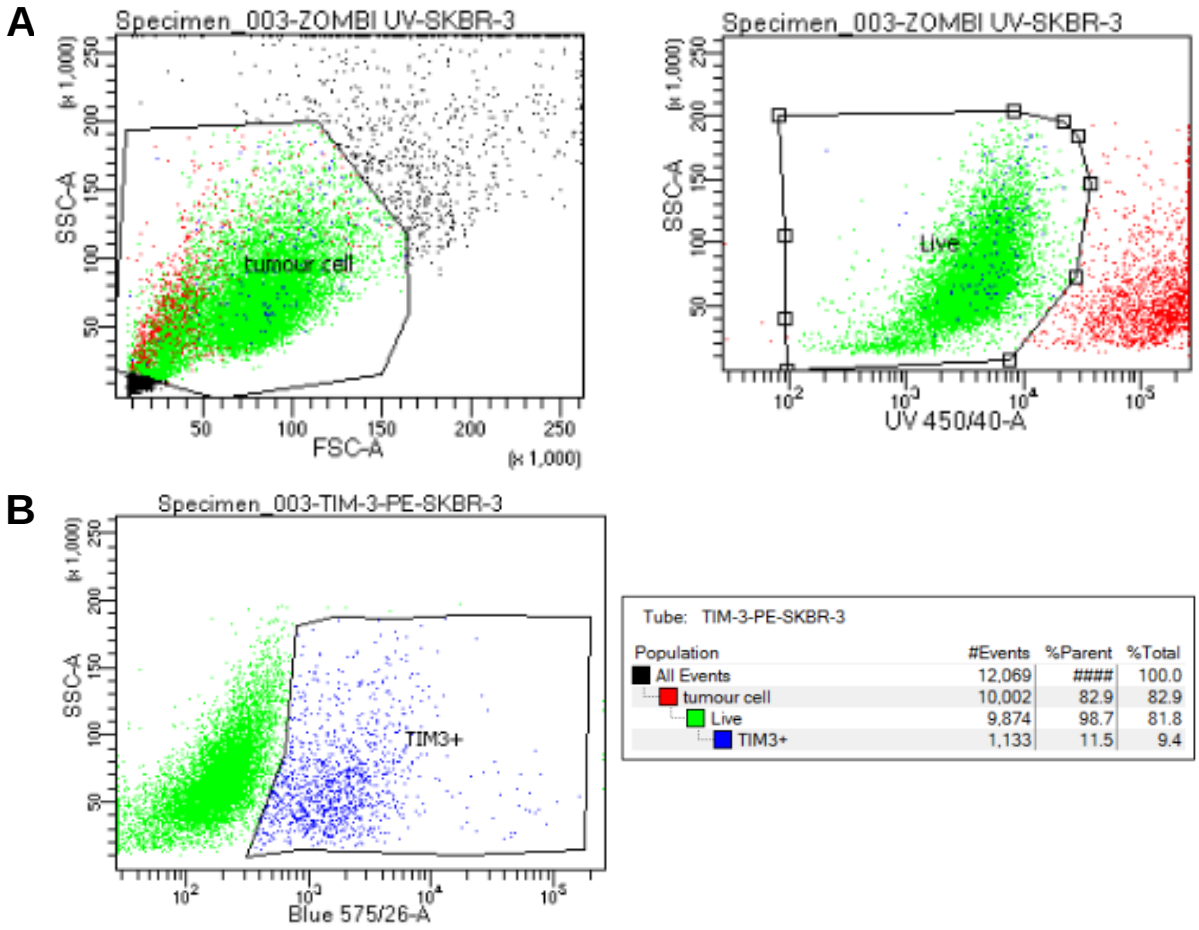

Figure 3.5. Representative Tim-3 expression on SKBR-3 human BC cells using Flow cytometry. ***A.*** *Upper left-hand dot plot was used to draw a gate around tumour cell population excluding cellular debris based on tumour cell side scatter-area (SSC-A) and forward scatter-area (FSC-A) profiles. Upper right-hand dot plot shows cells selected based on zombie UV uptake and used to draw a gate around alive tumour cell.* ***B.*** *Tim-3+cells were shown from gated alive cells. Data indicates the percentage of cells stained with 7 ul of anti-Tim-3 in half a million cells of n=1 experiment.*

3.3 Tim-3 is expressed on human PBMC and increased after co-culture with tumour cells conditioned medium

Buffy coats were obtained from NHSBT and PBMC isolated by Ficoll-Paque density gradient centrifugation as mentioned in **2.2.5**. A portion of the PBMCs was used for Flow cytometry analysis and the remaining cells were seeded into flasks and allowed to mature into macrophages over a period of 7 days (see section **2.2.5.1.**) Tim-3 expression was then examined on 1.

Healthy macrophages or macrophages exposed to BC cell line tumour conditioned medium (TCM) or fresh PMBC before/after co-culture with TCM (see section **2.2.5.2 & 4.**) were stained with various antibodies to identify cell types, including CD-4, CD-8 as markers of T cells (Reinherz et al., 1979); CD-14 as a monocyte/macrophage marker (Wu et al., 2019); CD80/86 as activated macrophage M1-like macrophage markers (Yunna et al., 2020); CD163 as a marker of M2 (Mantovani et al., 2017); HLA-DR as a marker of immune activation on most immune cells (Epstein et al., 2013) and analysed by Flow cytometry.

15% of all healthy macrophages expressed Tim-3 and when co-stained Tim-3 with macrophages markers (CD14, CD80, CD86, CD163 and HLA-DR) expression was between 4-11% (**Figure 3.7.1-3.7.2**). Interestingly, when macrophages were exposed to TCM, overall Tim-3 expression increased to >70% and 100% of CD14+ macrophages (**Figure 3.8.1-3.8.2**). Similarly, almost all of the CD80 and CD86 M1-like macrophages co-expressed Tim-3, whereas this was ~80% of all the M2 macrophages (CD163+) and 70% of HLA-DR+ macrophages.

Co-culture studies of PBMC with BC cancer cell lines was used to investigate Tim-3 expression profiles on fresh human PBMC before/after exposure to tumour cells (Moradpoor et al., 2020) were performed. In this study, they co-cultured the metastatic BC patients' PBMCs (patients=21, healthy=3) with cancer cell lines (MDA-MB-231 and MCF-7) in a chamber for five days. The PBMCs were placed in the lower compartment, while the cancer cells occupied the upper one, at a ratio of 1:7. Co-culture with patient PBMCs significantly impacted the expression of epithelial-to-mesenchymal transition (EMT) markers in both cell lines. MCF-7 cells exhibited upregulation of E-cadherin, N-cadherin, and vimentin, while MDA-MB-231 cells showed increased expression of N-cadherin and vimentin. This difference is likely due to pre-existing suppression of E-cadherin expression in MDA-MB-231 cells via promoter methylation. Furthermore, co-culture enhanced the invasion potential of both cell lines by approximately 4-fold. Interestingly, co-cultured cancer cells also displayed increased NF-κB transcriptional activity, with MCF-7 and MDA-MB-231 cells showing 1.4- and 2.2-fold increases, respectively. Gene Ontology pathway analysis of protein expression changes in co-cultured PBMCs compared to control PBMCs revealed three key subtypes: biological processes (BPs), molecular functions (MFs), and cellular components (CCs). Among BPs, pathways associated with cancer progression, including negative regulation of programmed cell death, positive regulation of cell morphogenesis, NF-κB signalling, and glucose metabolism, were significantly enriched. These findings suggest a complex crosstalk between PBMCs and cancer cells, where PBMCs potentially contribute to tumour progression through various mechanisms, including EMT induction, enhanced invasion, and NF-κB activation (Moradpoor et al., 2020).

Results showed that cell death occurred causing lots of cell debris (**Figure 3.6.)** and thus Flow cytometry data was not amenable for analysis. Therefore, it may have been better to use a chamber to separate the cells for future work. These studies were repeated using tumour-conditioned medium that should contain tumour-derived the factors.

Next, Tim-3 expression profiles on fresh human PBMC before or after exposure to TCM was investigated (**Figure 3.9. and Figure 3.10.**). It was found that overall expression of Tim-3 was 38.6% in healthy PBMC, and this decreased to 23% PBMC cultured with tumour-conditioned medium. However, CD4+T cells and CD14+ monocytes exposed to TCM upregulated expression from 20%, 10% to 49% & 23% respectively, while CD8+T cells exhibited a decrease in expression from 26% to 15%. Most abundance was observed on CD14+Tim-3+ monocytes from 20% to 69% in response to TCM, although CD4, CD8 also upregulated expression of Tim-3 in TCM. Overall, the results of the experiments revealed that Tim-3 expression was upregulated on macrophages and PBMC in the presence of TCM (**Figure 3.11.-3.12**).

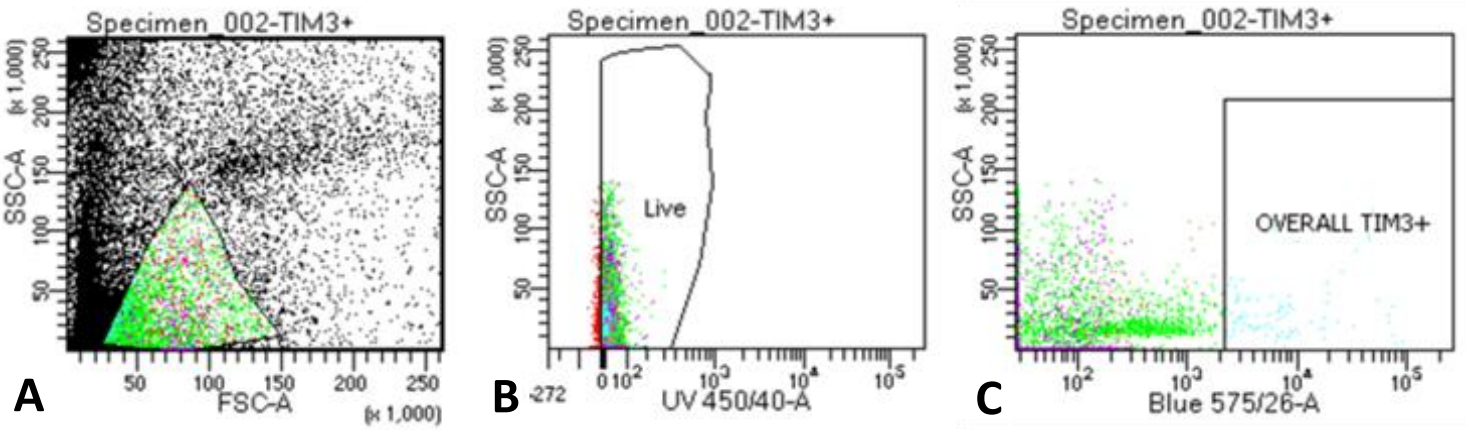

Figure 3.6. An example showing excessive cell debris after exposure of PBMC to tumour cells*. Side scatter-area (SSC-A) and forward scatter-area (FSC-A) profiles were used to create a gate* ***(A).*** *Following that viable cells* ***(B)*** *and positive cells* ***(C)*** *were selected based on that gate and exclusion of dead cells based on staining with the zombie UV viability dye.*

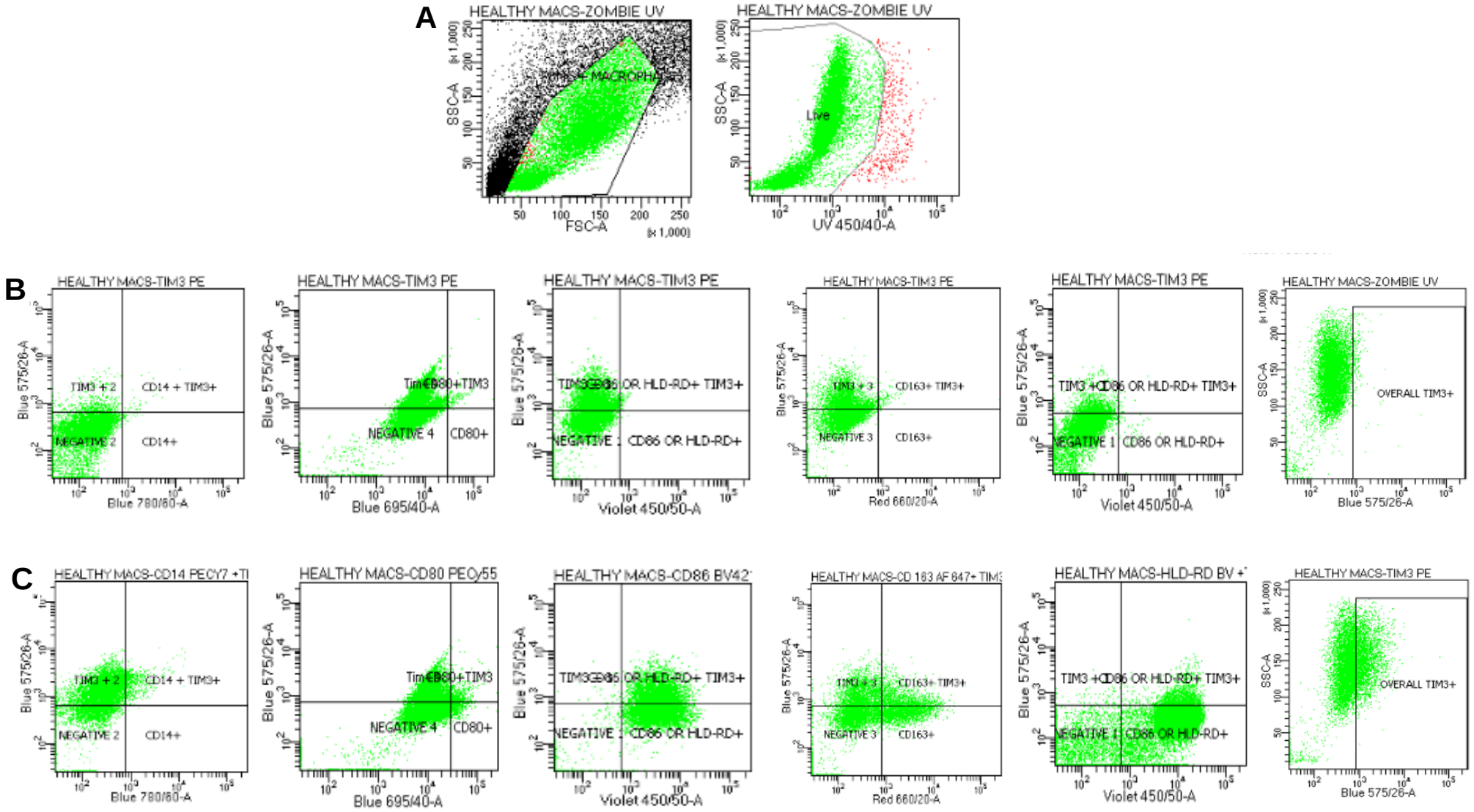

***Figure 3.7.1. Tim-3 expression on healthy human monocyte-derived macrophages*. A.** *Side scatter-area (SSC-A) and forward scatter-area (FSC-A) profiles were used to create a gate. Following that viable cells and positive cells were selected based on that gate and exclusion of dead cells based on staining with the zombie UV viability dye.* **B.** *Representative flow cytometry quadrant dot plots include 4 regions and top-left shows the only Tim-3 staining to position the correct gate.* **C.** *Gated dot plots show CD14+ Tim-3+, CD80+ Tim-3+, CD86+ Tim-3+, CD163+ Tim-3+, and HLA-DR+Tim-3+ stained cell population in top-right quadrants based on changes in fluorescence. The data is generated with n=3 independent blood donors.*

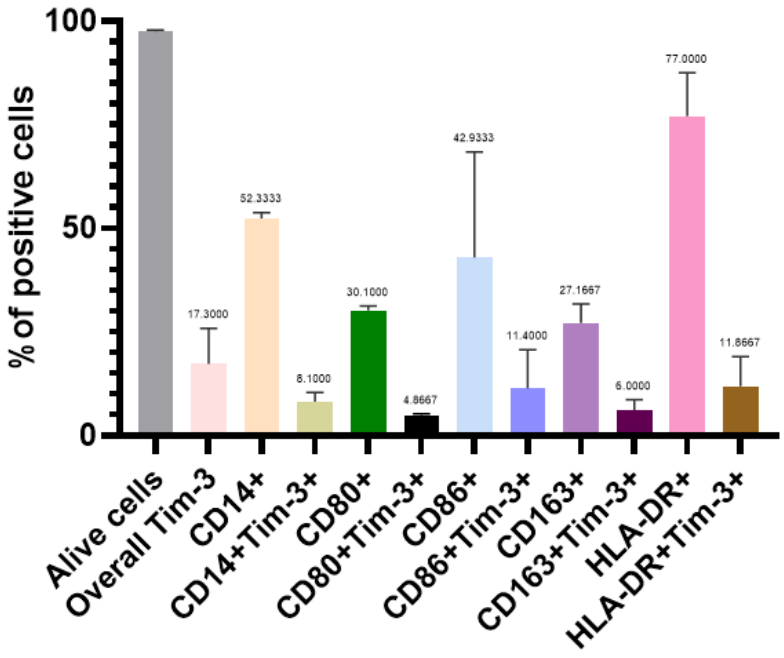

Figure 3.7.2. Tim-3 expression on healthy human monocyte-derived macrophages. *XY graph shows the percentage expression on healthy human monocyte-derived macrophages where the data is the mean and SEM for n=3 independent blood donors.*

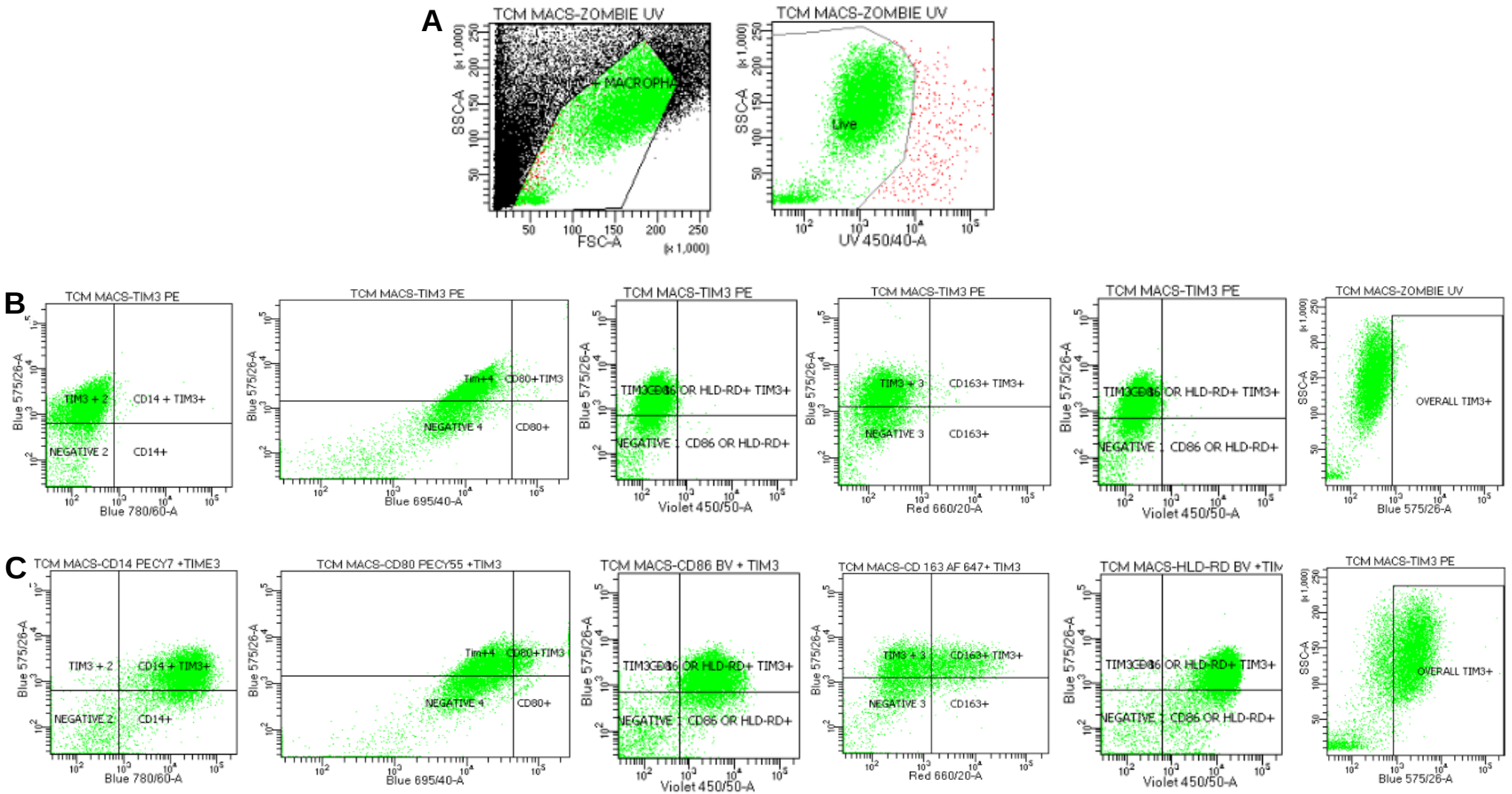

Figure 3.8.1. Tim-3 expression on healthy human monocyte-derived macrophages increased after exposure to TCM. A. *Side scatter-area (SSC-A) and forward scatter-area (FSC-A) profiles were used to create a gate. Following that viable cells and positive cells were selected based on that gate and exclusion of dead cells based on staining with the zombie UV viability dye.* ***B.*** *Representative flow cytometry quadrant dot plots include 4 regions and top-left shows the only Tim-3 staining to position the correct gate.* ***C.*** *Gated dot plots show CD14+ Tim-3+, CD80+ Tim-3+, CD86+ Tim-3+, CD163+ Tim-3+, and HLA-DR+Tim-3+ stained cell population in top-right quadrants based on changes in fluorescence. The data is generated with n=3 independent blood donors.*

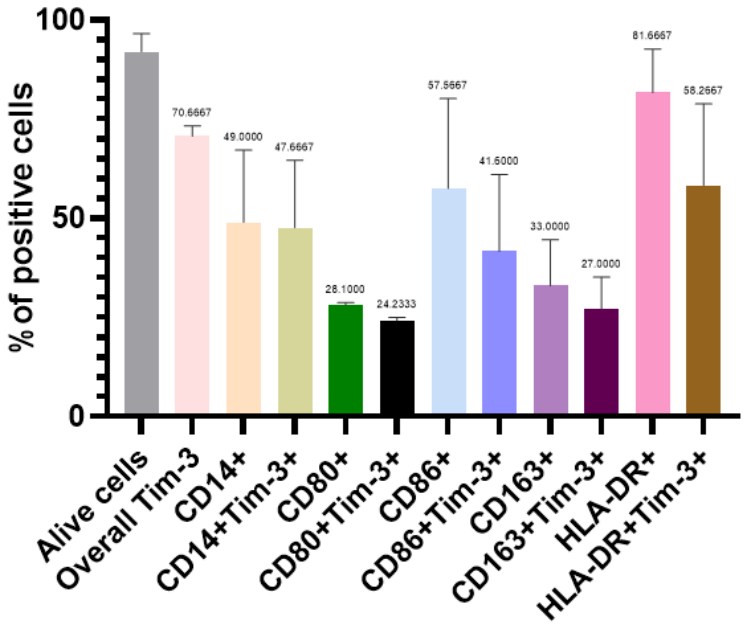

Figure 3.8.2. Tim-3 expression on healthy human monocyte-derived macrophages increased after exposure to TCM. *XY graph shows the percentage expression on human monocyte-derived macrophages exposed to TCM where the data is the mean and SEM for n=3 independent blood donors.*

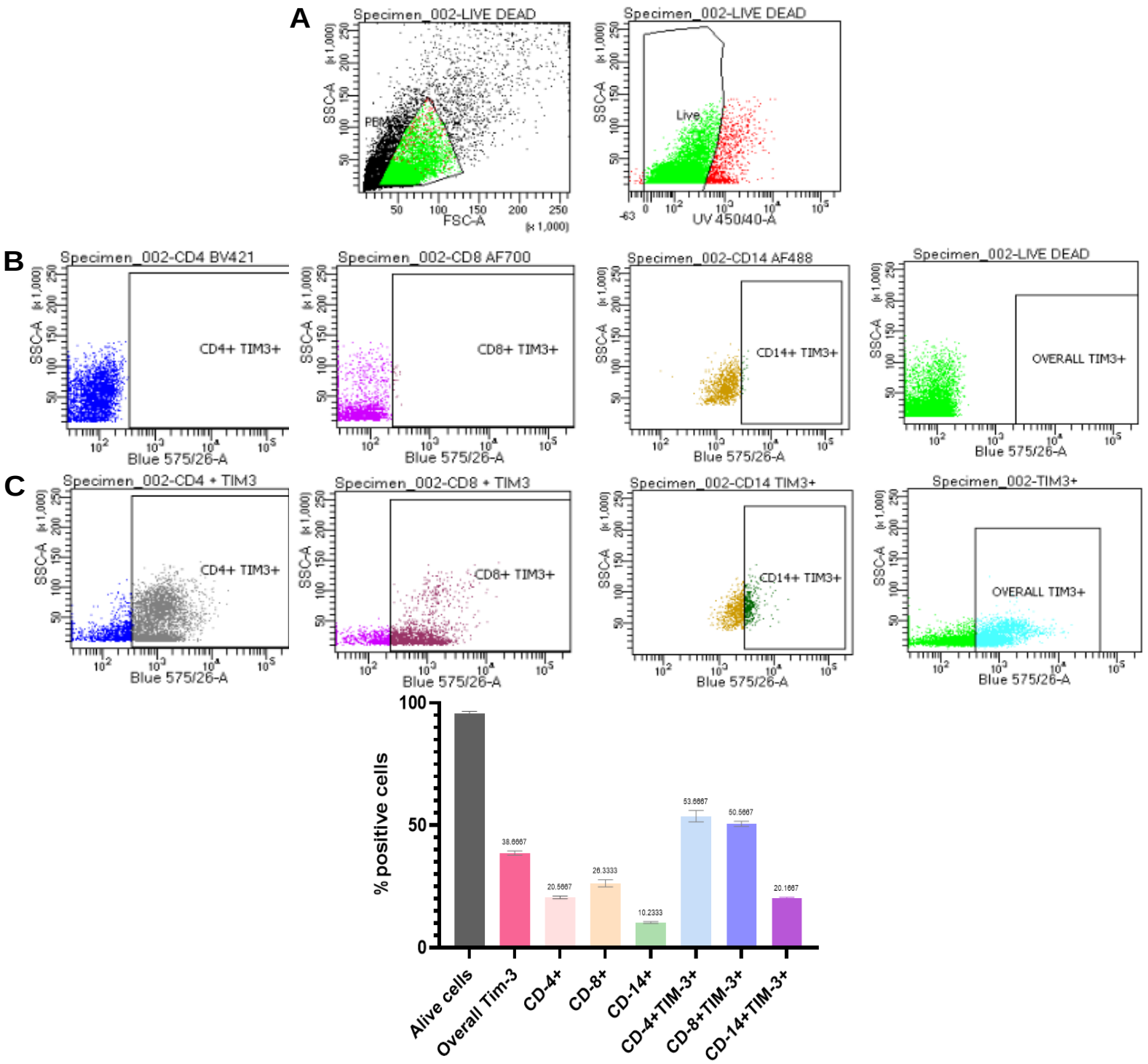

Figure 3.9. Tim-3 expression on monocytes and T cells isolated from human PBMC. A. *Side scatter-area (SSC-A) and forward scatter-area (FSC-A) profiles were used to create a gate. Following that viable cells and positive cells were selected based on that gate and exclusion of dead cells based on staining with the zombie UV viability dye.* ***B.*** *Representative flow cytometry quadrant dot plots include 2 regions and left shows the only Tim-3 staining to position the correct gate.* ***C.*** *Gated dot plots show the overall Tim-3, CD4+ Tim-3+, CD8+ Tim-3+, CD14+Tim-3+ stained cell population in right quadrants based on changes in fluorescence. XY graph shows the percentage expression and data are the means and SEM for n=3 independent experiments.*

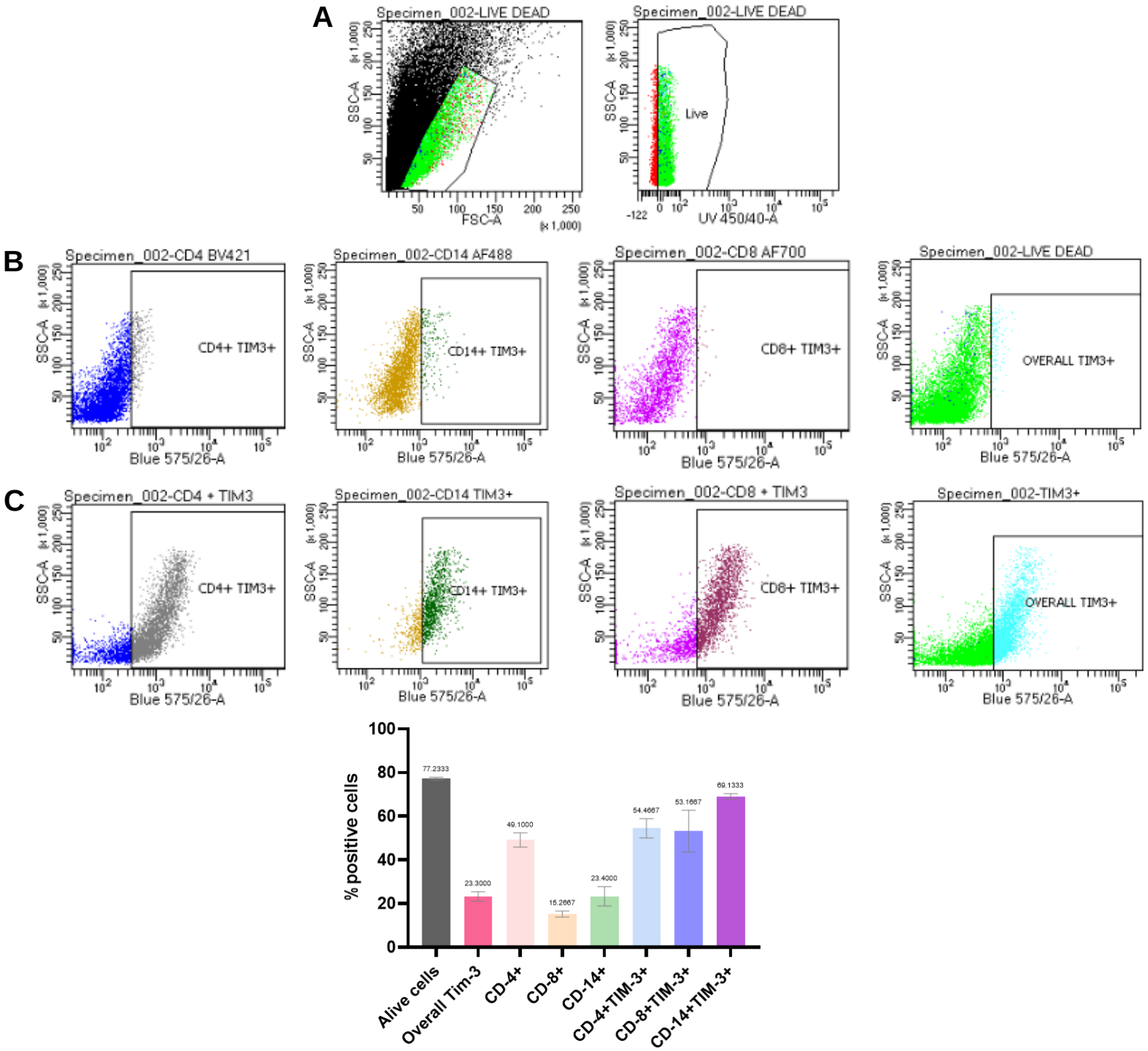

Figure 3.10. Tim-3, monocytes, and T cells markers detection on human PBMC co-cultured TCM using Flow cytometry A. *Side scatter-area (SSC-A) and forward scatter-area (FSC-A) profiles were used to create a gate. Following that viable cells and positive cells were selected based on that gate and exclusion of dead cells based on staining with the zombie UV viability dye.* ***B.*** *Representative flow cytometry quadrant dot plots include 2 regions and left shows the only Tim-3 staining to position the correct gate.* ***C.*** *Gated dot plots show the overall Tim-3, CD4+ Tim-3+, CD8+ Tim-3+, CD14+Tim-3+ stained cell population in right quadrants based on changes in fluorescence. XY graph shows the percentage expression and data are the means and SEM for n=3 independent experiments.*

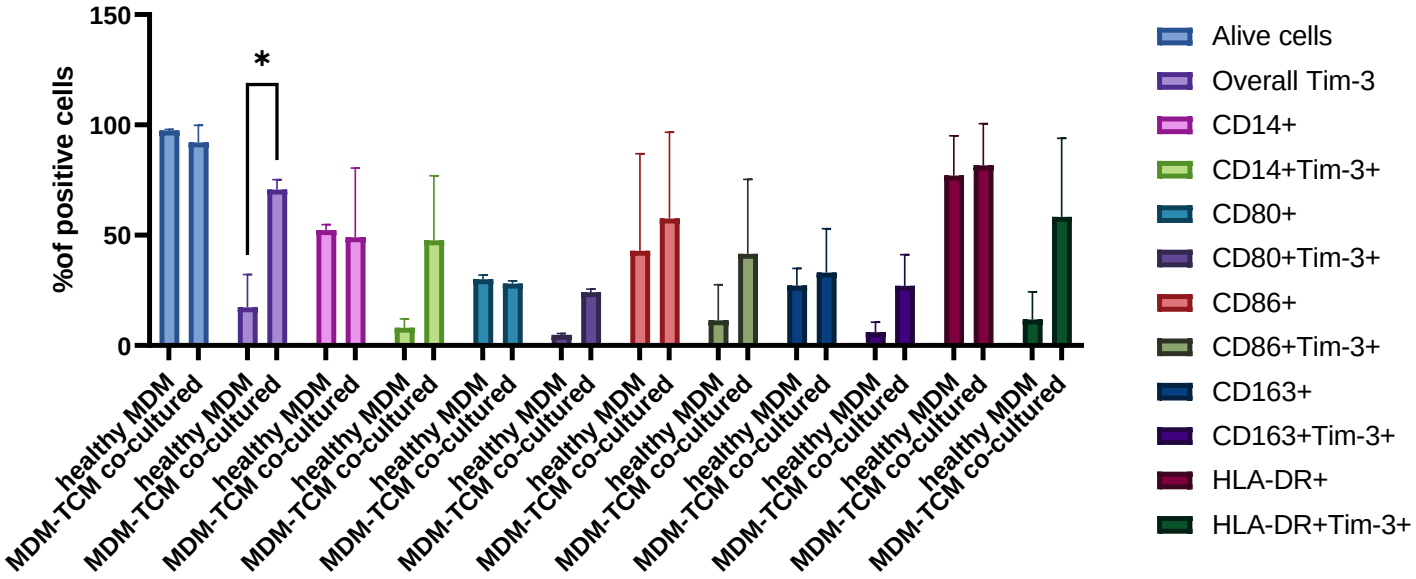

Figure 3.11. Tim-3 abundance comparison of human monocyte-derived macrophages (MDM) and after exposure to TCM. *XY graph shows the percentage expression of overall Tim-3, CD14+ Tim-3+, CD80+ Tim-3+, CD86+Tim-3+, CD163+Tim-3+, and HLA-DR+Tim-3+. The graphs generated using GraphPad Prism software and the Mean ± SD for n=3 independent experiments, where * = 0.0266 after the application of a 2Way ANOVA with multiple comparison to control.*

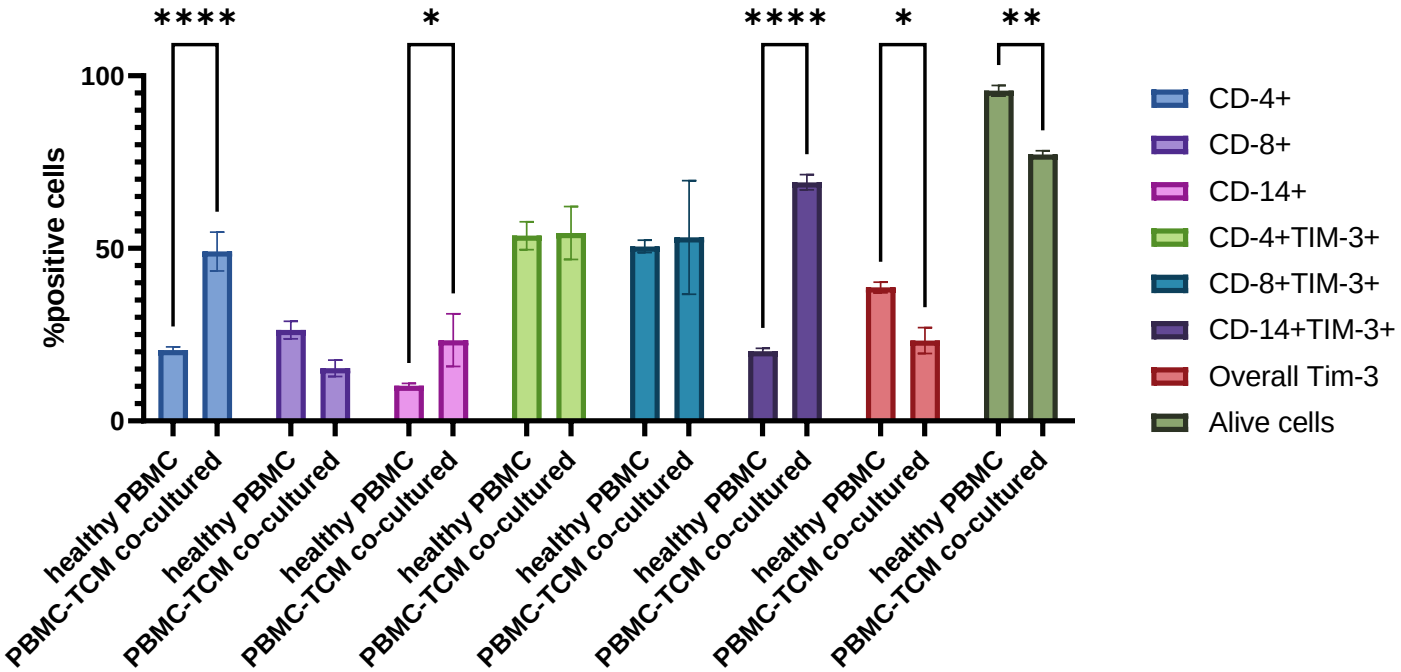

Figure 3.12. Tim-3 abundance comparison of human PBMC and after exposure to TCM. *XY graph shows the percentage expression of the overall Tim-3, CD4+ Tim-3+, CD8+ Tim-3+, CD14+Tim-3+. The graphs generated using GraphPad Prism software and the Mean ± SD for n=3 independent experiments, where * * = P<0.05, **** = P<0.0001 after the application of a 2Way ANOVA with multiple comparison to control.*

3.4 Tim-3 is expressed by human BC TME tissue

Next, the expression of Tim-3 on human BC tissue was investigated. Paraffin wax-embedded tissue from BC patients (N=20) were obtained from Prof. Penelope Ottewell (University of Sheffield). In this experiment, Tim-3 was co-stained with CD-3, CD-4, CD-8 as T cell markers (Reinherz *et al.*, 1979; Greaves *et al.*, 1981; Norman, 1995),CD-31 as an endothelial marker for vessels (Mourik *et al.*, 1987; DeLisser, Newman and Albelda, 1994), and CD-163 as a TAM marker (Lau, Chu and Weiss, 2004) to determine the expression ratio of Tim-3 on these immune cells within TME. Macrophages are the most well-characterised type of tumour-infiltrating immune cell in BC and are of interest in this project as they have been shown to express immune checkpoints including Tim-3.

In brief, slides were dewaxed with xylene and hydrated through alcohol gradients (100%, 95%,90% and 70%) before being rinsed in tap water. Following antigen retrieval, tissues were blocked and stained with antibodies **(Table 2.8., section 2.2.10.1.).**

A marked presence of Tim-3 expression was detected in the TME (**Figure 3.13 and 3.14A**.). These comprised approximately 60% of the tumour microenvironment. Within the TME, 35% of TAMs (CD163+) co-expressed Tim-3. Cytotoxic T cells (CD8+) constituted 34% of the population, with 70% displaying Tim-3 receptors. T helper cells (CD4+) accounted for 36% and 80% of these cells co-expressed Tim-3. This data is promising and supports the use of Tim-3 inhibitors targeting this immune checkpoint. For these tissue samples it was unable to obtain the patient subtypes and therefore this data provides a global view of expression in BC.

However, it was possible to access N=38 TNBC tissue obtained from patients who either received treatment prior to and after their biopsies from NeoGenomics for use in this study (Kindly provided by Richard Allen under the supervision of Prof. Claire Lewis). These slides were stained by Neogenomics using the MultiOmyx technique to examine CD68, CD163 and Tim-3.

This data was provided in an excel spreadsheet and analysed by an MSc student Zoi Papasavva under my supervision using GraphPad Prism. The average tumour size was comprised of a total 69,077 DAPI+ cells. Of these cells 21% were CD68+ macrophages and 38% expressed the M2-like CD163 macrophage marker. Tim-3 abundance was 21%. Interestingly, 63% of CD163+ TAMs expressed Tim-3 supporting a role for these cells in immunosuppression via checkpoint inhibition (**Figure 3.14B.**).

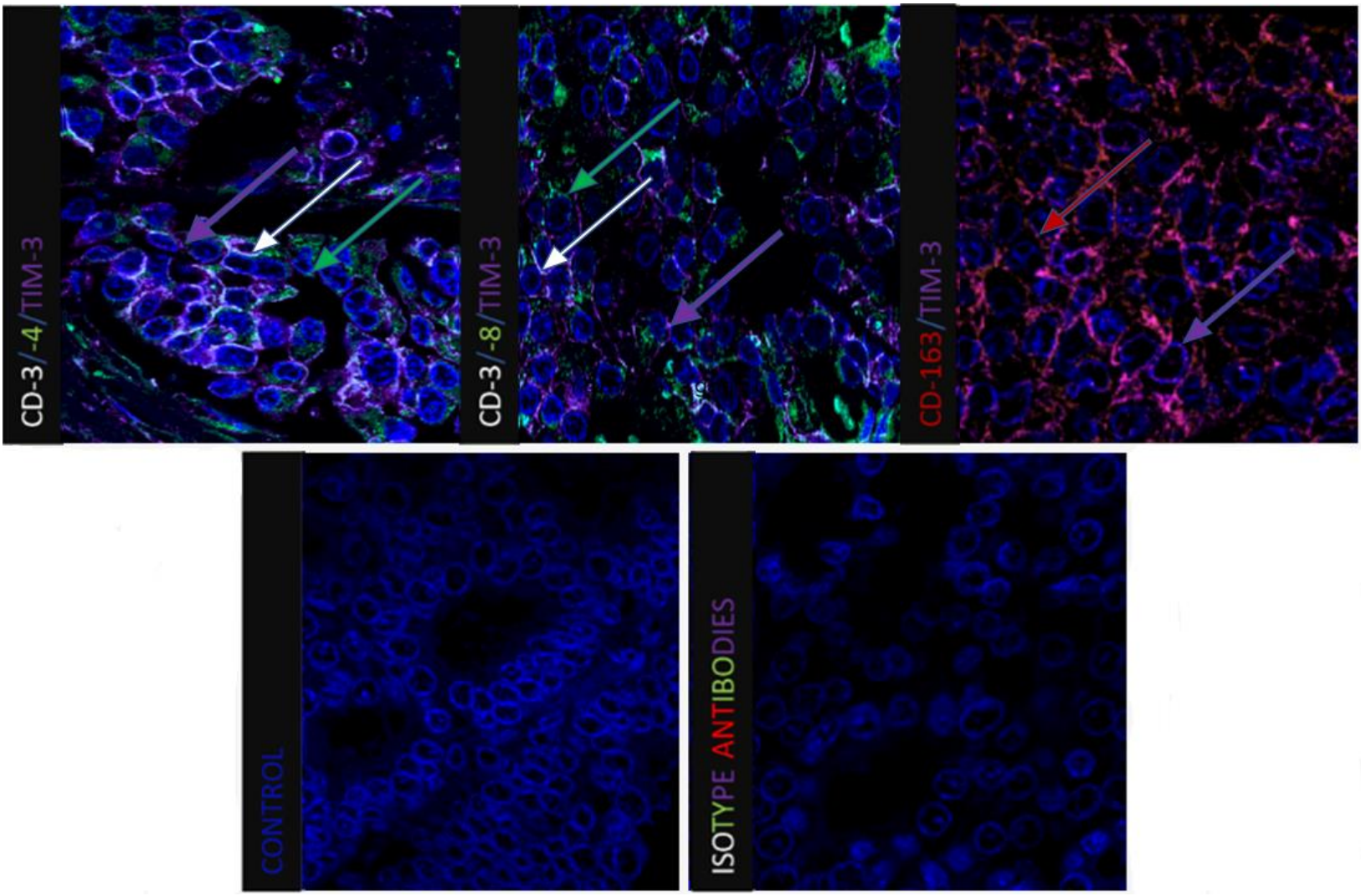

Figure 3.13. Tim-3 is expressed by macrophage and T cells in human BC tissue. *Representative images show expression of Tim-3, CD-3, CD-4, CD-8, CD-163 and cells expressing them together on human BC tissue. Images represent the immunofluorescence staining of each marker. Green is CD4/8, White=CD3, Purple-Tim-3, Red=CD163 and blue is DAPI stained nuclei.*

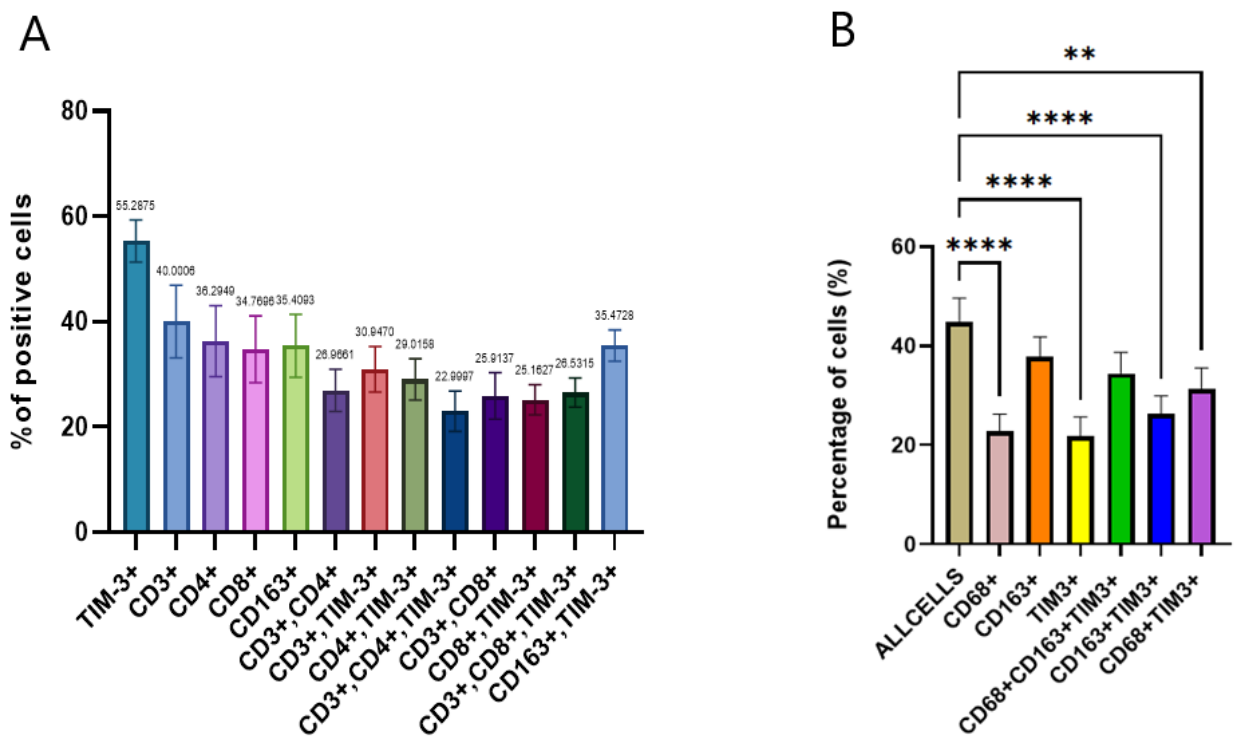

Figure 3.14. Tim-3 is expressed by macrophage and T cells in the human BC TME. (A) *The XY graph shows expression percentages of Tim-3, CD-3, -4, -8, -163 and cells expressing them together on human BC tissue. Data are presented as mean SD for n=20.* ***(B)*** *Graphic representation of the normalized data provided by the NeoGenomics (n=38) company along with the of the statistical analysis One-way ANOVA, where ****=P<0.0001, **=P=0.0038.*

Overall, this study revealed that Tim-3 was expressed in human breast tumour tissue and that all T cells markers were co-expressed with Tim-3 **(Figure 3.14A.)**. However, the Tim-3 expression levels between tissue samples obtained locally and those from NeoGenomics yielded contrasting results **(Figure 3.14B.)**. NeoGenomics specimens were exclusively from the triple-negative BC (TNBC) subtype, while NHS samples encompassed various subtypes, including ER+/PR+/HER2+/TNBC. Notably, all TAMs and most of T cells co-expressed Tim-3. This pattern of Tim-3 expression was consistent with the results obtained from the (co-cultured TCM) Flow cytometry results. It is crucial to note that while the study investigated Tim-3 expression in immune cells, the overall Tim-3 percentage encompasses other TME cell types and tumour cells.

3.6. Discussion

Immune checkpoint ligands are proteins expressed on the surface of both cancer cells and immune cells. When these ligands interact with their corresponding receptors on immune cells, they can inhibit or modulate the function of immune cells such as T cells (Wherry, 2011), enabling cancer cells to evade immune attack (Dyck and Mills, 2017). Tim-3 is an example of an immune checkpoint ligand that has been demonstrated to be expressed on both immune cells (Freeman et al., 2010; Gleason et al., 2012) and cancer cells (Cao et al., 2013; Cheng et al., 2018; Jiang et al., 2013; Zhou et al., 2015).

This chapter investigates the expression of Tim-3 in human BC cell lines, human breast tissue samples and immune cell populations in the circulation as the TME includes macrophages, and PBMCs. Overall, the findings confirm that Tim-3 is expressed on all of these cell types. Additionally, the Human Protein Atlas website was probed to provide further evidence of Tim-3 expression. According to the Human Protein Atlas (https://www.proteinatlas.org/), MCF-7 (0.2 nTPM) and MDA-MB-231 (0.2 nTPM) human BC cell lines have same and higher Tim-3 expression levels than SKBR-3 (0.1 nTPM). (**Figure 3.2.**)

Data presented in this chapter confirms these findings, with MDA-MB-231 exhibiting the highest Tim-3 expression level among the three cell lines, while MCF-7 and SKBR-3 have approximately equal expression levels (**Figure 3.3.-3.5.**). However, considerable data reproducibility issues with the F38-2E2 antibody used in this assay were encountered, despite multiple attempts and its prior validation by other researchers (Hastings et al., 2009; Limagne et al., 2019). Consequently, the F38-2E2 clone used here may have a stability issue impacting its affinity leading to unreliable Tim-3 staining.(Gu et al., 2010). Another consideration is that the cancer cell lines do not stably express the Tim-3 receptor and there is no literature on Tim-3 expression by Flow cytometry, mostly western blotting. Perhaps Tim-3 is located intracellular and if time permitted western blots or intracellular staining (after fixing and permeabilising of cells) by flow cytometry would be performed to determine this.

Tim-3 clone (7D3) was next investigated. Tim-3 expression in human healthy PBMCs and tumour-conditioned PBMCs to mimic tumour conditions using Flow Cytometry staining with various markers, including CD14, CD80, CD86, CD163, and HLA-DR. These markers not only serve as cell identification tools but also provide insights into immune modulation. For instance,

- CD14 may contribute to tumour cell proliferation in cancer cells and immunosuppressive TME formation (Gregory, 2000),
- CD80/86 are classical markers of macrophage activation and could cause T cell dysfunction (Ohue and Nishikawa, 2019),
- CD163 is associated with anti-inflammatory functions and considered a TAM marker (Allison et al., 2023; Skytthe et al., 2020),
- HLA-DR downregulation or absence can aid in immune escape (Fei et al., 2022).

These markers were investigated in healthy macrophages and tumour-conditioned macrophages by Flow cytometry. Notably, both healthy and TCM-co-cultured macrophages displayed cell surface Tim-3 receptors, with expression levels increased by 4-6 times for each marker. Interestingly, monocytes in fresh PBMCs displayed a 3.5-fold increase in Tim-3 expression, while T cells showed only a slight increase in Tim-3 population after co-culturing with TCM. Additionally, CD8+T cells abundance decreased from 26% to 15% while CD4+ T cells increased almost 2.5-fold.

This observation aligns with the concept of MHC-driven lineage selection, where specific TCR-MHC interactions influence the survival and development of different T cell lineages. As Fowlkes and Schweighoffer (1995) highlight, binding of class I MHC to CD8 promotes downregulation of CD4, while MHC class II binding to CD4 promotes downregulation of CD8 (Fowlkes and Schweighoffer, 1995). As class II MHC molecules primarily present exogenous proteins recognizing by helper (CD4) T cells and Class I MHC molecules primarily present intrinsic peptide products cytotoxic (CD8) T cells (Kamal et al., 2023),in the co-culture setting, the observed increase in CD4+ T cells and decrease in CD8+ T cells suggest a potential role of class II MHC-specific TCR interactions in shaping T cell populations.

This interaction induces an immune response leading to increased IC expression including Tim-3 to prevent excessive response in health condition and to escape in cancer (Topalian et al., 2016). Studies have shown that Tim-3 expression on CD8+ and/or CD4+ T cells in non-small cell lung cancer patients impairs their effector functions (Gao et al., 2012b). Similarly, in BC patients, elevated PD-1 and Tim-3 levels on follicular T helper cells (a subset of CD4 T cells) were associated with exhaustion markers (Zhu et al., 2016). Therefore, further investigation using additional T cell subtype and function markers could be highly informative to gain a deeper understanding of this phenomenon.

Data from the tissue sections by IF staining showed Tim-3 expression in breast tumours while it was not possible to see this reliably in the BC cell lines. This may be due to the anti-Tim-3 antibody being better for IF than flow cytometry or tumour cells in a 3D environment (as in tissue) express more Tim-3 than cells in 2D (monolayers). Immune cells in tissue are different from cells in the blood due to the tumour microenvironment due to the presence of tumour factors and indeed increased expression on immune cells upon culture with tumour cell derived conditioned medium provides some evidence of this.

In conclusion, the data presented in this chapter confirms the presence of Tim-3 on PBMCs and cancer cells, corroborating findings from the Human Protein Atlas website (**Figure 3.15.**). Data from the Protein Atlas shows that myeloid dendritic cells and natural killer cells have the highest nTPM. In line with data presented here, subsets of monocytes including classical monocytes also express Tim 3. Data presented in this chapter now show expression of Tim-3 on human monocyte-derived macrophage. It would have been interesting to compare the different phenotypes of macrophages with our TCM-treated macrophages and if skewing these to become M1-like or M2-like impacts Tim-3 expression. This could be achieved by culturing the macrophages in LPS stimulator for inflammatory macrophages (M1-like phenotype) (Fang et al., 2004) or IL-4 stimulator for M2-like macrophages (M. Z. Zhang et al., 2017).

Previous studies have shown that Tim-3 is expressed at low levels by M1-like macrophages and have inflammatory activity including the production of pro-inflammatory cytokines (e.g. IL-12, TNF and IFN-g), antigen presentation capability and are phagocytic (Yan et al., 2015). However, following recruitment to tumours these cells change to become more like TAMs (express CD163, CD206) with regulatory like properties and an increase in Tim-3 expression. This change in phenotype is typical of macrophages and fits with their plasticity. This offers an opportunity to reprogramme these cells, which will be achieved in this thesis using cancer-killing oncolytic viruses. Our team have shown that OVs can reprogram TAMs to have an inflammatory anti-cancer phenotype (Kwan et al., 2021). Lymphocytes on the other hand, do not exhibit this plasticity they are polarised towards a particular effector profile, where their chromatin is modified significantly. This results in a genetic profile that can be altered in response to the stimulus, albeit based on the type of stimuli, the concentration used and how long the stimulus is present (Cassetta et al., 2011; Martinez et al., 2006). Therefore, targeting TAMs holds promise when considering drugs that reprogramme the TME.

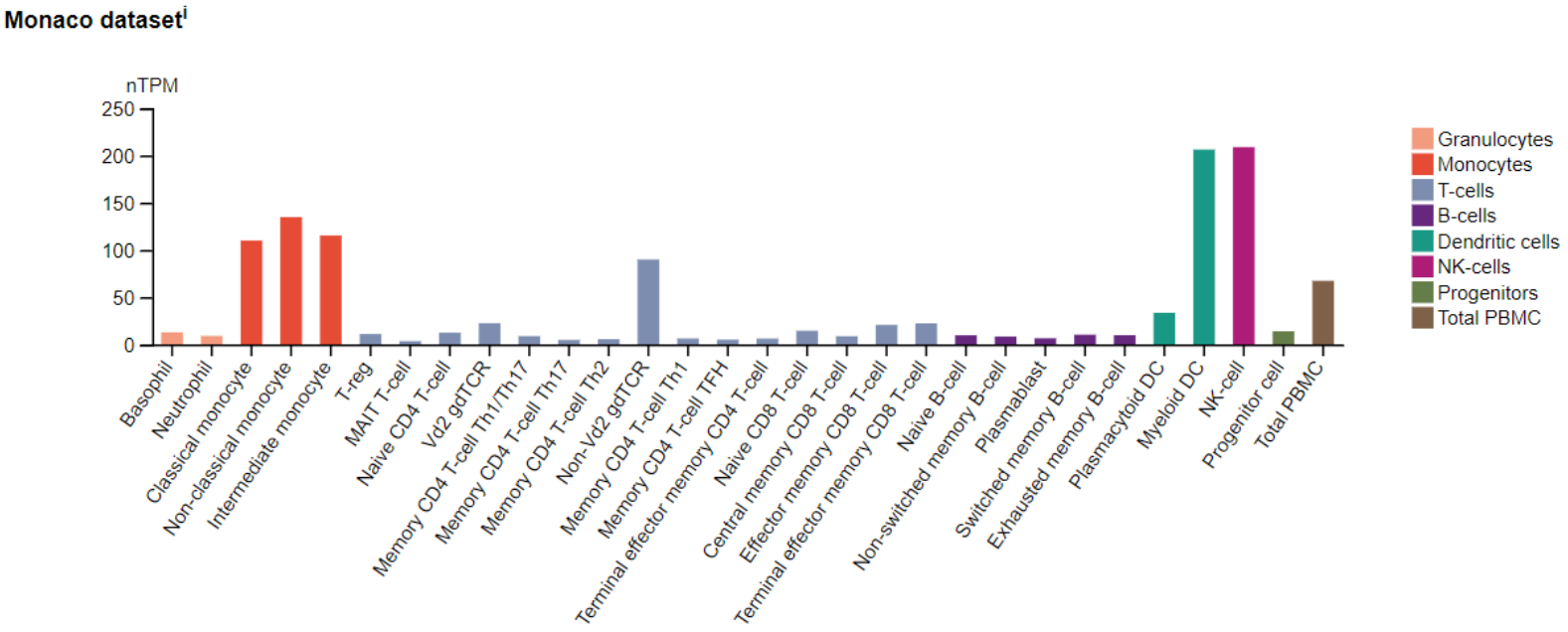

Figure 3.15.: Expression of Tim-3 in immune cell lines. *Image obtained from the website Human Protein Atlas (https://www.proteinatlas.org/).*

Indeed, findings also demonstrate that immune cell exposure to TCM upregulates Tim-3 expression on monocytes (CD14+), this could be preconditioning the monocytes into becoming TAMs. Next, Tim-3 expression on human BC tissue was investigated where macrophages including TAMs (CD163+), and cytotoxic T cells (CD8+ T cells) displayed expressed Tim-3. This aligns with observations in other cancers, like HCC and CRC, where TAMs exhibit increased Tim-3 due to the tumour microenvironment (Katagata et al., 2023; Yan et al., 2015). This upregulation effect is also observed on CD14+Tim-3+ monocytes in glioma patients compared to healthy donors (X. Li et al., 2018).

Supporting this trend, a separate study comparing Renal Cell Carcinoma patients and healthy controls revealed significantly higher Tim-3 expression on tumour-infiltrating lymphocytes (TILs) (14.6% for CD4+ T cells and 30.9% for CD8+ T cells), compared to 7.6% and 10.7%, respectively (Cai et al., 2016). Notably, peripheral blood T cells in these patients showed no significant difference (Cai et al., 2016).

Summary

In conclusion, the data in this chapter reinforces the presence of Tim-3 on various immune and tumour cell subsets in BC, and its enhanced expression upon interaction with TCM. This aligns with observations in other malignancies and supports the notion of a dynamic interplay between cancer and the immune system, where both environmental factors and direct interaction can influence Tim-3 expression and potentially impact tumour progression. The following chapter will delve into the potential functions of Tim-3 blockade with/without oHSV in vitro.

Chapter 4

Combination of anti-Tim-3 and oncolytic virotherapy in BCs cells

4.1. Introduction

Tim-3 upregulation has been implicated in promoting tumour cell proliferation, migration, and invasion in vitro (Cheng et al., 2018; Guo et al., 2022a; Lin et al., 2017). Preclinical studies have demonstrated that inhibiting Tim-3 or silencing its expression through siRNA can impede these processes in various cancer types, including breast, glioma, prostate, colorectal, and clear cell renal cell carcinoma (Cheng et al., 2018; Guo et al., 2022b; Huo et al., 2022; Piao et al., 2013; M. Yu et al., 2017b, 2017a; Zhang and Zhang, 2020; Zheng et al., 2015).

In the context of breast cancer, a few studies have shown that Tim-3 blockade on breast cancer immune cells can improve the anti-tumour response in vitro. γδ T-cells from breast cancer patients were cultured and demonstrated that Tim-3 upregulation during ex vivo expansion contributed to dysfunction and markedly promoted apoptosis of these cells. Importantly, Tim-3 inhibition effectively restored their function in vitro (Guo et al., 2020). Another study revealed Tim-3 upregulation on tumour-infiltrating immune cells from human primary breast cancer explant cultures. Notably, Tim-3 blockades enhanced immune responses and suppressed cancer-related pathways, exerting anti-tumorigenic effects in vitro (Saleh et al., 2020).

Additionally, oncolytic viruses are already used clinically for certain cancer types and are under clinical trials for many others, including breast cancer, as mentioned in section 1.3. These viruses, including adenovirus, vaccinia virus, reovirus, and HSV-1, have demonstrated anti-tumour effects showing effective cytotoxicity resulting in efficient killing of BC cells in vitro (Zeng et al.,2013; Cody et al.,2014; Ghouse et al.,2020; Cheng et al.,2018; Fan et al.,2016; Chen et al.,2016; Liu and Rabkin,2005; Wang et al.,2012; Nanni et al.,2013; Zeng et al.,2013; Guo et al.,2020). Moreover, as previously mentioned, OVs can be armed with reporter genes, cytotoxic transgenes, and have the potential to induce immune responses that modify the tumour microenvironment. Some studies have combined OVs with other agents or genetically modified them to enhance therapeutic effects. For instance, combining histone deacetylase inhibitors or paclitaxel with oncolytic HSV has shown improved anti-tumour activity including inducing of mitotic arrest and

apoptosis (Zeng et al.,2013) or improvement of virus replication (Cody et al.,2014) in vitro. Furthermore, arming an oncolytic HSV with interleukin-12 or the carboxyl-terminus of protein phosphatase 1 regulatory subunit 15A (MyD116/GADD34) has led to enhanced viral replication, cytotoxicity in vitro (Ghouse et al.,2020; Cheng et al.,2018) and inhibition of tumour growth, tumour angiogenesis, and prevention of lung metastasis in vivo (Ghouse et al.,2020).

Overall, although both Tim-3 inhibition and oHSV have shown promise in preclinical studies, their monotherapy is not sufficient to complete anti-tumour responses. Thus, combination therapy of Tim-3 inhibition and oHSV could provide better therapeutic outcomes.

Subsequently, the aim of this chapter was to assess the outcomes of inhibiting Tim-3 with/without oHSV-1 in BC cell lines. This was investigated by Alamar Blue, cell migration and invasion assays following treatment of a panel of human BC cell lines.

The specific aims were to determine;

- IC50 values of 3 oHSV-1 viruses
- Cytotoxicity analysis via Alamar Blue assay on human and mouse BC cell lines
- BC cell migration using a scratch/wound healing assay
- BC cell Invasion using the flouroblock transwell Matrigel assay.

4.2. IC50 evaluation of BC cell lines in response to the oncolytic viruses HSV-1716, HSV-E17RL1del7, HSV-V17RL1del2

The oncolytic effect of three oHSV-1 viruses (HSV-1716, HSV-E17RL1del7, HSV-V17RL1del2) was assessed in 3 BC cell lines. HSV-E17RL1del7, HSV-V17RL1del2 were provided by Dr Joe Conner and are genetic variants of HSV-1716 that have not yet been investigated. IC50 values were determined by Alamar blue assay on 1st,2nd,5th, and 7th day post infection. The concentration of virus used was MOI 30, 10, 3, 1, 0.3, 0.1 and, 0.03, this range has been determined by HSV-1716 on MDA-MB-231. In this experiment the IC50 for infected cells was measured. This determines the concentration of a virus that causes death of half the number of total cells (**See Appendix 7.3. for raw data**). Therefore, it could be used to compare their effectiveness and determine concentrations for other experiments.

In MCF-7 cells, which are ER+, PR+, HER2-, all 3 virus types caused a significant decrease in cell viability in the first 24 hours (**Figure 4.1.**), with the highest cell death and the lowest IC50 value (0.1863) in the HSV-1716 group. HSV-E17RL1del7 was also effective at the 24 h time point with an IC50 of 0.2489. However, at 48 hours to 168 hours the IC50 for HSV-1716 and HSV-E17RL1del7 increases suggesting these viruses were more effective at the earlier time point. On the other hand, HSV-V17RL1del2 activity exhibited the lowest IC50 at the 48 (0.04970) and 120 hours (0.2652) post-infection compared to the other viruses. This suggests that this virus is more effective at later time points. At 168 hours, a decrease in the efficiency of all 3 virus types was observed and the lowest IC50 value was in the HSV-E17RL1del7 group.

Similar to MCF-7 cell line, all 3 virus types caused a significant decrease in cell viability in the first 24 hours in the MDA-MB-231 cell line which belongs to the TNBC group (**Figure 4.2.**). In this cell line the lowest IC50 value (0.08964) with the highest cell death was observed with the HSV-1716 treatment group at 24 h, and this IC50 value was low compared to that of the other 2 groups (IC50 values HSV-E17RL1del7 = 0.9906, HSV-V17 RL1del2 = 0.4682). However, HSV-1716 was less effective over time. At 120 and 168 hours, the HSV-V17RL1del2 group exhibited a significant increase in cell death compared to the other viruses and displayed the lowest IC50 (0.3474 and 0.1480, respectively) compared to the other treatments. This suggests that this virus is more effective at later time points for MDA-MB-231 cells, and this may be important for long term treatment.

All 3 virus types in the SKBR-3 cell line caused a significant decrease in cell viability in the first 24 hours (**Figure 4.3.**). The lowest IC50 value (0.1101) with the highest cell death was observed in the HSV-1716 group. After 48-hours evaluation, there was an increase in cell death of all groups and the lowest IC50 value (0.08171) was in the HSV-1716 group. At 120 hours, only the HSVV17RL1del2 group continued this increasing trend of cell death. At the end of the 168 hours period, the lowest IC50 value (0.6315) was also found in this group. This suggests that HSV-1716 is more effective at the earlier time points while HSV-V17RL1del2 is more effective at later time points.

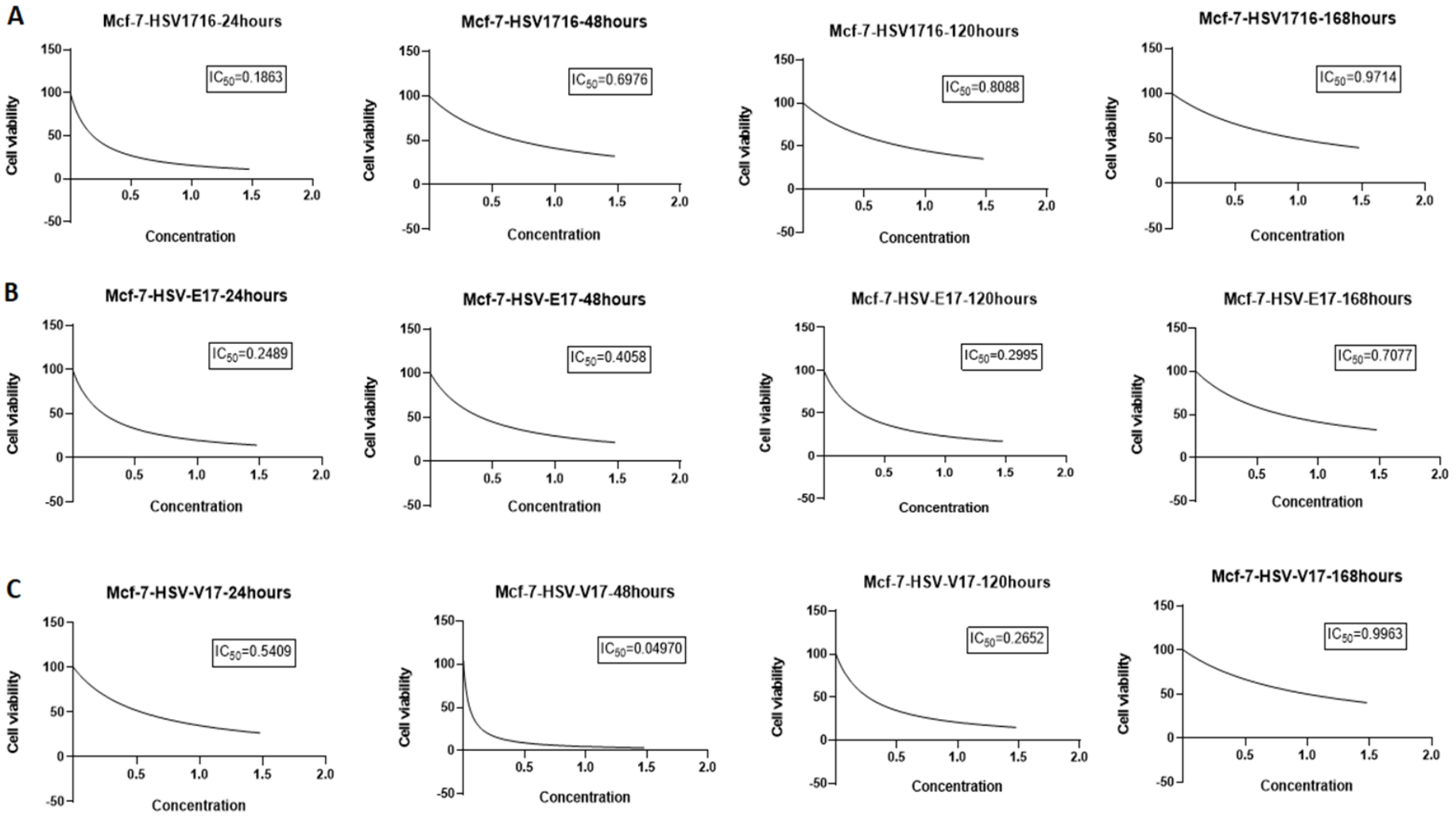

Figure 4.1. HSV-1716, HSV-E17RL1del7, HSV-V17RL1del2 reduce cell viability in MCF7 BC cells. *MCF7 cells were plated into 96 well plates at 5x10^3 and infected with 3 types of HSV at concentrations of MOI 30,10,3,1,0.3,0.1,0.03. Alamar blue reagent was added, and plates were read at 24-, 48-, 120- and 168-hours post infection on a fluorescent plate reader at excitation peak 570nm and emission peak 585nm. The data are normalised to the corresponding non-treated control cells the graphs generated using GraphPad Prism software for IC50 calculations. Data are the Mean ± SEM for n=3 independent experiments.*

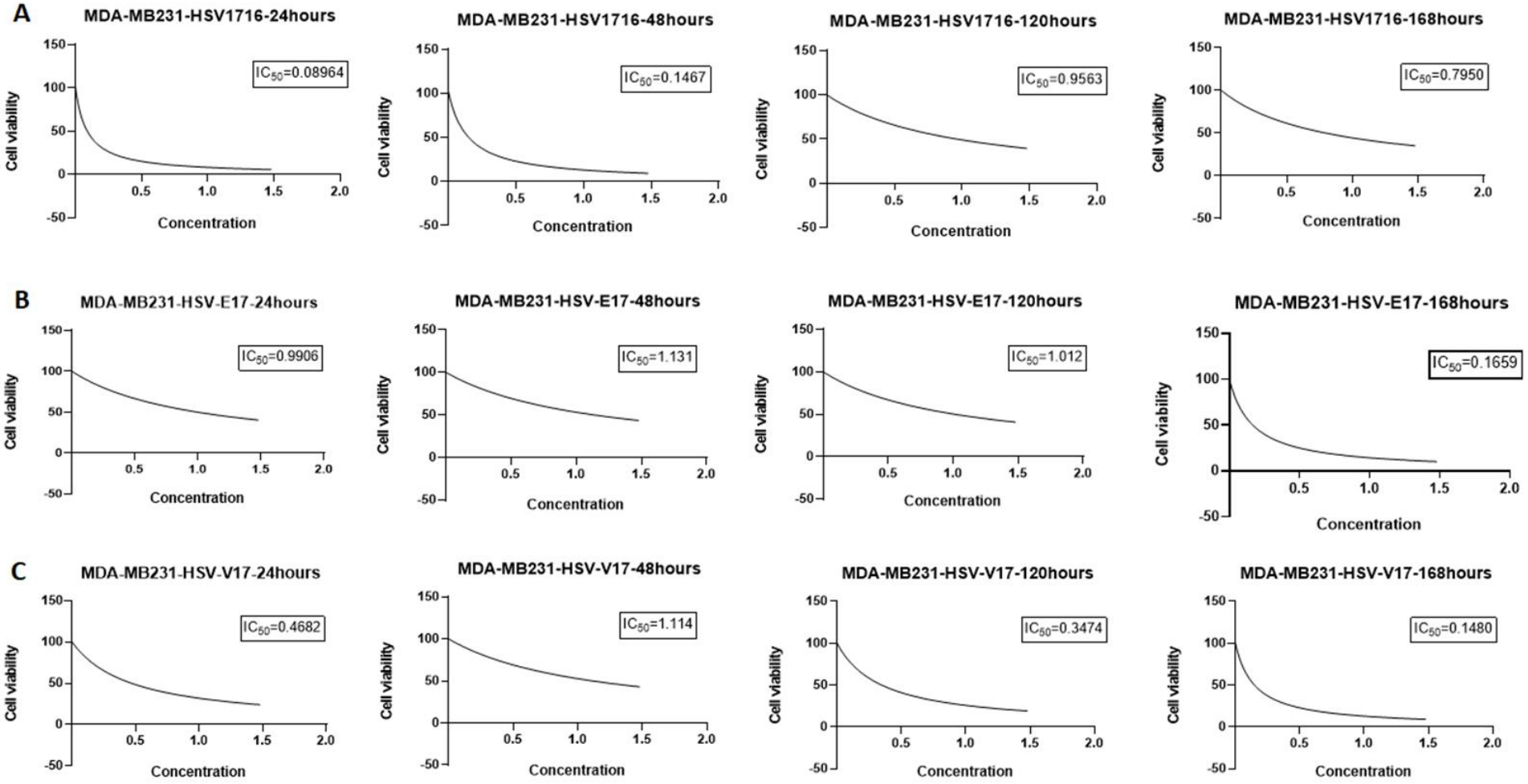

Figure 4.2. HSV-1716, HSV-E17RL1del7, HSV-V17RL1del2 reduce cell viability in MDA-MB-231 BC cells. *Cells were plated into 96 well plates at 5x10^3 and infected with 3 types of HSV at concentrations of MOI 30,10,3,1,0.3,0.1,0.03. Alamar blue reagent was added, and plates were read at 24-, 48-, 120- and 168-hours post infection on a fluorescent plate reader at excitation peak 570nm and emission peak 585nm. The data are normalised to the corresponding non-treated control cells the graphs generated using GraphPad Prism software for IC50 calculations. Data are the Mean ± SEM for n=3 independent experiments*.

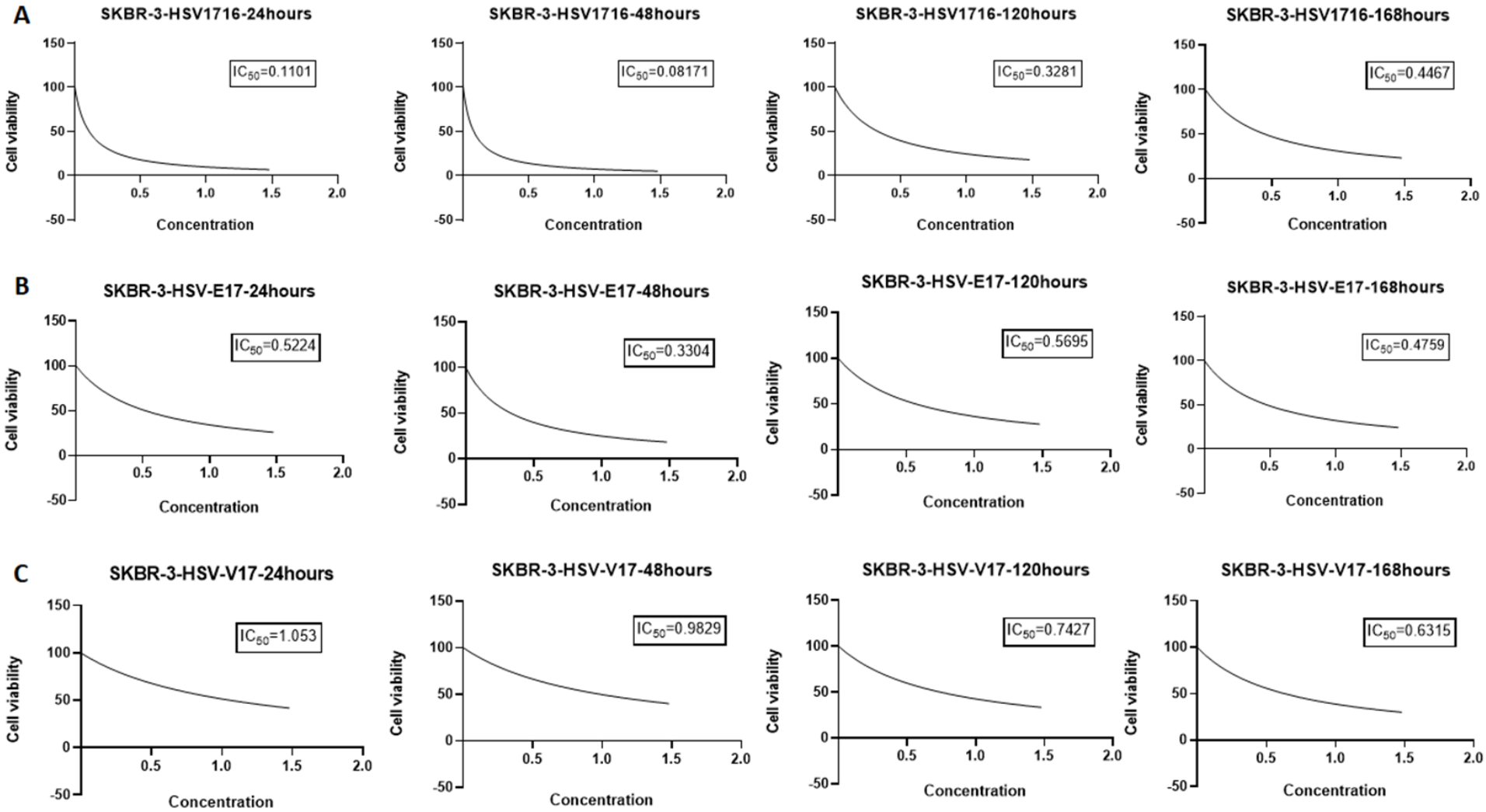

Figure 4.3. HSV-1716, HSV-E17RL1del7, HSV-V17RL1del2 reduce cell viability in SKBR-3 BC cells. *SKBR-3 cells were plated into 96 well plates at 5x10^3 and infected with 3 types of HSV at concentrations of MOI 30,10,3,1,0.3,0.1,0.03. Alamar blue reagent was added, and plates were read at 24-, 48-, 120- and 168-hours post infection on a fluorescent plate reader at excitation peak 570nm and emission peak 585nm. The data are normalised to the corresponding non-treated control cells the graphs generated using GraphPad Prism software for IC50 calculations. Data are the Mean ± SEM for n=3 independent experiments.*

4.2. Use of Alamar blue assays to investigate the cytotoxicity of HSV-1716, HSV-E17RL1del7, HSV-V17RL1del2 on BC cell lines in combination with Tim-3

The IC50 values were used to determine optimal virus concentrations. For the following Tim-3 experiment, HSV-1716 was used initially as this is the most characterised virus. of MOI 1 was used for the HSV-1716 virus concentration, since this induced cell death over a 7-day period. The anti-Tim-3 concentration range administered was 5 mg/mL, 2.5 mg/mL, 1.25 mg/mL, this range was selected from the literature (Hastings et al., 2009). The experimental design included untreated cells, Ig control, anti-Tim-3, HSV-1716 + anti-Tim-3 and medium only for background.

In the MCF7 cells, Tim-3 showed a trend towards reducing cell viability at 24 h but this was only significant at a concentration of 2.5 mg/ml and not at higher or lower concentrations of Tim-3. Further experimental repeats would help to confirm if this is reproducible. However, the combination of HSV-1716 + anti-Tim-3 treatment significantly reduced cell viability at all concentrations and time intervals compared to the control group (**Figure 4.4.**). Moreover, this effect was sustained and most prominent 7 days post -treatment, where nearly all the cells lost viability.

Next, Tim-3 inhibition was assessed in the MDA-MB-231 cell line (**Figure 4.5.**). This cell line was significantly more sensitive to anti-Tim-3 when given alone particularly at the 5 mg/ml where cell viability reduced over time compared to the control group. Loss of viability with TIM-3 treatment was dose-dependent at all times tested. In addition, when combined with HSV-1716 a more synergistic effect was observed whereby all concentrations of anti-Tim-3 led to a reduction in cell viability at all the time points.

Finally, the same experiments as above were repeated in the SKBR-3 cell line. Here the anti-Tim-3 group showed no significant effects on cell viability at most concentrations and time points compared to the control group (**Figure 4.6.**). However, the HSV-1716 + anti-Tim-3 treatment group significantly reduced cell viability at most concentrations and time points compared to the control group. This cell line was the least sensitive to Tim-3 inhibition alone or in combination with HSV-1716.

Following the human BC cell line, these treatment groups were performed in mouse cell lines by MSc student Soumya Rupangudi under my supervision. E0771 and 4T-1 BC cell lines mimicking human TNBC subtype (Schrörs et al., 2020) were used. Experiments were carried out identical to the human BC cell lines. The combination treatment demonstrated more cell death till 72 hours, all treatment groups presented a trend towards declining cell viability over time compared to the control group. Moreover, the least cell viability was obtained in HSV-1716 alone and combination treatment groups. However, these 2 groups exhibited a similar reduction considering that adding Tim-3 did not contribute to viability declining as Tim-3 alone group showed less cell viability than the combination **(Figure 4.7.).**

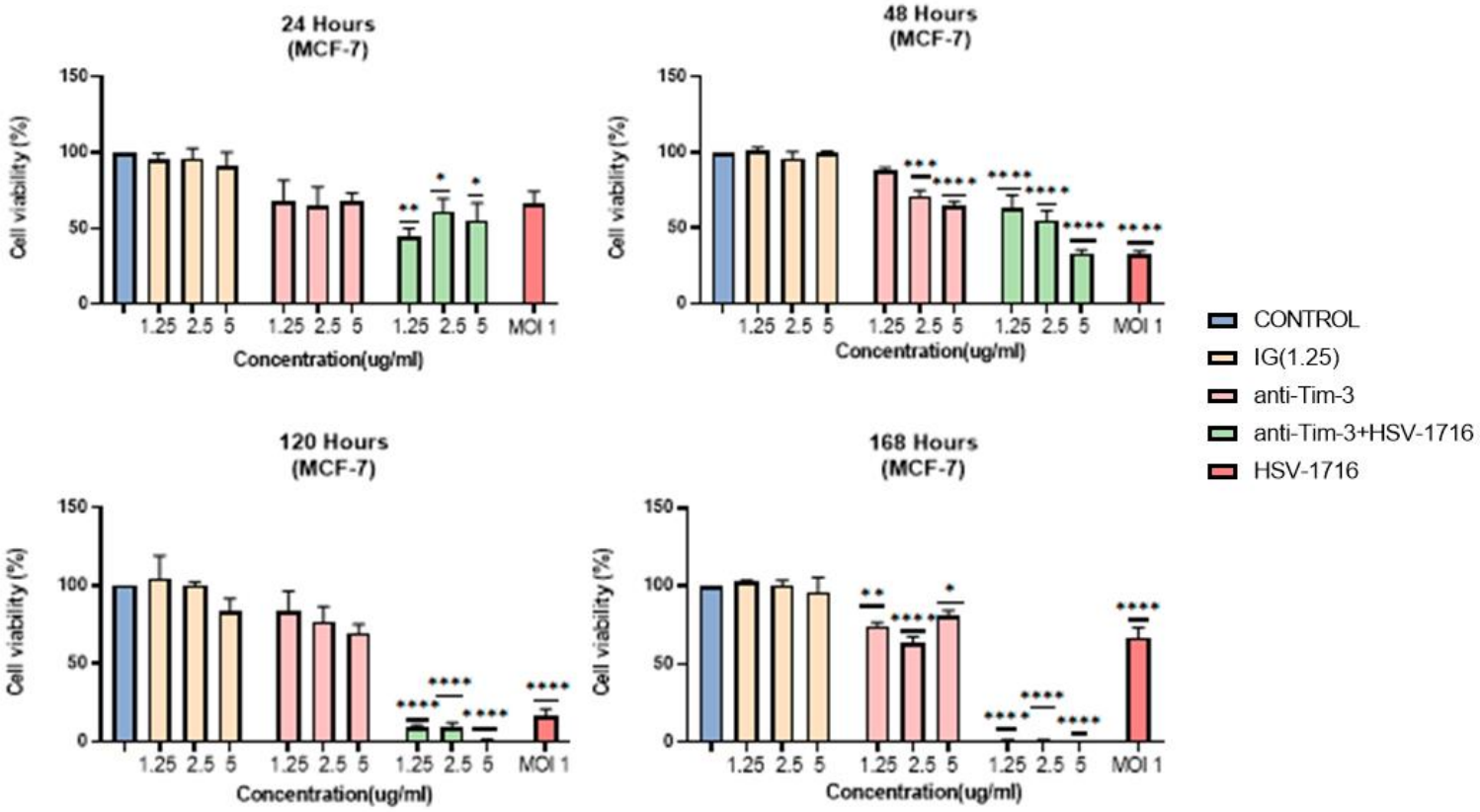

Figure 4.4. Combination treatment with Tim-3 inhibition and HSV-1716 infection reduces cell viability in MCF-7. *Anti-Tim-3 antibody and, HSV-1716+ anti-Tim-3 antibody were administrated on MCF-7 at different concentrations which are 5 mg/ml, 2.5 mg/ml, 1.25 mg/ml for antibodies: MOI 1 for HSV-1716. Alamar blue reagent was added, and plates were read at 24-, 48-, 120- and 168-hours post infection on a fluorescent plate reader at excitation peak 570 nm and emission peak 585 nm. Data is shown as mean ± SEM for n=3 independent experiments, where * = P<0.05 after the application of a Three Way AMOVA with multiple comparison to control*.

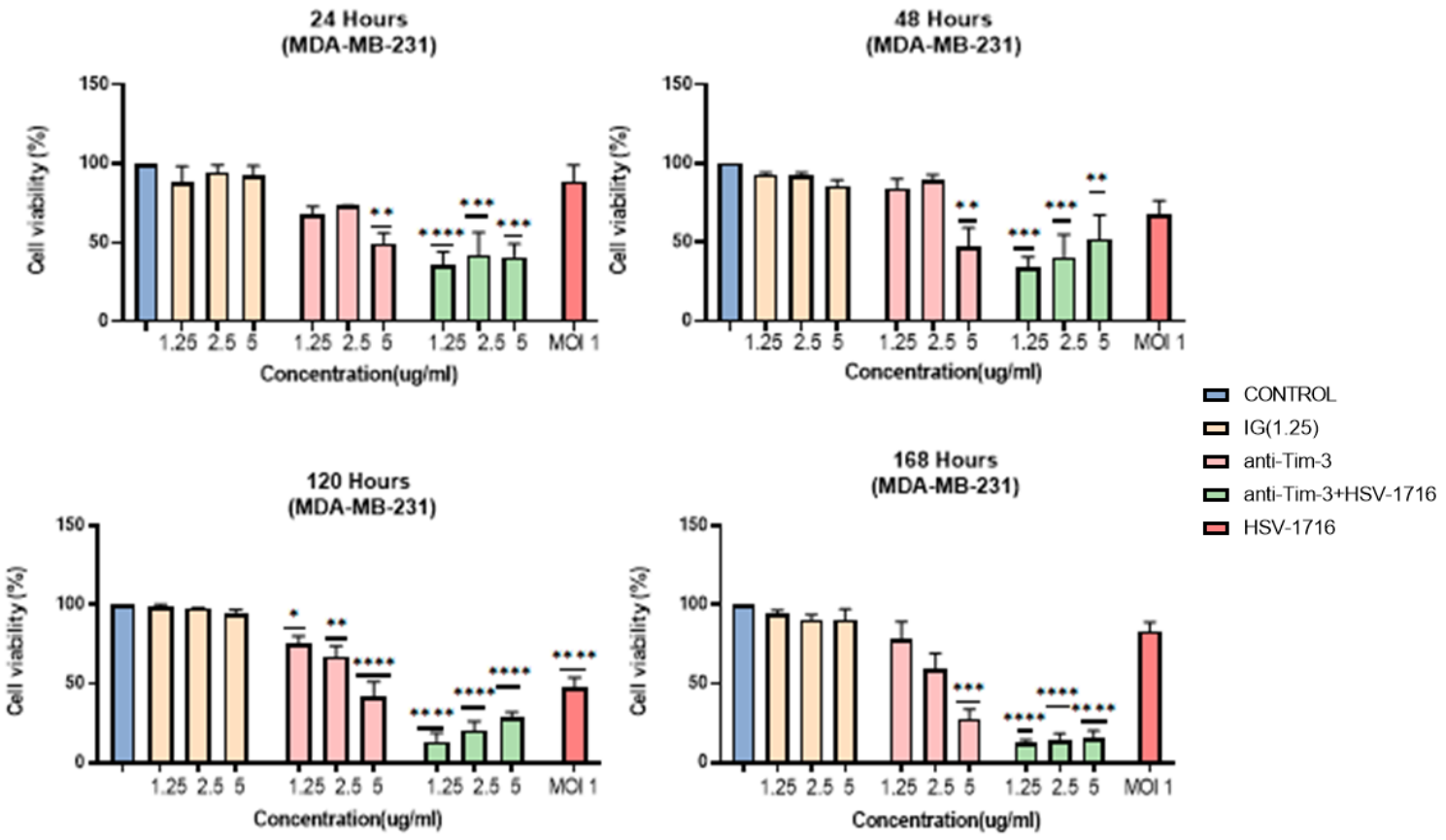

Figure 4.5. Combination treatment with Tim-3 inhibition and HSV-1716 infection reduces cell viability in MDA-MB-231. *Anti-Tim-3 antibody and, HSV-1716+ anti-Tim-3 antibody were administrated on MDA-MB-231 at different concentrations which are 5 mg/ml, 2.5 mg/ml, 1.25 mg/ml for antibodies: MOI 1 for HSV-1716. Alamar blue reagent was added, and plates were read at 24-, 48-, 120- and 168-hours post infection on a fluorescent plate reader at excitation peak 570 nm and emission peak 585 nm. Data is shown as mean ± SEM for n=3 independent experiments, where * = P<0.05 after the application of a Three-Way ANOVA multiple comparison to control.*

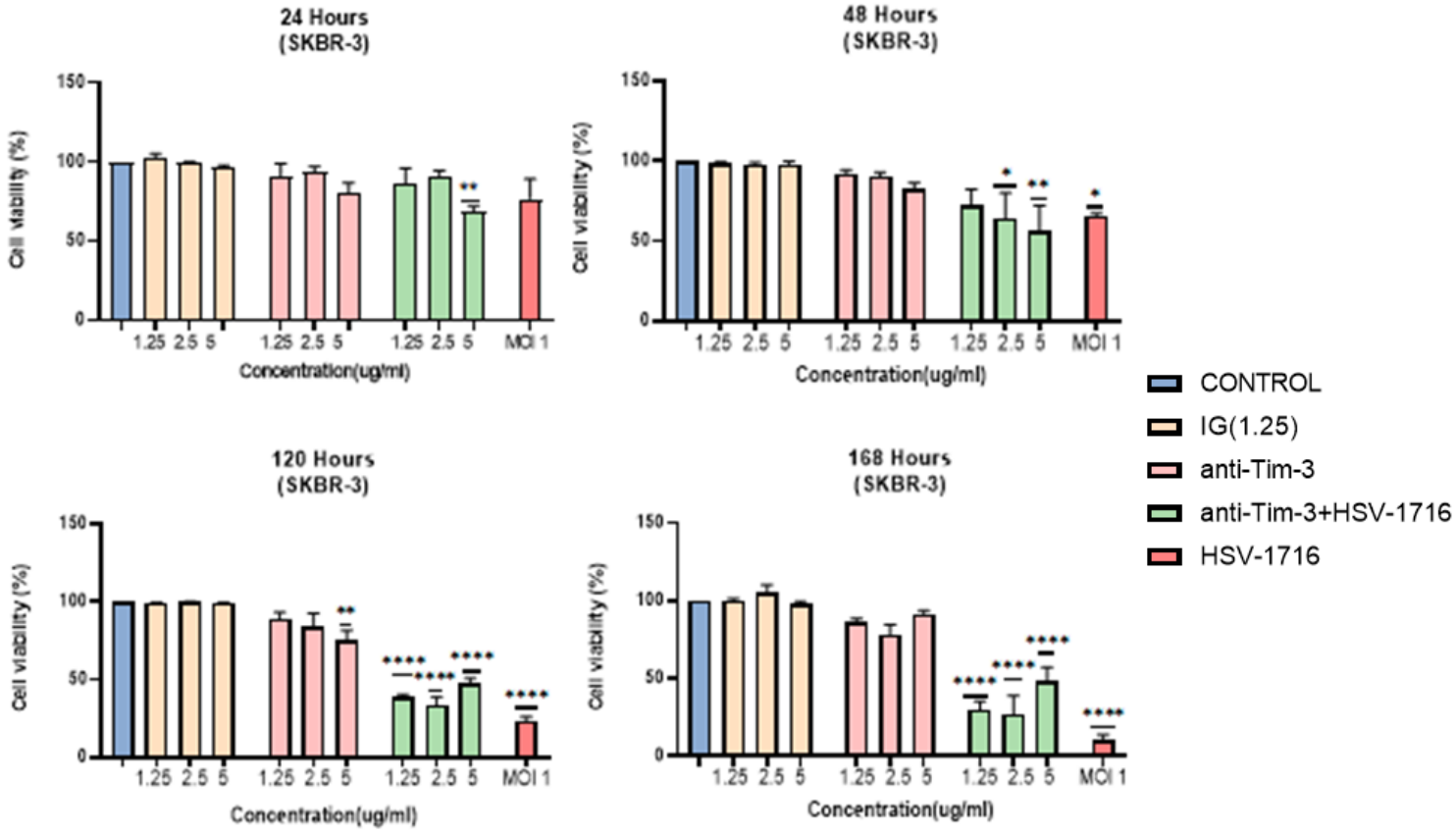

Figure 4.6. Combination treatment with Tim-3 inhibition and HSV-1716 infection reduces cell viability in SKBR-3. *Anti-Tim-3 antibody and, HSV-1716+ anti-Tim-3 antibody were administrated on SKBR-3 at different concentrations which are 5 mg/ml, 2.5 mg/ml, 1.25 mg/ml for antibodies: MOI 1 for HSV-1716. Alamar blue reagent was added, and plates were read at 24-, 48-, 120- and 168-hours post infection on a fluorescent plate reader at excitation peak 570 nm and emission peak 585 nm. Data is shown as mean ± SEM for n=3 independent experiments, where * = P<0.05 after the application of a Three Way ANOVA with multiple comparison to control.*

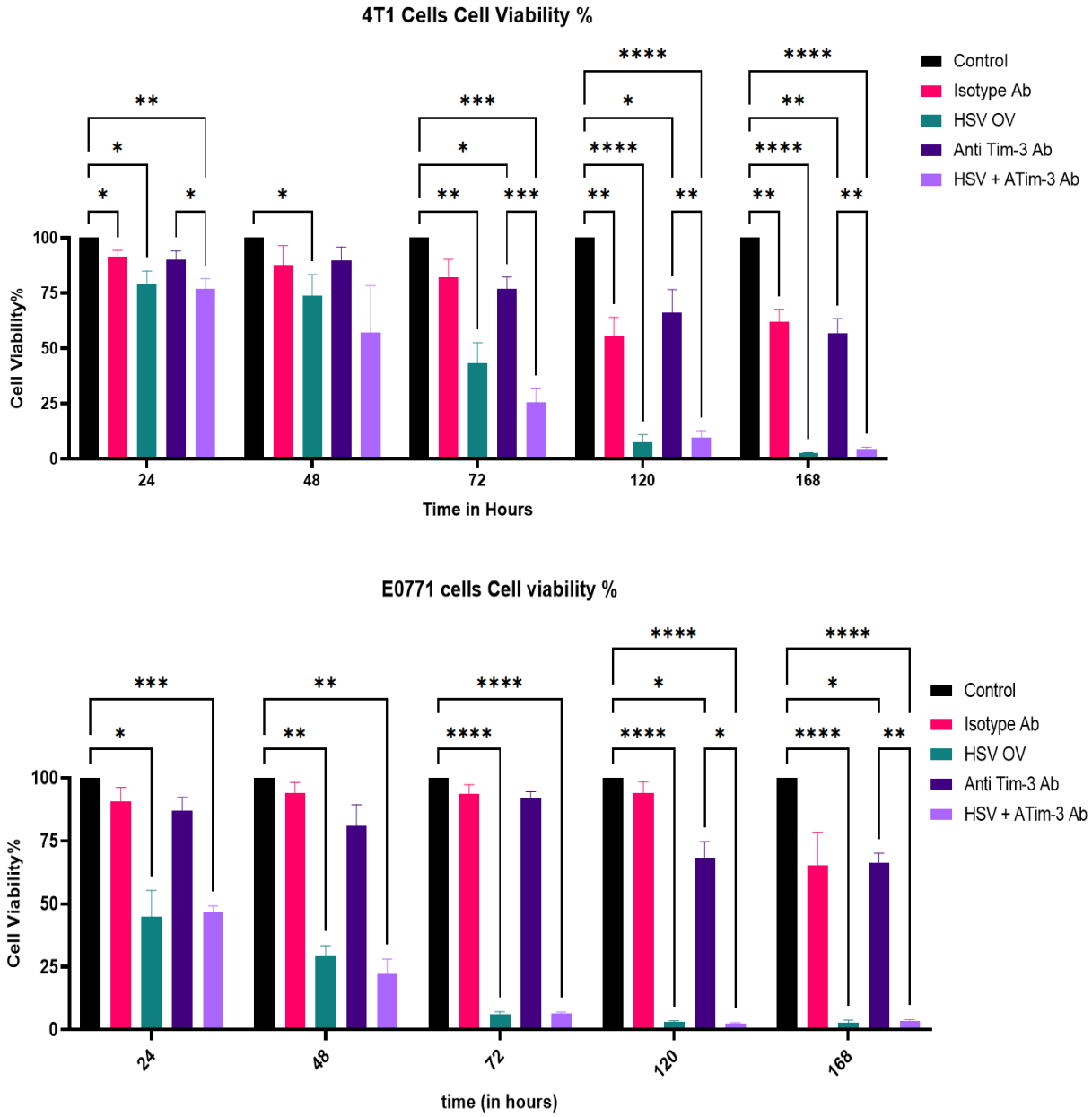

Figure 4.7. Combination treatment with Tim-3 inhibition and HSV-1716 infection reduces cell viability in mice BC cell lines which are 4T1 and E0771. *Anti-Tim-3 antibody and HSV-1716 + anti-Tim-3 antibody were administered on 4T1 and E0771 at concentration of 5 mg/ml for antibodies: MOI 3 for HSV-1716. Alamar blue reagent was added, and plates were read at 24-, 48-, 72-, 120- and 168-hours post infection on a fluorescent plate reader at excitation peak 570 nm and emission peak 585 nm. The data, n=3 independent trials, is displayed as mean with Standard Deviation (SD). A two-way ANOVA is employed to analyse and compare mean of each treatment trial with each other. Here *=P<0.05 and ****=P<0.01 as observed between the control and HSV-1716 the control and the combination treatment on the 5th and 7th day post treatment.*

4.3. The effect of anti-Tim-3 and oHSVs on migratory potential of BC cell lines

Wound healing assays were performed to evaluate cell migration behaviour. This was carried out by scratching the cell surface of the cell monolayers with a pipette tip followed by exposing to cells to the treatments below. Cells were then imaged until the scratch closed completely at dedicated time periods as mentioned in the method **section 2.2.8**.

The nine treatment groups using in the assay on BC cell lines;

- Control cells treated with serum-free medium
- Cells treated with control (IG) antibody
- Cells treated with TIM-3 antibody
- Cells infected with HSV-1716
- Cells infected with HSV-E17
- Cells infected with HSV-V17
- Cells infected with HSV-1716 + anti-Tim-3 antibody
- Cells infected with HSV-E17 + anti-Tim-3 antibody
- Cells infected with HSV-V17 + anti-Tim-3 antibody

The scratch was imaged using the EVOS microscope and the data normalised to the corresponding non-treated control cells. All the graphs were generated using GraphPad Prism software using Two-way ANOVA as shown in **Figures 4.8. to 4.10.**

MCF-7 cells were treated with 9 different groups and imaged at 0, 6, 18 and 24 hours. After 6 hours of treatment, all groups, except theHSV-E17 + anti-Tim-3 combination group, demonstrated a statistically significant decreases in migration compared to the control group (**Figure 4.8.**). Furthermore, the greatest inhibition of cell migration was seen in the HSV-V17 group at 6 hours.

At the end of 18 hours, it was determined that this significant inhibitory effect was maintained only by the HSV-1716 + anti-Tim-3 combination group. When the last time period was evaluated, all groups caused considerable decreased migration. To conclude, in the last two time periods, the distinguished result was obtained from the HSV-1716 + anti-Tim-3 combination groups.

The same treatment groups were applied to MDA-MB-231 cells and imaged at 0, 18 and 24 hours. However, no significant difference was obtained in any group or time period tested (**Figure 4.9.**).

For SKBR-3 cells, migration was evaluated at 24, 48 and 72 hours. At 48 hours post treatment the HSV-1716 + anti-Tim-3 and HSV-E17 + anti-Tim-3 combination treatment groups resulted in significantly reduced BC migration **(Figure 4.10.)**. Although at this time point, most of the group treatments appeared to prevent migration (blue lines presented visual size differences compared to the control group). However, no statistical difference was observed. At 72 hours, all groups excluding the HSV-V17 + anti-Tim-3 combination group exhibited a significant decrease in migration. The most evident decrease in both periods of time was detected in the combination group of HSV-1716+anti-Tim-3. To conclude, HSV-E17, HSV-E17 + anti-Tim-3 and HSV-1716 + anti-Tim-3 combination treatment groups showed statistically significant reductions in BC cell migration.

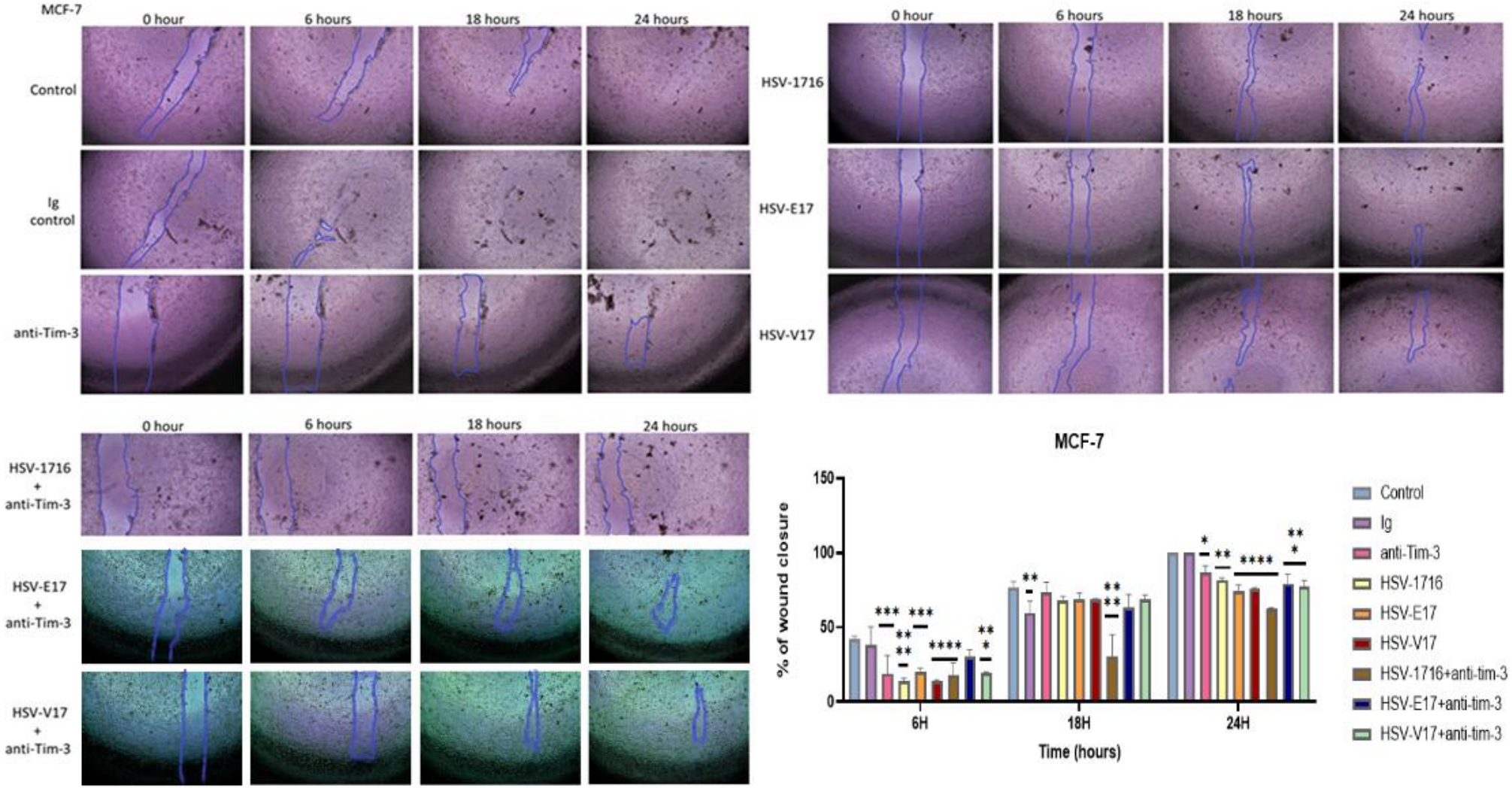

Figure 4.8. Representative images of migration assay by Tim-3 blocking with/without HSV-1716/-E17/-V17 on MCF-7 cell lines. *Cells were blocked with anti-TIM-3 at concentration of 5 mg/ml, with/without viruses at MOI 1. This experiment was repeated 3 times and images were taken at 0, 6, 18 and 24 hours. Data are mean ± SEM. The data normalised to the corresponding non-treated control cells and analysed by Two-way ANOVA.*

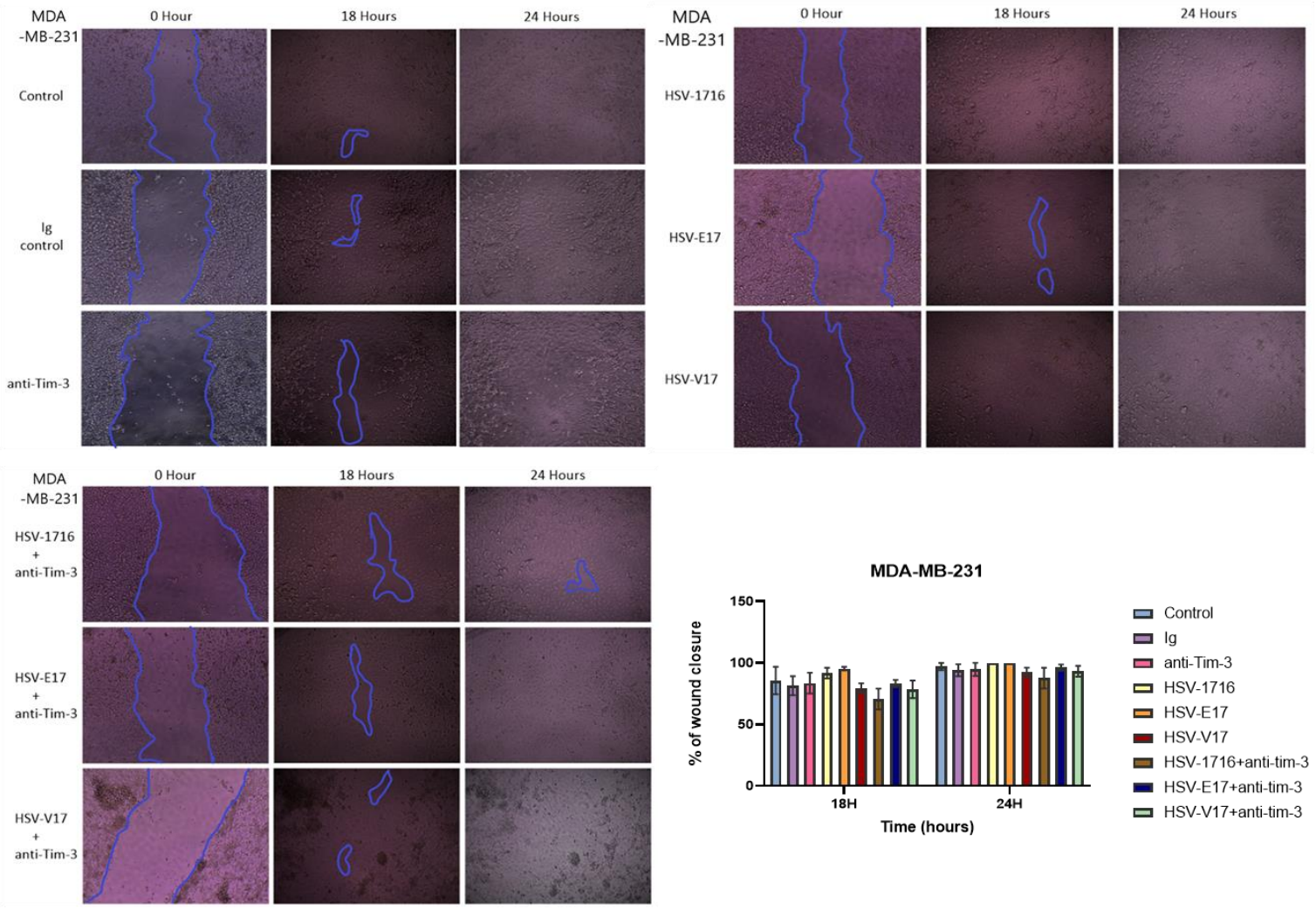

Figure 4.9. Representative images of migration assay by Tim-3 blocking with/without HSV-1716/-E17/-V17 on MDA-MB-231 cell lines. *Cells were blocked with anti-TIM-3 at concentration of 5 mg/ml, with/without viruses at MOI 1. This experiment was repeated 3 times and images were taken at 0, 18, and 24 hours. Data are presented as mean ± SEM. The data are normalised to the corresponding non-treated control cells and analysed by Two-way ANOVA.*

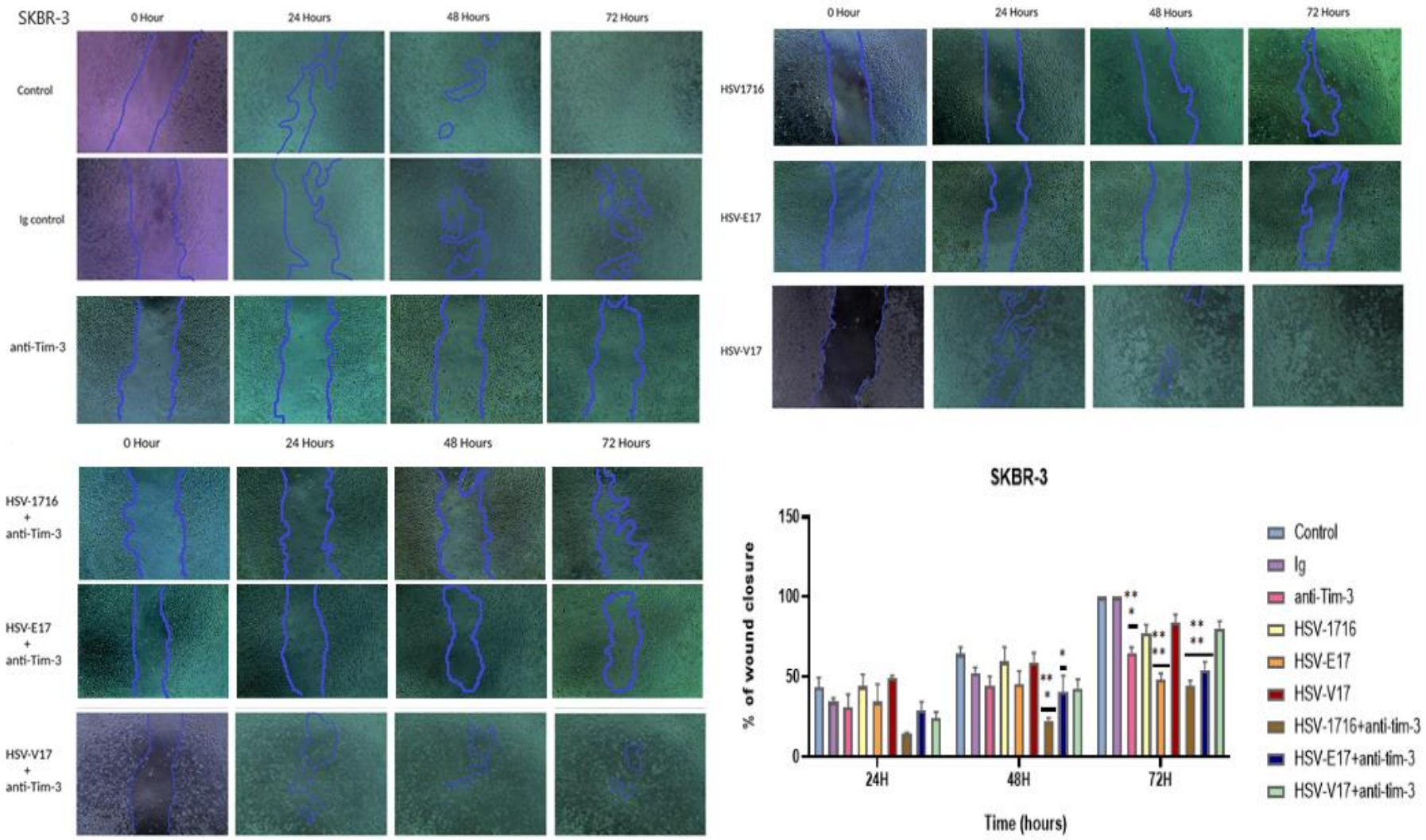

Figure 4.10. Representative images of migration assay by Tim-3 blocking with/without HSV-1716/-E17/-V17 on SKBR-3 cell lines. *Cells were blocked with anti-TIM-3 at concentration of 5 mg/ml, with/without viruses at MOI 1. This experiment was repeated 3 times and images were taken at 0, 24,4 8 and 72 hours. Data are presented as mean ± SEM. The data are normalised to the corresponding non-treated control cells and analysed by Two-way ANOVA*.

4.4. The effect of anti-Tim-3 and oHSVs on the invasion potential BC cell lines

Invasion assays were performed to evaluate treatment on behaviour of BC cell invasion. Briefly, cells were exposed to Mitomycin C and Matrigel was added to Flouroblock Transwells by incubating for 2 hours. Cells and treatments were mixed and then added to the transwells. After 24 hours incubation (48 hours for SKBR-3), wells were stained with Calcein AM followed by 45 min incubation.

Tests were carried out including nine treatment groups on 3 BC cell lines;

1. Control cells treated with serum-free medium
2. Cells treated with control (IG) antibody
3. Cells treated with TIM-3 antibody
4. Cells infected with HSV-1716
5. Cells infected with HSV-E17
6. Cells infected with HSV-V17
7. Cells infected with HSV-1716 + anti-TIM-3 antibody
8. Cells infected with HSV-E17 + anti-TIM-3 antibody
9. Cells infected with HSV-V17 + anti-TIM-3 antibody

Wells then were imaged by EVOS microscope at 4x magnification, and the data are normalised to the corresponding non-treated control cells the graphs generated using GraphPad Prism software using Two-way ANOVA as shown in **Figures 4.12.,4.14.,4.16.**

This experiment is based on movement of the treated/untreated cells from the top of transwell to the bottom of the well through the Matrigel. FBS provides the factors that attract cells across the barrier as they a have high content of migration stimulating proteins. Furthermore, Matrigel is a solubilized basement membrane extracted from mouse sarcoma, rich in such ECM proteins as laminin (a major component), collagen IV, heparan sulphate proteoglycans, entactin/nidogen, and a number of growth factors, and so mimics the *in vivo* tumour microenvironment. Cells then passing through the Matrigel are considered invasive while those staying on the top of the transwells are non-invasive cells in this experiment. Imagining was carried out from the top of wells showing non-invasive cells labelled green.

MCF-7 cells were treated with 9 different groups and imaged at 24 hours using the EVOS microscope. Tim-3 inhibition (**Figure 4.11.-number 3**) and HSV-V17 exposed treatment group (**Figure 4.11.-number 9**) had more green labelled cells (that had not invaded the Matrigel) compared to other treatments and control group. Furthermore, statistical analysis showed considerable changes in the same groups (**Figure 4.12.**).

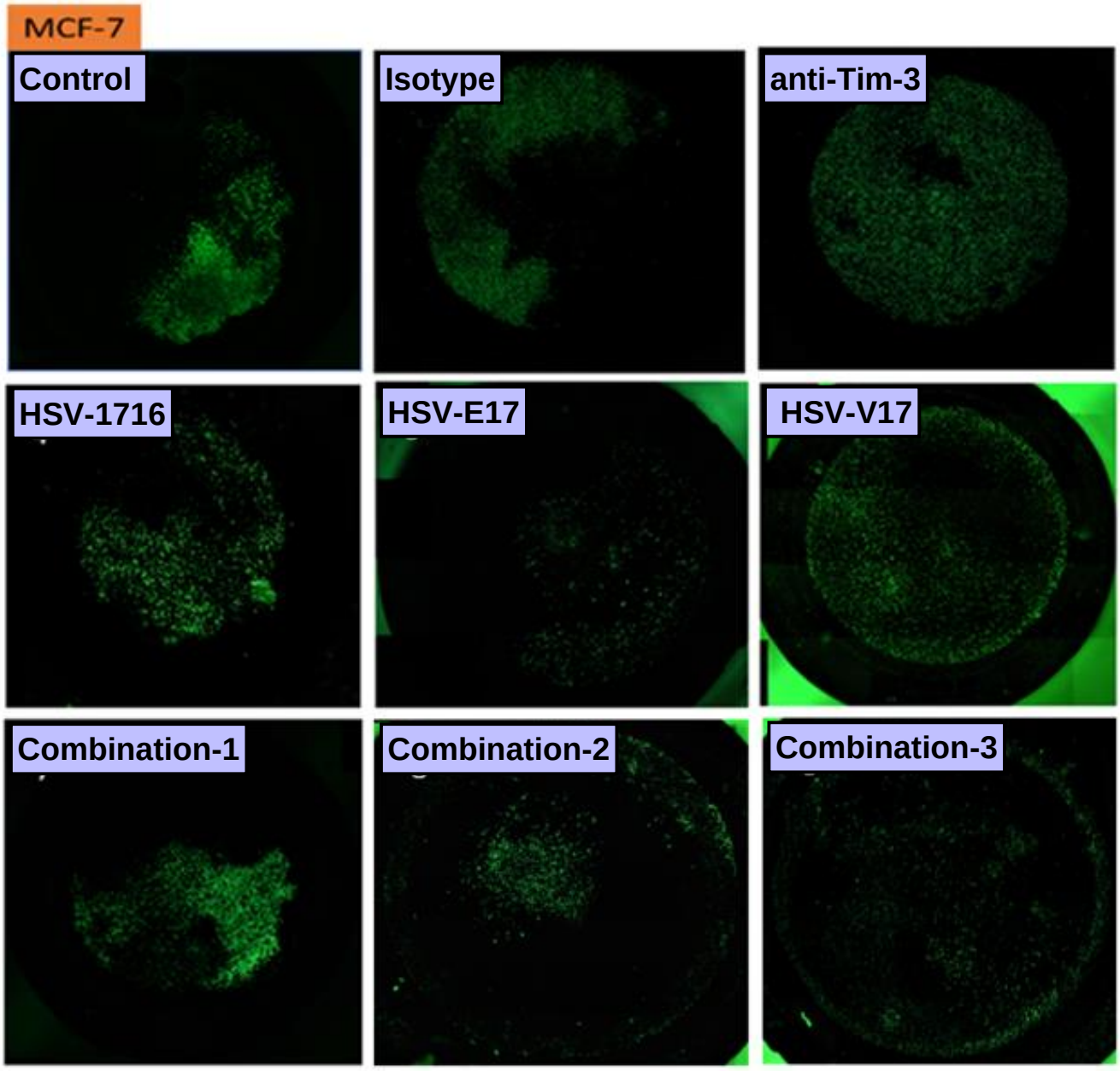

Figure 4.11. Representative images of an invasion assay following treatment with Tim-3 blocking with/without HSV-1716/-E17/-V17 on MCF-7 cell lines. *Cells were blocked with anti-TIM-3 at concentration of 5 ug/ml, with/without HSV-1716, -E17, -V17 viruses at MOI 1,3,10 respectively. Combination treatment groups were labelled with numbers and combination-1: combination of HSV-1716 and anti-Tim-3 antibody, -2: combination of HSV-E17 and anti-Tim-3 antibody, -3: combination of HSV-V17 and anti-Tim-3 antibody. Images represent non-invasive cells by green fluorescence dye and were taken from top of the transwells. This experiment was repeated 3 times and images were taken at 24 hours.*

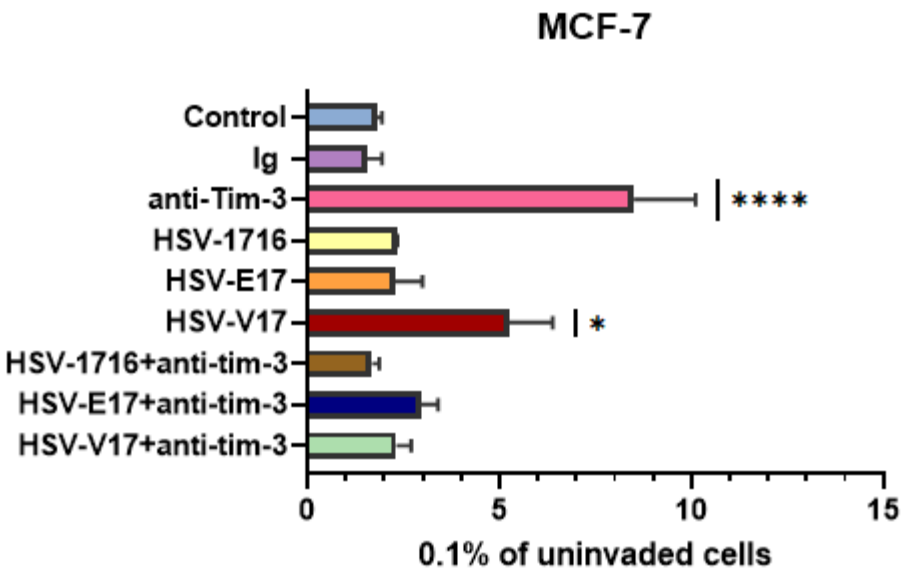

Figure 4.12. Combination of Tim-3 inhibition and HSV-V17 treatment showed reduced in invasiveness of MCF-7 cells. *Cells were blocked with anti-TIM-3 at concentration of 5 mg/ml, with/without HSV-1716, -E17, -V17 viruses at MOI 1,3,10 respectively. Treatment groups were labelled with numbers and number 1: control ,2: Ig antibody, 3: anti-Tim-3 antibody, 4: HSV-1716, 5: HSV-E17, 6: HSV-V17, 7: combination of HSV-1716 and anti-Tim-3 antibody, 8: combination of HSV-E17 and anti-Tim-3 antibody, 9: combination of HSV-V17 and anti-Tim-3 antibody. Data are mean ± SEM. This experiment was repeated 3 times, and the data are normalised to the corresponding non-treated control cells. The graphs show the uninvaded cells and were generated using GraphPad Prism software and analysed using One-way ANOVA.*

The same treatment groups were applied to MDA-MB-231 cells as in MCF-7 cell lines and imaged at 24 hours. However, no meaningful results were obtained in any group. Although the Tim-3 treatment group did not show statistical significance evaluated in terms of cell count, they exhibited a tend towards less invasion (**Figure 4.13.-number 3 and Figure 4.14.**).

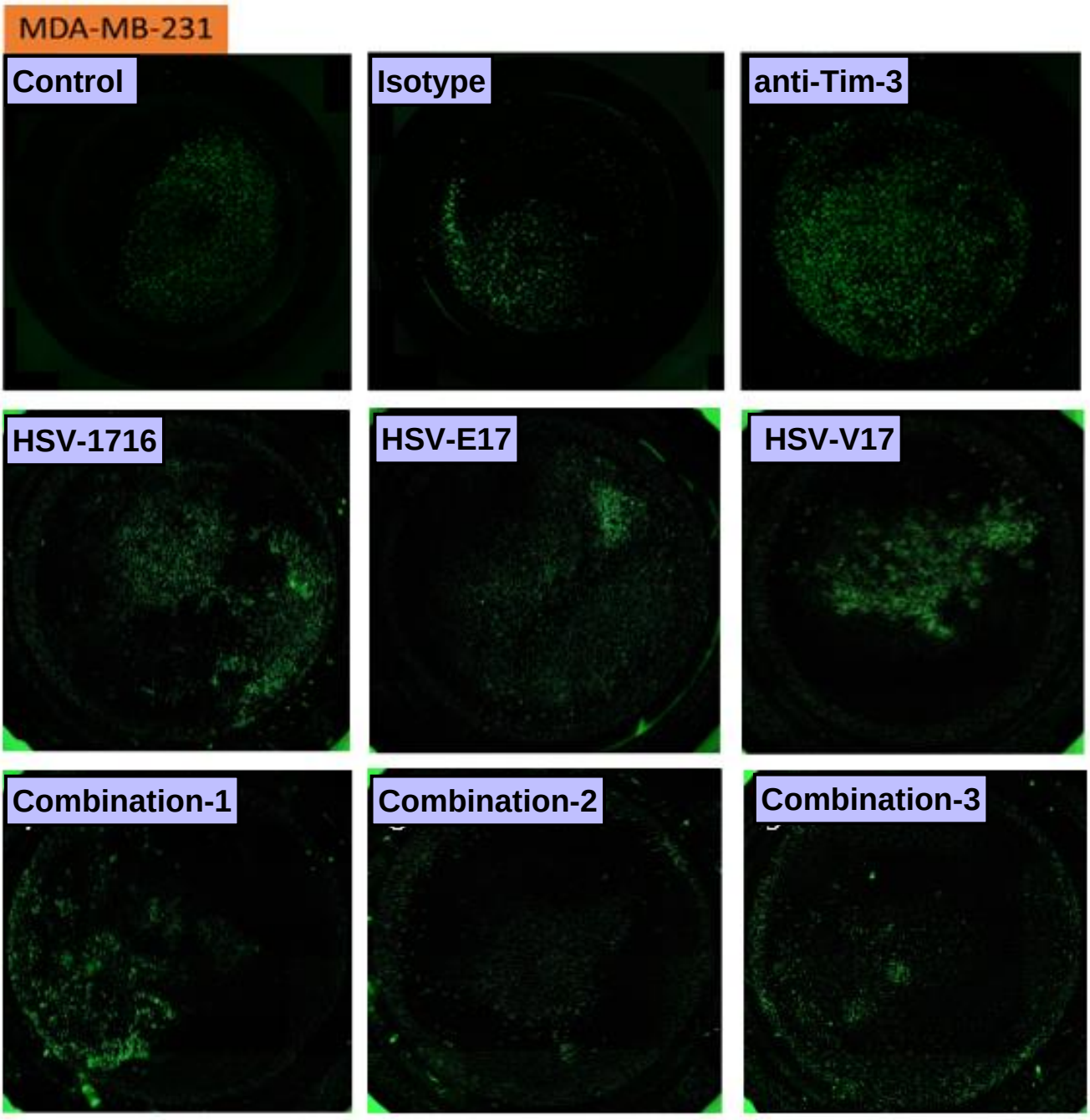

Figure 4.13. Representative images of an invasion assay following treatment with Tim-3 blocking with/without HSV-1716/-E17/-V17 on MDA-MB-231 cells. *Cells were blocked with anti-TIM-3 at concentration of 5 mg/ml, with/without HSV-1716, -E17, -V17 viruses at MOI 3,30,30 respectively. Combination treatment groups were labelled with numbers and combination-1: combination of HSV-1716 and anti-Tim-3 antibody, -2: combination of HSV-E17 and anti-Tim-3 antibody, -3: combination of HSV-V17 and anti-Tim-3 antibody. Images represent non-invasive cells by green fluorescence dye and were taken from top of the transwells. Data are mean ± SEM. This experiment was repeated 3 times and images were taken at 24 hours. This experiment was repeated 3 times and images were taken at 24 hours.*

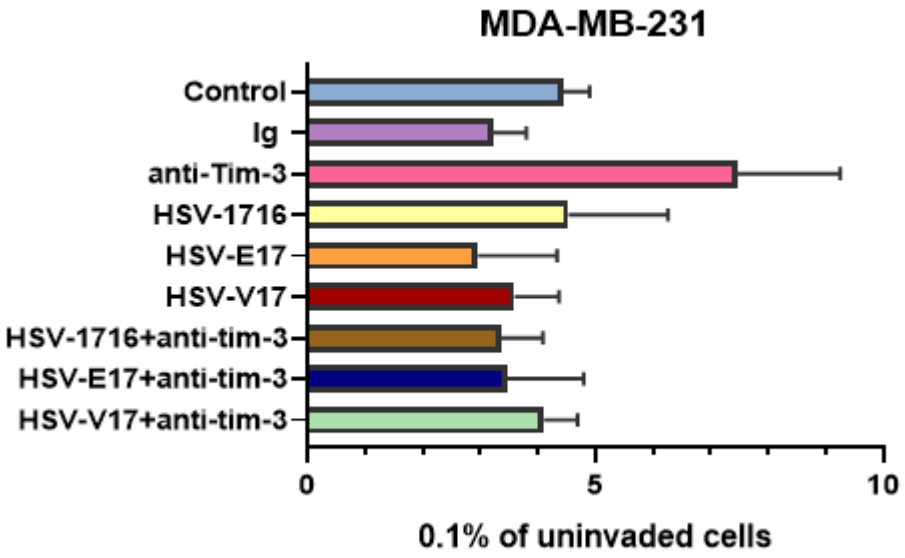

Figure 4.14. There are no significant differences on all treatment groups in invasiveness of MDA-MB-231 cells. *Cells were blocked with anti-TIM-3 at concentration of 5 mg/ml, with/without HSV-1716, -E17, -V17 viruses at MOI 1, 3, 10 respectively. Treatment groups were labelled with numbers and number 1: control ,2: Ig antibody, 3: anti-Tim-3 antibody, 4: HSV-1716, 5: HSV-E17, 6: HSV-V17, 7: combination of HSV-1716 and anti-Tim-3 antibody, 8: combination of HSV-E17 and anti-Tim-3 antibody, 9: combination of HSV-V17 and anti-Tim-3 antibody. Data are mean ± SEM. This experiment was repeated 3 times, and the data are normalised to the corresponding non-treated control cells. The graphs show uninvaded cells and were generated using GraphPad Prism software and analysed using One-way ANOVA.*

Finally, the same experiments as above were repeated in the SKBR-3 cell line and imaged at 48 hours. All HSV types exposed treatment groups (**Figure 4.15.-number-4, -5, -6**) and one of combination groups HSV-1716+anti-Tim-3 exposed treatment group (**Figure 4.15.-number 7**) had more green labelled cells (that had not invaded the Matrigel) compared to other treatment groups and control group. Furthermore, statistical analysis showed considerable changes in the same groups (**Figure 4.16.**). Although the HSV-V17 + anti-Tim-3 exposed treatment group did not show statistical significance evaluated in terms of cell count, they exhibited a tend towards less invasion (**Figure 4.15.-number 9 and Figure 4.16.**).

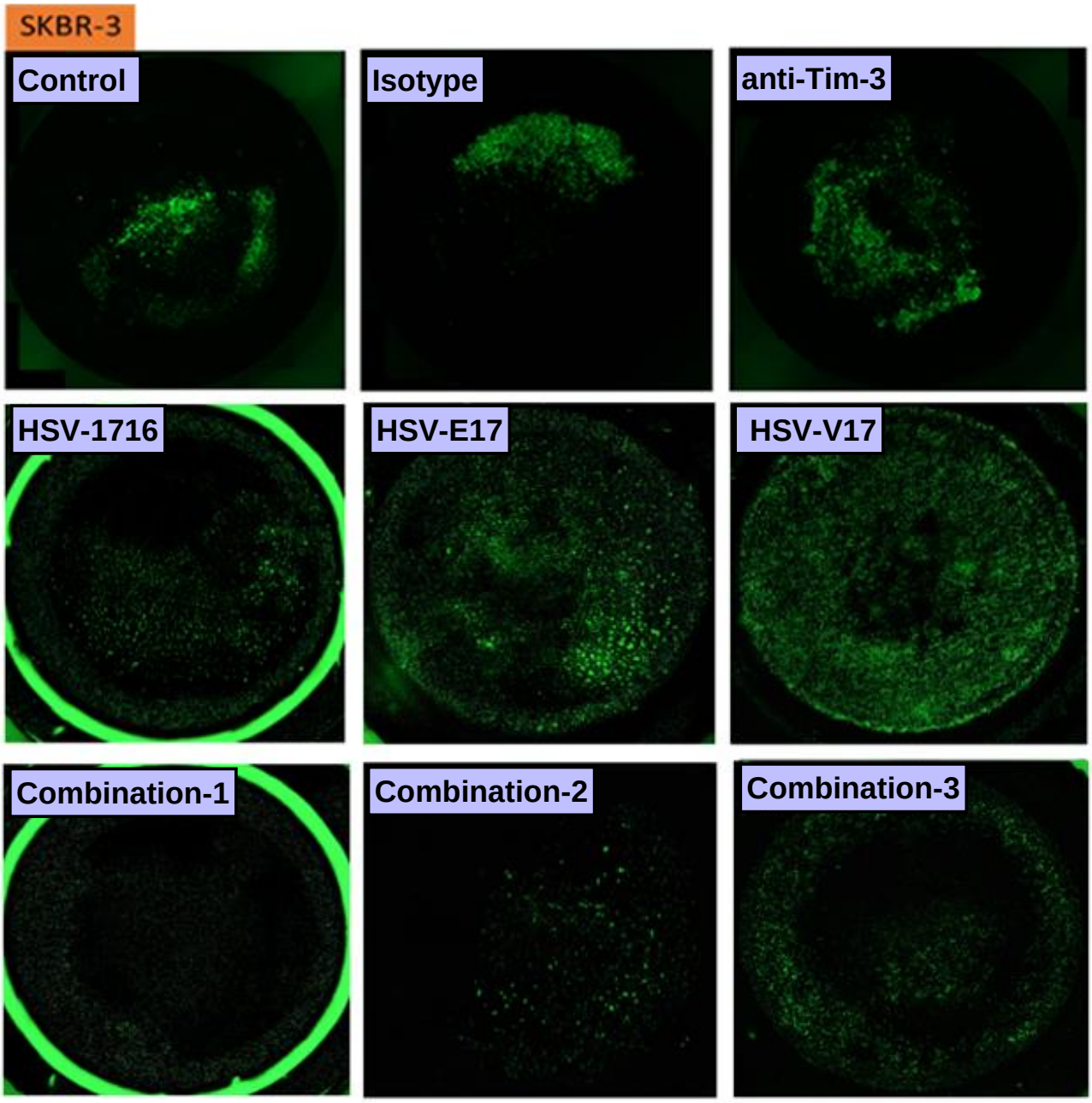

Figure 4.15. Representative images of an invasion assay following treatment with Tim-3 blocking with/without HSV-1716/-E17/-V17 on SKBR-3 cell lines. *Cells were blocked with anti-TIM-3 at concentration of 5 mg/ml, with/without HSV-1716, -E17, -V17 viruses at MOI 1, 3, 10 respectively. Combination treatment groups were labelled with numbers and combination-1: combination of HSV-1716 and anti-Tim-3 antibody, -2: combination of HSV-E17 and anti-Tim-3 antibody, -3: combination of HSV-V17 and anti-Tim-3 antibody. Images represent non-invasive cells by green fluorescent cells and were taken from top of the transwells. This experiment was repeated 3 times and images were taken at 48 hours.*

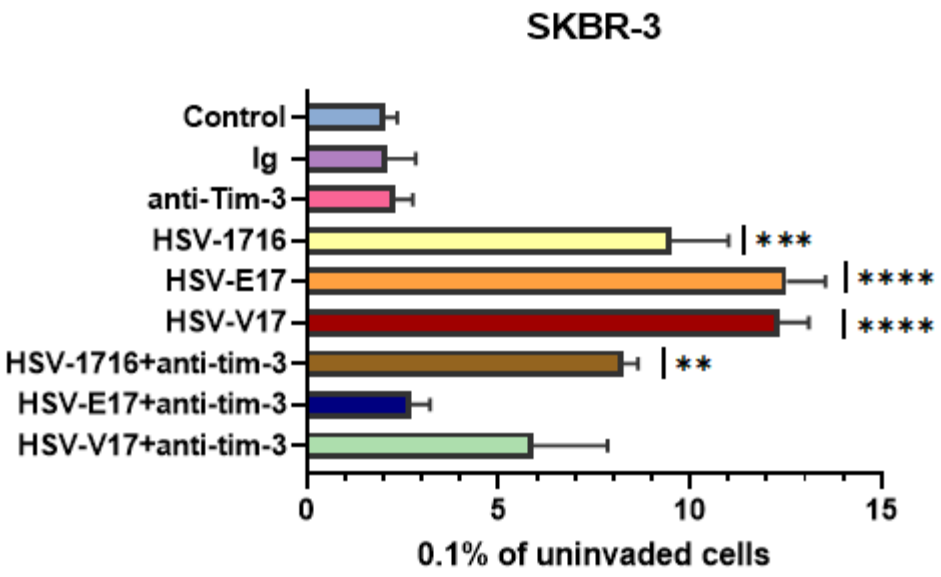

Figure 4.16. Combination of Tim-3 inhibition HSV-1716 and each of all HSV types exposed treatments showed reduced in invasiveness of SKBR-3 cells. *Cells were blocked with anti-TIM-3 at concentration of 5 mg/ml, with/without HSV-1716, -E17, -V17 viruses at MOI 1, 3, 10 respectively. Treatment groups were labelled with numbers and number1: control ,2: Ig antibody, 3: anti-Tim-3 antibody, 4: HSV-1716, 5: HSV-E17, 6: HSV-V17, 7: combination of HSV-1716 and anti-Tim-3 antibody, 8: combination of HSV-E17 and anti-Tim-3 antibody, 9: combination of HSV-V17 and anti-Tim-3 antibody. Data are mean ± SEM. This experiment was repeated 3 times, and the data are normalised to the corresponding non-treated control cells. The graphs show uninvaded cells and were generated using GraphPad Prism software and analysed using One-way ANOVA.*

4.6. Discussion

Immune checkpoints (ICs) normally prevent excessive T cell activation and maintain self-tolerance. However, disruptions in this balance, often due to epigenetic or genetic factors, can lead to cancer and upregulation of ICs, thereby suppressing T cell activity (Huang et al., 2019; Sakowska et al., 2022). This upregulation has been implicated in tumour progression across various cancers (Lisi et al., 2022; Shukla and Steinmetz, 2016; Topalian et al., 2014) and has led to the clinical use of IC inhibitors (ICIs). While ICIs have shown clinical benefits (Hargadon et al., 2018), the efficacy of these new drugs is limited in some patients, particularly with "cold" tumours that lack sufficient immune infiltration needed for the inhibitors to work(Liu and Sun, 2021). Oncolytic viruses (OVs) like the HSVs used in this chapter can reshape the tumour microenvironment (TME) by inducing immunogenic cell death and recruiting immune cells (Achard et al., 2018). This enhanced immune response can synergize with ICIs, improving their efficacy by enabling T cell infiltration into tumours (Chon et al., 2019).

This chapter investigated the effects of arming of oHSV with a Tim-3 inhibitor on cell viability, migration, and invasion *in vitro.*

First of all, the IC50 data confirmed that all three viruses reduced cell viability across all the human BC cell lines. The most studied of these viruses (HSV-1716) had a more pronounced effect on cell viability in the first 24 hours in all cell lines. However, this effect was not so evident over the 7 days period. The other 2 viruses (HSV-E17, HSV-V17) were also effective, and this is the first time this has been demonstrated in any cancer. For instance, in the MCF-7 cell line, HSV-E17RL1del7 showed a decreasing-increasing-decreasing graph on 2nd, 5th, and 7th post infection days, respectively, while the efficacy in the SKBR-3 cell line showed an increasing-decreasing-increasing cell viability. It is not clear why this is the case and more experimental repeats may help confirm if this is a genuine phenomenon. It could be that the different subtypes of BC influence their sensitivity to HSV.

For example, the doubling time of MCF-7 is 30-40 hours, while this time is 20 hours for MDA-MB-231 and so the rate of cell growth may influence infection. Also, the HSV viral life cycle is 18-20 hours. Therefore, the doubling time of the MDA-MB-231 cell line and the virus are close to each other and may have an effect on the transformation of the efficacy in a decreasing and then increasing trend. It is also possible that the different BC cells express different levels of HSV-1 cell surface receptors, and this could affect infection kinetics.

Furthermore, these viruses have different genetic modifications, and this could lead to the differences observed, as mutations in the virus glycoproteins could affect HSV-1 cell attachment factors (Peters and Rabkin, 2015). It is interesting that HSV-V17RL1del2 works better at the longer time point, and this could be important in a therapeutic setting as it would give longevity to the response. It is the first time that we have seen long lasting responses to a HSV virus our previous research on HSV-1716 was limited to earlier timepoints (Kwan et al., 2021). If time was permitting, additional methods for investigating cell death would be employed to confirm these data and confirm mechanisms of cell death. For example, previous studies from our team have shown that HSV-1716 (MOI 10) induces immunogenic cell death in BC cells (MDA-MB-231 and E0771) with an upregulation in ATP, HMGB1 and expression of calreticulin, in immunogenic cell death (ICD) markers (IFN-ϒ, HSPA1A, NF-κβ, and TNF-α), non-ICD marker (LC3B) and apoptosis (CASP3 and CASP8) were significantly upregulated (Howard et al., 2022). This could be done using ELISA assay, ENLITEN ATP assay and, Real Time PCR.

Once the IC50 data for the viruses were obtained, the effect of Tim-3 blocking alone and, in combination with HSV-1716 in all the human BC cell lines was investigated. Tim-3 inhibition on its own was least effective at reducing cell death even across the 7 days incubation. However, the combination with HSV-1716 showed a significant decrease across all the anti-Tim-3 antibody concentrations suggesting that OV makes the cell lines more sensitive to the inhibitor.

Next the effect of the OV and anti-Tim-3 ICI on 2 mouse BC cell lines was investigated. 4T-1 and E0771 cells are different subtypes of BC. For instance, 4T-1 has a metastatic profile and the doubling is 12.6 hours. Whereas E0771 is poorly metastatic compared to 4T-1 and doubling occurs in 5-6 days, while the HSV viral life cycle is 18-20 hours, which may have an effect on the transformation of the efficacy and stability of the antibody. The decreased viability of Murine BC cells after HSV-1716 infection in vitro suggests that HSV-1716 has cancer cell-killing capacity at a MOI 3.

Across the research, there was a significant decrease in the viability of BC cells in both the HSV-1716 treated groups, whether alone or in combination with an Ab. Both mAbs (Isotype Ab and Anti-Tim-3 Ab) were examined in the viability assay to determine their role in toxicity and cancer cell growth. They show no symptoms of toxicity to cells at first, but there is a decrease in cells viability on days 5 and 7. The identical findings of the combination therapy and standalone OVT demonstrate that the addition of the anti-Tim-3 Ab together with the OV HSV-1716 does not impair viral function. Because HSV-1716 alone and in combination with the Ab have a similar cytotoxic impact on BC cells, it may be concluded that HSV-1716 and anti-Tim-3 Ab are complimentary in vitro.

Previous studies have established that TIM-3 is upregulated in various cancers (Baitsch et al., 2011; Fourcade et al., 2010; Gao et al., 2012a). This upregulation has been linked to increased cell proliferation, migration, and invasion including BC cells (Cheng et al., 2018), HCC cells (Lin et al., 2017), glioblastoma (Guo et al., 2022a). Furthermore, it was found to be significantly correlated with clinical stage and metastasis (Cheng et al., 2018) in BC patients and with pathogenesis and cancer progression in NSCLC patients (Gao et al., 2012a). Our own findings from the migration and invasion assays align with these observations. In MCF-7 and SKBR-3 cell lines, all treatment groups significantly impeded migration, with the HSV-1716 + anti-Tim-3 combination showing the most potent effect. Similar patterns were observed in the invasion assay. In MCF-7 cells, anti-Tim-3 treatment alone and HSV-V17 significantly inhibited invasion, with anti-Tim-3 again showing the strongest effect.

In SKBR-3 cells, all HSV-based treatments and the HSV-1716 + anti-Tim-3 combination significantly reduced cell invasion. However, MDA-MB-231 cells, a more aggressive subtype, exhibited any significant resistance to all treatments for migration and minimal response to invasion (**Figure 4.9. and 4.14.**). This suggests that the efficacy of this treatment approach may vary depending on tumour subtype and aggressiveness and this may need to be considered for patient treatment. Of note, the invasion assay used in this project counted noninvaded cells, therefore another invasion methods could be used to improve the data such as staining and counting cells that had invaded (Justus et al., 2014).

Our findings align with previous studies demonstrating the pro-migratory and pro-invasive roles of TIM-3 in epithelial ovarian cancer and BC. These previous studies examined the migration and invasion effects on over-expression and depleted Tim-3 genes using pcDNA/ADV-Tim-3 (recombinant adenovirus vectors containing a fragment of Tim-3 cDNA) or siRNA to knockdown Tim-3, in vitro. Silencing the Tim-3 inhibited the migratory and invasiveness of cells while over-expression of Tim-3 improved these abilities (Cheng et al., 2018; Huo et al., 2022) .

Whilst this chapter focuses on cells grown in 2D, our findings indicate the diverse responses of BC cell lines to treatment, even within the same disease. This variability likely stems from differences in tumour subtypes and their associated ER/PR/HER2 status, as well as varying levels of Tim-3 expression observed in section **3.2**. Additionally, the order of treatment administration could impact efficacy. HSV infection might neutralize the anti-Tim-3 antibody, suggesting that delaying antibody treatment after HSV infection (2-4 hours) might be more effective. Optimizing treatment schedules and considering subtype-specific responses will be crucial for maximizing therapeutic benefit.

Despite these divergences, our findings provide compelling evidence for the potential of combining oHSV and anti-Tim-3 antibodies to suppress migration and invasion in BC cell lines. This aligns with previous studies highlighting the pro-migratory and pro-invasive roles of TIM-3.

If more time was permitted, it would be important to determine how this drug combination works in 3D models of BC using tumour spheroids and is discussed in the future work section (chapter 6). The next chapter will delve further into exploring this promising treatment strategy in an animal model of BC.

Summary

This chapter showed for the first time the effects of inhibiting Tim-3 in combination with the virus HSV-1716 in BC cell lines *in vitro*. The data showed a significant reduction on tumour cell viability, cell migration and invasion in MCF-7 and SKBR-3 but this was not statistically significant in the aggressive MDA-MB-231 cells.

CHAPTER 5

The effect of anti-Tim-3 and HSV-1716 in animal models of BC

5.1. Introduction

Animal models are often used to investigate drug mechanisms/efficacy and disease pathways in preclinical research to mimic human pathology. These include syngeneic and xenograft models offering a tumour microenvironment (Le Naour et al., 2020a) with normal immune system function. These are called immunocompetent murine models (Tao et al., 2008a). Moreover, orthotopic transplantation of tumour cells, such as BC mouse cells into the mammary fat pad, mimics primary tumour growth leading to spontaneous metastasis similar to human cancers including tumour vascularity, metastatic pathway, histology, gene expression, resistance to chemotherapy (Khanna and Hunter, 2005). Cancer cells can also be implanted into the blood circulation such as intracardiac infusion for bone metastasis, tail vein injection for lung metastasises or portal vein injection for liver metastasis. However, implanting into the circulation is an opportunity for assessing organ colonization, not for metastatic processes (Fantozzi and Christofori, 2006).

Xenograft models is where the cancer cells are derived from different species such as human cancer cells. For this to be successful the immune system is suppressed in these mice to prevent graft reaction and these are called immunocompromised animals (Khanna and Hunter, 2005). These mice tend to lack an adaptive immune system and whilst useful for studying human tumours it is not possible to study complexed immunity (Clarke, 1996). Therefore, the advantage of syngeneic models is that they have normal immune system function allowing us to investigate cancer processes/therapeutics and the immune response (Fantozzi and Christofori, 2006; Khanna and Hunter, 2005). Two very common strains of mice for studying BC are C57BL/6 and Balb/c (Le Naour et al., 2020b). C57BL/6 became the first genome sequenced inbred strain (Waterston et al., 2002) and is receptive to mutations for genetic engineered research while refractory to many tumours including BCs (Le Naour et al., 2020b). Balb/c mice are useful as tumours implanted in these mice have the ability to spontaneously metastasise, and it has been showed they mimic advanced malignant BC metastasis in humans (Kau et al., 2012; Rashid et al., 2013; Tao et al., 2008b). For instance, in the 4T-1 syngeneic model, tumour cells quickly metastasise to brain, lung, liver and bone (Fantozzi and Christofori, 2006).

There are genetically engineered mouse models (GEMMs) (Regua et al., 2021) and organoid models of BC (Srivastava et al., 2020). GEMMS are used to investigate genetic modifications on BC progression and types include tumour suppressor gene knock-out, tumorigenesis by cell fate/differentiation modulators, tumorigenesis by cell cycle regulators, tumour induction by virally-derived oncogenes, spontaneous tumorigenesis by receptor signalling, tumour induction by specific promoters and inducible transgenic BC murine models (Regua et al., 2021). An example of a GEMMS model, is the Polyoma Middle T (PyMT) antigen-derived model, which is used for studying TNBC in C57BL/6 or FVB mice and was first described in 1992. PyMT is transmembrane protein and promotes tumorigenesis activating PI3-kinase/AKT, MAP kinase, and PLC-γ signalling pathways (Regua et al., 2021). A disadvantage of this model is that it can take many weeks for multiple primary tumours to develop (14 weeks) and as a result it is no longer viable for studying metastasis as the animals need to be culled due to the substantive tumour burden caused by the primary tumours (Attalla et al., 2020). As mentioned above, there are a number of preclinical BC models that pertain to the different BC subtypes in different murine strains. The majority of these are TNBC, most likely because these are aggressive and grow well. This limits the models to some extent but can be overcome by using xenograft or patient derived xenograft (PDX) models (Souto et al., 2022). Mouse models of BC are highlighted in **Table 5.1.**

BC Organoid models are an exciting recent alternative that entail embedding mammary epithelial fragments usually derived from patient samples in extracellular matrix and growing these in 3D cultures. These provide a platform that allow investigation of cellular and structural functions such as cell adhesion and matrix interactions, tissue morphology and environmental factors that impact on tumorigenesis (Srivastava et al., 2020). This important for clinically relevant cancer research and investigating treatment modalities in vitro in a more sophisticated preclinical model. Organoids are still early in their development as models and a downside to their use is sustaining the cultures long-term as the cells often die after a few days of culture. It is also necessary to have more standardised methods for processing organoids and understanding their culture and storage.

Table 5.1. Examples of murine BC models, the subtypes, strain of mice and method for implantation.

BC cell subtypes	Mice strain	Implantation method	Reference
4T1/4T07 (TNBC)	BALB/c	Tail vein/ orthotopic – mammary fat pat	(Aslakson and Miller2, 1992)
E0771 (ER+, PR-, HER2-)	C57BL/6	Subcutaneous/ orthotopic – mammary fat pat	(Sugiura and Ciiester Stock, n.d.) (Johnstone et al., 2015a)
E0771 (ER+, PR-, HER2-)	C57BL/6	Intracardiac and intramammary	(Hiraga and Ninomiya, 2019)
D20R/D2A1 (ER+, PR-, HER2-)	SCID	Tail vein	(Naumov et al., 2003)
EMT-6 (TNBC)	BALB/c	Tail vein	(Gauthier et al., 2004)
LM3 (ER+, PR+, HER2-)	BALB/c	Tail vein/ orthotopic – mammary fat pat	(Peters et al., 2003)
M6C (TNBC)	FVB	subcutaneous	(Holzer et al., 2003)
Metastatic BC	FVB-PyMT	GEMMS	(Guy et al., 1992; Lifsted et al., 1998)

In the previous chapter it was shown that anti-Tim-3 and oHSVs displayed cytotoxic and anti-tumour-properties *in vitro*. The aim of this chapter was to assess the effects of anti-Tim-3 with/without HSV-1716 treatment in primary mouse mammary carcinoma models. This will allow an investigation into antitumour immunity in a more complex model. HSV-1716 was used as this was the most characterised of our oHSVs and has been widely tested in mouse models by us and others (Benencia et al., 2008; F. Howard et al., 2022; Kwan et al., 2021; Lambright et al., 1999; Toyoizumi et al., 1999).

Two types of BC mouse cell lines (E0771 and 4T-1) were used and implanted into the mammary fat pads of C57BL/6 and Balb/c mice, respectively. EO771 is a murine breast adenocarcinoma cell line derived from C57BL/6 mouse at the Jackson laboratory in 1940(Dunham and Stewart, 1953.; Sugiura and Ciiester Stock, 1952). EO771 is a basal-like BC, which is positive for ER, negative for PR and HER2, and develops metastasis to the lung in C57BL/6 mice (Johnstone et al., 2015b). 4T-1 is a murine BC cell line isolated from Balb/c mice (Miller et al., 1988)and metastasises to the lungs, liver, bone and brain (Yoneda et al., 2000; Lelekakis et al., 1999; Yang et al., 2004).

The specific objectives were to determine the anti-tumour effects of;

- Anti-Tim-3 and HSV-1716 on mouse body weight and mouse survival in E0771 and 4T-1 preclinical mouse models.
- Anti-Tim-3 and HSV-1716 on mammary tumour growth in E0771 and 4T-1 preclinical mouse models.
- Anti-Tim-3 and HSV-1716 on tumour necrosis in E0771 and 4T-1 preclinical mouse models.
- Anti-Tim-3 and HSV-1716 on tumour metastasis to the lung/liver in E0771 and 4T-1 preclinical mouse models.

5.2. *In vivo* study design

4T1-LUC cells and E0771-LUC cells (1x10^5 cells/mice) were implanted via intranipple injection into Balb/c and C57BL/6, respectively. Tumour progression was monitored every 2 days by manual measurement using callipers, alongside daily animal weighing. Each mouse strain was randomly divided into groups of n=8 mice. They received the first treatment when tumour size reached ~100 mm^3. For Balb/c mice three doses were given in each treatment group on consecutive days, while C57BL/6 were given once a week. This treatment was based on tolerability to HSV-1716 as determined by our research group (Howard et al., 2022). HSV-1716 treatment was given intravenously (IV) while anti-Tim-3 antibodies were received via the intratumoural route (Ju et al., 2022b) (**Figure 5.1.**).

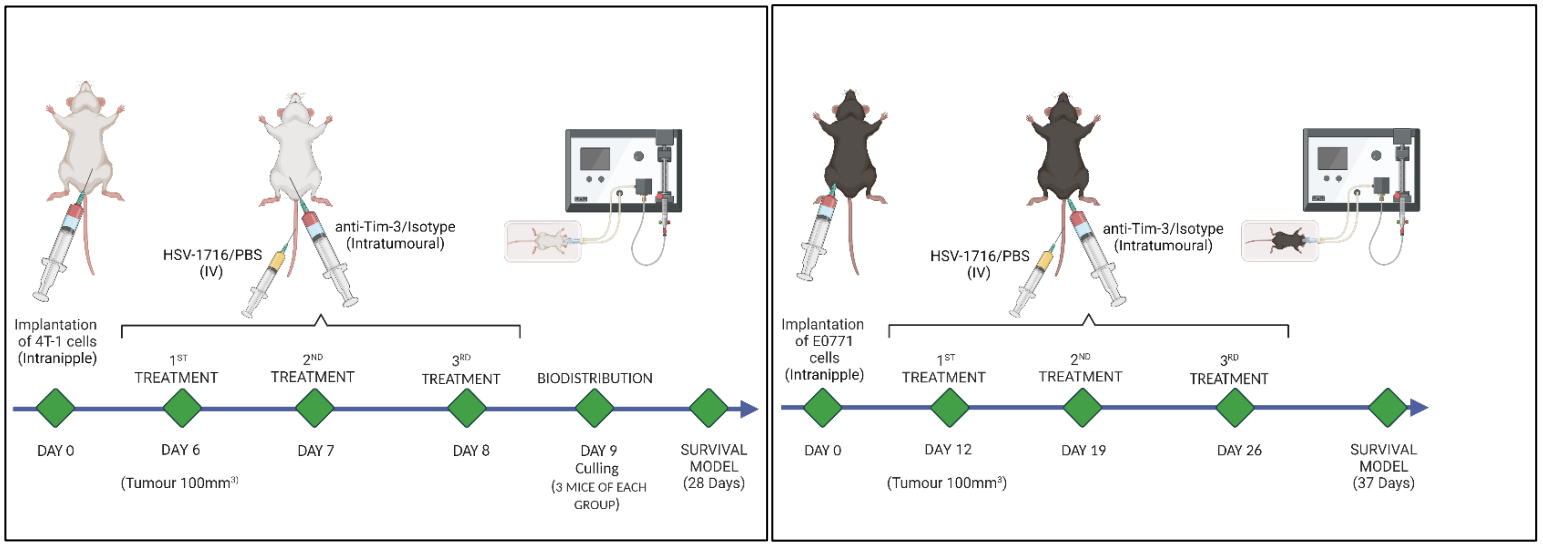

Figure 5.1. Schematic diagram to demonstrate the in vivo study design and treatment regimens for both mice strain.

The 5 treatment groups were as follows;

1. **Control mice:** Injected IV with PBS in a volume 0.1 mL.

2. **Isotype mice:** Injected intratumourally with isotype antibody (200 mg/mice) in a volume 0.1 mL.

3. **Anti-Tim-3 mice:** Injected intratumourally with anti-Tim-3 antibody (200 mg/mice) in a volume 0.1 mL.

4. **HSV-1716 mice:** Injected IV with HSV-1716 (10^5 pfu/mice for Balb/c and 10^6 pfu/mice for c57bl/6) in a volume 0.1 mL.

5. **Combination therapy:** Injected IV with HSV-1716 (10^5 pfu/mice for Balb/c and 10^6 pfu/mice for C57BL/6) in a volume 0.L ml and intratumoural with anti-Tim-3 antibody (200 mg/mice) in a volume 0.1 mL.

Treatments were conducted in the same manner for both strains except for treatment days. Firstly, a small study of n=3 mice of each treatment group were culled for biodistribution study after 24 hours of the final treatment. Blood and organs (kidneys, spleen, brain, lung and liver) and tumours were extracted for post-mortem analysis studies. Following that, the remaining mice were allowed to reach the maximum permitted size of an average of 12 mm diameter. Overall, humane endpoints for this study included ulceration of tumours, neurological deficit (mobility issues, head tilting, extreme sensitivity and seizures), weight loss prior to culling, extraction of blood/organs/tumours same as biodistribution study for survival model. Mice experiencing any of these were culled immediately (**See Appendix 7.1. for ISP**)

5.3. Tumour growth in response to anti-Tim-3 and HSV-1716 treatment

To evaluate the impact of anti-Tim-3 with/without HSV-1716 treatment on tumour growth, 4T-1-bearing Balb/c mice were used (n=40) and E0771-bearing C57BL/6 mice (n=40) were used. Tumour volume was measured 3-4 times weekly using callipers. Once tumours reached approximately ~100 mm^3, treatment began as described in **section 2.2.11.1**. In the Balb/c model, tumours grew steadily, and treatment commenced on days 6, 7, and 8. While not statistically significant, all treatment groups displayed reduced tumour growth compared to the control group (**Figure 5.2.**). Notably, HSV-1716 monotherapy showed the most pronounced reduction, followed by the combination therapy group.

Tumour growth in the C57BL/6 model was more variable, with treatment starting on days 14, 21, and 28. Diverse trends were observed in response to treatments, and this was not expected as normally these tumours grow relatively quick. Initially, tumour growth in mice receiving HSV-1716, anti-Tim-3, or in combination was delayed until the second dose. Notably, the combination therapy group showed a reduction in tumour growth between the second and third doses, but then a sharp increase before the final dose. Interestingly, the combination group maintained the smallest overall tumour volume, even though the differences were not statistically significant (**Figures 5.3.**).

Further analysis revealed that all treatment groups initially resembled each other in terms of tumour growth for the first four days after the first dose. However, a sudden increase in tumour volume occurred for all groups by day 18, continuing until the third treatment. Notably, following the final dose, the combination group's tumour volume increased at a significantly slower rate than the other groups, hinting at a potential regulatory effect (**see Appendix Figure 7.2.2.**). It is also important to note that no significant differences in body weight were observed across all treatment groups compared to the control group, confirming no adverse effects on overall health (**Figure 5.4.**).

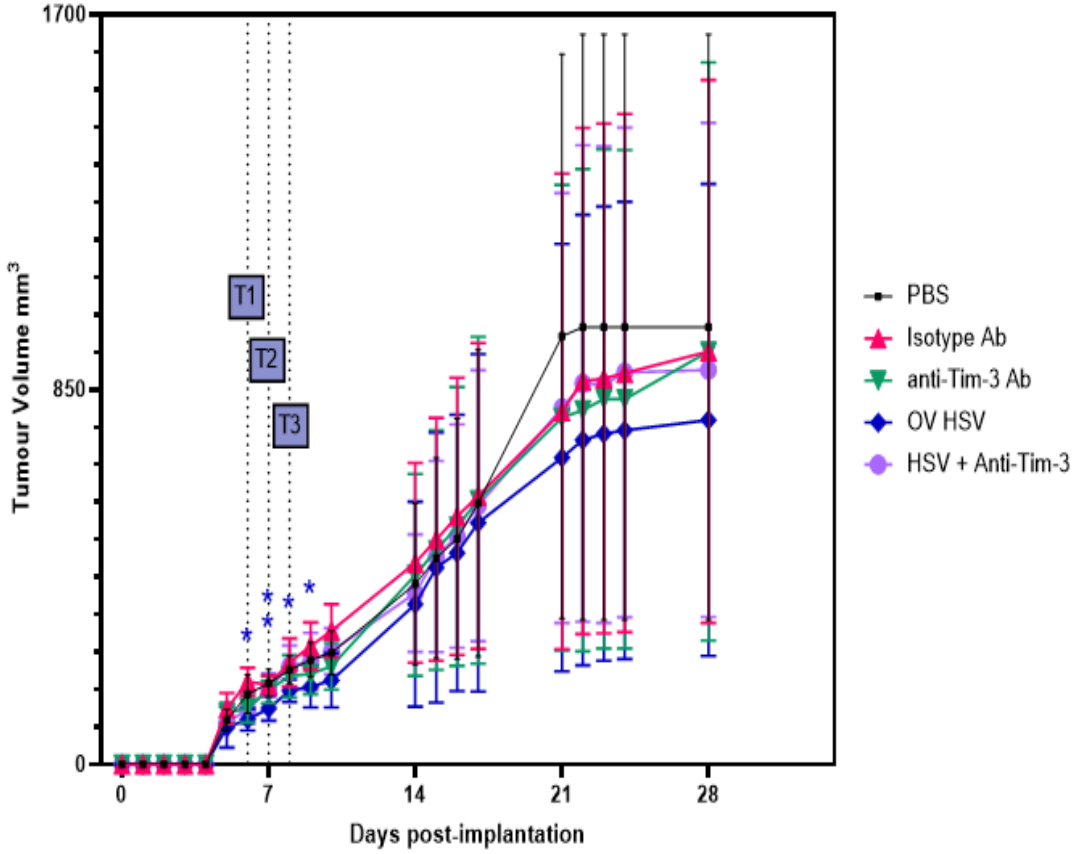

Figure 5.2. Overall tumour volume (mm3) post treatment of mice following implantation of 4T1. *Balb/c mice tumour volume was measured daily across all treatment groups including control (black), Isotype ab (pink), anti-Tim-3 ab (green), HSV-1716 (dark purple), combination (light purple) until when the last surviving mice of the study reached their humane endpoint. Result shown as mean ± SEM for a last observation carried forward with an n=8 mice per treatment group where * = p<0.05 after the 2-way ANOVA with multiple comparisons between each treatment group.*

.

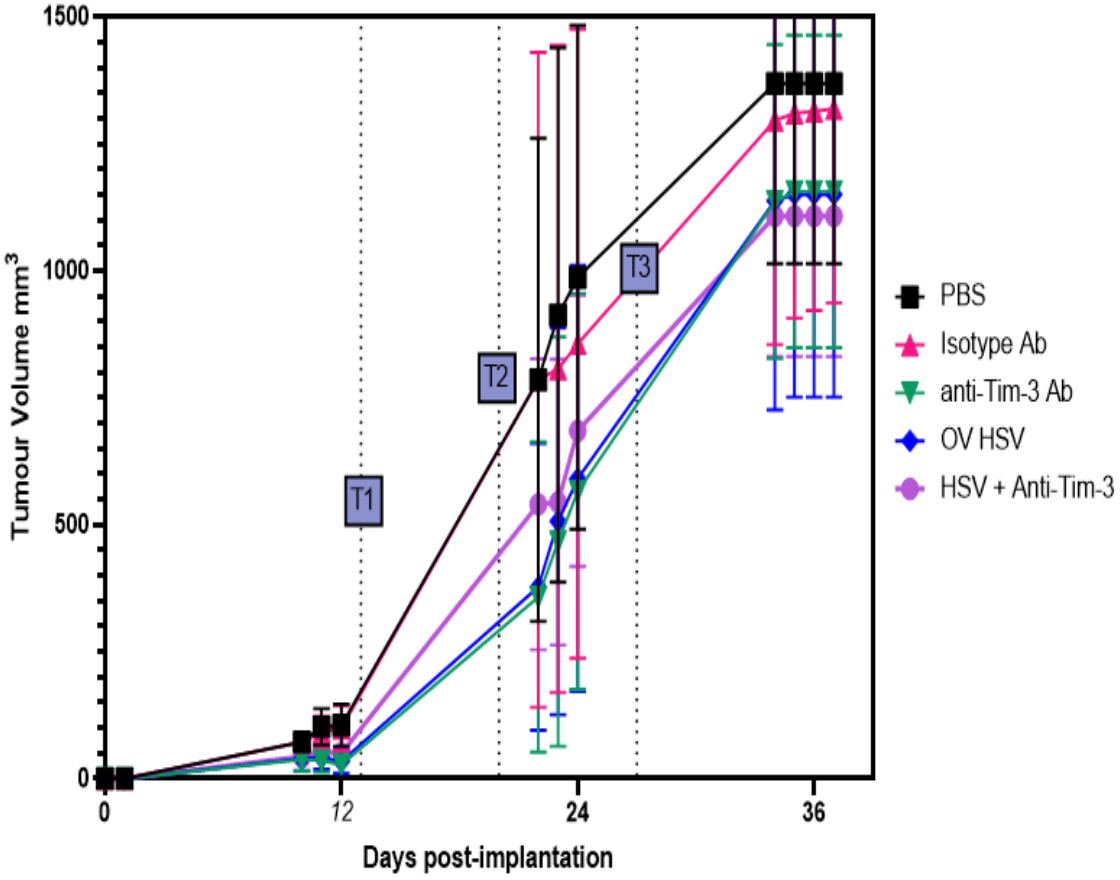

Figure 5.3. Tumour volume (mm^3) post treatment of mice following implantation of E0771. *C57BL/6 tumour volume was measured daily across all treatment groups including control (black), Isotype Ab (pink), anti-Tim-3 Ab (green), HSV-1716 (dark purple), combination (light purple) until when the last surviving mice of the study reached their humane endpoint. Result shown as mean ± SEM for a last observation carried forward with an n=8 mice per treatment group where * = p<0.05 after the 2-way ANOVA with multiple comparisons between each treatment group.*

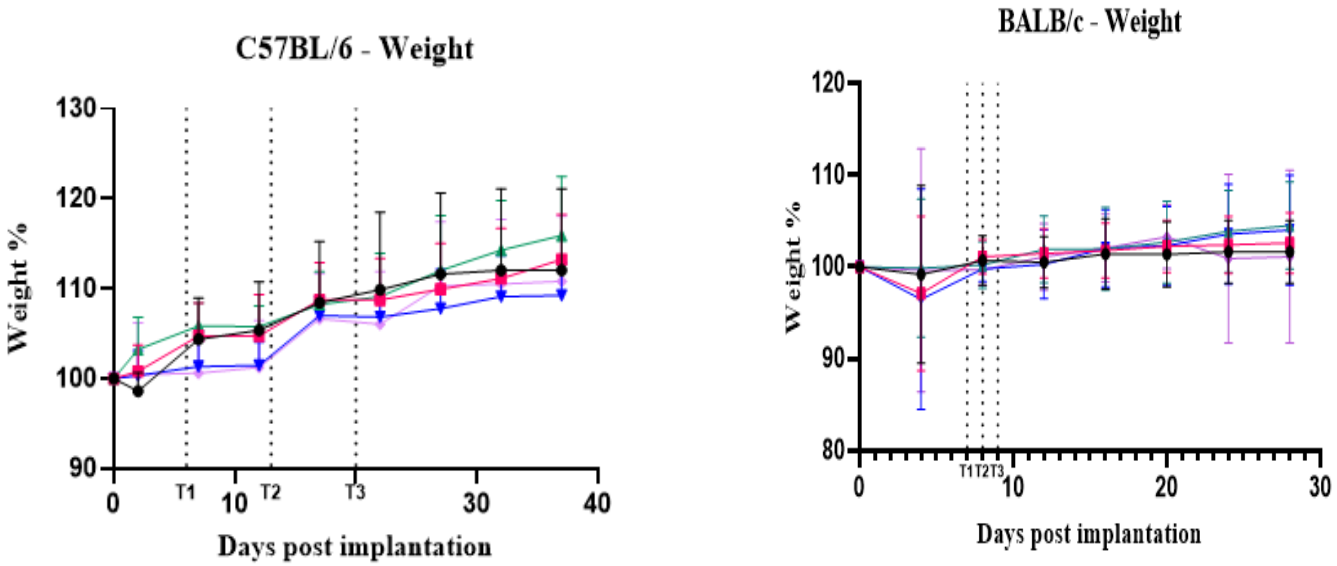

Figure 5.4. Anti-Tim-3 and HSV-1716 treatment did not affect mouse weight. *Balb/c and C57BL/6 mouse body weights were measured daily across all treatment groups including control (black), Isotype ab (pink), anti-Tim-3 ab (green), HSV-1716 (dark purple), combination (light purple) until they were culled. Result shown as mean ± SEM with n=8 mice per treatment group*.

5.4. Mouse survival in response to anti-Tim-3 and HSV-1716 treatment

To assess the impact of anti-Tim-3 with/without oHSV treatment on survival, 4T-1 tumour-bearing Balb/c mice (excluding the biodistribution group) and all E0771 tumour-bearing C57BL/6 mice were used. Survival times were recorded until humane endpoints were reached, as defined in **section 2.2.11.1** (e.g., ulceration, neurological deficit, weight loss). Overall survival was analysed using the Kaplan-Meier survival test.

In the 4T-1 model (Balb/c mice), anti-Tim-3 and isotype antibody groups displayed improved survival rates compared to control mice (**Figure 5.5.**). Although there is not a statistically significant distinction between the control group and treatment groups, control group mice presented 6 days shorter survival period than the anti-Tim-3 treated mice. Unfortunately, in the HSV-1716 alone and combination therapies some mice were culled before maximum tumour size was reached and this has likely impacted on the survival data. This was because a substantial number of mice developed ulceration, necessitating early euthanasia and limiting sample size for endpoint analysis. For instance, in the HSV-1716 and combination groups, the last surviving mouse was culled on day 25, while the last surviving mouse in the antibody only groups were culled on day 28.

Similarly, in the E0771 model (C57BL/6 mice), no statistically significant differences in survival were observed between control and treatment groups **(Figure 5.6.)**. However, it is noteworthy that the last surviving mouse in the HSV-1716 alone group and two in the anti-Tim-3 alone group were sacrificed due to ulceration on day 35. Despite the lack of statistical significance, these observations hint at a trend towards improvement in survival with HSV-1716 and anti-Tim-3 treatments.

Overall, all treatments were well-tolerated with no cancer-related mortality. The observed ulceration, however, likely impacted survival rates and may mask potential treatment benefits. Future studies with improved ulceration management strategies are needed to provide a more definitive assessment of the survival impact of these treatments.

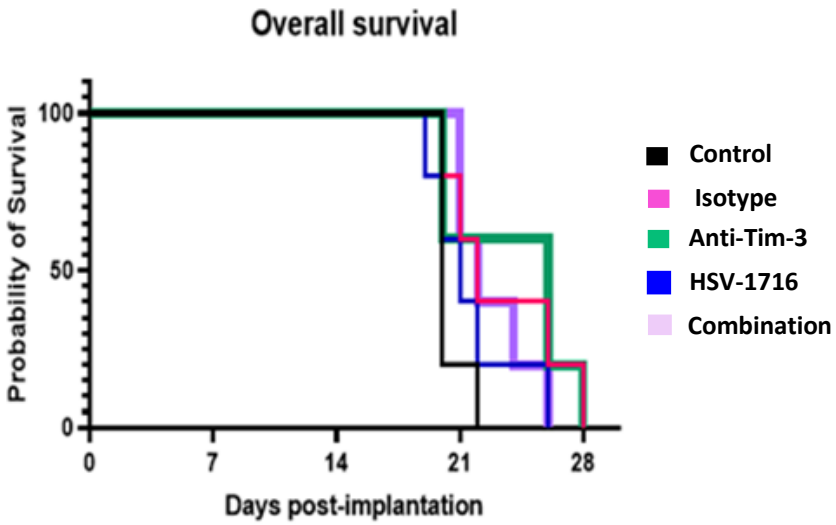

Figure 5.5. Overall animal survival post treatment of mice following implantation of 4T1*. A graph of survival plotted against Days (post implantation) to understand the survival rates of the BALB/c mice treated with the 5 different treatment groups including control (black), Isotype ab (pink), anti-Tim-3 ab (green), HSV-1716 (blue), combination (light purple). A Log-rank (Mantel Cox) test was conducted to analyse the survival curve with n=8 mice in each treatment group.*

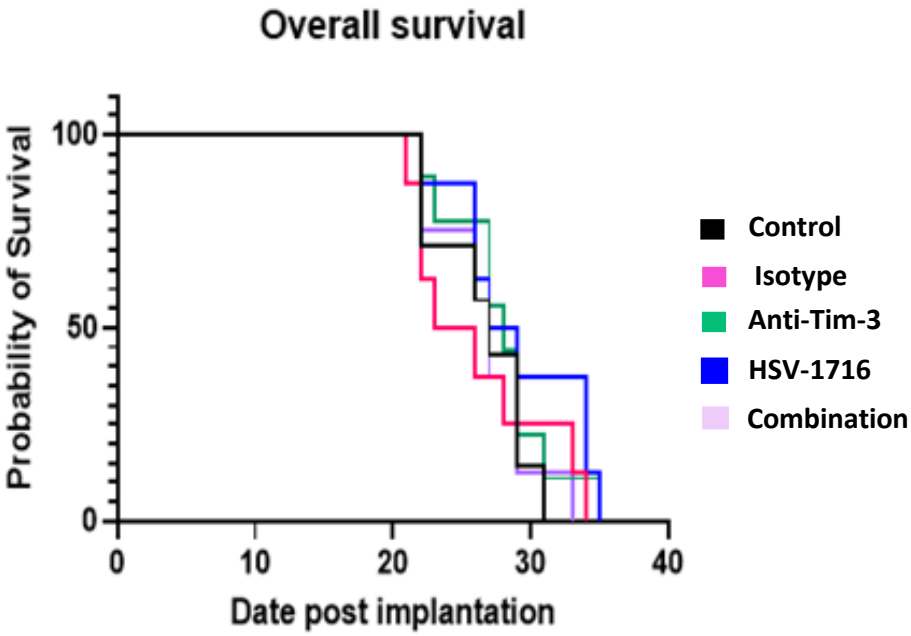

Figure 5.6. Overall animal survival post treatment of mice following implantation of E0771. *A graph of survival plotted against Days (post implantation) to understand the survival rates of the C57BL/6 mice treated with the 5 different treatment groups groups including control (black), Isotype ab (pink), anti-Tim-3 ab (green), HSV-1716 (blue), combination (light purple). A Log-rank (Mantel Cox) test was conducted to analyse the survival curve with n=8 mice in each treatment group.*

5.5. Anti-Tim-3 and HSV-1716 increased tumour necrosis in 4T1 and E0771 mouse models of BC

H&E staining is a simple but powerful technique that is used to identify different tissue types and structural changes in cancer. Haematoxylin stains nuclei a deep blue-purple colour, while eosin stains proteins in the cytoplasm and extracellular matrix pink. In a healthy tissue sample, the nuclei are clearly defined, and the cytoplasm and extracellular matrix are evenly distributed. In cancerous tissue, the nuclei are often enlarged or misshapen, and the cytoplasm and extracellular matrix may be disrupted or altered. These changes can be used to identify cancer and to determine the type, stage and grade of the tumour (Fischer et al., 2008).

Mouse tumour samples were immediately embedded in OCT following removal from mice and then stored in -80°C until these were cryosectioned. Slides were imaged after staining with H&E and imaged with a Panoramic slide scanner as described in **section 2.2.11.2.** These images were used to assess the impact of treatments on tumour necrosis. Necrosis is a type of cell death resulting from leaking of intracellular contents as a danger signal to the extracellular environment displaying cytoplasmic swelling, irreversible plasma membrane damage and organelle breakdown (Festjens et al., 2006). Necrotic areas in the images are demonstrated by light pink patches (no cells, no haematoxylin).

Data showed that all treatments caused increased necrotic areas in both tumour models compared to the control groups (**Figure 5.7.**). In the 4T1 model (Balb/c mice), the highest percentage of necrosis was obtained in anti-Tim-3 and HSV-1716 alone treated groups (6-fold) compared to control and 7-fold compared to isotype treated mice. Although, the combination group exhibited necrosis compared to the anti-Tim-3/ HSV-1716 alone, it was still significant with 4.5-fold compared to the control group.

In the EO771 model (C57BL/6 mice), the highest percentage of necrosis was obtained in the combination treatment groups with an almost 10-fold increase compared to control and isotype-treated mice. The individual treatments (anti-Tim-3 and HSV-1716 alone) also significantly increased necrosis (**Figure 5.7.**) suggesting that these treatments were effective at inducing cell death within tumour bearing mice.

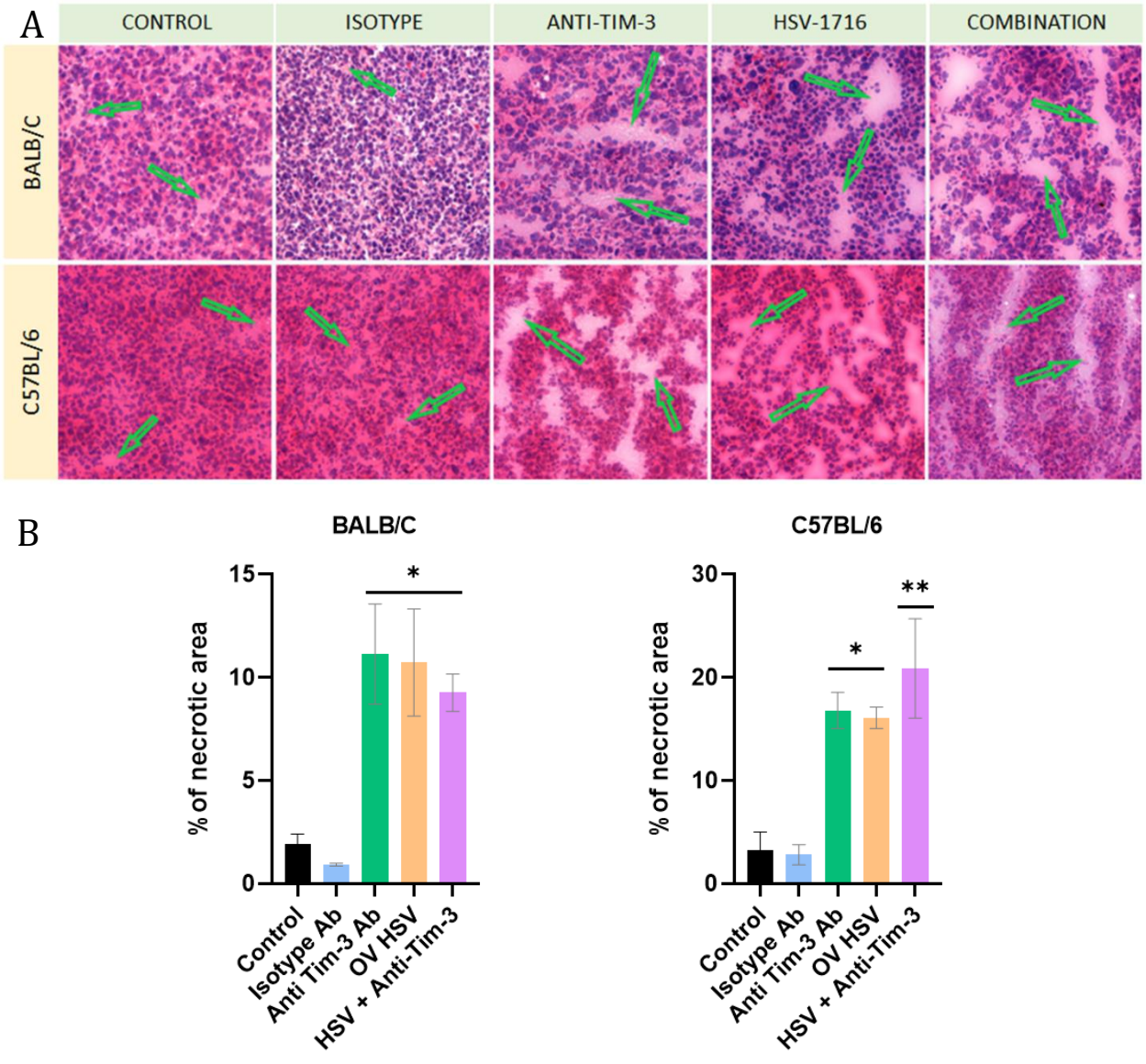

Figure 5.7. All treatments increased necrosis in 4T1 and EO771 tumour models. A. *Representative images of H&E staining indicating necrotic areas with green arrow.* ***B.*** *Percentages of necrotic areas is quantified using ImageJ software and result shown as mean ± SEM with an n=3-5 mice per treatment group where * = p<0.05 after the 2-way ANOVA with multiple comparisons between each treatment group against the control.*

5.6. Anti-Tim-3 and HSV-1716 reduced tumour metastasis in the 4T1 and Eo771 mouse models of BC

Mouse organs were embedded in paraffin wax and stored at room temperature. These were sectioned, stained with H&E and imaged using a Panoramic slide scanner as mentioned in **section 2.2.11.2.** These images were used to assess the impact of treatments on metastasis to the liver and lungs of the treated mice. Tumour metastasis is assessed by counting 10 or more tightly packed haematoxylin-stained cells. Training to spot metastasis was provided and corroborated by Prof. Muthana.

Analysis in the 4T1 BALB/C model showed that treatment with anti-Tim-3 and HSV-1716 significantly restricted the spread of tumours to the liver/lung of mice. The most reduction was obtained with Tim-3 inhibition (6-fold) alone or in combination with HSV-1716 (5.5-fold) compared to control for liver metastasis while the HSV-1716 treatment only group was the most effective at reducing metastasis to the lung compared to the control (**Figure 5.8.**).

In the EO771 C57BL/6 model all treatments significantly inhibited metastasis to the liver and lungs of mice. The most reduction was obtained in the combination treatment group in both organs (2.5 and 4-fold compared to control) (**Figure 5.9.**).

Despite the tumour growth data not showing any significance, all treatments significantly induced tumour necrosis and suppressed metastasis. Future studies are needed to further characterise the anti-tumour properties of these therapies and samples have been collected to help do this.

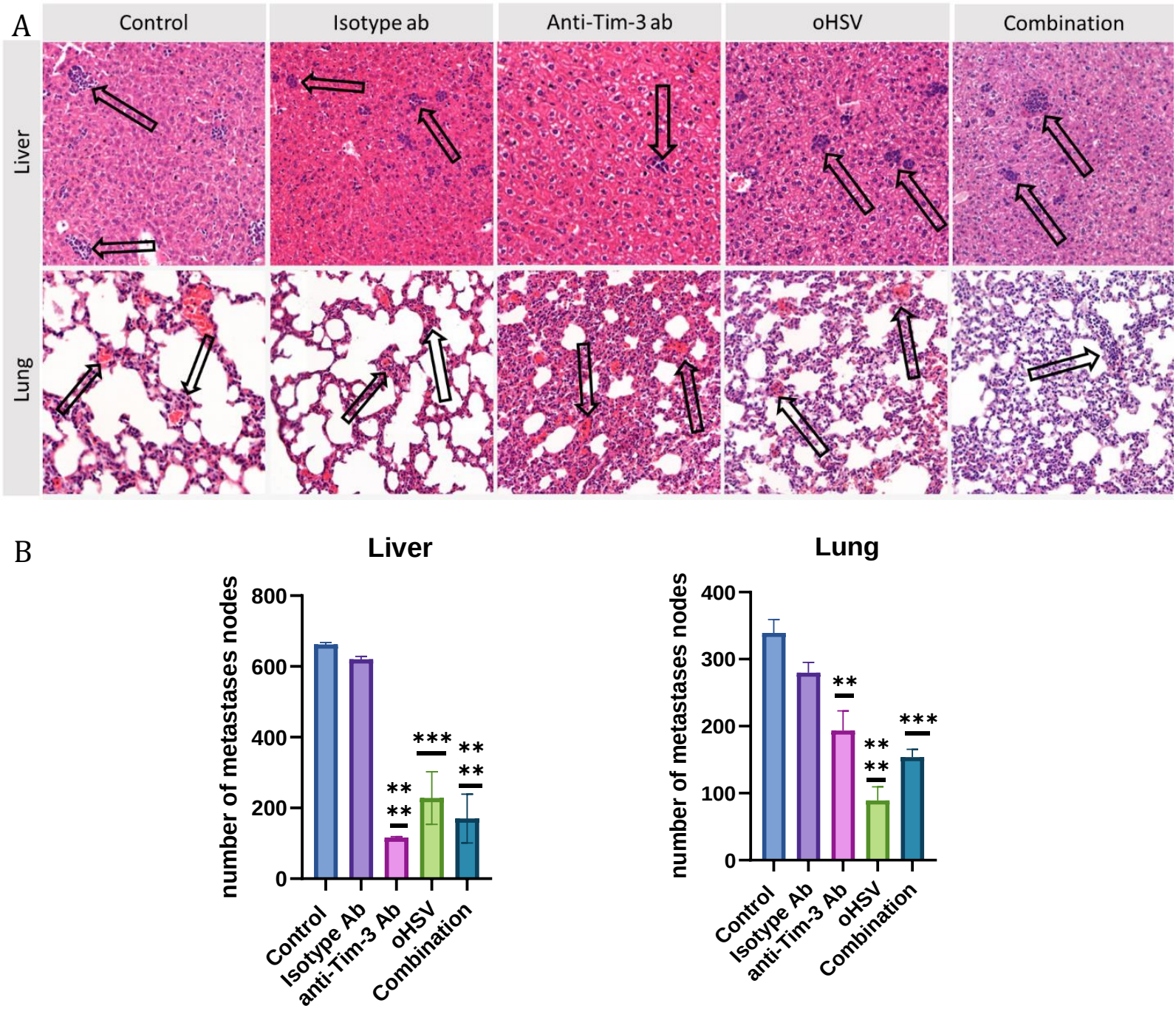

Figure 5.8. All treatments reduced metastasis in the 4T1 and EO771 mouse models of BC. A. *Representative images of H&E staining (metastatic nodes are shown with arrows).* ***B.*** *The number of metastatic nodes is quantified using Case Viewer software and result shown as mean ± SEM with an n=3 mice per treatment group where * = p<0.05, **** = p<0.0001, *** = p<0.0003 after a One-way ANOVA with multiple comparisons between each treatment group against the control.*

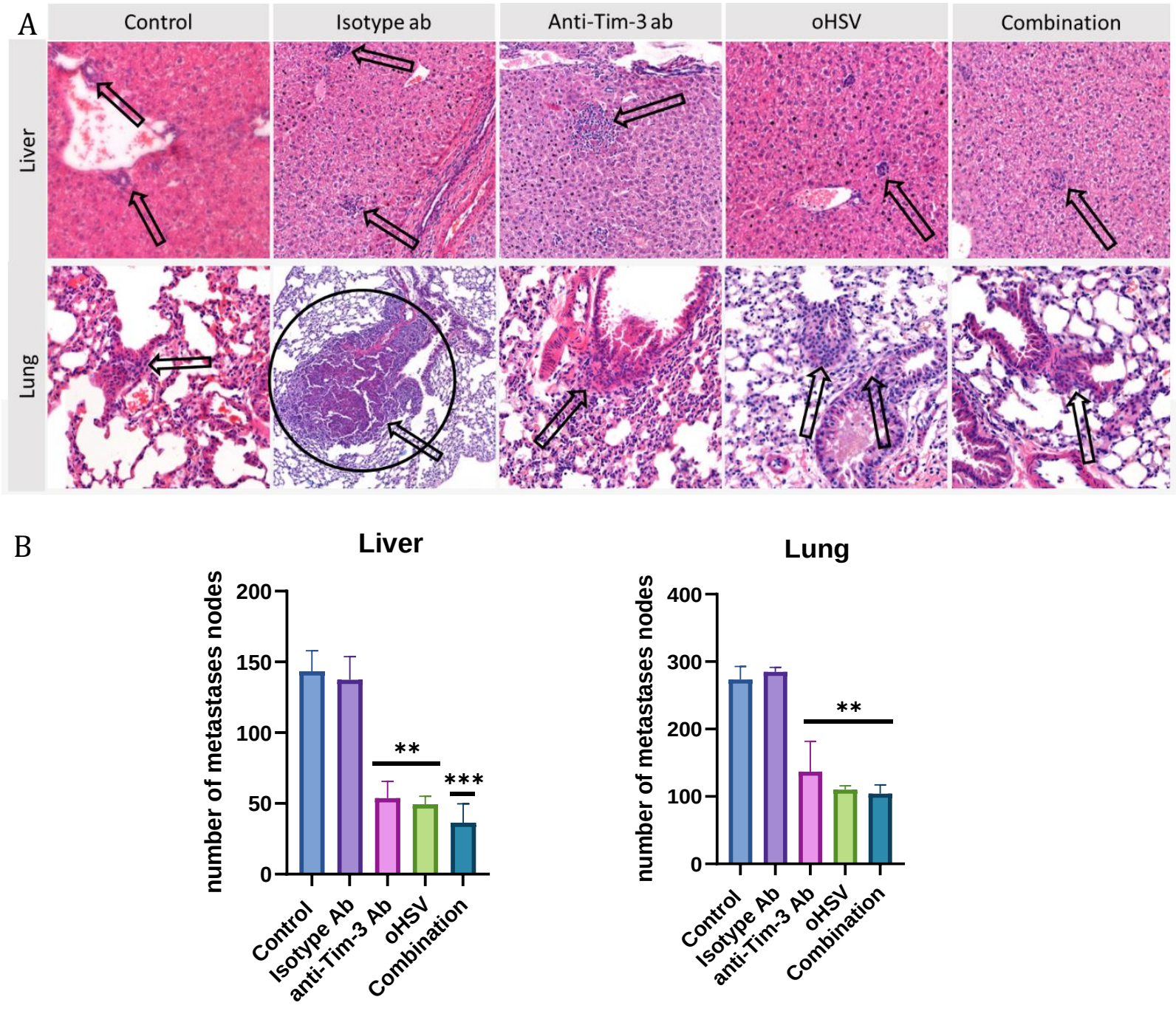

Figure 5.9. All treatments reduced metastasis in C57BL/6 mice model tumour. A. *Representative images of H&E staining indicating metastatic nodes with arrow.* ***B.*** *Number of metastatic nodes is quantified using Case Viewer software and result shown as mean ± SEM with an n=3 mice per treatment group where *** = p<0.0006, ** = p<0.0064 after the One-way ANOVA with multiple comparisons between each treatment group against the control.*

5.2. Discussion

Immune checkpoints inhibitors have been used for treatment of various cancer types including BC as described in chapter 1 (Berg and Zavazava, 2008; Naidoo et al., 2017; Topalian et al., 2014; Wei et al., 2018). However, there are some serious immune-related adverse effects and poor patient response in certain cancer types especially those with a cold TME, such as BC where there are currently clinical trials using CTLA-4, PD-1/PD-L1 (Riley et al., 2019).

Tim-3 is a less-well known immune checkpoint molecule that is expressed on many tumour types including lung cancer, osteosarcoma, HCC, BC, and it has been suggested that Tim-3 in tumours correlates with tumour progress, overall survival and clinical stage (Cheng et al., 2018; Dannenmann et al., 2013; Han et al., 2016; J. Li et al., 2013). A small number of clinical trials with Tim-3 inhibitors have been reported where these have been used alone or in combination with PD1/CTLA-4 and is well-tolerated and safe to use ("ESMO Congress 2022 | OncologyPRO," n.d.; Hollebecque et al., 2021; Sakuishi et al., 2010a; Yan et al., 2015).

The use of anti-Tim-3 in combination with OVs was explored in this chapter. The purpose of the virus was to switch the cold TME to hot TME leading to the recruitment of immune cells thus enabling improved response to this immune checkpoint treatment. This approach has the potential to expand the use of ICIs in cancers that are currently poorly responsive to these therapies, like BC (Chon et al., 2019). There are a small number of approved OVs for clinical use (**Table 5.2.**).

Table 5.2. Currently approved oncolytic viruses clinically (Shalhout et al., 2023)

Derived virus	**Treated disease**	**Country**
H101(Adenovirus)	Nasopharyngeal carcinoma	China (2005)
T-VEC(HSV-1)	Unresectable stage IIIB–IV melanoma	Australia (2016), Europe (2015), Israel (2017), USA (2015)
Teserpaturev (HSV-1)	R/R glioblastoma following	Japan (2021)
Nadofaragene firadenovec (Adenovirus)	BCG-unresponsive non-muscle invasive bladder cancer	USA (2022)

OVs are armed with reporter genes, cytotoxic transgenes for increasing tumour cytotoxicity and, inducing immune responses that change the tumour microenvironment as mentioned in section 1.3. Furthermore, they can be used in combination with conventional treatments including chemotherapy, radiotherapy, and more recently with immune checkpoint inhibitors (Bernstock et al., 2020; Ribas et al., 2017; Saha et al., 2020; Vito et al., 2021). For example, Vito et al. investigated the combination effects of 5-fluorouracil, epirubicin, and cyclophosphamide (FEC) with oHSV-1 in C57/BL6 mice bearing E0771 mouse BC cells. Mice were treated with FEC after tumours reached a dedicated volume and then treated with oHSV-1 at the 2nd, 3rd, 4th day. The results showed in combination therapy groups, tumour growth was impeded while M1-like macrophages number increased suggesting TAMs expressed an inflammatory phenotype (Vito et al., 2021).

Already, combination of OVs and ICIs studies have been reported *in vivo* and in clinical trials. These are reshaping the TME with an upregulation in immune modulation genes, M1 polarisation genes, Th1-Th2 responses, immune checkpoints (*pd-1, pd-l1, Ctla-4*, and *lag-3*) genes, observed tumour reductions and higher objective response rate (Chesney et al., 2018; Chon et al., 2019; Kelly et al., 2020; Liikanen et al., 2022) as described in chapter 1.

Furthermore, T-Vec (oHSV) has been combined with anti-PD-1 antibody (Pembrolizumab) in advanced melanoma patients in a phase 1b clinical trial (Ribas et al., 2017). 8 of 12 patients that responded to combined therapy have more infiltrating cytotoxic CD8+ T cells, which has the potential to kill tumour cells and change the tumour microenvironment profile. Moreover, combining anti-PD-1 did not exhibit side effects/ toxicity compared to T-Vec monotherapy (Ribas et al., 2017).

Another study was conducted combining the HSV-1 expressing PD-1 blocker gene and anti-Tim-3 antibody in the syngeneic BALB/c mice bearing Hepa1-6 tumour. Here, tumour growth in the combination groups presented considerable regression against monotherapy groups (Ju et al., 2022a). There are a small number of studies where anti-Tim-3 inhibition in combination with chemo/radiotherapy/ICIs/OVs has been investigated in different preclinical cancer types (as listed in **Table 5.3.).** Overall, this data has shown promising results. These studies have helped guide the dosage and treatment regime used in this study together with the expertise of our team on HSV-1716 a safe treatment regime was developed.

In this study, HSV-1716 tolerability was tested in mice bearing mLUC-E0771, TS1, and mLUC-4T1 BCs in C57/Bl6 and BalB/C mice, respectively. We already know there is strain-dependent tolerability to HSV-1716. For example, between $1x10^4$ - $1x10^6$ PFU HSV-1716 can be administered IV in C57Bl/6 with no adverse effects at higher dosage. These, mice were deemed to be Th1 biased after analysis using immunomodulatory driving Th bias response. However, the same dose of HSV-1716 cannot be tolerated by Balb/c mice with only a $1x10^4$ inoculation showing no adverse effects after IV administration (Howard et al., 2022). BalB/c mice have a Th2 background and are more sensitive to this virus, high doses result in lethal side effects including decreased respiration, pallor, piloerection, and reduced activity (Howard et al., 2022; Pinchuk and Filipov, 2008). This information is important as it is likely that humans may also respond differently to HSV-1716 and this should be taken into consideration such as not given if patients have Th2 disease background.

Table 5.3. in vivo anti-Tim-3 antibody treatment regimen examples

Dose (per mouse)	Dose repetition	Injection time scale	Regime	Mice strain	Delivery route	Outcomes	Cancer model	Reference
1mg followed 0.5 mg	3	4 days gap	Anti-Tim-3+ Chemotherapy	C57BL/6J	IP	Enhanced an immune mediated response to chemotherapy	Breast cancer	(de Mingo Pulido et al., 2018)
200 ug	3	2 days gap	HSV1 (encoding PD-1)+Tim-3 atsame time	C57BL/6	IT	Increased tumour immunogenicity and activated antitumor adaptive immune responses	Liver cancer	(Ju et al., 2022b)
250 ug	3	3 days gap	Anti-Tim-3 +Radiotherapy	C57BL/6J	IP	Long-term survival, increased immune cell infiltration and immune memory	Hepatocellular carcinoma	(Kim et al., 2017a)
100 ug	5	1 day gap	PD-1+Tim-3 Same day	C57BL/6	IP	Preventing CD8(+) T-cell exhaustion	Advanced acute myelogenous leukemia	(Zhou et al., 2011)
200 ug followed 100 ug	3	2 days gap	PD-1+Tim-3 interval day	BALB/c	IP	Delayed tumour growth, synergized with PD-1 antibody in prolonging the survival, enhancing T cell function	Colon carcinoma	(Gefen et al., 2017)
250 ug	3	4 days gap	CD137+Tim-3 at same point	C57BL/6	IP	Synergized with CD137 increasing $CD4^+$/ $CD8^+$ cells, decreasing regulatory T cells	Ovarian cancer	(Guo et al., 2013)
100 ug	3	1 day gap	PD-1+Tim-3 Interval day	BALB/c	IP	Synergized with PD-1 controlling tumour growth	Colon carcinoma	(Sakuishi et al., 2010b)
100 ug	6	Twice a week	Adenovirus (encoding both DC- and T cell-activating genes)+Tim-3 at same point	C57BL/6J	IT+IP	Increased infiltration of $CD8^+$ T cells, natural killer (NK) cells, and $CD103^+$ DCs, IFN-γ, TNF-α, IL-27, reduced tumour growth	Skin cancer	(Wenthe et al., 2022)

Immune related side effect following treatment with anti-Tim-3 or HSV-1716 were not observed. This is in line with other studies listed above that reported that anti-Tim-3 antibody was tolerated well. A study on anti-tumour efficacy of TIM-3 blockade alone and in combination with anti-PD-1 and Radiotherapy (SRS) in a glioma C57BL/6 model also showed this effect. This study looked at the impact of these treatments on median/overall survival. Tim-3 inhibition had no significant impact on survival nor did SRS, although anti-PD-1 monotherapy improved median survival to 33 days in comparison to the control (22 days) (Kim et al., 2017b).

Likewise, in the *in vivo* models of BC in this study, Tim-3 inhibition did not show changes on overall survival (OS) as a monotherapy **(Figure 5.5. and 5.6)**. Kim et al., combined the anti-Tim-3 and SRS resulting in 100 days median survival compared to control (22 days) and SRS monotherapy (27 days). Anti-Tim-3 + anti-PD-1 combination treatment elevated the median survival from 33 days (anti-PD-1 monotherapy) to 100 days and OS from 27.8% to 57.9%. This is exciting as glioma is very difficult to treat and this data suggest that Tim-3 inhibition in combination therapies is more effective as a treatment for cancer.

Similar correlation was seen in another study which investigated Tim-3 inhibition with/without PD-1 inhibition in CT26 colon tumours in BALB/c mice and B16 melanoma tumours in C57BL/6 mice. In the colon carcinoma models, Tim-3 inhibition monotherapy had no effect on tumour volume while combined with anti-PD-1 suppressed tumour growth dramatically with complete tumour regression in 50% of mice. In the melanoma model the authors demonstrated an even longer survival in the combination treatment compared to control, anti-Tim-3 alone, and anti-PD-L1 alone (Sakuishi et al., 2010c). These studies support that combining Tim-3 inhibition with other treatments improved the outcomes.

With respect to BC, there are no studies combining anti-Tim-3 with HSV-1716, so this study is the first to attempt this. It was shown that HSV-1716 displayed a trend towards reducing tumour volume in the 4T1 Balb/c model more so than in combination with anti-Tim-3. However, anti-Tim-3 in combination with HSV-1716 was more inhibitory in the EO771 C57BL/6 model. These data need to be interpreted with caution as they were not statistically significant, and the dosing regimen differed in the two models. Administration of anti-Tim-3 with HSV-1716 in the 4T1 Balb/c mice was given on consecutive days for 6, 7,8 days and in C57BL/6 was applied on 6-day intervals for 14, 21, 28 days. Therefore, it is impossible to compare side by side. Ideally both models would have received identical treatment, but this was possible due to the rate of tumour growth ben significantly delayed in the E0771 C57BL/6 mice.

The combination of another ICI plus OV has been investigated using oncolytic Reovirus (oRV) with anti-PD-L1 in a syngeneic EMT6 murine model of BC in BALB/c mice. Monotherapy of both therapies showed a significant reduction in tumour volume and this impact was elevated with combination treatment compared to oRV monotherapy ($p < 0.05$) or anti-PD-1 monotherapy ($p < 0.01$). This improvement was obtained for overall survival which cured ~70% of treated mice (at day 110 post tumour injection) (Mostafa et al., 2018). This study is very promising and shows that the combination of an ICI with OV might prove useful for BC treatment. Besides using a different immune checkpoint their study used a different treatment scheme and drug dose. oRV was administered four times on days 6, 9, 12 and 14 and then anti-PD-1 antibody was given six times at days 14, 17, 20, 23, 26 and 29) (Mostafa et al., 2018). Indeed, by starting with the OV there was more time for infection, replication and infiltration of the immune cells in response to the virus, prior to giving the ICI and could contribute to the ICI working. This is something that should be repeated in future work with our treatment combination.

As mentioned above, C57BL/6 mice are considered to be Th1-biased driving $CD8^+$ T cell-mediated responses and this may correlate with the prolonged survival and good clinical outcome in the EMT6 (TNBC) model. Whilst we did not see a reduction of tumour growth in E0771 (ER+) in the C57BL/6 mice in our studies, this may be improved using the dosing schedule described by Mostafa *et al* above. By contrast, the 4T1 model in the Balb/c mice is considered to have a Th2-biased response driven by activation of B cells and production of the cytokine IL-10 correlating with tumour aggressiveness (Fridman et al., 2012). Therefore, this could be the reason that overall survival is improved in the E0771 C57BL/6 mice even though this is not statistically significant.

Nevertheless, this data was largely affected due to tumour ulceration resulting in early sacrifice of the mice due to ethical reasons. Ulceration can change the tumour growth pattern and lead to body fluid loss and infections. This means that tumours were not allowed to grow to permitted maximum size (12mm diameter) for the survival studies and therefore the duration is reduced and is too short to fully determine the effect of anti-Tim-3 and HSV-1716. In addition, this reduces the statistical significance of the data. Interestingly, studies in other cancer types that lead to ulceration of subcutaneous tumours, advise that the mammary fat pad be used as an alternative injection to prevent this (Obodozie et al., 2019) but we were unable to prevent ulceration in our tumour. If more time were available the experiments would be repeated with larger group sizes included to factor in the loss of mice due to ulceration. This experiment could also be performed by reducing the number of injected cells to see if this helps prevent ulceration or choosing a different BC cell line e.g., EMT6, TS1.as these are slower growing.

Despite a lack of significance on tumour volume and survival in the mouse models, the anti-Tim-3 and HSV-1716 alone or in combination resulted in significant tumour necrosis in both mouse models of BC. The E0771 model displayed the highest necrosis (7-10-fold) in the combination therapy treated mice. As mentioned above, this could be due to the Th1 bias of these mice which may activate the Th1 pathway leading to antitumour toxicity.

Whilst it cannot completely be rule out that necrosis is due to anti-Tim-3 cell toxicity after intratumoural injection, the mice did not display any adverse effects. This needs to be investigated further with additional staining for cell death markers. It would be interesting to determine the type of cell death by staining for apoptotic or immunogenic cell death markers such as HMGB1, HSPA1A, Caspase 3/8, LC3B. Full analysis of the tumour microenvironment was not completed to fully understand why necrosis and metastasis was reduced. However, all the tumour and organs were collected for further analysis but the antibodies did not arrive in sufficient time to perform these studies. This included antibodies to stain for viral delivery with an anti-HSV antibody in the biodistribution studies and to see if Tim-3 was sufficiently blocked in the tumours as this will help determine efficacy. Other antibodies included a panel for immune markers and these ae described in the final chapter.

If more time were available, it would have been useful to perform a pilot study to determine the optimal concentration of anti-Tim-3, as well as experiments with alternative treatment schedules. For example, pre-treatment with HSV-1716 to recruit immune cells as in the study by Mostafa et al (Mostafa et al., 2018) followed by anti-Tim-3 inhibition. Future work would also compare the different oHSVs described in chapter 4 as these were promising agents for inducing BC cell death.

Summary

This chapter showed for the first time the effects of inhibiting Tim-3 in combination with the virus HSV-1716 in preclinical mouse models of BC. The data showed a trend in reducing tumour growth and prolonging mouse survival, but this was not statistically significant. However, there was a clear reduction in tumour necrosis and a reduction in pulmonary and liver metastasis. Together, this suggests that this drug concentration might be a useful strategy for the treatment of BC.

CHAPTER 6

GENERAL DISCUSSION

6.1. Major outcomes

The 6 hallmarks of an immunosuppressive TME include defects of antigen-presenting cells, lack of tumour antigens, impairment of T-cell infiltration, activation of an immunosuppressive signalling pathway, heterogeneity of constitution and enhancement of immunosuppressive metabolism (Tang et al., 2021). The immunosuppressive cells consist of tumour cells, suppressive myeloid cells (such as tumour-associated macrophages, monocytes, and granulocytes), vascular endothelial cells, cancer-associated fibroblasts (CAFs), regulatory T (Treg) cells, and regulatory B cell. Immunotherapy with OVs provides an opportunity to generate an immune response to both viral and tumour antigens and overcome this immunosuppressive TME. OVs infect the tumour cells resulting in oncolysis which leads to the release of soluble tumour-associated antigens, viral pathogen-associated molecular patterns (PAMPs) and cell-derived damage-associated molecular patterns (DAMPs) into the TME (Kaufman et al., 2016). These patterns inducing immunogenic cell death contribute to reshaping the TME by cross-presenting of tumour antigen and recruiting immune cells into tumours leading to the induction of a robust and long-lasting antitumor immune response (Achard et al., 2018).

ICIs have been used in clinics (Hargadon et al., 2018), however benefits are limited to patients that present with immunologically 'hot` TME profile meaning higher density of infiltrating immune cells. Patients where tumours are immunogenically 'cold' are benefiting from these therapies. In this project we propose that regulation of the TME by OVs might increase sensitivity to ICIs by enabling T cell infiltration and exerting the checkpoint inhibitors expression (Chon et al., 2019). Studies in mouse Renca tumours which are typically immunologically cold, show that CD8+ cytotoxic T cells, CD11c+ dendritic cells, PD-L1 levels increased following OV injection leading to upregulation of immune modulation genes, M1 polarisation genes, Th1-Th2 responses, immune checkpoints (Pd-1, Pd-l1, Ctla-4, and Lag-3) genes. They also assessed the combination of OV and anti-PD-1/anti-CTLA-4 ICI antibodies and observed tumour growth reductions were 23% in anti-PD-1 alone; 20% in anti-CTLA-4; 44% in OV alone; 70% in OV+anti-PD-1; 57.6% in OV+anti-CTLA-4. The results of this study are promising and suggest that OVs could be used to overcome ICI resistance in patients with immunologically cold tumours (Chon et al., 2019).

Furthermore, a clinical trial for the HSV-1 T-Vec plus ipilimumab (anti-CTLA-4) indicates that OV combination with ICI exhibited a higher objective response rate suggesting due to greater antitumour activity (Chesney et al., 2018). The phase II study enrolled 198 advanced melanoma patients treating 98 patients with combination (T-Vec plus anti-CTLA-4) and 100 patients with anti-CTLA-4 alone. Objective response rate (ORR) among randomly assigned patients were 39% in the combination arm; 18% in the ipilimumab arm this was even higher than T-Vec alone data in literature (Chesney et al., 2018). Another clinical phase ll trial investigated T-Vec plus pembrolizumab (anti-PD-1) in 20 patients with advanced sarcoma (Kelly et al., 2020). Data showed that this regimen increased the ORR to 35% while standard neoadjuvant regimen has a response range of 16-28%. In this study 64% of patients exhibited higher PD-1 and CD3+/CD8+ TILs after treatment with the virus and ICI, this antitumour response was evident in advanced disease and across different sarcoma subtypes based on histology, importantly the treatment combination was safe with limited toxicity (Kelly et al., 2020).

Further, another research team investigated the impact of oncolytic adenovirus (Ad5/3Δ24-GM CSF) on Tim-3 modulation in a B16 melanoma C57BL/6 model and in 15 patients with advanced-stage cancer (colorectal, prostate, mesothelioma, melanoma, lung (NSCLC), cervical, ovarian, breast (Liikanen et al., 2022). For the clinical study, microarray analysis on patients before/after OV treatment showed that Tim-3 levels decreased in 9 patients while increasing in 6 patients. Patients with increased Tim-3 upregulated the acute inflammatory response genes *SAA1* and *ORM1/2* and metabolic enzymes *PHGDH* and *SHMT1/2* that are important in effector T-cell expansion. Also, in this group the induction of Th17 cells was observed and considered to enhance long-term antitumour immunity. Of note, in patients where Tim-3 decreased an upregulated profile of core CD8+T cell exhaustion was exhibited. Next, CD8+ T cell infiltration to the tumour was investigated. Data showed significantly higher infiltration of T cells when Tim-3 decreased in patients. Notably, median OS was 204 days in patients with lower Tim-3 while 64 days in patients where Tim-3 was elevated. This suggests that oncolytic adenovirus can reshape the tumour microenvironment to reduce T cell exhaustion, induce CD8+ T cell influx into the tumour, and correlates with longer survival in patients with decreased Tim-3 expression (Liikanen et al., 2022).

In line with this, the authors also demonstrated the presence of exhausted Tim-3+ CD8+ TIL in mouse tumours. This phenotype of TILs was significantly reduced following treatment with oncolytic adenovirus (Liikanen et al., 2022). Together, this study demonstrated an important role for Tim-3 as a biomarker for OV.

This PhD investigated for first time the combination of an oHSV plus Tim-3 inhibition in preclinical models of BC *in vitro* and *in vivo.*

In results chapter 3, Tim-3 expression was confirmed on human BC cell lines (**Figure 3.3.-3.5.**) and human BC tumour tissue samples (**Figure 3.12.**), this is in agreement with data reported by the Human Protein Atlas (**Figure 3.2.**) as well as other published studies (Sasidharan Nair et al., 2018; Tu et al., 2020; Yasinska et al., 2019; H. Zhang et al., 2017). Moreover, in the literature, it has been reported that Tim-3 is upregulated on immune cells such as CD-4, -8 T cells in cancers including BC, glioma, ovarian cancer, colorectal cancer, chronic myeloid leukaemia (Han et al., 2014; Irani et al., 2023; Shariati et al., 2020; Toor et al., 2019; Wu et al., 2013; Yilmaz et al., 2023).

Consistent with the literature, in our data, Tim-3 was upregulated on CD-4, -8 T cell following exposure of healthy PBMC to tumour-derived factors in TCM. Tim-3 upregulation on CD8 T cells was associated with higher tumour grade (Shariati et al., 2020), T cell exhaustion (Yilmaz et al., 2023), and Tim-3 upregulation on $CD4^+$ T cells was correlated with the number of metastatic lymph nodes in BC patients (Shariati et al., 2020). We did not have time in this study to investigate Tim-3 expression by immune cells in our BC tissue, but this should be part of future work as we have access to the tissue and patient data.

Tim-3 upregulation was also seen on CD68 and CD163 TAMs following TCM exposure of healthy macrophages. Tim-3 expression by macrophages was associated with shorter overall survival and worst prognosis in NSCLC and malignancy grade in glioma (Li et al., 2016; Moamin et al., 2023; Wang et al., 2018; Zhang et al., 2023a, 2023b). A recent study from the University of Sheffield, used multiplex immunofluorescence imaging to investigate the difference in immune cells in untreated and neoadjuvant treated patients with TNBC.

Interestingly, the patients displayed Tim-3+/CD163+ TAMS in the stroma and this was linked to patients with high risk of disease relapse (Moamin et al., 2023.) This suggest that Tim-3 expressing macrophages could be used as a biomarker for this patient group. It would be useful to perform a larger study looking at the different subtypes of BC to see if this is also the case. Moreover, does this suggest that given Tim-3 is expressed in the BC TME that anti-TIM-3 could be a more useful checkpoint inhibitor in these patients.

Once we had confirmed the Tim-3 expression/upregulation we investigated whether Tim-3 inhibition with/without oHSV impact the cell viability, migration, and invasion functions in chapter 4. First, we looked at cell viability to determine the IC50 values for three oHSVs and found that all 3 reduced cell viability across all the human and mouse BC cell lines. This is the first time that some of these viruses have been tested in BC and show very promising oncolytic activity. In future work these will be taken into our animal models. Next, we looked at cell viability following Tim-3 inhibition on its own and in combination with oHSV. A significant decrease in cell viability across all the anti-Tim-3 antibody concentrations was noted in the presence of oHSVs suggesting that the virus makes the cell lines more sensitive to the inhibitor in human BC cell lines. However, in mouse BC cell lines the oHSV alone and in combination with the anti-Tim-3 have similar cytotoxic effects. We did not have time to determine the IC50 values in the mouse cell lines and further optimisation is needed including anti-Tim-3 antibody dose optimization experiments on mouse cell lines instead of human cell lines data.

It has been already reported that Tim-3 upregulation contributes to tumour cell proliferation, migration, and invasion in vitro (Cheng et al., 2018; Guo et al., 2022a; Lin et al., 2017). In our hands, MCF-7 and SKBR-3 cell lines, the oHSV + anti-Tim-3 combination treatment significantly impeded tumour cell migration and invasion. However, MDA-MB-231 cells, a more aggressive subtype, exhibited significant resistance to all treatments for migration and minimal response to invasion.

Literature suggests that Tim-3 inhibition/siRNA knockdown impedes the migration and invasion in BC, glioma, prostate cancer, colorectal cancer, clear cell renal cell carcinoma in vitro. (Cheng et al., 2018; Guo et al., 2022b; Huo et al., 2022; Piao et al., 2013; M. Yu et al., 2017b, 2017a; Zhang and Zhang, 2020; Zheng et al., 2015). Moreover, these studies aimed to understand which signals Tim-3 used to suppress migration/invasion and looked at the Akt/GSK-3β/Snail signalling pathway or epithelial marker E-cadherin and mesenchymal markers N-cadherin and vimentin. They found that Tim-3 could play role in prevention of M2 polarization to M1 or in epithelial cell attachment for tumour growth. Therefore, it would be beneficial to consider these markers in further work.

In Chapter 5, the effect of anti-Tim-3 with the OV HSV-1716 in our in vivo data, we saw a trend towards tumour reduction in our combination therapy over the individual treatments. However, this data needs to be interpreted with caution as there was no significance. Other studies have reported that ICI monotherapy was not as effective compared to oHSV and oHSV encoding ICI. For instance, anti-PD-1 monotherapy was not effective compared to oHSV or oHSV encoding anti-PD-1 in a murine aggressive B16–F10 melanoma model (Tian et al., 2021) and in a murine CT26 colon adenocarcinoma model (Xie et al., 2022), which is agreement with our in vivo data. Nevertheless, this immunotherapy drug combination impeded tumour metastasis to the lung/liver with HSV-1716 & anti-Tim-3 showing the most potent effect compared to untreated mice. Unfortunately, there was not enough time to analyse the tumours and organs collected from the mice to better understand the mechanism behind this. Zhou et al., assessed tumour cell death in a preclinical model of subcutaneous MC38 colon carcinoma. They used TUNEL labelling for apoptosis markers and used an oncolytic chimpanzee adenovirus expressing full length anti-PD1. This treatment induced apoptotic cell death and immune memory leading to the protection of animals rechallenged with MC38 cells. A major limitation of this study is that they did not investigate the immune landscape in the TME following the treatment (Zhou et al., 2022).

We also calculated the necrotic area to assess cell death with the HSV-1716 & anti-Tim-3 combination and found this treatment to be very effective at inducing cell death over anti-Tim-3 alone, which may be responsible for preventing metastasis. Tian et al., observed downregulation on angiogenesis genes such as Cdh5, Aplnr, Cyplb1 and cell adhesion genes such as Col5a3, Postn suggesting that OVs expressing/encoding ICIs contributes to tumour vessel destruction to prevent metastasis (Tian et al., 2021).

Future work will aim to interrogate some of these markers in the tumour tissue that was collected post-mortem. A panel of caspases (3,7,8,9), immunogenic cell death markers (Calreticulin, HMGB-1) and CD31 for measuring tumour vascular was planned for immunofluorescent staining on the post-mortem tumour tissue but there was not enough time to do this.

Engineering OV expressing ICIs rather than OV plus antibody therapy is an area of interest (Chaurasiya et al., 2022; Hamdan et al., 2021; Ju et al., 2022c, 2022d; Tian et al., 2021; Xie et al., 2022; Zhou et al., 2022; Zuo et al., 2021) and already a study is mentioned above. This could be an excellent approach of overcoming the toxicities of using ICIs whilst using the virus to activate immunity and recruit immune cells to the tumour site. Not only will this help promote oncolysis and antitumour immunity, but this could be used for BC or cancers that are immunogenically cold.

An exciting recent study engineered an adenovirus encoding Tim-3 for liver cancer (Qiang et al., 2023). They engineered oncolytic Ad-GD55 (MOI-10) and Ad-GD55–α-Tim-3 (MOI-10). BALB/c nude mice were implanted with co-cultured of PBMCs activated by anti-CD-3/-28 and BEL-7404 into the flank to mimic the local tumour microenvironment in a manner more consistent with that in HCC patients. Tumour bearing mice were treated with 2 times of intratumorally injections of PBS/Ad-GD55/Ad-GD55–α-Tim-3 at an interval of 2 days. This improved tumour inhibition, overall survival of the mice, T cell infiltration, and response to ICIs. In vivo immune related gene expression and quantitative analysis revealed significantly upregulated T cell markers CD4/8 in Ad-GD55–α-Tim-3 treated mice compared to PBS/Ad-GD55 treated mice, which indicates TME regulation ability. H&E staining data showed downregulation on proliferation-related Ki-67 antigen expression with more extensive tumour cell death in Ad-GD55–α-Tim-3 treated mice to PBS/Ad-GD55 treated mice.

Tim-3 inhibition and OV alone/together also considerably improved antitumour immunity but OV encoding Tim-3 treatment was the most effective approach in this model (Qiang et al., 2023). Together all these studies with ours point to OV in combination with anti-Tim-3 as a potential strategy to treat BC.

6.2. Limitations of study

One of the major limitations of this study is that the commercial human anti-Tim-3 antibody did not show reproducible data *in vitro.* Flow cytometry experiments in BC cell lines were repeated 8-10 times changing antibody volume/cell number/incubation time/incubation temperature. In the literature, Tim-3 detection has been performed mostly by Western blotting, we could have taken this approach however, for Tim-3 inhibition this would need to be on the surface, and this is why we wanted to check this by Flow Cytometry. Due to the unreliable results this prevented further studies looking at Tim-3 expression following inhibition with the anti-Tim-3 inhibitor. If more time was available Tim-3 expression would be repeated using a different antibody clone.

We also determined Tim-3 expression on human PBMC co-cultured with human BC cell lines, however this resulted in PBMC cell death (**Figure 3.6**.). We therefore replaced with the BC cells with tumour conditioned medium taken from the cell lines. This showed an upregulation of Tim-3 in the PBMC. However, this is a very simplistic model to mimic the TME and the factors (metabolites, secreted cytokine and growth factors) within the TCM that induce this upregulation need to be identified to understand this better.

For in vivo work, time and delays in receiving ordered antibodies was a major factor preventing further analysis. We had planned to examine the immune landscape, expression of Tim-3, and to observe the TME reshaping, following treatment in mouse organs/tumours by Flow cytometry and histology. We have designed an immune panel including CD8a Monoclonal Antibody (53-6.7), Anti-Mouse F4/80 Antigen (BM8.1), Anti-Mouse CD3 (17A2), Anti-Mouse CD45, Anti-Mouse CD4 (RM4-5), Anti-Mouse NK1.1, Anti-Mouse CD19, Anti-Mouse Anti-TIM-3 (RMT3-23), Anti-Mouse CD274 (PD-L1, B7-H1) to run the samples by Flow cytometry (**Table 6.1.**). However, the antibodies have not arrived for us to test in our tumour tissue, and this will form part of future work.

Table 6.1. List of in vivo Flow cytometry experiment commercial anti-mouse antibodies

Marker	Clone	Fluorescent tag	Supplier
CD8	53-6.7	Super Bright 645	Thermo fisher
F4-80	BM8.1	APC-Cy7	Cytek Biosciences
CD3	17A2	FITC	Cytek Biosciences
CD45	30-F11	BUV395	Thermo fisher
CD4	RM4-5	PerCP-Cy5.5	Cytek Biosciences
CD161 (NK1.1)	PK136	APC	Cytek Biosciences
CD19	1D3	BV480	Thermo fisher
CD366 (Tim-3)	RMT3-23	PE	Cytek Biosciences
CD274 (PD-L1)	MIH5	BUV737	Thermo fisher
Viability		Ghost Dye UV 450	Cytek Biosciences
Glycoprotein B (HSV-1&HSV-2)		Qdot 800	Thermo fisher

6.3. Future work

There are lots of experiments that could be done to improve this study, and many have been discussed above. In the first instance, a more thorough in vivo investigation that defines the optimal treatment regime is needed. Giving HSV-1716 in advance of anti-Tim-3 could improve anti-tumour outcomes and give the ICI a better chance of working as the immune cells, particularly T cells are recruited to the tumour first (**Figure 6.1**.).

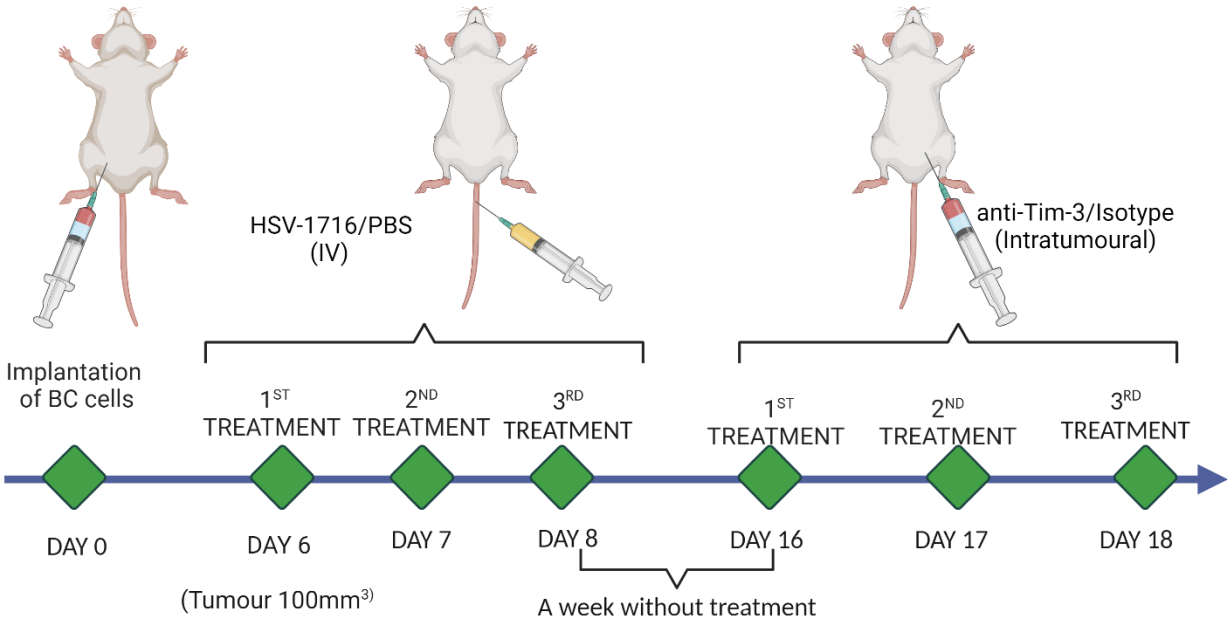

Figure 6.1. An example illustration treatment regime of oHSV with anti-Tim-3 antibody in vivo for further study. *Here we would treat the mice with one of the oHSVs prior to giving the anti-Tim-3. This would provide an opportunity for immune cells to be recruited to the tumours giving the ICI a chance to be effective.*

Currently, chemotherapy and radiotherapy are standard of care for BC, and it has been reported that these therapies help contribute to response to ICIs. Therefore, our future in vivo models would aim to combine drugs such as Epirubicin or radiotherapy with our oHSVs and anti-Tim-3.

We would also replace HSV-1716 with our new oHSV (HSV-E17RL1del7, HSV-V17RL1del2) as these have not been tested in vivo and may prove to be as effective as HSV-1716.

Moreover, bloodstream neutralisation of OVs and antibodies is an important barrier for treatment efficacy. An idea could be that we engineer oHSV encoding anti-Tim-3 as performed in liver cancer (Qiang et al., 2023). These could be delivered intravenously for targeting advanced cancers using some of our team's platform solutions for packaging and protecting OVs in circulation. Including cell therapies (Muthana et al., 2015), bioengineered cell membrane nanovehicles (Zhang et al., 2020), albumin-binding (Mato-Berciano et al., 2021), MSCs-encapsulation (Ghasemi Darestani et al., 2023), liposome encapsulation (Iscaro et al., 2022; Wang et al., 2019).

References

Achard, C., Surendran, A., Wedge, M.E., Ungerechts, G., Bell, J., Ilkow, C.S., 2018. Lighting a Fire in the Tumor Microenvironment Using Oncolytic Immunotherapy. EBioMedicine.

Actions of bisphosphonate on bone metastasis in animal models of breast carcinoma [WWW Document], n.d. URL https://acsjournals.onlinelibrary.wiley.com/doi/epdf/10.1002/1097-0142%2820000615%2988%3A12%2B%3C2979%3A%3AAID-CNCR13%3E3.0.CO%3B2-U (accessed 1.6.24).

Adusumilli, P.S., Stiles, B.M., Chan, M.-K., Eisenberg, D.P., Yu, Z., Stanziale, S.F., Huq, R., Wong, R.J., Rusch, V.W., Fong, Y., 2006. Real-time diagnostic imaging of tumors and metastases by use of a replication-competent herpes vector to facilitate minimally invasive oncological surgery. The FASEB Journal.

Alberts, P., Tilgase, A., Rasa, A., Bandere, K., Venskus, D., 2018. The advent of oncolytic virotherapy in oncology: The Rigvir® story. Eur J Pharmacol.

Allison, E., Edirimanne, S., Matthews, J., Fuller, S.J., 2023. Breast Cancer Survival Outcomes and Tumor-Associated Macrophage Markers: A Systematic Review and Meta-Analysis. Oncol Ther 11, 27.

Andreansky, S., He, B., Van Cott, J., McGhee, J., Markert, J.M., Gillespie, G.Y., Roizman, B., Whitley, R.J., 1998. Treatment of intracranial gliomas in immunocompetent mice using herpes simplex viruses that express murine interleukins. Gene Ther.

Aslakson, C.J., Miller2, F.R., 1992. Selective Events in the Metastatic Process Defined by Analysis of the Sequential Dissemination of Subpopulations of a Mouse Mammary Tumor1. Cancer Res 52, 1399–1405.

Attalla, S., Taifour, T., Bui, T., Muller, W., 2020. Insights from transgenic mouse models of PyMT-induced breast cancer: recapitulating human breast cancer progression in vivo. Oncogene 2020 40:3 40, 475–491.

Aurelian, L., 2016. Oncolytic viruses as immunotherapy: Progress and remaining challenges. Onco Targets Ther 9, 2627–2637.

Baitsch, L., Baumgaertner, P., Devêvre, E., Raghav, S.K., Legat, A., Barba, L., Wieckowski, S., Bouzourene, H., Deplancke, B., Romero, P., Rufer, N., Speiser, D.E., 2011. Exhaustion of tumor-specific CD8+ T cells in metastases from melanoma patients. Journal of Clinical Investigation.

Baitsch, L., Fuertes-Marraco, S.A., Legat, A., Meyer, C., Speiser, D.E., 2012. The three main stumbling blocks for anticancer T cells. Trends Immunol.

Bejarano, L., Jordão, M.J.C., Joyce, J.A., 2021. Therapeutic targeting of the tumor microenvironment. Cancer Discov.

Benencia, F., Courrèges, M.C., Fraser, N.W., Coukos, G., 2008. Herpes virus oncolytic therapy reverses tumor immune dysfunction and facilitates tumor antigen presentation. Cancer Biol Ther 7, 1194–1205.

Berg, M., Zavazava, N., 2008. Regulation of CD28 expression on CD8+ T cells by CTLA-4. J Leukoc Biol 83, 853–863.

Bernstock, J.D., Bag, A.K., Fiveash, J., Kachurak, K., Elsayed, G., Chagoya, G., Gessler, F., Valdes, P.A., Madan-Swain, A., Whitley, R., Markert, J.M., Gillespie, G.Y., Johnston, J.M., Friedman, G.K., 2020. Design and Rationale for First-in-Human Phase 1 Immunovirotherapy Clinical Trial of Oncolytic HSV G207 to Treat Malignant Pediatric Cerebellar Brain Tumors. Hum Gene Ther 31, 1132–1139.

Binnewies, M., Roberts, E.W., Kersten, K., Chan, V., Fearon, D.F., Merad, M., Coussens, L.M., Gabrilovich, D.I., Ostrand-Rosenberg, S., Hedrick, C.C., Vonderheide, R.H., Pittet, M.J., Jain, R.K., Zou, W., Howcroft, T.K., Woodhouse, E.C., Weinberg, R.A., Krummel, M.F., 2018. Understanding the tumor immune microenvironment (TIME) for effective therapy. Nat Med.

Bischoff, J.R., Kirn, D.H., Williams, A., Heise, C., Horn, S., Muna, M., Ng, L., Nye, J.A., Sampson-Johannes, A., Fattaey, A., McCormick, F., 1996. An adenovirus mutant that replicates selectively in p53-deficient human tumor cells. Science (1979).

Biswas, S.K., Mantovani, A., 2010. Macrophage plasticity and interaction with lymphocyte subsets: Cancer as a paradigm. Nat Immunol.

Body, J.J., Facon, T., Coleman, R.E., Lipton, A., Geurs, F., Fan, M., Holloway, D., Peterson, M.C. and Bekker, P.J., 2006. A study of the biological receptor activator of nuclear factor-kappaB ligand inhibitor, denosumab, in patients with multiple myeloma or bone metastases from breast cancer. *Clinical cancer research: an official journal of the American Association for Cancer Research*, *12*(4), pp.1221-1228.

Bommareddy, P.K., Peters, C., Saha, D., Rabkin, S.D., Kaufman, H.L., 2018. Oncolytic Herpes Simplex Viruses as a Paradigm for the Treatment of Cancer. Annu Rev Cancer Biol 2, 155–173.

Boon, T., Cerottini, J., Bruggen, P. Van Der, Pel, A. Van, 1994. Tumor Antigens Recognized. Annual Reviews in Immunology.

Bortner, C.D., Cidlowski, J.A., 2003. Uncoupling Cell Shrinkage from Apoptosis Reveals That Na+ Influx Is Required for Volume Loss during Programmed Cell Death*. Journal of Biological Chemistry 278, 39176–39184.

Breast cancer statistics | Cancer Research UK [WWW Document], n.d. URL https://www.cancerresearchuk.org/health-professional/cancer-statistics/statistics-by-cancer-type/breast-cancer#heading-Two (accessed 12.21.23).

Breitbach, C.J., Moon, A., Burke, J., Hwang, T.H., Kirn, D.H., 2015. A phase 2, open-label, randomized study of Pexa-Vec (JX-594) administered by intratumoral injection in patients with unresectable primary hepatocellular carcinoma. Methods in Molecular Biology.

Brunner, A.M., Esteve, J., Porkka, K., Knapper, S., Vey, N., Scholl, S., Garcia-Manero, G., Wermke, M., Janssen, J., Traer, E., Loo, S., Narayan, R., Tovar, N., Kontro, M., Ottmann, O., Naidu, P., Kurtulus, S., Makofske, J., Liao, S., Mohammed, A., Sabatos-Peyton, C.A., Rinne, M.L., Borate, U., Wei, A.H., 2020. Efficacy and Safety of Sabatolimab (MBG453) in Combination with Hypomethylating Agents (HMAs) in Patients with Acute Myeloid Leukemia (AML) and High-Risk Myelodysplastic Syndrome (HR-MDS): Updated Results from a Phase 1b Study. Blood 136, 1–2.

Buijs, P.R.A., Van Amerongen, G., Van Nieuwkoop, S., Bestebroer, T.M., Van Run, P.R.W.A., Kuiken, T., Fouchier, R.A.M., Van Eijck, C.H.J., Van Den Hoogen, B.G., 2014. Intravenously injected Newcastle disease virus in non-human primates is safe to use for oncolytic virotherapy. Cancer Gene Ther.

Buijs, P.R.A., Verhagen, J.H.E., van Eijck, C.H.J., van den Hoogen, B.G., 2015. Oncolytic viruses: From bench to bedside with a focus on safety. Hum Vaccin Immunother 11, 1573–1584.

Burnet, F.M., 1970. The concept of immunological surveillance. Progress in experimental tumor research. Fortschritte der experimentellen Tumorforschung. Progres de la recherche experimentale des tumeurs.

Burton, E.A., Bai, Q., Goins, W.F., Glorioso, J.C., 2002. Replication-defective genomic herpes simplex vectors: Design and production. Curr Opin Biotechnol.

Burugu, S., Gao, D., Leung, S., Chia, S.K., Nielsen, T.O., 2018. TIM-3 expression in breast cancer. Oncoimmunology 7.

Byun, K. Do, Hwang, H.J., Park, K.J., Kim, M.C., Cho, S.H., Ju, M.H., Lee, J.H., Jeong, J.S., 2018. T-Cell Immunoglobulin Mucin 3 Expression on Tumor Infiltrating Lymphocytes as a Positive Prognosticator in Triple-Negative Breast Cancer. J Breast Cancer 21, 406.

Cai, C., Xu, Y.F., Wu, Z.J., Dong, Q., Li, M.Y., Olson, J.C., Rabinowitz, Y.M., Wang, L.H., Sun, Y., 2016. Tim-3 expression represents dysfunctional tumor infiltrating T cells in renal cell carcinoma. World J Urol 34, 561–567.

Cai, L., Li, Yuchen, Tan, J., Xu, L., Li, Yangqiu, 2023. Targeting LAG-3, TIM-3, and TIGIT for cancer immunotherapy. J Hematol Oncol 16, 101.

Campadelli-Fiume, G., De Giovanni, C., Gatta, V., Nanni, P., Lollini, P.L., Menotti, L., 2011. Rethinking herpes simplex virus: The way to oncolytic agents. Rev Med Virol.

Cao, Y., Zhou, X., Huang, X., Li, Q., Gao, L., Jiang, L., Huang, M., Zhou, J., 2013. Tim-3 Expression in Cervical Cancer Promotes Tumor Metastasis. PLoS One 8.

Carter, M.E., Koch, A., Lauer, U.M., Hartkopf, A.D., 2021. Clinical Trials of Oncolytic Viruses in Breast Cancer. Front Oncol 11.

Cassetta, L., Cassol, E., Poli, G., 2011. Macrophage Polarization in Health and Disease. The Scientific World Journal 11, 2391.

Chase, M., Chung, R.Y., Antonio Chiocca, E., 1998. An oncolytic viral mutant that delivers the CYP2B1 transgene and augments cyclophosphamide chemotherapy. Nat Biotechnol.

Chaurasiya, S., Yang, A., Zhang, Z., Lu, J., Valencia, H., Kim, S.I., Woo, Y., Warner, S.G., Olafsen, T., Zhao, Y., Wu, X., Fein, S., Cheng, L., Cheng, M., Ede, N., Fong, Y., 2022. A comprehensive preclinical study supporting clinical trial of oncolytic chimeric poxvirus CF33-hNIS-anti-PD-L1 to treat breast cancer. Mol Ther Methods Clin Dev 24, 102.

Chávez-Galán, L., Olleros, M.L., Vesin, D., Garcia, I., 2015. Much more than M1 and M2 macrophages, there are also CD169+ and TCR+ macrophages. Front Immunol.

Chen, D.S., Mellman, I., 2013. Oncology meets immunology: The cancer-immunity cycle. Immunity.

Chen, P., Huang, Y., Bong, R., Ding, Y., Song, N., Wang, X., Song, X., Luo, Y., 2011. Tumor-associated macrophages promote angiogenesis and melanoma growth via adrenomedullin in a paracrine and autocrine manner. Clinical Cancer Research.

Chen, X., Han, J., Chu, J., Zhang, L., Zhang, J., Chen, C., Chen, L., Wang, Y., Wang, H., Yi, L. and Elder, J.B., 2016. A combinational therapy of EGFR-CAR NK cells and oncolytic herpes simplex virus 1 for breast cancer brain metastases. *Oncotarget*, *7*(19), p.27764.

Cheng, S., Han, F., Xu, Y., Qu, T., Ju, Y., 2018. Expression of Tim-3 in breast cancer tissue promotes tumor progression. Int J Clin Exp Pathol 11, 1157–1166.

Cheng, L., Jiang, H., Fan, J., Wang, J., Hu, P., Ruan, Y. and Liu, R., 2018. A novel oncolytic herpes simplex virus armed with the carboxyl-terminus of murine MyD116 has enhanced anti-tumour efficacy against human breast cancer cells. *Oncology Letters*, *15*(5), pp.7046-7052.

Chesney, J., Puzanov, I., Collichio, F., Singh, P., Milhem, M.M., Glaspy, J., Hamid, O., Ross, M., Friedlander, P., Garbe, C., Logan, T.F., Hauschild, A., Lebbé, C., Chen, L., Kim, J.J., Gansert, J., Andtbacka, R.H.I., Kaufman, H.L., 2018. Randomized, open-label phase II study evaluating the efficacy and safety of talimogene laherparepvec in combination with ipilimumab versus ipilimumab alone in patients with advanced, unresectable melanoma. Journal of Clinical Oncology 36.

Chiba, S., Baghdadi, M., Akiba, H., Yoshiyama, H., Kinoshita, I., Dosaka-Akita, H., Fujioka, Y., Ohba, Y., Gorman, J. V., Colgan, J.D., Hirashima, M., Uede, T., Takaoka, A., Yagita, H., Jinushi, M., 2012. Tumor-infiltrating DCs suppress nucleic acid-mediated innate immune responses through interactions between the receptor TIM-3 and the alarmin HMGB1. Nat Immunol.

Choi, A.H., O'Leary, M.P., Fong, Y., Chen, N.G., 2016. From benchtop to bedside: A review of oncolytic virotherapy. Biomedicines 4, 1–20.

Chon, H.J., Lee, W.S., Yang, H., Kong, S.J., Lee, N.K., Moon, E.S., Choi, J., Han, E.C., Kim, Joo Hoon, Ahn, J.B., Kim, Joo Hang, Kim, C., 2019. Tumor microenvironment remodeling by intratumoral oncolytic vaccinia virus enhances the efficacy of immune-checkpoint blockade. Clinical Cancer Research 25.

Clarke, R., 1996. H u m a n breast cancer cell line xenografts as models of breast cancer m The immunobiologies of recipient mice and the characteristics of several tumorigenic cell lines. Breast Cancer Res Treat 39, 69–86.

Clinic, T.A., Angeles, L., Oaks, T., Park, R., Food, U.S., 2019. Intratumoral Immunotherapy — Update 2019 1–16.

Cody, J.J., Markert, J.M. and Hurst, D.R., 2014. Histone deacetylase inhibitors improve the replication of oncolytic herpes simplex virus in breast cancer cells. *PloS one*, *9*(3), p.e92919.

Condeelis, J., Pollard, J.W., 2006. Macrophages: Obligate partners for tumor cell migration, invasion, and metastasis. Cell.

Conry, R.M., Westbrook, B., McKee, S., Norwood, T.G., 2018. Talimogene laherparepvec: First in class oncolytic virotherapy. Hum Vaccin Immunother 14, 839–846.

Cripe, T.P., Wang, P.Y., Marcato, P., Mahller, Y.Y., Lee, P.W.K., 2009. Targeting cancer-initiating cells with oncolytic viruses. Molecular Therapy.

Da Silva, I.P., Gallois, A., Jimenez-Baranda, S., Khan, S., Anderson, A.C., Kuchroo, V.K., Osman, I., Bhardwaj, N., 2014. Reversal of NK-cell exhaustion in advanced melanoma by Tim-3 blockade. Cancer Immunol Res.

Dannenmann, S.R., Thielicke, J., Stöckli, M., Matter, C., von Boehmer, L., Cecconi, V., Hermanns, T., Hefermehl, L., Schraml, P., Moch, H., Knuth, A., van den Broek, M., 2013. Tumor-associated macrophages subvert t-cell function and correlate with reduced survival in clear cell renal cell carcinoma. Oncoimmunology.

de Mingo Pulido, Á., Gardner, A., Hiebler, S., Soliman, H., Rugo, H.S., Krummel, M.F., Coussens, L.M., Ruffell, B., 2018. TIM-3 Regulates CD103+ Dendritic Cell Function and Response to Chemotherapy in Breast Cancer. Cancer Cell 33, 60-74.e6.

De Visser, K.E., Eichten, A., Coussens, L.M., 2006. Paradoxical roles of the immune system during cancer development. Nat Rev Cancer.

DeKruyff, R.H., Bu, X., Ballesteros, A., Santiago, C., Chim, Y.-L.E., Lee, H.-H., Karisola, P., Pichavant, M., Kaplan, G.G., Umetsu, D.T., Freeman, G.J., Casasnovas, J.M., 2010. T Cell/Transmembrane, Ig, and Mucin-3 Allelic Variants Differentially Recognize Phosphatidylserine and Mediate Phagocytosis of Apoptotic Cells. J Immunol 184, 1918.

Department of Neurosurgery, The University of Tokyo, Tokyo, Japan, 2008. 2060–2064.

Dmitrieva, N., Yu, L., Viapiano, M., Cripe, T.P., Chiocca, E.A., Glorioso, J.C., Kaur, B., 2011. Chondroitinase ABC I-mediated enhancement of oncolytic virus spread and antitumor efficacy. Clinical Cancer Research.

Domschke, C., Schneeweiss, A., Stefanovic, S., Wallwiener, M., Heil, J., Rom, J., Sohn, C., Schuetz, F., 2016. Cellular Immune Responses and Immune Escape Mechanisms in Breast Cancer: Determinants of Immunotherapy. Breast Care 11, 102–107.

Doniņą, S., Strele, I., Proboka, G., Auziņš, J., Alberts, P., Jonsson, B., Venskus, D., Muceniece, A., 2015a. Adapted ECHO-7 virus Rigvir immunotherapy (oncolytic virotherapy) prolongs survival in melanoma patients after surgical excision of the tumour in a retrospective study. Melanoma Res.

Doniņą, S., Strele, I., Proboka, G., Auziņš, J., Alberts, P., Jonsson, B., Venskus, D., Muceniece, A., 2015b. Adapted ECHO-7 virus Rigvir immunotherapy (oncolytic virotherapy) prolongs survival in melanoma patients after surgical excision of the tumour in a retrospective study. Melanoma Res.

Du, W., Yang, M., Turner, A., Xu, C., Ferris, R.L., Huang, J., Kane, L.P., Lu, B., 2017. Tim-3 as a target for cancer immunotherapy and mechanisms of action. Int J Mol Sci.

Dunham, L.J., Stewart, H.L., n.d. A Survey of Transplantable and Trans-missible Animal Tumors.

Dunn, G.P., Old, L.J., Schreiber, R.D., 2004. The Three Es of Cancer Immunoediting. Annu Rev Immunol.

Dyck, L., Mills, K.H.G., 2017. Immune checkpoints and their inhibition in cancer and infectious diseases. Eur J Immunol 47, 765–779.

Epstein, S.P., Gadaria-Rathod, N., Wei, Y., Maguire, M.G., Asbell, P.A., 2013. HLA-DR expression as a biomarker of inflammation for multicenter clinical trials of ocular surface disease. Exp Eye Res.

Errington, F., Steele, L., Prestwich, R., Harrington, K.J., Pandha, H.S., Vidal, L., de Bono, J., Selby, P., Coffey, M., Vile, R., Melcher, A., 2008. Reovirus Activates Human Dendritic Cells to Promote Innate Antitumor Immunity. The Journal of Immunology.

ESMO Congress 2022 | OncologyPRO [WWW Document], n.d. URL https://oncologypro.esmo.org/meeting-resources/esmo-congress-2022/first-in-human-phase-i-study-of-incagn02390-a-Tim-3-monoclonal-antibody-antagonist-in-patients-with-advanced-malignancies (accessed 12.11.23).

Fan, Y., He, S., 2022. The Characteristics of Tumor Microenvironment in Triple Negative Breast Cancer. Cancer Manag Res.

Fan, J., Jiang, H., Cheng, L. and Liu, R., 2016. The oncolytic herpes simplex virus vector, G47Δ, effectively targets tamoxifen-resistant breast cancer cells. *Oncology Reports*, *35*(3), pp.1741-1749.

Fang, H., Pengal, R.A., Cao, X., Ganesan, L.P., Wewers, M.D., Marsh, C.B., Tridandapani, S., 2004. Lipopolysaccharide-Induced Macrophage Inflammatory Response Is Regulated by SHIP. The Journal of Immunology 173, 360–366.

Fantozzi, A., Christofori, G., 2006. Mouse models of breast cancer metastasis. Breast Cancer Research 8, 212.

Fei, F., Rong, L., Jiang, N., Wayne, A.S., Xie, J., 2022. Targeting HLA-DR loss in hematologic malignancies with an inhibitory chimeric antigen receptor. Molecular Therapy 30, 1215.

Ferguson, M.S., Lemoine, N.R., Wang, Y., 2012. Systemic delivery of oncolytic viruses: Hopes and hurdles. Adv Virol 2012.

Festjens, N., Vanden Berghe, T., Vandenabeele, P., 2006. Necrosis, a well-orchestrated form of cell demise: Signalling cascades, important mediators and concomitant immune response. Biochimica et Biophysica Acta (BBA) - Bioenergetics 1757, 1371–1387.

Fields, B.N., Knipe, D.M., Howley, P.M., 2007. Fields Virology, 5th Edition, Fields Virology.

Fife, B.T., Bluestone, J.A., 2008. Control of peripheral T-cell tolerance and autoimmunity via the CTLA-4 and PD-1 pathways. Immunol Rev 224, 166–182.

Fischer, A.H., Jacobson, K.A., Rose, J., Zeller, R., 2008. Hematoxylin and Eosin Staining of Tissue and Cell Sections. Cold Spring Harb Protoc 2008, pdb.prot4986.

Fountzilas, C., Patel, S., Mahalingam, D., 2017. Review: Oncolytic virotherapy, updates and future directions. Oncotarget 8, 102617–102639.

Fourcade, J., Sun, Z., Benallaoua, M., Guillaume, P., Luescher, I.F., Sander, C., Kirkwood, J.M., Kuchroo, V., Zarour, H.M., 2010. Upregulation of Tim-3 and PD-1 expression is associated with tumor antigen-specific CD8+ T cell dysfunction in melanoma patients. Journal of Experimental Medicine.

Fowlkes, B.J., Schweighoffer, E., 1995. Positive selection of T cells. Curr Opin Immunol 7, 188–195.

Frampton, A.R., Goins, W.F., Nakano, K., Burton, E.A., Glorioso, J.C., 2005. HSV trafficking and development of gene therapy vectors with applications in the nervous system. Gene Ther.

Freeman, G.J., Casasnovas, J.M., Umetsu, D.T., Dekruyff, R.H., 2010. TIM genes: A family of cell surface phosphatidylserine receptors that regulate innate and adaptive immunity. Immunol Rev.

Fridman, W.H., Pagès, F., Sauts-Fridman, C., Galon, J., 2012. The immune contexture in human tumours: impact on clinical outcome. Nature Reviews Cancer 2012 12:4 12, 298–306.

Frisancho-Kiss, S., Nyland, J.F., Davis, S.E., Barrett, M.A., Gatewood, S.J.L., Njoku, D.B., Cihakova, D., Silbergeld, E.K., Rose, N.R., Fairweather, D., 2006. Cutting Edge: T Cell Ig Mucin-3 Reduces Inflammatory Heart Disease by Increasing CTLA-4 during Innate Immunity. The Journal of Immunology.

Fukuhara, H., Martuza, R.L., Rabkin, S.D., Ito, Y., Todo, T., 2005. Oncolytic herpes simplex virus vector G47Δ in combination with androgen ablation for the treatment of human prostate adenocarcinoma. Clinical Cancer Research.

Gabrilovich, D.I., Ostrand-Rosenberg, S., Bronte, V., 2012. Coordinated regulation of myeloid cells by tumours. Nat Rev Immunol.

Galanis, E., Markovic, S.N., Suman, V.J., Nuovo, G.J., Vile, R.G., Kottke, T.J., Nevala, W.K., Thompson, M.A., Lewis, J.E., Rumilla, K.M., Roulstone, V., Harrington, K., Linette, G.P., Maples, W.J., Coffey, M., Zwiebel, J., Kendra, K., 2012. Phase II trial of intravenous administration of reolysin ® (reovirus serotype-3-dearing strain) in patients with metastatic melanoma. Molecular Therapy.

Gao, X., Zhu, Y., Li, G., Huang, H., Zhang, G., Wang, F., Sun, J., Yang, Q., Zhang, X., Lu, B., 2012a. TIM-3 expression characterizes regulatory T cells in tumor tissues and is associated with lung cancer progression. PLoS One.

Gao, X., Zhu, Y., Li, G., Huang, H., Zhang, G., Wang, F., Sun, J., Yang, Q., Zhang, X., Lu, B., 2012b. TIM-3 Expression Characterizes Regulatory T Cells in Tumor Tissues and Is Associated with Lung Cancer Progression. PLoS One 7.

Gauthier, N., Lohm, S., Touzery, C., Chantôme, A., Perette, B., Reveneau, S., Brunotte, F., Juillerat-Jeanneret, L., Jeannin, J.F., 2004. Tumour-derived and host-derived nitric oxide differentially regulate breast carcinoma metastasis to the lungs. Carcinogenesis 25, 1559–1565.

Geevarghese, S.K., Geller, D.A., De Haan, H.A., Hörer, M., Knoll, A.E., Mescheder, A., Nemunaitis, J., Reid, T.R., Sze, D.Y., Tanabe, K.K., Tawfik, H., 2010. Phase I/II study of oncolytic herpes simplex virus NV1020 in patients with extensively pretreated refractory colorectal cancer metastatic to the liver. Hum Gene Ther 21, 1119–1128.

Gefen, T., Castro, I., Muharemagic, D., Puplampu-Dove, Y., Patel, S., Gilboa, E., 2017. A TIM-3 Oligonucleotide Aptamer Enhances T Cell Functions and Potentiates Tumor Immunity in Mice. Mol Ther 25, 2280–2288.

Genard, G., Lucas, S., Michiels, C., 2017. Reprogramming of tumor-associated macrophages with anticancer therapies: Radiotherapy versus chemo- and immunotherapies. Front Immunol.

Gennari, A., André, F., Barrios, C.H., Cortes, J., de Azambuja, E., DeMichele, A., Dent, R., Fenlon, D.,

Gligorov, J., Hurvitz, S.A. and Im, S.A., 2021. ESMO Clinical Practice Guideline for the diagnosis, staging

and treatment of patients with metastatic breast cancer☆. *Annals of oncology*, *32*(12), pp.1475-1495.

Ghasemi Darestani, N., Gilmanova, A.I., Al-Gazally, M.E., Zekiy, A.O., Ansari, M.J., Zabibah, R.S., Jawad, M.A., Al-Shalah, S.A.J., Rizaev, J.A., Alnassar, Y.S., Mohammed, N.M., Mustafa, Y.F., Darvishi, M., Akhavan-Sigari, R., 2023. Mesenchymal stem cell-released oncolytic virus: an innovative strategy for cancer treatment. Cell Commun Signal 21, 43.

Ghouse, S.M., Nguyen, H.M., Bommareddy, P.K., Guz-Montgomery, K. and Saha, D., 2020. Oncolytic herpes simplex virus encoding IL12 controls triple-negative breast cancer growth and metastasis. *Frontiers in oncology*, *10*, p.384.

Gleason, M.K., Lenvik, T.R., McCullar, V., Felices, M., O'Brien, M.S., Cooley, S.A., Verneris, M.R., Cichocki, F., Holman, C.J., Panoskaltsis-Mortari, A., Niki, T., Hirashima, M., Blazar, B.R., Miller, J.S., 2012. Tim-3 is an inducible human natural killer cell receptor that enhances interferon gamma production in response to galectin-9. Blood.

Golden-Mason, L., Palmer, B.E., Kassam, N., Townshend-Bulson, L., Livingston, S., McMahon, B.J., Castelblanco, N., Kuchroo, V., Gretch, D.R., Rosen, H.R., 2009. Negative Immune Regulator Tim-3 Is Overexpressed on T Cells in Hepatitis C Virus Infection and Its Blockade Rescues Dysfunctional CD4+ and CD8+ T Cells. J Virol.

Goldufsky, J., Sivendran, S., Harcharik, S., Pan, M., Bernardo, S., Stern, R., Friedlander, P., Ruby, C., Saenger, Y., Kaufman, H., 2013. Oncolytic virus therapy for cancer. Oncolytic Virother 2, 31–46.

Goradel, N.H., Baker, A.T., Arashkia, A., Ebrahimi, N., Ghorghanlu, S., Negahdari, B., 2021. Oncolytic virotherapy: Challenges and solutions. Curr Probl Cancer 45, 100639.

Gregory, C.D., 2000. CD14-dependent clearance of apoptotic cells: relevance to the immune system. Curr Opin Immunol 12, 27–34.

Grossardt, C., Engeland, C.E., Bossow, S., Halama, N., Zaoui, K., Leber, M.F., Springfeld, C., Jaeger, D., Von Kalle, C., Ungerechts, G., 2013. Granulocyte-macrophage colony-stimulating factor-armed oncolytic measles virus is an effective therapeutic cancer vaccine. Hum Gene Ther.

Gu, X., Jia, X., Feng, J., Shen, B., Huang, Y., Geng, S., Sun, Y., Wang, Y., Li, Y., Long, M., 2010. Molecular modeling and affinity determination of scFv antibody: proper linker peptide enhances its activity. Ann Biomed Eng 38, 537–549.

Gu, Y., Li, J., Gu, L., Bi, Y., Li, X., Liao, C., Liao, X., Huang, Z., Chen, L., Huang, Y., 2020. Tim-3 expression on t cells is correlated with liver inflammation, fibrosis and virological characteristics in treatment-naïve chronic hepatitis B patients: a cross-sectional study. Ann Blood.

Guffey, M.B., Parker, J.N., Luckett, W.S., Gillespie, G.Y., Meleth, S., Whitley, R.J., Markert, J.M., 2007. Engineered herpes simplex virus expressing bacterial cytosine deaminase for experimental therapy of brain tumors. Cancer Gene Ther.

Guo, Q., Shen, S., Guan, G., Zhu, C., Zou, C., Cao, J., Cheng, W., Xu, X., Yu, J., Lin, Z., Wang, G., Chen, L., Cheng, P., Wu, A., 2022a. Cancer cell intrinsic TIM-3 induces glioblastoma progression. iScience 25.

Guo, Q., Zhao, P., Zhang, Z., Zhang, J., Zhang, Z., Hua, Y., Han, B., Li, N., Zhao, X. and Hou, L., 2020. TIM-3 blockade combined with bispecific antibody MT110 enhances the anti-tumor effect of γδ T cells. *Cancer Immunology, Immunotherapy*, *69*, pp.2571-2587.

Guo, W., Fensom, G.K., Reeves, G.K., Key, T.J., 2020. Physical activity and breast cancer risk: results from the UK Biobank prospective cohort. British Journal of Cancer 2020 122:5 122, 726–732.

Guo, Z., Cheng, D., Xia, Z., Luan, M., Wu, L., Wang, G., Zhang, S., 2013. Combined TIM-3 blockade and CD137 activation affords the long-term protection in a murine model of ovarian cancer. J Transl Med 11.

Guy, C.T., Cardiff, R.D., Muller`*, W.J., 1992. Induction of Mammary Tumors by Expression of Polyomavirus Middle T Oncogene: A Transgenic Mouse Model for Metastatic Disease. Mol Cell Biol 12, 954–961.

Hamdan, F., Ylosmaki, E., Chiaro, J., Giannoula, Y., Long, M., Fusciello, M., Feola, S., Martins, B., Feodoroff, M., Antignani, G., Russo, S., Kari, O., Lee, M., Jarvinen, P., Nisen, H., Kreutzman, A., Leusen, J., Mustjoki, S., McWilliams, T.G., Gronholm, M., Cerullo, V., 2021. Original research: Novel oncolytic adenovirus expressing enhanced cross-hybrid IgGA Fc PD-L1 inhibitor activates multiple immune effector populations leading to enhanced tumor killing in vitro, in vivo and with patient-derived tumor organoids. J Immunother Cancer 9, 3000.

Hamilton, J.A., 2008. Colony-stimulating factors in inflammation and autoimmunity. Nat Rev Immunol.

Han, Q., Shi, H., Liu, F., 2016. CD163+ M2-type tumor-associated macrophage support the suppression of tumor-infiltrating T cells in osteosarcoma. Int Immunopharmacol 34, 101–106.

Han, S., Feng, S., Xu, L., Shi, W., Wang, X., Wang, H., Yu, C., Dong, T., Xu, M., Liang, G., 2014. Tim-3 on Peripheral CD4+ and CD8+ T Cells Is Involved in the Development of Glioma. https://home.liebertpub.com/dna 33, 245–250.

Han, X., Yu, S., Li, A., Liu, Q., Yuan, X., Xu, H., Jiao, D., Pestell, R.G., Wu, K., 2017. Recent advances of bispecific antibodies in solid tumors. J Hematol Oncol.

Hanahan, D., Weinberg, R.A., 2011. Hallmarks of cancer: The next generation. Cell.

Hanahan, D., 2022. Hallmarks of cancer: new dimensions. *Cancer discovery*, *12*(1), pp.31-46.

Hardcastle, J., Kurozumi, K., Dmitrieva, N., Sayers, M.P., Ahmad, S., Waterman, P., Weissleder, R., Chiocca, E.A., Kaur, B., 2010. Enhanced antitumor efficacy of vasculostatin (Vstat120) expressing oncolytic HSV-1. Molecular Therapy.

Hargadon, K.M., Johnson, C.E., Williams, C.J., 2018. Immune checkpoint blockade therapy for cancer: An overview of FDA-approved immune checkpoint inhibitors. Int Immunopharmacol.

Harrington, K., Freeman, D.J., Kelly, B., Harper, J., Soria, J.C., 2019. Optimizing oncolytic virotherapy in cancer treatment. Nat Rev Drug Discov 18, 689–706.

Hastings, W.D., Anderson, D.E., Kassam, N., Koguchi, K., Greenfield, E.A., Kent, S.C., Xin, X.Z., Strom, T.B., Hafler, D.A., Kuchroo, V.K., 2009. TIM-3 is expressed on activated human CD4+ T cells and regulates Th1 and Th17 cytokines. Eur J Immunol 39, 2492–2501.

He, Y., Cao, J., Zhao, C., Li, X., Zhou, C., Hirsch, F.R., 2018. TIM-3, a promising target for cancer immunotherapy. Onco Targets Ther.

Hiraga, T., Ninomiya, T., 2019. Establishment and characterization of a C57BL/6 mouse model of bone metastasis of breast cancer. J Bone Miner Metab 37, 235–242.

Hollebecque, A., Chung, H.C., Miguel, M.J.D., Italiano, A., MacHiels, J.P., Lin, C.C., Dhani, N.C., Peeters, M., Moreno, V., Su, W.C., Chow, K.H., Galvao, V.R., Carlse, M., Yu, D., Szpurka, A.M., Zhao, Y., Schmidt, S.L., Gandhi, L., Xu, X., Bang, Y.J., 2021. Safety and Antitumor Activity of a-PD-L1 Antibody as Monotherapy or in Combination witha-TIM-3 Antibody in Patients with Microsatellite Instability-High/Mismatch Repair-Deficient Tumors. Clinical Cancer Research 27, 6393–6404.

Holzer, R.G., MacDougall, C., Cortright, G., Atwood, K., Green, J.E., Jorcyk, C.L., 2003. Development and characterization of a progressive series of mammary adenocarcinoma cell lines derived from the C3(1)/SV40 Large T-antigen transgenic mouse model. Breast Cancer Res Treat 77, 65–76.

Howard, F., Conner, J., Danson, S., Muthana, M., 2022. Inconsistencies in Modeling the Efficacy of the Oncolytic Virus HSV1716 Reveal Potential Predictive Biomarkers for Tolerability. Front Mol Biosci 9, 889395.

Howard, Faith H N, Al-Janabi, Haider, Patel, Priya, Cox, Katie, Smith, Emily, Vadakekolathu, Jayakumar, Pockley, A Graham, Conner, J., Nohl, James F, Allwood, Dan A, Collado-Rojas, Cristal, Kennerley, Aneurin, Staniland, S., Muthana, Munitta, Howard, F H N, Al-Janabi, H, Patel, P, Cox, K, Collado-Rojas, C, Muthana, M, Smith, E, Vadakekolathu, J, Pockley, A G, Van, J., Cancer, G., Nohl, J F, Allwood, D A, Kennerley, A, 2022. Nanobugs as Drugs: Bacterial Derived Nanomagnets Enhance Tumor Targeting and Oncolytic Activity of HSV-1 Virus. Small 18, 2104763.

Howard, Faith H.N., Kwan, A., Winder, N., Mughal, A., Collado-Rojas, C., Muthana, M., 2022. Understanding Immune Responses to Viruses-Do Underlying Th1/Th2 Cell Biases Predict Outcome? Viruses 14.

Howells, A., Marelli, G., Lemoine, N.R., Wang, Y., 2017a. Oncolytic viruses-interaction of virus and tumor cells in the battle to eliminate cancer. Front Oncol 7.

Howells, A., Marelli, G., Lemoine, N.R., Wang, Y., 2017b. Oncolytic viruses-interaction of virus and tumor cells in the battle to eliminate cancer. Front Oncol 7.

Hu, G., Xu, F., Zhong, K., Wang, S., Huang, L., Chen, W., 2018. Activated tumor-infiltrating fibroblasts predict worse prognosis in breast cancer patients. J Cancer 9.

Huang, C., Zhu, H.X., Yao, Y., Bian, Z.H., Zheng, Y.J., Li, L., Moutsopoulos, H.M., Gershwin, M.E., Lian, Z.X., 2019. Immune checkpoint molecules. Possible future therapeutic implications in autoimmune diseases. J Autoimmun 104, 102333.

Huang, P., Watanabe, M., Kaku, H., Kashiwakura, Y., Chen, J., Saika, T., Nasu, Y., Fujiwara, T., Urata, Y., Kumon, H., 2008. Direct and distant antitumor effects of a telomerase-selective oncolytic adenoviral agent, OBP-301, in a mouse prostate cancer model. Cancer Gene Ther.

Huang, Y.H., Zhu, C., Kondo, Y., Anderson, A.C., Gandhi, A., Russell, A., Dougan, S.K., Petersen, B.S., Melum, E., Pertel, T., Clayton, K.L., Raab, M., Chen, Q., Beauchemin, N., Yazaki, P.J., Pyzik, M., Ostrowski, M.A., Glickman, J.N., Rudd, C.E., Ploegh, H.L., Franke, A., Petsko, G.A., Kuchroo, V.K., Blumberg, R.S., 2015. CEACAM1 regulates TIM-3-mediated tolerance and exhaustion. Nature.

Huo, W., Yang, X., Wang, B., Cao, L., Fang, Z., Li, Z., Liu, H., Liang, X. jie, Zhang, J., Jin, Y., 2022. Biomineralized hydrogel DC vaccine for cancer immunotherapy: A boosting strategy via improving immunogenicity and reversing immune-inhibitory microenvironment. Biomaterials 288, 121722.

Hurvitz, S.A., Hu, Y., O'Brien, N., Finn, R.S., 2013. Current approaches and future directions in the treatment of HER2-positive breast cancer. Cancer Treat Rev.

Irani, Y.D., Kok, C.H., Clarson, J., Shanmuganathan, N., Branford, S., Yeung, D.T., Ross, D.M., Hughes, T.P., Yong, A.S.M., 2023. Association of TIM-3 checkpoint receptor expression on T cells with treatment-free remission in chronic myeloid leukemia. Blood Adv 7, 2364.

Iscaro, A., Jones, C., Forbes, N., Mughal, A., Howard, F.N., Janabi, H. Al, Demiral, S., Perrie, Y., Essand, M., Weglarz, A., Cruz, L.J., Lewis, C.E., Muthana, M., 2022. Targeting circulating monocytes with CCL2-loaded liposomes armed with an oncolytic adenovirus. Nanomedicine 40, 102506.

Jackson III, W., Krishnan, V. and Mastro, A.M., 2013. The Breast Cancer Metastases in Bone Conundrum. In *Madame Curie Bioscience Database [Internet]*. Landes Bioscience.

Jenkins, S., Wesolowski, R., Gatti-Mays, M.E., 2021. Improving Breast Cancer Responses to Immunotherapy—a Search for the Achilles Heel of the Tumor Microenvironment. Curr Oncol Rep.

Jia, T., Liu, Y., Fan, Y., Wang, L., Jiang, E., 2022. Association of Healthy Diet and Physical Activity with Breast Cancer: Lifestyle Interventions and Oncology Education. Front Public Health 10, 797794.

Jiang, J., Jin, M.S., Kong, F., Cao, D., Ma, H.X., Jia, Z., Wang, Y.P., Suo, J., Cao, X., 2013. Decreased Galectin-9 and Increased Tim-3 Expression Are Related to Poor Prognosis in Gastric Cancer. PLoS One 8.

Jiang, W., Li, F., Jiang, Y., Li, S., Liu, X., Xu, Y., Li, B., Feng, X., Zheng, C., 2022. Tim-3 Blockade Elicits Potent Anti-Multiple Myeloma Immunity of Natural Killer Cells. Front Oncol 12, 739976.

Jin, H.T., Anderson, A.C., Tan, W.G., West, E.E., Ha, S.J., Araki, K., Freeman, G.J., Kuchroo, V.K., Ahmed, R., 2010. Cooperation of Tim-3 and PD-1 in CD8 T-cell exhaustion during chronic viral infection. Proc Natl Acad Sci U S A.

Jinushi, M., Yoneda, A., 2013. T cell immunoglobulin domain and mucin domain-3 as an emerging target for immunotherapy in cancer management. Immunotargets Ther.

Johnstone, C.N., Smith, Y.E., Cao, Y., Burrows, A.D., Cross, R.S.N., Ling, X., Redvers, R.P., Doherty, J.P., Eckhardt, B.L., Natoli, A.L., Restall, C.M., Lucas, E., Pearson, H.B., Deb, S., Britt, K.L., Rizzitelli, A., Li, J., Harmey, J.H., Pouliot, N., Anderson, R.L., 2015a. Functional and molecular characterisation of EO771.LMB tumours, a new C57BL/6-mouse-derived model of spontaneously metastatic mammary cancer. DMM Disease Models and Mechanisms 8, 237–251.

Johnstone, C.N., Smith, Y.E., Cao, Y., Burrows, A.D., Cross, R.S.N., Ling, X., Redvers, R.P., Doherty, J.P., Eckhardt, B.L., Natoli, A.L., Restall, C.M., Lucas, E., Pearson, H.B., Deb, S., Britt, K.L., Rizzitelli, A., Li, J., Harmey, J.H., Pouliot, N., Anderson, R.L., 2015b. Functional and molecular characterisation of EO771.LMB tumours, a new C57BL/6-mouse-derived model of spontaneously metastatic mammary cancer. DMM Disease Models and Mechanisms 8, 237–251.

Jones, R.B., Ndhlovu, L.C., Barbour, J.D., Sheth, P.M., Jha, A.R., Long, B.R., Wong, J.C., Satkunarajah, M., Schweneker, M., Chapman, J.M., Gyenes, G., Vali, B., Hyrcza, M.D., Yue, F.Y., Kovacs, C., Sassi, A., Loutfy, M., Halpenny, R., Persad, D., Spotts, G., Hecht, F.M., Chun, T.W., McCune, J.M., Kaul, R., Rini, J.M., Nixon, D.F., Ostrowski, M.A., 2008. Tim-3 expression defines a novel population of dysfunctional T cells with highly elevated frequencies in progressive HIV-1 infection. Journal of Experimental Medicine.

Ju, F., Luo, Y., Lin, C., Jia, X., Xu, Z., Tian, R., Lin, Y., Zhao, M., Chang, Y., Huang, X., Li, S., Ren, W., Qin, Y., Yu, M., Jia, J., Han, J., Luo, W., Zhang, J., Fu, G., Ye, X., Huang, C., Xia, N., 2022a. Original research: Oncolytic virus expressing PD-1 inhibitors activates a collaborative intratumoral immune response to control tumor and synergizes with CTLA-4 or TIM-3 blockade. J Immunother Cancer 10, 4762.

Ju, F., Luo, Y., Lin, C., Jia, X., Xu, Z., Tian, R., Lin, Y., Zhao, M., Chang, Y., Huang, X., Li, S., Ren, W., Qin, Y., Yu, M., Jia, J., Han, J., Luo, W., Zhang, J., Fu, G., Ye, X., Huang, C., Xia, N., 2022b. Oncolytic virus

expressing PD-1 inhibitors activates a collaborative intratumoral immune response to control tumor and synergizes with CTLA-4 or TIM-3 blockade. J Immunother Cancer 10.

Ju, F., Luo, Y., Lin, C., Jia, X., Xu, Z., Tian, R., Lin, Y., Zhao, M., Chang, Y., Huang, X., Li, S., Ren, W., Qin, Y., Yu, M., Jia, J., Han, J., Luo, W., Zhang, J., Fu, G., Ye, X., Huang, C., Xia, N., 2022c. Original research: Oncolytic virus expressing PD-1 inhibitors activates a collaborative intratumoral immune response to control tumor and synergizes with CTLA-4 or TIM-3 blockade. J Immunother Cancer 10, 4762.

Ju, F., Luo, Y., Lin, C., Jia, X., Xu, Z., Tian, R., Lin, Y., Zhao, M., Chang, Y., Huang, X., Li, S., Ren, W., Qin, Y., Yu, M., Jia, J., Han, J., Luo, W., Zhang, J., Fu, G., Ye, X., Huang, C., Xia, N., 2022d. Original research: Oncolytic virus expressing PD-1 inhibitors activates a collaborative intratumoral immune response to control tumor and synergizes with CTLA-4 or TIM-3 blockade. J Immunother Cancer 10, 4762.

Justus, C.R., Leffler, N., Ruiz-Echevarria, M., Yang, L. V., 2014. In vitro Cell Migration and Invasion Assays. J Vis Exp 88, 51046.

Kahramanian, A., Kuroda, T., Wakimoto, H., 2019. with Therapeutic Genes of Interest 1937, 177–188.

Kamal, S., Kerndt, C.C., Lappin, S.L., 2023. Genetics, Histocompatibility Antigen. StatPearls.

Kanai, R., Zaupa, C., Sgubin, D., Antoszczyk, S.J., Martuza, R.L., Wakimoto, H., Rabkin, S.D., Wilcox, D.R., Longnecker, R., 2016. Effect of γ34.5 Deletions on Oncolytic Herpes Simplex Virus Activity in Brain Tumors. PLoS Pathog.

Kantarjian, H.M., Talpaz, M., O'Brien, S., Kurzrock, R., Gutterman, J., Keating, M.J., McCredie, K.B., Freireich, E.J., 1997. Chronic myelogenous leukemia - Progress at the M. D. Anderson Cancer Center over the past two decades and future directions: First Emil J Freireich Award Lecture. In: Clinical Cancer Research.

Karachaliou, N., Cao, M.G., Teixidó, C., Viteri, S., Morales-Espinosa, D., Santarpia, M., Rosell, R., 2015. Understanding the function and dysfunction of the immune system in lung cancer: the role of immune checkpoints. Cancer Biol Med 12, 79.

Katagata, M., Okayama, H., Nakajima, S., Saito, K., Sato, T., Sakuma, M., Fukai, S., Endo, E., Sakamoto, W., Saito, M., Saze, Z., Momma, T., Mimura, K., Kono, K., 2023. TIM-3 Expression and M2 Polarization of Macrophages in the TGFβ-Activated Tumor Microenvironment in Colorectal Cancer. Cancers (Basel) 15.

Kau, P., Nagaraja, G.M., Zheng, H., Gizachew, D., Galukande, M., Krishnan, S., Asea, A., 2012. A mouse model for triple-negative breast cancer tumor-initiating cells (TNBC-TICs) exhibits similar aggressive phenotype to the human disease. BMC Cancer 12, 120.

Kaufman, H.L., Kohlhapp, F.J., Zloza, A., 2015. Oncolytic viruses: A new class of immunotherapy drugs. Nat Rev Drug Discov.

Kaufman, H.L., Kohlhapp, F.J., Zloza, A., 2016. Erratum: Oncolytic viruses: a new class of immunotherapy drugs. Nat Rev Drug Discov 15.

Keenan, T.E., Tolaney, S.M., 2020. Role of immunotherapy in triple-negative breast cancer. JNCCN Journal of the National Comprehensive Cancer Network.

Kelly, C.M., Antonescu, C.R., Bowler, T., Munhoz, R., Chi, P., Dickson, M.A., Gounder, M.M., Keohan, M.L., Movva, S., Dholakia, R., Ahmad, H., Biniakewitz, M., Condy, M., Phelan, H., Callahan, M., Wong, P.,

Singer, S., Ariyan, C., Bartlett, E.K., Crago, A., Yoon, S., Hwang, S., Erinjeri, J.P., Qin, L.X., Tap, W.D., D'Angelo, S.P., 2020. Objective Response Rate among Patients with Locally Advanced or Metastatic Sarcoma Treated with Talimogene Laherparepvec in Combination with Pembrolizumab: A Phase 2 Clinical Trial. JAMA Oncol 6.

Kelly, E., Russell, S.J., 2007. History of oncolytic viruses: Genesis to genetic engineering. Molecular Therapy.

Khan, U., Biran, T., Ocean, A.J., Popa, E.C., Ruggiero, J.T., Paul, D., Garcia, C., Carr-Locke, D., Sharaiha, R., Urata, Y., Shah, M.A., 2019. Phase II study of a telomerase-specific oncolytic adenovirus (OBP-301, Telomelysin) in combination with pembrolizumab in gastric and gastroesophageal junction adenocarcinoma. Journal of Clinical Oncology.

Khanna, C., Hunter, K., 2005. Modeling metastasis in vivo. Carcinogenesis 26, 513–523.

Kim, J.E., Patel, M.A., Mangraviti, A., Kim, E.S., Theodros, D., Velarde, E., Liu, A., Sankey, E.W., Tam, A., Xu, H., Mathios, D., Jackson, C.M., Harris-Bookman, S., Garzon-Muvdi, T., Sheu, M., Martin, A.M., Tyler, B.M., Tran, P.T., Ye, X., Olivi, A., Taube, J.M., Burger, P.C., Drake, C.G., Brem, H., Pardoll, D.M., Lim, M., 2017a. Combination Therapy with Anti-PD-1, Anti-TIM-3, and Focal Radiation Results in Regression of Murine Gliomas. Clin Cancer Res 23, 124–136.

Kim, J.E., Patel, M.A., Mangraviti, A., Kim, E.S., Theodros, D., Velarde, E., Liu, A., Sankey, E.W., Tam, A., Xu, H., Mathios, D., Jackson, C.M., Harris-Bookman, S., Garzon-Muvdi, T., Sheu, M., Martin, A.M., Tyler, B.M., Tran, P.T., Ye, X., Olivi, A., Taube, J.M., Burger, P.C., Drake, C.G., Brem, H., Pardoll, D.M., Lim, M., 2017b. Combination Therapy with Anti-PD-1, Anti-TIM-3, and Focal Radiation Results in Regression of Murine Gliomas. Clin Cancer Res 23, 124.

Kim, R., Emi, M., Tanabe, K., 2007. Cancer immunoediting from immune surveillance to immune escape. Immunology.

Kirkwood, J.M., Butterfield, L.H., Tarhini, A.A., Zarour, H., Kalinski, P., Ferrone, S., 2012. Immunotherapy of cancer in 2012. CA Cancer J Clin 62, 309–335.

Kohlhapp, F.J., Kaufman, H.L., 2016. Molecular pathways: Mechanism of action for talimogene laherparepvec, a new oncolytic virus immunotherapy. Clinical Cancer Research 22, 1048–1054.

Kohrt, H.E., Nouri, N., Nowels, K., Johnson, D., Holmes, S., Lee, P.P., 2005. Profile of immune cells in axillary lymph nodes predicts disease-free survival in breast cancer. PLoS Med 2.

Krisky, D.M., Marconi, P.C., Oligino, T.J., Rouse, R.J.D., Fink, D.J., Cohen, J.B., Watkins, S.C., Glorioso, J.C., 1998. Development of herpes simplex virus replication-defective multigene vectors for combination gene therapy applications. Gene Ther.

Kulu, Y., Dorfman, J.D., Kuruppu, D., Fuchs, B.C., Goodwin, J.M., Fujii, T., Kuroda, T., Lanuti, M., Tanabe, K.K., 2009. Comparison of intravenous versus intraperitoneal administration of oncolytic herpes simplex virus 1 for peritoneal carcinomatosis in mice. Cancer Gene Ther.

Kwa, M.J., Adams, S., 2018. Checkpoint inhibitors in triple-negative breast cancer (TNBC): Where to go from here. Cancer.

Kwan, A., Winder, N., Atkinson, E., Al-Janabi, H., Allen, R.J., Hughes, R., Moamin, M., Louie, R., Evans, D., Hutchinson, M., Capper, D., Cox, K., Handley, J., Wilshaw, A., Kim, T., Tazzyman, S.J., Srivastava, S., Ottewell, P., Vadakekolathu, J., Pockley, G., Lewis, C.E., Brown, J.E., Danson, S.J., Conner, J., Muthana,

M., 2021. Macrophages mediate the antitumor effects of the oncolytic virus HSV1716 in mammary tumors. Mol Cancer Ther 20, 589–601.

Lambright, E.S., Caparrelli, D.J., Abbas, A.E., Toyoizumi, T., Coukos, G., Molnar-Kimber, K.L., Kaiser, L.R., 1999. Oncolytic therapy using a mutant type-1 herpes simplex virus and the role of the immune system. Ann Thorac Surg 68, 1756–1760.

Lan, M., Lu, W., Zou, T., Li, L., Liu, F., Cai, T., Cai, Y., 2021. Role of inflammatory microenvironment: potential implications for improved breast cancer nano-targeted therapy. Cellular and Molecular Life Sciences.

Lang, F.F., Conrad, C., Gomez-Manzano, C., Alfred Yung, W.K., Sawaya, R., Weinberg, J.S., Prabhu, S.S., Rao, G., Fuller, G.N., Aldape, K.D., Gumin, J., Vence, L.M., Wistuba, I., Rodriguez-Canales, J., Villalobos, P.A., Dirven, C.M.F., Tejada, S., Valle, R.D., Alonso, M.M., Ewald, B., Peterkin, J.J., Tufaro, F., Fueyo, J., 2018. Phase I study of DNX-2401 (delta-24-RGD) oncolytic adenovirus: replication and immunotherapeutic effects in recurrent malignant glioma. Journal of Clinical Oncology.

Lauer, U.M., Schell, M., Beil, J., Berchtold, S., Koppenhofer, U., Glatzle, J., Konigsrainer, A., Mohle, R., Nann, D., Fend, F., Pfannenberg, C., Bitzer, M., Malek, N.P., 2018. Phase I study of oncolytic vaccinia virus GL-ONC1 in patients with peritoneal carcinomatosis. Clinical Cancer Research.

Laurent, S., Carrega, P., Saverino, D., Piccioli, P., Camoriano, M., Morabito, A., Dozin, B., Fontana, V., Simone, R., Mortara, L., Mingari, M.C., Ferlazzo, G., Pistillo, M.P., 2010. CTLA-4 is expressed by human monocyte-derived dendritic cells and regulates their functions. Hum Immunol 71, 934–941.

Lawler, S.E., Speranza, M.C., Cho, C.F., Chiocca, E.A., 2017. Oncolytic viruses in cancer treatment a review. JAMA Oncol 3, 841–849.

Le Naour, A., Koffi, Y., Diab, M., Le Guennec, D., Rougé, S., Aldekwer, S., Goncalves-Mendes, N., Talvas, J., Farges, M.C., Caldefie-Chezet, F., Vasson, M.P., Rossary, A., 2020a. EO771, the first luminal B mammary cancer cell line from C57BL/6 mice. Cancer Cell Int 20.

Le Naour, A., Rossary, A., Vasson, M.P., 2020b. EO771, is it a well-characterized cell line for mouse mammary cancer model? Limit and uncertainty. Cancer Med 9, 8074.

Lelekakis, M., Moseley, J.M., Martin, T.J., Hards, D., Williams, E., Ho, P., Lowen, D., Javni, J., Miller, F.R., Slavin, J., Anderson, R.L., 1999. A novel orthotopic model of breast cancer metastasis to bone. Clin Exp Metastasis 17, 163–170.

Li, J., Cao, D., Guo, G., Wu, Y., Chen, Y., 2013. Expression and anatomical distribution of TIM-containing molecules in Langerhans cell sarcoma. J Mol Histol.

Li, L., Yang, L., Wang, L., Wang, F., Zhang, Z., Li, J., Yue, D., Chen, X., Ping, Y., Huang, L., Zhang, B., Zhang, Y., 2016. Impaired T cell function in malignant pleural effusion is caused by TGF-β derived predominantly from macrophages. Int J Cancer 139, 2261–2269.

Li, X., Wang, B., Gu, L., Zhang, J., Li, Xiaoyan, Gao, L., Ma, C., Liang, X., Li, Xingang, 2018. Tim-3 expression predicts the abnormal innate immune status and poor prognosis of glioma patients. Clinica Chimica Acta 476.

Li, Z., Ju, Z., Frieri, M., 2013. The T-cell immunoglobulin and mucin domain (Tim) gene family in asthma, allergy, and autoimmunity. Allergy Asthma Proc.

Li, Z., Qiu, Y., Lu, W., Jiang, Y., Wang, J., 2018. Immunotherapeutic interventions of Triple Negative Breast Cancer. J Transl Med.

Liang, M., 2018. Oncorine, the World First Oncolytic Virus Medicine and its Update in China. Curr Cancer Drug Targets.

Lifsted, T., Le Voyer, T., Williams, M., Muller, W., Klein-Szanto, A., Buetow, K.H., Hunter, K.W., 1998. IDENTIFICATION OF INBRED MOUSE STRAINS HARBORING GENETIC MODIFIERS OF MAMMARY TUMOR AGE OF ONSET AND METASTATIC PROGRESSION. Int. J. Cancer 77, 640–644.

Liikanen, I., Basnet, S., Quixabeira, D.C.A., Taipale, K., Hemminki, O., Oksanen, M., Kankainen, M., Juhila, J., Kanerva, A., Joensuu, T., Tähtinen, S., Hemminki, A., 2022. Oncolytic adenovirus decreases the proportion of TIM-3 + subset of tumor-infiltrating CD8 + T cells with correlation to improved survival in patients with cancer. J Immunother Cancer 10.

Limagne, E., Richard, C., Thibaudin, M., Fumet, J.D., Truntzer, C., Lagrange, A., Favier, L., Coudert, B., Ghiringhelli, F., 2019. Tim-3/galectin-9 pathway and mMDSC control primary and secondary resistances to PD-1 blockade in lung cancer patients. Oncoimmunology 8.

Lin, E.Y., Nguyen, A. V., Russell, R.G., Pollard, J.W., 2001. Colony-stimulating factor 1 promotes progression of mammary tumors to malignancy. Journal of Experimental Medicine.

Lin, H., Yang, B., Teng, M., 2017. T-cell immunoglobulin mucin-3 as a potential inducer of the epithelial-mesenchymal transition in hepatocellular carcinoma. Oncol Lett 14, 5899.

Lin, X.J., Li, Q.J., Lao, X.M., Yang, H., Li, S.P., 2015. Transarterial injection of recombinant human type-5 adenovirus H101 in combination with transarterial chemoembolization (TACE) improves overall and progressive-free survival in unresectable hepatocellular carcinoma (HCC). BMC Cancer.

Lin, Y., Wang, W., Wan, J., Yang, Y., Fu, W., Pan, D., Cai, L., Cheng, T., Huang, X., Wang, Y., 2018. Oncolytic activity of a coxsackievirus B3 strain in human endometrial cancer cell lines. Virol J.

Lipton, A., Steger, G.G., Figueroa, J., Alvarado, C., Solal-Celigny, P., Body, J.J., De Boer, R., Berardi, R., Gascon, P., Tonkin, K.S. and Coleman, R., 2007. Randomized active-controlled phase II study of denosumab efficacy and safety in patients with breast cancer-related bone metastases. *Journal of Clinical Oncology*, *25*(28), pp.4431-4437.

Lipton, A., Steger, G.G., Figueroa, J., Alvarado, C., Solal-Celigny, P., Body, J.J., De Boer, R., Berardi, R., Gascon, P., Tonkin, K.S. and Coleman, R.E., 2008. Extended efficacy and safety of denosumab in breast cancer patients with bone metastases not receiving prior bisphosphonate therapy. Clinical Cancer Research, 14(20), pp.6690-6696.

Lisi, L., Lacal, P.M., Martire, M., Navarra, P., Graziani, G., 2022. Clinical experience with CTLA-4 blockade for cancer immunotherapy: From the monospecific monoclonal antibody ipilimumab to probodies and bispecific molecules targeting the tumor microenvironment. Pharmacol Res 175.

Liu, R.B. and Rabkin, S.D., 2005. Oncolytic herpes simplex virus vectors for the treatment of human breast cancer. *Chinese medical journal*, *118*(04), pp.307-312.

Liu,B.L.,Robinson,M.,Han,Z.Q.,Branston,R.H.,English,C.,Reay,P.,McGrath,Y.,Thomas,S.K.,Thornton,M.,Bullok ,P., Love, C.A., Coffin, R.S., 2003. ICP34.5 deleted herpes simplex virus with enhanced oncolytic, immune stimulating, and anti-tumour properties. Gene Ther 10, 292–303.

Liu, C., Yang, M., Zhang, D., Chen, M., Zhu, D., 2022. Clinical cancer immunotherapy: Current progress and prospects. Front Immunol 13.

Liu, R., Martuza, R.L., Rabkin, S.D., 2005. Intracarotid delivery of oncolytic HSV vector G47Δ to metastatic breast cancer in the brain. Gene Ther.

Liu, Y.T., Sun, Z.J., 2021. Turning cold tumors into hot tumors by improving T-cell infiltration. Theranostics 11, 5365.

Loibl, S., André, F., Bachelot, T., Barrios, C.H., Bergh, J., Burstein, H.J., Cardoso, M.J., Carey, L.A., Dawood, S., Del Mastro, L. and Denkert, C., 2023. Early breast cancer: ESMO Clinical Practice Guideline for diagnosis, treatment and follow-up☆. *Annals of Oncology*, *35*(2), pp.159-182.

López-Soto, A., Gonzalez, S., Smyth, M.J., Galluzzi, L., 2017. Control of Metastasis by NK Cells. Cancer Cell.

Lou, E., 2003. Oncolytic Herpes Viruses as a Potential Mechanism for Cancer Therapy. Acta Oncol (Madr) 42, 660–671.

Ma, W., He, H., Wang, H., 2018a. Oncolytic herpes simplex virus and immunotherapy. BMC Immunol 19, 1–11.

Ma, W., He, H., Wang, H., 2018b. Oncolytic herpes simplex virus and immunotherapy. BMC Immunol 19, 1–11.

Mahller, Y.Y., Vaikunth, S.S., Ripberger, M.C., Baird, W.H., Saeki, Y., Cancelas, J.A., Crombleholme, T.M., Cripe, T.P., 2008. Tissue inhibitor of metalloproteinase-3 via oncolytic herpesvirus inhibits tumor growth and vascular progenitors. Cancer Res.

Malhotra, Sandeep, K., Teresa, Z., Jonathan, B., Joseph, E., Michael, D., Michael, F., Yuman, 2007. Use of an oncolytic virus secreting GM-CSF as combined oncolytic and immunotherapy for treatment of colorectal and hepatic adenocarcinomas. Surgery.

Malmberg, K.J., Carlsten, M., Björklund, A., Sohlberg, E., Bryceson, Y.T., Ljunggren, H.G., 2017. Natural killer cell-mediated immunosurveillance of human cancer. Semin Immunol.

Manservigi, R., Argnani, R., Marconi, P., 2010. HSV Recombinant Vectors for Gene Therapy~!2009-12-17~!2010-13-31~!2010-06-17~! Open Virol J 4, 123–156.

Mantovani, A., Biswas, S.K., Galdiero, M.R., Sica, A., Locati, M., 2013. Macrophage plasticity and polarization in tissue repair and remodelling. Journal of Pathology.

Mantovani, A., Marchesi, F., Malesci, A., Laghi, L., Allavena, P., 2017. Tumour-associated macrophages as treatment targets in oncology. Nature Reviews Clinical Oncology 2017 14:7 14, 399–416.

Marchini, A., Scott, E.M., Rommelaere, J., 2016. Overcoming barriers in oncolytic virotherapy with HDAC inhibitors and immune checkpoint blockade. Viruses 8, 1–22.

Marin-Acevedo, J.A., Kimbrough, E.M.O., Lou, Y., 2021. Next generation of immune checkpoint inhibitors and beyond. Journal of Hematology & Oncology 2021 14:1 14, 1–29.

Marin-Acevedo, J.A., Soyano, A.E., Dholaria, B., Knutson, K.L., Lou, Y., 2018. Cancer immunotherapy beyond immune checkpoint inhibitors. J Hematol Oncol.

Markert, J.M., Liechty, P.G., Wang, W., Gaston, S., Braz, E., Karrasch, M., Nabors, L.B., Markiewicz, M., Lakeman, A.D., Palmer, C.A., Parker, J.N., Whitley, R.J., Gillespie, G.Y., 2009. Phase Ib trial of mutant herpes simplex virus G207 inoculated pre-and post-tumor resection for recurrent GBM. Molecular Therapy.

Markert, J.M., Medlock, M.D., Rabkin, S.D., Gillespie, G.Y., Todo, T., Hunter, W.D., Palmer, C.A., Feigenbaum, F., Tornatore, C., Tufaro, F., Martuza, R.L., 2000. Conditionally replicating herpes simplex virus mutant G207 for the treatment of malignant glioma: Results of a phase I trial. Gene Ther.

Maroun, J., Muñoz-Alía, M., Ammayappan, A., Schulze, A., Peng, K.W., Russell, S., 2017. Designing and building oncolytic viruses. Future Virol 12, 193–213.

Martin, T.J., 2002. Manipulating the environment of cancer cells in bone: a novel therapeutic approach. *The Journal of clinical investigation*, *110*(10), pp.1399-1401.

Martinez, F.O., Gordon, S., Locati, M., Mantovani, A., 2006. Transcriptional Profiling of the Human Monocyte-to-Macrophage Differentiation and Polarization: New Molecules and Patterns of Gene Expression. The Journal of Immunology 177, 7303–7311.

Martuza, R.L., Malick, A., Markert, J.M., Ruffner, K.L., Coen, D.M., 1991. Experimental therapy of human glioma by means of a genetically engineered virus mutant. Science (1979).

Mato-Berciano, A., Morgado, S., Maliandi, M. V., Farrera-Sal, M., Gimenez-Alejandre, M., Ginestà, M.M., Moreno, R., Torres-Manjon, S., Moreno, P., Arias-Badia, M., Rojas, L.A., Capellà, G., Alemany, R., Cascallo, M., Bazan-Peregrino, M., 2021. Oncolytic adenovirus with hyaluronidase activity that evades neutralizing antibodies: VCN-11. J Control Release 332, 517–528.

Miller, F.R., McInerney, D., Rogers, C., Miller, B.E., 1988. Spontaneous fusion between metastatic mammary tumor subpopulations. J Cell Biochem 36, 129–136.

Mineta, T., Rabkin, S.D., Yazaki, T., Hunter, W.D., Martuza, R.L., 1995. Attenuated multi-mutated herpes simplex virus-1 for the treatment of malignant gliomas. Nat Med.

Mitchem, J.B., Brennan, D.J., Knolhoff, B.L., Belt, B.A., Zhu, Y., Sanford, D.E., Belaygorod, L., Carpenter, D., Collins, L., Piwnica-Worms, D., Hewitt, S., Udupi, G.M., Gallagher, W.M., Wegner, C., West, B.L., Wang-Gillam, A., Goedegebuure, P., Linehan, D.C., DeNardo, D.G., 2013. Targeting tumor-infiltrating macrophages decreases tumor-initiating cells, relieves immunosuppression, and improves chemotherapeutic responses. Cancer Res.

Mittal, D., Gubin, M.M., Schreiber, R.D., Smyth, M.J., 2014. New insights into cancer immunoediting and its three component phases-elimination, equilibrium and escape. Curr Opin Immunol.

Moamin, M.R., Allen, R., Woods, S.L., Brown, J.E., Nunns, H., Juncker-Jensen, A., Lewis, C.E., 2023. Changes in the immune landscape of TNBC after neoadjuvant chemotherapy: correlation with relapse. Front Immunol 14, 1291643.

Monney, L., Sabatos, C.A., Gaglia, J.L., Ryu, A., Waldner, H., Chernova, T., Manning, S., Greenfield, E.A., Coyle, A.J., Sobel, R.A., Freeman, G.J., Kuchroo, V.K., 2002a. Th1-specific cell surface protein Tim-3 regulates macrophage activation and severity of an autoimmune disease. Nature.

Monney, L., Sabatos, C.A., Gaglia, J.L., Ryu, A., Waldner, H., Chernova, T., Manning, S., Greenfield, E.A., Coyle, A.J., Sobel, R.A., Freeman, G.J., Kuchroo, V.K., 2002b. Th1-specific cell surface protein Tim-

3 regulates macrophage activation and severity of an autoimmune disease. Nature 2002 415:6871 415, 536–541.

Moradpoor, R., Gharebaghian, A., Shahi, F., Mousavi, A., Salari, S., Akbari, M.E., Ajdari, S., Salimi, M., 2020. Identification and Validation of Stage-Associated PBMC Biomarkers in Breast Cancer Using MS-Based Proteomics. Front Oncol 10, 1101.

Mosser, D.M., Edwards, J.P., 2008. Exploring the full spectrum of macrophage activation. Nat Rev Immunol.

Mostafa, A.A., Meyers, D.E., Thirukkumaran, C.M., Liu, P.J., Gratton, K., Spurrell, J., Shi, Q., Thakur, S., Morris, D.G., 2018. Oncolytic Reovirus and Immune Checkpoint Inhibition as a Novel Immunotherapeutic Strategy for Breast Cancer. Cancers (Basel) 10.

Muller, A., Homey, B., Soto, H., Ge, N., Catron, D., Buchanan, M.E., McClanahan, T., Murphy, E., Yuan, W., Wagner, S.N. and Barrera, J.L., 2001. Involvement of chemokine receptors in breast cancer metastasis. Nature, 410(6824).

Muntasell, A., Rojo, F., Servitja, S., Rubio-Perez, C., Cabo, M., Tamborero, D., Costa-García, M., Martínez-Garcia, M., Menendez, S., Vazquez, I., Lluch, A., Gonzalez-Perez, A., Rovira, A., Lopez-Botet, M., Albanell, J., 2019. NK cell infiltrates and HLA class I expression in primary HER2 þ breast cancer predict and uncouple pathological response and disease-free survival. Clinical Cancer Research 25.

Muthana, M., Kennerley, A.J., Hughes, R., Fagnano, E., Richardson, J., Paul, M., Murdoch, C., Wright, F., Payne, C., Lythgoe, M.F., Farrow, N., Dobson, J., Conner, J., Wild, J.M., Lewis, C., 2015. Directing cell therapy to anatomic target sites in vivo with magnetic resonance targeting. Nat Commun 6.

Nagahara, K., Arikawa, T., Oomizu, S., Kontani, K., Nobumoto, A., Tateno, H., Watanabe, K., Niki, T., Katoh, S., Miyake, M., Nagahata, S.-I., Hirabayashi, J., Kuchroo, V.K., Yamauchi, A., Hirashima, M., 2008. Galectin-9 Increases Tim-3 + Dendritic Cells and CD8 + T Cells and Enhances Antitumor Immunity via Galectin-9-Tim-3 Interactions. The Journal of Immunology 181, 7660–7669.

Naidoo, J., Wang, X., Woo, K.M., Iyriboz, T., Halpenny, D., Cunningham, J., Chaft, J.E., Segal, N.H., Callahan, M.K., Lesokhin, A.M., Rosenberg, J., Voss, M.H., Rudin, C.M., Rizvi, H., Hou, X., Rodriguez, K., Albano, M., Gordon, R.A., Leduc, C., Rekhtman, N., Harris, B., Menzies, A.M., Guminski, A.D., Carlino, M.S., Kong, B.Y., Wolchok, J.D., Postow, M.A., Long, G. V., Hellmann, M.D., 2017. Pneumonitis in patients treated with anti-programmed death-1/programmed death ligand 1 therapy. Journal of Clinical Oncology 35, 709–717.

Nakamura, H., Mullen, J.T., Chandrasekhar, S., Pawlik, T.M., Yoon, S.S., Tanabe, K.K., 2001. Multimodality therapy with a replication-conditional herpes simplex virus 1 mutant that expresses yeast cytosine deaminase for intratumoral conversion of 5-fluorocytosine to 5-fluorouracil. Cancer Res.

Nakayama, M., Akiba, H., Takeda, K., Kojima, Y., Hashiguchi, M., Azuma, M., Yagita, H., Okumura, K., 2009. Tim-3 mediates phagocytosis of apoptotic cells and cross-presentation. Blood.

Nanni, P., Gatta, V., Menotti, L., De Giovanni, C., Ianzano, M., Palladini, A., Grosso, V., Dall'Ora, M., Croci, S., Nicoletti, G. and Landuzzi, L., 2013. Preclinical therapy of disseminated HER-2+ ovarian and breast carcinomas with a HER-2-retargeted oncolytic herpesvirus. *PLoS pathogens*, *9*(1), p.e1003155.

Naran, K., Nundalall, T., Chetty, S., Barth, S., 2018. Principles of Immunotherapy: Implications for Treatment Strategies in Cancer and Infectious Diseases. Front Microbiol.

Naumov, G.N., Townson, J.L., Macdonald, I.C., Wilson, S.M., Bramwell, V.H.C., Groom, A.C., Chambers, A.F., 2003. Ineffectiveness of doxorubicin treatment on solitary dormant mammary carcinoma cells or late-developing metastases. Breast Cancer Res Treat 82, 199–206.

Ndhlovu, L.C., Lopez-Vergès, S., Barbour, J.D., Brad Jones, R., Jha, A.R., Long, B.R., Schoeffler, E.C., Fujita, T., Nixon, D.F., Lanier, L.L., 2012. Tim-3 marks human natural killer cell maturation and suppresses cell-mediated cytotoxicity. In: Blood.

Obodozie, C., Beshay, J., Stahnke, B., Bijelic, G., Moor, S., Giesen, B., Leisegang, U., Weber, H., 2019. Prevention of tumor ulceration in mice – Mammary fat pad injection of tumor cells. Eur J Cancer 110, S16.

Ohue, Y., Nishikawa, H., 2019. Regulatory T (Treg) cells in cancer: Can Treg cells be a new therapeutic target? Cancer Sci 110, 2080–2089.

Old, M.O., Wise-Draper, T., Wright, C.L., Kaur, B., Teknos, T., 2016. The current status of oncolytic viral therapy for head and neck cancer. World Journal of Otorhinolaryngology-Head and Neck Surgery.

Ono, M., Tsuda, H., Shimizu, C., Yamamoto, S., Shibata, T., Yamamoto, H., Hirata, T., Yonemori, K., Ando, M., Tamura, K., Katsumata, N., Kinoshita, T., Takiguchi, Y., Tanzawa, H., Fujiwara, Y., 2012. Tumor-infiltrating lymphocytes are correlated with response to neoadjuvant chemotherapy in triple-negative breast cancer. Breast Cancer Res Treat.

Orimo, A., Gupta, P.B., Sgroi, D.C., Arenzana-Seisdedos, F., Delaunay, T., Naeem, R., Carey, V.J., Richardson, A.L., Weinberg, R.A., 2005. Stromal fibroblasts present in invasive human breast carcinomas promote tumor growth and angiogenesis through elevated SDF-1/CXCL12 secretion. Cell 121.

Packiam, V.T., Lamm, D.L., Barocas, D.A., Trainer, A., Fand, B., Davis, R.L., Clark, W., Kroeger, M., Dumbadze, I., Chamie, K., Kader, A.K., Curran, D., Gutheil, J., Kuan, A., Yeung, A.W., Steinberg, G.D., 2018. An open label, single-arm, phase II multicenter study of the safety and efficacy of CG0070 oncolytic vector regimen in patients with BCG-unresponsive non–muscle-invasive bladder cancer: Interim results. Urologic Oncology: Seminars and Original Investigations.

Pandha, H.S., Annels, N.E., Simpson, G., Mostafid, H., Harrington, K.J., Melcher, A., Grose, M., Davies, B., Au, G.G., Karpathy, R., Shafren, D., 2016. Phase I/II canon study: Oncolytic immunotherapy for the treatment of non-muscle invasive bladder (NMIBC) cancer using intravesical coxsackievirus A21. https://doi.org/10.1200/JCO.2016.34.15_suppl.e16016 34, e16016–e16016.

Pardoll, D.M., 2012a. The blockade of immune checkpoints in cancer immunotherapy. Nature Reviews Cancer 2012 12:4 12, 252–264.

Pardoll, D.M., 2012b. The blockade of immune checkpoints in cancer immunotherapy. Nature Reviews Cancer 2012 12:4 12, 252–264.

Park, S.H., Breitbach, C.J., Lee, J., Park, J.O., Lim, H.Y., Kang, W.K., Moon, A., Mun, J.H., Sommermann, E.M., Maruri Avidal, L., Patt, R., Pelusio, A., Burke, J., Hwang, T.H., Kirn, D., Park, Y.S., 2015. Phase 1b Trial of Biweekly Intravenous Pexa-Vec (JX-594), an Oncolytic and Immunotherapeutic Vaccinia Virus in Colorectal Cancer. Molecular Therapy.

Pawlik, T.M., Nakamura, H., Yoon, S.S., Mullen, J.T., Chandrasekhar, S., Chiocca, E.A., Tanabe, K.K., 2000. Oncolysis of diffuse hepatocellular carcinoma by intravascular administration of a replication-competent, genetically engineered herpesvirus. Cancer Res 60, 2790–2795.

Pecora, A.L., Rizvi, N., Cohen, G.I., Meropol, N.J., Sterman, D., Marshall, J.L., Goldberg, S., Gross, P., O'Neil, J.D., Groene, W.S., Roberts, M.S., Rabin, H., Bamat, M.K., Lorence, R.M., 2002. Phase I trial of intravenous administration of PV701, an oncolytic virus, in patients with advanced solid cancers. Journal of Clinical Oncology.

Perou, C.M., Sørile, T., Eisen, M.B., Van De Rijn, M., Jeffrey, S.S., Ress, C.A., Pollack, J.R., Ross, D.T., Johnsen, H., Akslen, L.A., Fluge, Ø., Pergammenschlkov, A., Williams, C., Zhu, S.X., Lønning, P.E., Børresen-Dale, A.L., Brown, P.O., Botstein, D., 2000. Molecular portraits of human breast tumours. Nature.

Peters, C., Rabkin, S.D., 2015. Designing herpes viruses as oncolytics. Mol Ther Oncolytics 2, 15010.

Peters, M.G., Farías, E., Colombo, L., Filmus, J., Puricelli, L., Bal De Kier Joffé, E., 2003. Inhibition of invasion and metastasis by glypican-3 in a syngeneic breast cancer model. Breast Cancer Res Treat 80, 221–232.

Piao, Y.R., Piao, L.Z., Zhu, L.H., Jin, Z.H., Dong, X.Z., 2013. Prognostic value of T cell immunoglobulin mucin-3 in prostate cancer. Asian Pac J Cancer Prev 14, 3897–3901.

Pinchuk, L.M., Filipov, N.M., 2008. Differential effects of age on circulating and splenic leukocyte populations in C57BL/6 and BALB/c male mice. Immun Ageing 5, 1.

Prabhakar, S., Messerli, S.M., Stemmer-Rachamimov, A.O., Liu, T.C., Rabkin, S., Martuza, R., Breakefield, X.O., 2007. Treatment of implantable NF2 schwannoma tumor models with oncolytic herpes simplex virus G47Δ. Cancer Gene Ther.

Prognostic implication of TIM-3 in clear cell renal cell carcinoma - PubMed [WWW Document], n.d. URL https://pubmed.ncbi.nlm.nih.gov/24195506/ (accessed 1.23.24).

Powell, G.J., Southby, J., Danks, J.A., Stillwell, R.G., Hayman, J.A., Henderson, M.A., Bennett, R.C. and Martin, T.J., 1991. Localization of parathyroid hormone-related protein in breast cancer metastases: increased incidence in bone compared with other sites. Cancer research, 51(11), pp.3059-3061.

Qiang, L., Huili, Z., Leilei, Z., Xiaoyan, W., Hui, W., Biao, H., Yigang, W., Fang, H., Yiqiang, W., 2023. Intratumoral delivery of a Tim-3 antibody-encoding oncolytic adenovirus engages an effective antitumor immune response in liver cancer. J Cancer Res Clin Oncol 149, 18201–18213.

Quatromoni, J.G., Eruslanov, E., 2012. Tumor-associated macrophages: Function, phenotype, and link to prognosis in human lung cancer. Am J Transl Res.

Raja, J., Ludwig, J.M., Gettinger, S.N., Schalper, K.A., Kim, H.S., 2018a. Oncolytic virus immunotherapy: future prospects for oncology. J Immunother Cancer 6, 1–13.

Raja, J., Ludwig, J.M., Gettinger, S.N., Schalper, K.A., Kim, H.S., 2018b. Oncolytic virus immunotherapy: future prospects for oncology. J Immunother Cancer 6, 1–13.

Rashid, O.M., Nagahashi, M., Ramachandran, S., Dumur, C.I., Schaum, J.C., Yamada, A., Aoyagi, T., Milstien, S., Spiegel, S., Takabe, K., 2013. Is tail vein injection a relevant breast cancer lung metastasis model? J Thorac Dis 5, 385.

Reale, A., Vitiello, A., Conciatori, V., Parolin, C., Calistri, A., Palù, G., 2019. Perspectives on immunotherapy via oncolytic viruses. Infect Agent Cancer 14, 1–8.

Regua, A.T., Arrigo, A., Doheny, D., Wong, G.L., Lo, H.W., 2021. Transgenic Mouse Models of Breast Cancer. Cancer Lett 516, 73.

Reinherz, E.L., Kung, P.C., Goldstein, G., Schlossman, S.F., 1979. Separation of functional subsets of human T cells by a monoclonal antibody. Proc Natl Acad Sci U S A 76.

Ribas, A., Dummer, R., Puzanov, I., VanderWalde, A., Andtbacka, R.H.I., Michielin, O., Olszanski, A.J., Malvehy, J., Cebon, J., Fernandez, E., Kirkwood, J.M., Gajewski, T.F., Chen, L., Gorski, K.S., Anderson, A.A., Diede, S.J., Lassman, M.E., Gansert, J., Hodi, F.S., Long, G. V., 2017. Oncolytic Virotherapy Promotes Intratumoral T Cell Infiltration and Improves Anti-PD-1 Immunotherapy. Cell 170, 1109.

Riley, R.S., June, C.H., Langer, R., Mitchell, M.J., 2019. Delivery technologies for cancer immunotherapy. Nat Rev Drug Discov.

Rouzbahani, F.N., Shirkhoda, M., Memari, F., Dana, H., Chalbatani, G.M., Mahmoodzadeh, H., Samarghandi, N., Gharagozlou, E., Hadloo, M.H.M., Maleki, A.R., Sadeghian, E., Nia, E.Z., Nia, N., Hadjilooei, F., Rezaeian, O., Meghdadi, S., Miri, S., Jafari, F., Rayzan, E., Marmari, V., 2018. Immunotherapy a new hope for cancer treatment: A review. Pakistan Journal of Biological Sciences 21, 135–150.

Rusch, T., Bayry, J., Werner, J., Shevchenko, I., Bazhin, A. V., 2018. Immunotherapy as an Option for Cancer Treatment. Arch Immunol Ther Exp (Warsz) 66, 89–96.

Russell, L., Peng, K.W., 2018a. The emerging role of oncolytic virus therapy against cancer. Chin Clin Oncol.

Russell, L., Peng, K.W., 2018b. The emerging role of oncolytic virus therapy against cancer. Chin Clin Oncol.

Russell, S.J., Peng, K.W., 2007. Viruses as anticancer drugs. Trends Pharmacol Sci.

Russell, S.J., Peng, K.W., 2017. Oncolytic Virotherapy: A Contest between Apples and Oranges. Molecular Therapy.

Sabatos, C.A., Chakravarti, S., Cha, E., Schubart, A., Sánchez-Fueyo, A., Zheng, X.X., Coyle, A.J., Strom, T.B., Freeman, G.J., Kuchroo, V.K., 2003a. Interaction of Tim-3 and Tim-3 ligand regulates T helper type 1 responses and induction of peripheral tolerance. Nat Immunol.

Sabatos, C.A., Chakravarti, S., Cha, E., Schubart, A., Sánchez-Fueyo, A., Zheng, X.X., Coyle, A.J., Strom, T.B., Freeman, G.J., Kuchroo, V.K., 2003b. Interaction of Tim-3 and Tim-3 ligand regulates T helper type 1 responses and induction of peripheral tolerance. Nature Immunology 2003 4:11 4, 1102–1110.

Saha, D., Rabkin, S.D., Martuza, R.L., 2020. Temozolomide antagonizes oncolytic immunovirotherapy in glioblastoma. J Immunother Cancer 8.

Sakowska, J., Arcimowicz, Ł., Jankowiak, M., Papak, I., Markiewicz, A., Dziubek, K., Kurkowiak, M., Kote, S., Kaźmierczak-Siedlecka, K., Połom, K., Marek-Trzonkowska, N., Trzonkowski, P., 2022. Autoimmunity and Cancer—Two Sides of the Same Coin. Front Immunol 13.

Sakuishi, K., Apetoh, L., Sullivan, J.M., Blazar, B.R., Kuchroo, V.K., Anderson, A.C., 2010a. Targeting Tim-3 and PD-1 pathways to reverse T cell exhaustion and restore anti-tumor immunity. Journal of Experimental Medicine.

Sakuishi, K., Apetoh, L., Sullivan, J.M., Blazar, B.R., Kuchroo, V.K., Anderson, A.C., 2010b. Targeting Tim-3 and PD-1 pathways to reverse T cell exhaustion and restore anti-tumor immunity. J Exp Med 207, 2187–2194.

Sakuishi, K., Apetoh, L., Sullivan, J.M., Blazar, B.R., Kuchroo, V.K., Anderson, A.C., 2010c. Targeting Tim-3 and PD-1 pathways to reverse T cell exhaustion and restore anti-tumor immunity. J Exp Med 207, 2187.

Saleh, R., Toor, S.M., Al-Ali, D., Sasidharan Nair, V. and Elkord, E., 2020. Blockade of PD-1, PD-L1, and TIM-3 altered distinct immune-and cancer-related signaling pathways in the transcriptome of human breast cancer explants. *Genes*, *11*(6), p.703.

Samaniego, L.A., Wu, N., DeLuca, N.A., 1997. The herpes simplex virus immediate-early protein ICP0 affects transcription from the viral genome and infected-cell survival in the absence of ICP4 and ICP27. J Virol.

Sanchala, D.S., Bhatt, L.K., Prabhavalkar, K.S., 2017. Oncolytic herpes simplex viral therapy: A stride toward selective targeting of cancer cells. Front Pharmacol 8, 1–9.

Sanghera, C., Sanghera, R., 2019. Immunotherapy – Strategies for Expanding Its Role in the Treatment of All Major Tumor Sites. Cureus 11, 1–12.

Sasidharan Nair, V., El Salhat, H., Taha, R.Z., John, A., Ali, B.R., Elkord, E., 2018. DNA methylation and repressive H3K9 and H3K27 trimethylation in the promoter regions of PD-1, CTLA-4, TIM-3, LAG-3, TIGIT, and PD-L1 genes in human primary breast cancer. Clin Epigenetics 10.

Sauer, N., Janicka, N., Szlasa, W., Skinderowicz, B., Kołodzińska, K., Dwernicka, W., Oślizło, M., Kulbacka, J., Novickij, V., Karłowicz-Bodalska, K., 2023. TIM-3 as a promising target for cancer immunotherapy in a wide range of tumors. Cancer Immunology, Immunotherapy 72, 3405.

Schreiber, R.D., Old, L.J., Smyth, M.J., 2011. Cancer immunoediting: Integrating immunity's roles in cancer suppression and promotion. Science (1979).

Schrörs, B., Boegel, S., Albrecht, C., Bukur, T., Bukur, V., Holtsträter, C., Ritzel, C., Manninen, K., Tadmor, A.D., Vormehr, M., Sahin, U., Löwer, M., 2020. Multi-Omics Characterization of the 4T1 Murine Mammary Gland Tumor Model. Front Oncol 10, 1195.

Schuster, S.J., Svoboda, J., Chong, E.A., Nasta, S.D., Mato, A.R., Anak, Ö., Brogdon, J.L., Pruteanu-Malinici, I., Bhoj, V., Landsburg, D., Wasik, M., Levine, B.L., Lacey, S.F., Melenhorst, J.J., Porter, D.L., June, C.H., 2017. Chimeric antigen receptor T Cells in refractory B-Cell lymphomas. New England Journal of Medicine.

Search of: herpes simplex oncolytic virus - List Results - ClinicalTrials.gov [WWW Document], n.d. URL https://classic.clinicaltrials.gov/ct2/results?term=herpes+simplex+oncolytic+virus&Search=Apply&age_v=&gndr=&type=&rslt= (accessed 12.25.23).

Search of: Oncolytic virus | Completed Studies - List Results - ClinicalTrials.gov [WWW Document], n.d. URL

https://classic.clinicaltrials.gov/ct2/results?term=Oncolytic+virus&Search=Apply&recrs=e&age_v=&gndr=&type=&rslt= (accessed 12.25.23).

Search of: Tim-3 combination - List Results - ClinicalTrials.gov [WWW Document], n.d. URL https://classic.clinicaltrials.gov/ct2/results?cond=&term=Tim-3+combination&cntry=&state=&city=&dist=&Search=Search (accessed 12.25.23).

Seymour, L.W., Fisher, K.D., 2016. Oncolytic viruses: Finally delivering. Br J Cancer 114, 357–361.

Shalhout, S.Z., Miller, D.M., Emerick, K.S., Kaufman, H.L., 2023. Therapy with oncolytic viruses: progress and challenges. Nature Reviews Clinical Oncology 2023 20:3 20, 160–177.

Shao, H. and Varamini, P., 2022. Breast cancer bone metastasis: a narrative review of emerging targeted drug delivery systems. *Cells*, *11*(3), p.388.).

Shariati, S., Ghods, A., Zohouri, M., Rasolmali, R., Talei, A.R., Mehdipour, F., Ghaderi, A., 2020. Significance of TIM-3 expression by CD4+ and CD8+ T lymphocytes in tumor-draining lymph nodes from patients with breast cancer. Mol Immunol 128, 47–54.

Shen, Y., Nemunaitis, J., 2006. Herpes simplex virus 1 (HSV-1) for cancer treatment. Cancer Gene Ther 13, 975–992.

Shore, N.D., 2015. Advances in the understanding of cancer immunotherapy. BJU Int 116, 321–329.

Shukla, S., Steinmetz, N.F., 2016. Emerging nanotechnologies for cancer immunotherapy. Exp Biol Med 241, 1116–1126.

Singh, P.K., Doley, J., Ravi Kumar, G., Sahoo, A.P., Tiwari, A.K., 2012. Oncolytic viruses & their specific targeting to tumour cells. Indian Journal of Medical Research.

Skytthe, M.K., Graversen, J.H., Moestrup, S.K., 2020. Targeting of CD163+ Macrophages in Inflammatory and Malignant Diseases. Int J Mol Sci 21, 1–31.

Sokolowski, N.A., Rizos, H., Diefenbach, R.J., 2015a. Oncolytic Virotherapy Dovepress Oncolytic virotherapy using herpes simplex virus: how far have we come? Oncolytic Virother 4, 207–219.

Sokolowski, N.A., Rizos, H., Diefenbach, R.J., 2015b. Oncolytic Virotherapy Dovepress Oncolytic virotherapy using herpes simplex virus: how far have we come? Oncolytic Virother 4, 207–219.

Southby, J., Kissin, M.W., Danks, J.A., Hayman, J.A., Moseley, J.M., Henderson, M.A., Bennett, R.C. and Martin, T.J., 1990. Immunohistochemical localization of parathyroid hormone-related protein in human breast cancer. Cancer research, 50(23), pp.7710-7716.

Souto, E.P., Dobrolecki, L.E., Villanueva, H., Sikora, A.G., Lewis, M.T., 2022. In Vivo Modeling of Human Breast Cancer Using Cell Line and Patient-Derived Xenografts. J Mammary Gland Biol Neoplasia 27, 211.

Srivastava, V., Huycke, T.R., Phong, K.T., Gartner, Z.J., 2020. Organoid models for mammary gland dynamics and breast cancer. Curr Opin Cell Biol 66, 51.

Stanton, S.E., Adams, S., Disis, M.L., 2016. Variation in the Incidence and Magnitude of Tumor-Infiltrating Lymphocytes in Breast Cancer Subtypes: A Systematic Review. JAMA Oncol.

Stanton, S.E., Disis, M.L., 2016. Clinical significance of tumor-infiltrating lymphocytes in breast cancer. J Immunother Cancer 4.

Su, C., Wang, H., Liu, Y., Guo, Q., Zhang, L., Li, J., Zhou, W., Yan, Y., Zhou, X., Zhang, J., 2020. Adverse Effects of Anti-PD-1/PD-L1 Therapy in Non-small Cell Lung Cancer. Front Oncol 10, 554313.

Su, J. xuan, Li, S. jia, Zhou, X. feng, Zhang, Z. jing, Yan, Y., Liu, S. lin, Qi, Q., 2023. Chemotherapy-induced metastasis: molecular mechanisms and clinical therapies. Acta Pharmacologica Sinica 2023 44:9 44, 1725–1736.

Sugiura, K., Ciiester Stock, A.C., n.d. STUDIES I N A TUMOR SPECTRUM I. Comparison of the Action of MethyEbis(2-chloroethy1)amine and 3-B is(2-ch loro et h y 1)am i no m e t hy 1-4-met hoxy m e t h y 1-5-h y droxy-6-methylpyridine on the Growth of a Variety of Mouse and Rat Tumors*.

Suva, L.J., Washam, C., Nicholas, R.W. and Griffin, R.J., 2011. Bone metastasis: mechanisms and therapeutic opportunities. Nature Reviews Endocrinology, 7(4), pp.208-218.

Tang, T., Huang, X., Zhang, G., Hong, Z., Bai, X., Liang, T., 2021. Advantages of targeting the tumor immune microenvironment over blocking immune checkpoint in cancer immunotherapy. Signal Transduct Target Ther.

Tao, K., Fang, M., Alroy, J., Gary, G.G., 2008a. Imagable 4T1 model for the study of late stage breast cancer. BMC Cancer 8, 228.

Tao, K., Fang, M., Alroy, J., Gary, G.G., 2008b. Imagable 4T1 model for the study of late stage breast cancer. BMC Cancer 8, 228.

Terceiro, L.E.L., Edechi, C.A., Ikeogu, N.M., Nickel, B.E., Hombach-Klonisch, S., Sharif, T., Leygue, E., Myal, Y., 2021. The Breast Tumor Microenvironment: A Key Player in Metastatic Spread. Cancers 2021, Vol. 13, Page 4798 13, 4798.

Tian, C., Liu, J., Zhou, H., Li, J., Sun, C., Zhu, W., Yin, Y., Li, X., 2021. Enhanced anti-tumor response elicited by a novel oncolytic HSV-1 engineered with an anti-PD-1 antibody. Cancer Lett 518, 49–58.

TIM-3 promotes the metastasis of esophageal squamous cell carcinoma by targeting epithelial-mesenchymal transition via the Akt/GSK-3β/Snail signaling pathway [WWW Document], n.d. URL https://www.spandidos-publications.com/or/36/3/1551 (accessed 1.23.24).

Timin, A.S., Litvak, M.M., Gorin, D.A., Atochina-Vasserman, E.N., Atochin, D.N., Sukhorukov, G.B., 2018. Cell-Based Drug Delivery and Use of Nano-and Microcarriers for Cell Functionalization. Adv Healthc Mater.

Todo, T., Martuza, R.L., Rabkin, S.D., Johnson, P.A., 2001. Oncolytic herpes simplex virus vector with enhanced MHC class I presentation and tumor cell killing. Proc Natl Acad Sci U S A.

Toor, S.M., Murshed, K., Al-Dhaheri, M., Khawar, M., Abu Nada, M., Elkord, E., 2019. Immune Checkpoints in Circulating and Tumor-Infiltrating CD4+ T Cell Subsets in Colorectal Cancer Patients. Front Immunol 10, 2936.

Topalian, S.L., Hodi, F.S., Brahmer, J.R., Gettinger, S.N., Smith, D.C., McDermott, D.F., Powderly, J.D., Carvajal, R.D., Sosman, J.A., Atkins, M.B., Leming, P.D., Spigel, D.R., Antonia, S.J., Horn, L., Drake, C.G., Pardoll, D.M., Chen, L., Sharfman, W.H., Anders, R.A., Taube, J.M., McMiller, T.L., Xu, H., Korman, A.J., Jure-Kunkel, M., Agrawal, S., McDonald, D., Kollia, G.D., Gupta, A., Wigginton, J.M., Sznol, M., 2012. Safety, activity, and immune correlates of anti-PD-1 antibody in cancer. N Engl J Med 366, 2443–2454.

Topalian, S.L., Sznol, M., McDermott, D.F., Kluger, H.M., Carvajal, R.D., Sharfman, W.H., Brahmer, J.R., Lawrence, D.P., Atkins, M.B., Powderly, J.D., Leming, P.D., Lipson, E.J., Puzanov, I., Smith, D.C., Taube, J.M., Wigginton, J.M., Kollia, G.D., Gupta, A., Pardoll, D.M., Sosman, J.A., Hodi, F.S., 2014. Survival, durable tumor remission, and long-term safety in patients with advanced melanoma receiving nivolumab. Journal of Clinical Oncology.

Topalian, S.L., Taube, J.M., Anders, R.A., Pardoll, D.M., 2016. Mechanism-driven biomarkers to guide immune checkpoint blockade in cancer therapy. Nature Reviews Cancer 2016 16:5 16, 275–287.

Tower, H., Ruppert, M., Britt, K., 2019. The Immune Microenvironment of Cancer. Cancers (Basel) 11, 1–15.

Toyoizumi, T., Mick, R., Abbas, A.E., Kang, E.H., Kaiser, L.R., Molnar-Kimber, K.L., 1999. Combined therapy with chemotherapeutic agents and herpes simplex virus type 1 ICP34.5 mutant (HSV-1716) in human non-small cell lung cancer. Hum Gene Ther 10, 3013–3029.

Tu, L., Guan, R., Yang, H., Zhou, Y., Hong, W., Ma, L., Zhao, G., Yu, M., 2020. Assessment of the expression of the immune checkpoint molecules PD-1, CTLA4, TIM-3 and LAG-3 across different cancers in relation to treatment response, tumor-infiltrating immune cells and survival. Int J Cancer 147, 423–439.

Tyminski, E., LeRoy, S., Terada, K., Finkelstein, D.M., Hyatt, J.L., Danks, M.K., Potter, P.M., Saeki, Y., Chiocca, E.A., 2005. Brain tumor oncolysis with replication-conditional herpes simplex virus type 1 expressing the prodrug-activating genes, CYP2B1 and secreted human intestinal carboxylesterase, in combination with cyclophosphamide and irinotecan. Cancer Res.

Vito, A., El-sayes, N., Salem, O., Wan, Y., Mossman, K.L., 2021. Response to FEC Chemotherapy and Oncolytic HSV-1 Is Associated with Macrophage Polarization and Increased Expression of S100A8/A9 in Triple Negative Breast Cancer. Cancers (Basel) 13.

Waldman, A.D., Fritz, J.M., Lenardo, M.J., 2020. A guide to cancer immunotherapy: from T cell basic science to clinical practice. Nature Reviews Immunology 2020 20:11 20, 651–668.

Wang, J., Xu, L., Zeng, W., Hu, P., Zeng, M., Rabkin, S.D., Liu, R., 2014. Treatment of human hepatocellular carcinoma by the oncolytic herpes simplex virus G47delta. Cancer Cell Int.

Wang, J.N., Hu, P., Zeng, M.S., Liu, R. Bin, 2011. Anti-tumor effect of oncolytic herpes simplex virus G47delta on human nasopharyngeal carcinoma. Chin J Cancer.

Wang, J., Hu, P., Zeng, M., Rabkin, S.D. and Liu, R., 2012. Oncolytic herpes simplex virus treatment of metastatic breast cancer. *International journal of oncology*, *40*(3), pp.757-763.

Wang, L., Zhang, C., Zhang, Z., Han, B., Shen, Z., Li, L., Liu, S., Zhao, X., Ye, F., Zhang, Y., 2018. Specific clinical and immune features of CD68 in glioma via 1,024 samples. Cancer Manag Res 10, 6409.

Wang, N., Liang, H., Zen, K., 2014. Molecular mechanisms that influence the macrophage M1-M2 polarization balance. Front Immunol.

Wang, Y., Huang, H., Zou, H., Tian, X., Hu, J., Qiu, P., Hu, H., Yan, G., 2019. Liposome Encapsulation of Oncolytic Virus M1 to Reduce Immunogenicity and Immune Clearance in Vivo. Mol Pharm 16, 779–785.

Wang, Y., Zhang, H., Liu, C., Wang, Z., Wu, W., Zhang, N., Zhang, L., Hu, J., Luo, P., Zhang, J., Liu, Zaoqu, Peng, Y., Liu, Zhixiong, Tang, L., Cheng, Q., 2022. Immune checkpoint modulators in cancer immunotherapy: recent advances and emerging concepts. J Hematol Oncol 15.

Wang, S., Wu, W., Lin, X., Zhang, K.M., Wu, Q., Luo, M. and Zhou, J., 2023. Predictive and prognostic biomarkers of bone metastasis in breast cancer: current status and future directions. Cell & Bioscience, 13(1), p.224.

Watanabe, T., Hioki, M., Fujiwara, Toshiya, Nishizaki, M., Kagawa, S., Taki, M., Kishimoto, H., Endo, Y., Urata, Y., Tanaka, N., Fujiwara, Toshiyoshi, 2006. Histone deacetylase inhibitor FR901228 enhances the antitumor effect of telomerase-specific replication-selective adenoviral agent OBP-301 in human lung cancer cells. Exp Cell Res.

Waterston, R.H., Lindblad-Toh, K., Birney, E., Rogers, J., Abril, J.F., Agarwal, P., Agarwala, R., Ainscough, R., Alexandersson, M., An, P., Antonarakis, S.E., Attwood, J., Baertsch, R., Bailey, J., Barlow, K., Beck, S., Berry, E., Birren, B., Bloom, T., Bork, P., Botcherby, M., Bray, N., Brent, M.R., Brown, D.G., Brown, S.D., Bult, C., Burton, J., Butler, J., Campbell, R.D., Carninci, P., Cawley, S., Chiaromonte, F., Chinwalla, A.T., Church, D.M., Clamp, M., Clee, C., Collins, F.S., Cook, L.L., Copley, R.R., Coulson, A., Couronne, O., Cuff, J., Curwen, V., Cutts, T., Daly, M., David, R., Davies, J., Delehaunty, K.D., Deri, J., Dermitzakis, E.T., Dewey, C., Dickens, N.J., Diekhans, M., Dodge, S., Dubchak, I., Dunn, D.M., Eddy, S.R., Elnitski, L., Emes, R.D., Eswara, P., Eyras, E., Felsenfeld, A., Fewell, G.A., Flicek, P., Foley, K., Frankel, W.N., Fulton, L.A., Fulton, R.S., Furey, T.S., Gage, D., Gibbs, R.A., Glusman, G., Gnerre, S., Goldman, N., Goodstadt, L., Grafham, D., Graves, T.A., Green, E.D., Gregory, S., Guigó, R., Guyer, M., Hardison, R.C., Haussler, D., Hayashizaki, Y., LaHillier, D.W., Hinrichs, A., Hlavina, W., Holzer, T., Hsu, F., Hua, A., Hubbard, T., Hunt, A., Jackson, I., Jaffe, D.B., Johnson, L.S., Jones, M., Jones, T.A., Joy, A., Kamal, M., Karlsson, E.K., Karolchik, D., Kasprzyk, A., Kawai, J., Keibler, E., Kells, C., Kent, W.J., Kirby, A., Kolbe, D.L., Korf, I., Kucherlapati, R.S., Kulbokas, E.J., Kulp, D., Landers, T., Leger, J.P., Leonard, S., Letunic, I., Levine, R., Li, J., Li, M., Lloyd, C., Lucas, S., Ma, B., Maglott, D.R., Mardis, E.R., Matthews, L., Mauceli, E., Mayer, J.H., McCarthy, M., McCombie, W.R., McLaren, S., McLay, K., McPherson, J.D., Meldrim, J., Meredith, B., Mesirov, J.P., Miller, W., Miner, T.L., Mongin, E., Montgomery, K.T., Morgan, M., Mott, R., Mullikin, J.C., Muzny, D.M., Nash, W.E., Nelson, J.O., Nhan, M.N., Nicol, R., Ning, Z., Nusbaum, C., O'Connor, M.J., Okazaki, Y., Oliver, K., Overton-Larty, E., Pachter, L., Parra, G., Pepin, K.H., Peterson, J., Pevzner, P., Plumb, R., Pohl, C.S., Poliakov, A., Ponce, T.C., Ponting, C.P., Potter, S., Quail, M., Reymond, A., Roe, B.A., Roskin, K.M., Rubin, E.M., Rust, A.G., Santos, R., Sapojnikov, V., Schultz, B., Schultz, J., Schwartz, M.S., Schwartz, S., Scott, C., Seaman, S., Searle, S., Sharpe, T., Sheridan, A., Shownkeen, R., Sims, S., Singer, J.B., Slater, G., Smit, A., Smith, D.R., Spencer, B., Stabenau, A., Stange-Thomann, N., Sugnet, C., Suyama, M., Tesler, G., Thompson, J., Torrents, D., Trevaskis, E., Tromp, J., Ucla, C., Ureta-Vidal, A., Vinson, J.P., von Niederhausern, A.C., Wade, C.M., Wall, M., Weber, R.J., Weiss, R.B., Wendl, M.C., West, A.P., Wetterstrand, K., Wheeler, R., Whelan, S., Wierzbowski, J., Willey, D., Williams, S., Wilson, R.K., Winter, E., Worley, K.C., Wyman, D., Yang, S., Yang, S.P., Zdobnov, E.M., Zody, M.C., Lander, E.S., 2002. Initial sequencing and comparative analysis of the mouse genome. Nature 2003 420:6915 420, 520–562.

Weber, J.S., O'Day, S., Urba, W., Powderly, J., Nichol, G., Yellin, M., Snively, J., Hersh, E., 2008. Phase I/II study of ipilimumab for patients with metastatic melanoma. J Clin Oncol 26, 5950–5956.

Wei, H., Wang, Z., Kuang, Y., Wu, Z., Zhao, S., Zhang, Z., Li, H., Zheng, M., Zhang, N., Long, C., Guo, W., Nie, C., Yang, H., Tong, A., 2020. Intercellular Adhesion Molecule-1 as Target for CAR-T-Cell Therapy of Triple-Negative Breast Cancer. Front Immunol 11, 573823.

Wei, S.C., Duffy, C.R., Allison, J.P., 2018. Fundamental mechanisms of immune checkpoint blockade therapy. Cancer Discov 8, 1069–1086.

Wenthe, J., Naseri, S., Hellström, A.C., Moreno, R., Ullenhag, G., Alemany, R., Lövgren, T., Eriksson, E., Loskog, A., 2022. Immune priming using DC- and T cell-targeting gene therapy sensitizes both treated and distant B16 tumors to checkpoint inhibition. Mol Ther Oncolytics 24, 429–442.

Wherry, E.J., 2011. T cell exhaustion. Nature Immunology 2011 12:6 12, 492–499.

Wilcox, D.R., Longnecker, R., 2016. The Herpes Simplex Virus Neurovirulence Factor γ34.5: Revealing Virus–Host Interactions. PLoS Pathog.

Wilkinson, M.J., Smith, H.G., Pencavel, T.D., Mansfield, D.C., Kyula-Currie, J., Khan, A.A., McEntee, G., Roulstone, V., Hayes, A.J., Harrington, K.J., 2016. Isolated limb perfusion with biochemotherapy and oncolytic virotherapy combines with radiotherapy and surgery to overcome treatment resistance in an animal model of extremity soft tissue sarcoma. Int J Cancer.

Wilson, C.B., Osenblum, M.L.I., 1983. Improved treatment of a brain-tumor model 58, 368–373.

Wolf, Y., Anderson, A.C. and Kuchroo, V.K., 2020. TIM3 comes of age as an inhibitory receptor. *Nature Reviews Immunology*, *20*(3), pp.173-185.

Wu, J., Liu, C., Qian, S., Hou, H., 2013. The Expression of Tim-3 in Peripheral Blood of Ovarian Cancer. https://home.liebertpub.com/dna 32, 648–653.

Wu, S., Du, X., Lou, G., Yu, S., Lai, K., Qi, J., Ni, S., Chen, Z., Chen, F., 2022. Expression changes of Tim-3 as one of supplementary indicators for monitoring prognosis of liver pathological changes in chronic HBV infection. BMC Infect Dis 22.

Wu, Z., Zhang, Z., Lei, Z., Lei, P., 2019. CD14: Biology and role in the pathogenesis of disease.

Xiang, Z., Gonzalez, R., Wang, Z., Ren, L., Xiao, Y., Li, J., Li, Y., Vernet, G., Paranhos-Baccalà, G., Jin, Q., Wang, J., 2012. Coxsackievirus A21, enterovirus 68, and acute respiratory tract infection, China. Emerg Infect Dis.

Xie, X., Lv, J., Zhu, W., Tian, C., Li, J., Liu, J., Zhou, H., Sun, C., Hu, Z., Li, X., 2022. The combination therapy of oncolytic HSV-1 armed with anti-PD-1 antibody and IL-12 enhances anti-tumor efficacy. Transl Oncol 15, 101287.

Xu, D. and Tang, M., 2023. Advances in the study of biomarkers related to bone metastasis in breast cancer. The British Journal of Radiology, 96(1150), p.20230117.

Xu, L., Huang, Y., Tan, L., Yu, W., Chen, D., Lu, C., He, J., Wu, G., Liu, X., Zhang, Y., 2015. Increased Tim-3 expression in peripheral NK cells predicts a poorer prognosis and Tim-3 blockade improves NK cell-mediated cytotoxicity in human lung adenocarcinoma. Int Immunopharmacol.

Yan, W., Liu, X., Ma, H., Zhang, H., Song, X., Gao, L., Liang, X., Ma, C., 2015. Tim-3 fosters HCC development by enhancing TGF-β-mediated alternative activation of macrophages. Gut 64.

Yang, J., Mani, S.A., Donaher, J.L., Ramaswamy, S., Itzykson, R.A., Come, C., Savagner, P., Gitelman, I., Richardson, A., Weinberg, R.A., 2004. Twist, a Master Regulator of Morphogenesis, Plays an Essential Role in Tumor Metastasis. Cell 117, 927–939.

Yasinska, I.M., Sakhnevych, S.S., Pavlova, L., Selnø, A.T.H., Abeleira, A.M.T., Benlaouer, O., Silva, I.G., Mosimann, M., Varani, L., Bardelli, M., Hussain, R., Siligardi, G., Cholewa, D., Berger, S.M., Gibbs, B.F., Ushkaryov, Y.A., Fasler-Kan, E., Klenova, E., Sumbayev, V. V., 2019. The Tim-3-galectin-9 pathway and its regulatory mechanisms in human breast cancer. Front Immunol 10, 1594.

Yeo, S.K., Guan, J.L., 2017. Breast Cancer: Multiple Subtypes within a Tumor? Trends Cancer.

Yi, M., Jiao, D., Xu, H., Liu, Q., Zhao, W., Han, X., Wu, K., 2018. Biomarkers for predicting efficacy of PD-1/PD-L1 inhibitors. Molecular Cancer 2018 17:1 17, 1–14.

Yilmaz, I., Tavukcuoglu, E., Horzum, U., Yilmaz, K.B., Akinci, M., Gulcelik, M.A., Oral, H.B., Esendagli, G., 2023. Immune checkpoint status and exhaustion-related phenotypes of CD8+ T cells from the tumor-draining regional lymph nodes in breast cancer. Cancer Med 12, 22196.

Yoo, J.Y., Haseley, A., Bratasz, A., Chiocca, E.A., Zhang, J., Powell, K., Kaur, B., 2012. Antitumor efficacy of 34.5ENVE: A transcriptionally retargeted and vstat120-expressing oncolytic virus. Molecular Therapy.

Yu, L., Liu, X., Wang, X., Yan, F., Wang, P., Jiang, Y., Du, J., Yang, Z., 2021. TIGIT+ TIM-3+ NK cells are correlated with NK cell exhaustion and disease progression in patients with hepatitis B virus-related hepatocellular carcinoma. Oncoimmunology 10.

Yu, M., Lu, B., Liu, Y., Me, Y., Wang, L., Li, H., 2017a. Interference with Tim-3 protein expression attenuates the invasion of clear cell renal cell carcinoma and aggravates anoikis. Mol Med Rep 15, 1103–1108.

Yu, M., Lu, B., Liu, Y., Me, Y., Wang, L., Zhang, P., 2017b. Tim-3 is upregulated in human colorectal carcinoma and associated with tumor progression. Mol Med Rep 15, 689–695.

Yu, S., Li, A., Liu, Q., Li, T., Yuan, X., Han, X., Wu, K., 2017. Chimeric antigen receptor T cells: a novel therapy for solid tumors. J Hematol Oncol.

Yunna, C., Mengru, H., Lei, W., Weidong, C., 2020. Macrophage M1/M2 polarization. Eur J Pharmacol 877, 173090.

Zeng, W., Hu, P., Wu, J., Wang, J., Li, J., Lei, L. and Liu, R., 2013. The oncolytic herpes simplex virus vector G47Δ effectively targets breast cancer stem cells. *Oncology reports*, *29*(3), pp.1108-1114.

Zhang, C., Xu, L., Ma, Y., Huang, Y., Zhou, L., Le, H., Chen, Z., Jones, J., 2023a. Increased TIM-3 expression in tumor-associated macrophages predicts a poorer prognosis in non-small cell lung cancer: a retrospective cohort study. J Thorac Dis 15, 1433–1444.

Zhang, C., Xu, L., Ma, Y., Huang, Y., Zhou, L., Le, H., Chen, Z., Jones, J., 2023b. Increased TIM-3 expression in tumor-associated macrophages predicts a poorer prognosis in non-small cell lung cancer: a retrospective cohort study. J Thorac Dis 15, 1433–1444.

Zhang, H., Xiang, R., Wu, B., Li, J., Luo, G., 2017. T-cell immunoglobulin mucin-3 expression in invasive ductal breast carcinoma: Clinicopathological correlations and association with tumor infiltration by cytotoxic lymphocytes. Mol Clin Oncol 7, 557.

Zhang, M.Z., Wang, X., Wang, Y., Niu, A., Wang, S., Zou, C., Harris, R.C., 2017. IL-4/IL-13–mediated polarization of renal macrophages/dendritic cells to an M2a phenotype is essential for recovery from acute kidney injury. Kidney Int 91, 375.

Zhang, R., Liu, Q., Li, T., Liao, Q., Zhao, Y., 2019. Role of the complement system in the tumor microenvironment. Cancer Cell Int.

Zhang, S.X., 2015. Turning Killer into cure - the story of oncolytic herpes simplex viruses. Discov Med.

Zhang, W., Fulci, G., Buhrman, J.S., Stemmer-Rachamimov, A.O., Chen, J.W., Wojtkiewicz, G.R., Weissleder, R., Rabkin, S.D., Martuza, R.L., 2012. Bevacizumab with angiostatin-armed oHSV increases antiangiogenesis and decreases bevacizumab-induced invasion in U87 glioma. Molecular Therapy.

Zhang, X., Zhang, Yang, Zhang, Yunming, Lv, P., Zhang, P., Chu, C., Mao, J., Wang, X., Li, W., Liu, G., 2020. Bio-engineered cell membrane nanovesicles as precision theranostics for perihilar cholangiocarcinoma. Biomater Sci 8, 1575–1579.

Zhang, Y., Cai, P., Li, L., Shi, L., Chang, P., Liang, T., Yang, Q., Liu, Y., Wang, L., Hu, L., 2017. Co-expression of TIM-3 and CEACAM1 promotes T cell exhaustion in colorectal cancer patients. Int Immunopharmacol.

Zhang, Y., Ma, C.J., Wang, J.M., Ji, X.J., Wu, X.Y., Moorman, J.P., Yao, Z.Q., 2012. Tim-3 regulates pro- and anti-inflammatory cytokine expression in human CD14 + monocytes . J Leukoc Biol.

Zhang, Y., Zhang, W., 2020. Tim-3 regulates the ability of macrophages to counter lipopolysaccharide-induced pulmonary epithelial barrier dysfunction via the PI3K/Akt pathway in epithelial cells. Mol Med Rep 22, 534–542.

Zhang, Z.Y., Schluesener, H.J., Zhang, Z., 2011. Distinct expression of Tim-3 during different stages of rat experimental autoimmune neuritis. Brain Res Bull.

Zheng, H., Guo, X., Tian, Q., Li, H., Zhu, Y., 2015. Distinct role of Tim-3 in systemic lupus erythematosus and clear cell renal cell carcinoma. Int J Clin Exp Med 8, 7029.

Zheng, M., Huang, J., Tong, A., Yang, H., 2019. Oncolytic viruses for cancer therapy: barriers and recent advances. Mol Ther Oncolytics.

Zhou, E., Huang, Q., Wang, J., Fang, C., Yang, L., Zhu, M., Chen, J., Chen, L., Dong, M., 2015. Up-regulation of Tim-3 is associated with poor prognosis of patients with colon cancer. Int J Clin Exp Pathol 8, 8018.

Zhou, P., Wang, Xuchen, Xing, M., Yang, X., Wu, M., Shi, H., Zhu, C., Wang, Xiang, Guo, Y., Tang, S., Huang, Z., Zhou, D., 2022. Intratumoral delivery of a novel oncolytic adenovirus encoding human antibody against PD-1 elicits enhanced antitumor efficacy. Mol Ther Oncolytics 25, 236.

Zhou, Q., Munger, M.E., Veenstra, R.G., Weigel, B.J., Hirashima, M., Munn, D.H., Murphy, W.J., Azuma, M., Anderson, A.C., Kuchroo, V.K., Blazar, B.R., 2011. Coexpression of Tim-3 and PD-1 identifies a CD8+ T-cell exhaustion phenotype in mice with disseminated acute myelogenous leukemia. Blood 117, 4501–4510.

Zhu, C., Anderson, A.C., Schubart, A., Xiong, H., Imitola, J., Khoury, S.J., Zheng, X.X., Strom, T.B., Kuchroo, V.K., 2005. The Tim-3 ligand galectin-9 negatively regulates T helper type 1 immunity. Nat Immunol.

Zhu, S., Lin, J., Qiao, G., Wang, X., Xu, Y., 2016. Tim-3 identifies exhausted follicular helper T cells in breast cancer patients. Immunobiology 221, 986–993.

Zuo, S., Wei, M., Xu, T., Kong, L., He, B., Wang, Shiqun, Wang, Shibing, Wu, J., Dong, J., Wei, J., 2021. Original research: An engineered oncolytic vaccinia virus encoding a single-chain variable fragment against

TIGIT induces effective antitumor immunity and synergizes with PD-1 or LAG-3 blockade. J Immunother Cancer 9, 2843.

Yoneda, T., Michigami, T., Yi, B., Williams, P.J., Niewolna, M. and Hiraga, T. (2000), Actions of bisphosphonate on bone metastasis in animal models of breast carcinoma. Cancer, 88: 2979-2988.

7. SCIENTIFIC APPENDIX

7.1. Individual study plan (ISP)

ISP reference (e.g. JMB 1) This must be written on the cage card	SD_VIV001 and HBM_VIV001
PPL number	PP1099883
Name of PPL holder	Munitta Muthana
Protocol number (or 19b number) and severity	Protocol 1 Tumour models Moderate
PIL/Researcher name(s): Researcher:	Secil Demiral (I02143396) Faith Howard, Hawari Bin Mansour, Zijian Gao Soumya Rupangudi

Animal holding room	Start date of experiment	End date
FU311	09/05/23	09/06/23

ANIMALS:

Species/strain	Number of animals per group	Number of groups
Mouse Balb/c	8	5 – Treatments
Mouse Balb/c	1	1 – Tolerance
Mouse C57BL/6	8	5 – Treatments

AIM OF THE EXPERIMENT:

To investigate the delivery and efficacy of oncolytic viruses on primary murine mammary tumours including in combination with the immune checkpoint inhibitor TIM-3. Tumour growth will be monitored by callipers measurements and live tracking of luciferase expressing virus will be monitored by IVIS.

EXPERIMENT DETAILS:

Day of experiment (+/- 7 days)	Procedure
0 Implantation of tumour cells	$1x10^5$ murine BC 4T1 parental cells injected intra-nipple (25 µL) in 1:1 mix of PBS:GFR-Matrigel **Daily health monitoring including weight and tumour caliper measurement. Once tumours reach an average diameter of 7.2mm (60% of permitted maximum diameter), tumours will be measured daily.**
Tumour $100mm^3$ (T0)	**Treatment 1** – Treatment administered to group 1 and monitored for 30 minutes. Dosing of all other groups will commence after the initial tolerability assessment as per table below.
T+2 days	**Treatment 2** – Tumours will be measured and treatment administered as per table below.
T+4 days	**Treatment 3** – Tumours will be measured and treatment administered as per table below.
T+5 days	3 mice from groups 2-9 will undergo IVIS for detection of virus. Mice will not be permitted to recover from the anaesthetic but will undergo terminal blood sample and euthanasia. Ex vivo IVIS will be performed on harvested organs prior to storage for distribution analyses (liver, kidney, lung, spleen, heart, brain and tumour).
EOP survival model when each mice reach experimental limits.	Terminal blood sample will be collected prior to euthanasia. Ex vivo IVIS will be performed on harvested organs prior to storage for post-mortem analyses (liver, kidney, lung, spleen, and tumour tissue).

Exp group	No. mice	Treatment	Route Admin	Concentration	Volume (µl)
1	3	Anti-Tim-3 (Tolerance)	IP	200ug	100ul
2	8	PBS	IV	-	
3	8	Isotype antibody	IP	200ug	
4	8	Anti-Tim-3 antibody	IP	200ug	
5	8	HSV-1716-GFP	IV	10e5pfu/ml	
6	8	Anti-Tim-3 + HSV-1716-GFP	IP + IV	200ug + 10e5 pfu/ml	

Implantation of tumour cells:

- Animals will be anaesthetised using aerosolised isofluorane.
- Analgesic administered via subcutaneous injection (Metacam 5mg/kg).

- Remove hair around the lower mammary fat pads with depilatory cream.
- Prepare surgical incision site – apply drapes and sterilise skin with Hibiscrub.
- Grip nipple 4 with blunt ended forceps and slowly inject 20ul of cell suspension using an insulin syringe.
- Recover and monitor animal in incubator. Return to clean cage when fully alert.

Treatment:

- Following IV/IP injection of treatment, mice will be monitored for 30 minutes.

For **surgery**, please provide details of the following:

Anaesthesia: drug(s), dose rate and route	Vaporised Isofluorane (5% induction and 0.5-2% maintenance via tube)
Analgesia: drug(s), dose rate and route	Metacam 5mg/kg SC
Antibiotics: drug, dose rate and route	Na
Wound closure: method and materials (e.g. suturing with 5-0 Vicryl)	Na

Planned fate of the animals at the end of the experiment (e.g. Schedule 1 or a terminal procedure):
The animals will be culled by exsanguination followed by cervical dislocation.

ADVERSE EFFECTS and END-POINTS (for **these** animals):

Expected adverse effects	Principal adverse effects anticipated: a. Impeded ambulation, large tumour growth impeding movement b. Weight loss due to virotherapy or impeded movement c. Ulceration (minimal risk)
Humane end-points	When the tumours reach a mean diameter of 12 mm, the animal will be culled as per the approved schedule 1 method. In addition, if the body weight decreases by over 20%, the animal will be culled as per the approved schedule 1 method. If the posture of the animal demonstrates marked discomfort the animal will be culled

UNEXPECTED DEATHS:

If an animal reaches its end-point or has to be culled on welfare grounds and the researcher is unavailable, describe how you would like the cadaver to be stored (e.g. fridge, freezer) and any tissues to be taken:
If the animal reaches its end point, please cull the animal and leave in the fridge. If the animal has to be culled on welfare grounds, please discard the animal.

HEALTH AND SAFETY:

I have filled out a COSHH risk assessment for this work (delete as applicable) YES

SIGNATURES:

I confirm that I have checked that the PPL, and my PIL, contain the necessary authority for all of the work proposed under this study plan. I confirm that I have read and understood the Personal Licence Standard Conditions, including the requirement for appropriate supervision and declaration of competency before carrying out any regulated procedure.

This ISP has also been read by:

Role	Name	Signature	Date
PPL holder*	**Munitta Muthana**		**26/04/2023**

***Must** sign the ISP before the experiment commences, to confirm that work is covered under the PPL**.**

7.2 Tumour Volume graph for each day measurements

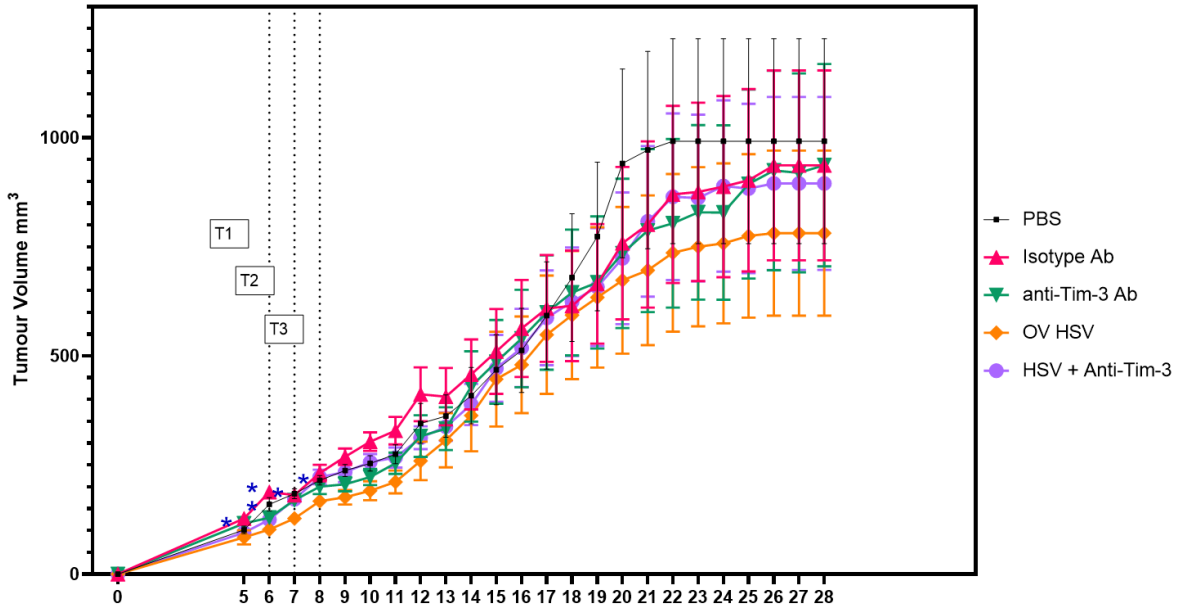

Figure 7.2.1: The figure displays tumour volume percentage measured every day of BALB/c mice over a 28-day period following the implantation of 4T1 BC cells. The study comprises 5 distinct treatment categories: PBS as a control, Iso Ab, Anti-Tim-3 Ab, HSV-1716, and a combination of OV with Anti-Tim-3 Ab. A total of 40 BALB/c mice were divided into 5 groups, each containing 8 mice. Within each of these 5 groups, the mice were subjected to 3 administrations of the specified treatments. These treatment doses were administered on days 6, 7, and 8 after the implantation of 4T1 cells into the mammary fat pads of the mice. 3 mice in each treatment group were culled on day 9 for biodistribution study. The remaining mice in each group were allowed for survival and were euthanized in cases of abnormal occurrences, such as the development of ulcerations or the presence of large tumours exceeding a diameter of 12mm. The results are presented as the Mean ± Standard Error of the Mean (SEM) using a last observation carried forward approach. Statistical analysis included a two-way ANOVA followed by multiple comparisons between the treatment groups, where significance (* symbol) was observed at a P=<0.05. Graph made using GraphPad Prism.

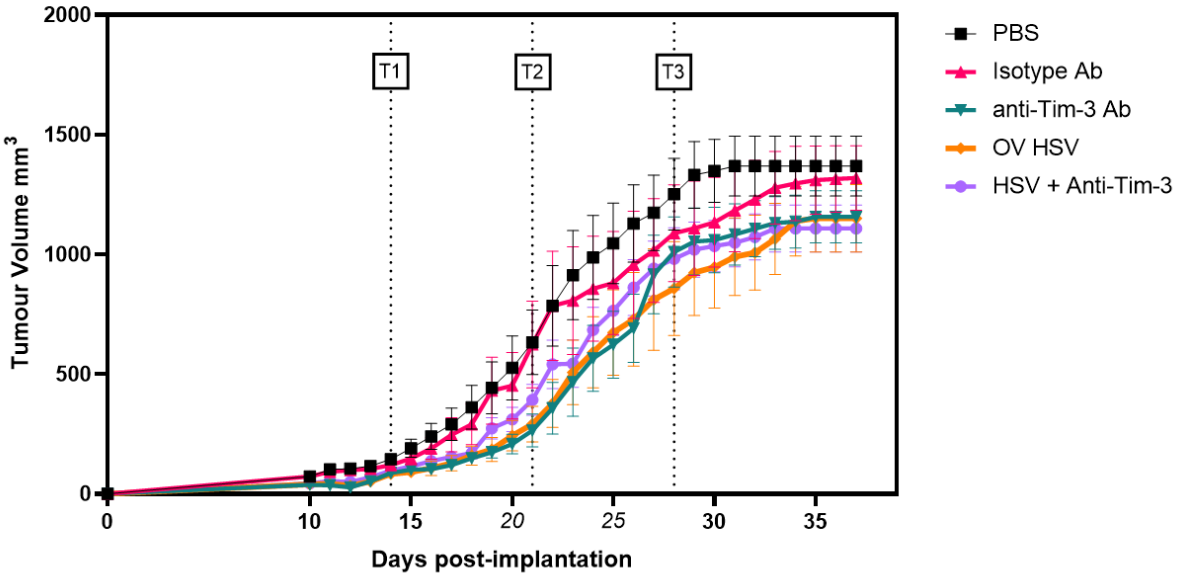

Figure 7.2.2: The curve graph above shows tumour growth by calculating the tumour volume percentage measured every day of C57BL/6 strain mice over the span of 37 days post implantation of E0771 BC cells. Based on the 5 treatment groups, PBS as control, Iso Ab, Anti-Tim-3 Ab, HSV-1716 and combination of HSV-1716 with Anti-Tim-3 Ab, a total of 40 mice were segregated into 5 groups of 8 mice in each group (n=8). Each of the 5 mice group were treated on days 14, 21 and 28 post implantations of BC cells. They were allowed for survival and Mice were euthanized in cases of abnormal conditions, such as the occurrence of ulcerations or the presence of large tumours exceeding a diameter of 12mm. The results are presented as the Mean ± SEM using a last observation carried forward approach. Statistical analysis included a two-way ANOVA followed by multiple comparisons between the treatment groups, where significance (* symbol) was observed at a P=<0.05. Graph made using GraphPad Prism.

7.3. MOI raw data

Table 7.1. Cell viability percentages of MOI values ranging from 0.01 to 30 for HSV-1716 in MCF-7 cell lines.

MCF-7	HSV-1716											
	24h			48h			120h			168h		
MOIs	Percentage of cell viability (n=3)			Percentage of cell viability (n=3)			Percentage of cell viability (n=3)			Percentage of cell viability (n=3)		
30	45,17108	58,2128	58,64894	33,79106	22,69	27,24652	13,33238	11,41993	13,67976	94,89683	77,3541	33,9366
10	44,32246	68,82165	79,03377	38,57047	24,44192	25,87858	15,66936	13,49208	9,181387	79,18244	80,10408	46,54701
3	53,31702	72,07992	79,94995	38,42764	26,56553	32,32281	28,30839	15,30633	6,96318	76,49103	75,22997	23,79269
1	53,6101	64,78569	81,03354	35,32599	26,82473	34,83368	25,0454	14,48709	10,45823	72,96772	73,54956	54,94536
0.3	91,05039	67,64164	85,06771	61,59433	29,66655	37,23834	40,11696	23,74431	29,93847	51,55736	45,00957	61,52229
0.1	100,304	81,71839	79,39375	97,45995	34,66478	40,55858	75,02554	22,77674	42,31809	69,93494	55,27942	71,9423
0.03	95,29077	88,10594	92,07071	97,51996	40,74701	59,79516	79,68833	10,12707	70,39517	68,18975	66,20699	66,4559
0.01	100	100	100	100	100	100	100	100	100	100	100	100

Table 7.2. Cell viability percentages of MOI values ranging from 0.01 to 30 for HSV-E17 in MCF-7 cell lines.

MCF-7	HSV-E17											
	24h			48h			120h			168h		
MOIs	Percentage of cell viability (n=3)			Percentage of cell viability (n=3)			Percentage of cell viability (n=3)			Percentage of cell viability (n=3)		
30	41,15364	68,47711	64,81791	46,8624	37,30464	43,74091	21,82632	9,521651	5,354397	4,354146	2,269315	4,884494
10	82,62078	72,74603	81,44078	86,24088	60,1538	24,38713	30,51596	15,74421	6,452817	5,74922	4,731559	3,493531
3	101,0851	91,6691	101,8021	89,87672	75,68417	45,22432	52,24833	22,52277	11,00566	21,05179	7,708874	9,625034
1	87,6245	82,40852	109,9828	90,3391	78,98142	62,67708	59,32972	33,88286	15,72573	10,82023	13,08602	9,557511
0.3	47,91425	94,9656	92,1877	93,00396	99,16009	86,3887	73,86463	50,77207	33,52119	38,74946	17,36135	20,35291
0.1	92,86242	69,76433	99,68402	99,10755	81,15396	97,81061	91,26071	55,85801	74,97796	38,63316	22,20764	28,75112
0.03	65,53604	86,02385	99,38315	100,5488	90,85355	95,54995	100,7775	79,36396	79,10788	79,32966	46,61751	46,94256
0.01	100	100	100	100	100	100	100	100	100	100	100	100

Table 7.3. Cell viability percentages of MOI values ranging from 0.01 to 30 for HSV-V17 in MCF-7 cell lines.

MCF-7	HSV-V17											
	24h			48h			120h			168h		
MOIs	Percentage of cell viability (n=3)			Percentage of cell viability (n=3)			Percentage of cell viability (n=3)			Percentage of cell viability (n=3)		
30	94,30503	62,02652	79,5718	67,26369	63,30288	36,53038	9,030052	16,13405	18,97837	4,480073	2,760634	5,901945
10	101,2826	76,04517	77,76251	80,89727	77,3369	59,02302	18,89822	18,82226	27,95503	5,496839	1,927625	5,398307
3	97,40503	75,98559	78,53154	98,39976	81,54939	86,52962	23,06109	18,2818	36,87898	13,08082	6,894905	10,21306
1	96,83009	86,42897	77,48782	92,4717	81,35997	85,3859	42,89116	34,47345	50,83998	18,56723	9,681742	11,31517
0.3	97,49952	80,95739	82,80107	87,58939	71,01232	89,26688	59,74288	50,86979	60,11465	27,2313	12,18094	14,93959
0.1	87,08988	76,32383	88,27025	85,05061	84,33256	72,60761	67,21167	105,6627	82,85803	16,41415	52,29928	33,85501
0.03	81,85021	45,61604	53,88418	48,31467	44,88242	62,6837	53,30132	30,47694	55,13289	19,23927	19,97415	50,23811
0.01	100	100	100	100	100	100	100	100	100	100	100	100

Table 7.4. Cell viability percentages of MOI values ranging from 0.01 to 30 for HSV-1716 in MDA-MB-231 cell lines.

MDA-MB-231	HSV-1716											
	24h			48h			120h			168h		
MOIs	Percentage of cell viability (n=3)			Percentage of cell viability (n=3)			Percentage of cell viability (n=3)			Percentage of cell viability (n=3)		
30	88,69956	94,09262	79,40198	45,41974	53,22736	39,14499	76,71719	65,56207	40,92907	74,94843	82,33544	81,81993
10	82,7687	95,1429	51,05073	50,16399	58,40574	41,96049	66,10751	63,01964	29,73134	70,09238	71,85347	85,54247
3	95,12674	97,73216	80,0779	55,9383	53,56997	53,53786	46,14599	17,20991	49,42579	70,15728	78,73955	86,79084
1	97,54274	100,5371	67,99285	78,81626	74,15002	50,12329	45,60971	38,62945	59,30247	87,87378	71,54842	89,85397
0.3	98,89972	107,2814	72,39792	85,89706	94,29539	51,06174	56,28826	50,78651	70,04812	79,74671	61,25607	75,04528
0.1	95,7489	120,5949	95,41513	93,99166	99,86758	24,26886	84,68055	58,10432	50,52848	86,90935	72,06467	73,54894
0.03	97,75632	115,7113	89,40625	96,57815	94,01368	16,29942	104,7375	36,92975	31,17455	91,46717	94,84956	69,71167
0.01	100	100	100	100	100	100	100	100	100	100	100	100

Table 7.5. Cell viability percentages of MOI values ranging from 0.01 to 30 for HSV-E17 in MDA-MB-231 cell lines.

MDA-MB-231	HSV-E17											
	24h			48h			120h			168h		
MOI	Percentage of cell viability (n=3)			Percentage of cell viability (n=3)			Percentage of cell viability (n=3)			Percentage of cell viability (n=3)		
30	66,75483	68,32205	39,06716	58,79729	27,02651	53,92761	48,797	96,80235	52,4196	52,86462	89,03013	66,38647
10	67,19145	76,90979	24,64424	92,37129	25,64037	55,49489	61,64128	45,25925	93,51468	59,48895	65,8716	48,70991
3	40,35437	79,56988	54,13212	61,75502	21,12523	51,05785	89,98736	71,92695	83,26223	54,84192	90,95956	45,81404
1	51,54958	74,56377	45,04744	66,63679	10,13552	64,11663	73,80222	75,55177	86,30277	50,81314	90,97911	61,99751
0.3	60,92857	77,82882	52,51633	55,18436	16,70993	65,65639	69,29853	75,40628	85,38211	94,58474	86,09655	75,49087
0.1	48,48429	66,09594	60,57918	59,48263	31,75962	49,03765	69,47257	79,1054	80,99875	110,7049	86,93495	69,29231
0.03	58,00761	64,05151	82,79885	58,35189	13,76319	41,04878	55,90811	83,55672	83,31258	76,37936	87,95058	58,26763
0.01	100	100	100	100	100	100	100	100	100	100	100	100

Table 7.6. Cell viability percentages of MOI values ranging from 0.01 to 30 for HSV-V17 in MDA-MB-231 cell lines.

MDA-MB-231	HSV-V17											
	24h			48h			120h			168h		
MOIs	Percentage of cell viability (n=3)			Percentage of cell viability (n=3)			Percentage of cell viability (n=3)			Percentage of cell viability (n=3)		
30	75,71322	83,40233	53,61572	33,96715	39,87997	42,38863	5,580901	2,432515	5,476292	1,499119	1,421218	0,68574
10	86,01127	104,6837	93,4837	69,84894	95,18012	82,95427	7,286072	9,362465	17,57311	4,178136	5,00265	5,931856
3	99,84607	99,22191	92,27561	111,2376	93,42544	82,63648	40,99103	39,67166	46,63137	16,74557	26,30284	18,82602
1	104,7948	104,6618	98,21791	116,8126	100,5821	99,54784	82,84169	92,13932	75,75117	56,2948	77,66812	58,29709
0.3	95,00778	104,3305	85,10534	118,3145	96,90556	94,93173	102,794	108,8458	96,58987	88,58017	96,46115	88,44164
0.1	92,1105	84,71158	79,65896	102,1274	88,20817	93,1381	105,6293	90,81194	91,8787	94,30536	101,4422	84,684
0.03	100,6945	97,54051	96,74931	94,02586	89,69445	92,298	105,6349	97,53527	97,12526	97,21429	100,3352	88,57772
0.01	100	100	100	100	100	100	100	100	100	100	100	100

Table 7.7. Cell viability percentages of MOI values ranging from 0.01 to 30 for HSV-1716 in SKBR-3 cell lines.

SKBR-3	HSV-1716											
	24h			48h			120h			168h		
MOIs	Percentage of cell viability (n=3)			Percentage of cell viability (n=3)			Percentage of cell viability (n=3)			Percentage of cell viability (n=3)		
30	61,62946	47,38363	71,15806	44,91421	45,38511	57,15875	15,904	17,12396	19,96565	3,953022	3,704083	7,113488
10	51,91273	47,43833	66,69057	48,35437	43,49546	37,70979	13,46855	13,41382	18,15279	7,008528	2,197331	6,67698
3	62,89263	46,96732	74,21076	57,03995	43,47487	56,03263	13,23519	15,39378	19,1444	4,464185	1,542092	6,156624
1	72,61576	57,79851	100,0385	67,40267	63,59177	67,24089	18,57875	23,73595	27,74864	6,776923	6,478189	17,31017
0.3	76,47218	50,34407	109,7354	94,14792	71,79933	85,22383	37,87092	62,10364	57,91756	25,31694	33,12571	51,32205
0.1	70,06819	47,73996	93,5563	100,5727	42,52079	86,77121	75,85543	52,05762	82,33996	67,00074	33,57584	68,81853
0.03	89,16763	63,76668	61,62008	99,82603	76,69243	90,57515	100,2519	57,91288	75,69677	100,5714	43,32466	61,14236
0.01	100	100	100	100	100	100	100	100	100	100	100	100

Table 7.8. Cell viability percentages of MOI values ranging from 0.01 to 30 for HSV-E17 in SKBR-3 cell lines.

SKBR-3	HSV-E17											
	24h			48h			120h			168h		
MOIs	Percentage of cell viability (n=3)			Percentage of cell viability (n=3)			Percentage of cell viability (n=3)			Percentage of cell viability (n=3)		
30	94,90585	97,10349	96,81808	91,2106	64,78028	100,0952	97,1731	82,78192	102,1132	73,75798	42,04614	49,02359
10	99,36508	99,59303	94,60919	95,92832	71,39591	95,63961	99,40844	94,00389	96,9331	93,88847	72,81971	72,75686
3	84,08912	108,1646	96,47604	84,82223	67,5038	97,59899	98,45278	94,76093	98,47242	102,8467	70,72843	79,72257
1	94,74899	100,1163	100,0293	86,32262	72,91011	100,1856	102,1187	90,97663	99,55658	97,56222	73,71748	73,52118
0.3	85,43806	91,65666	97,23949	93,28576	63,72759	96,31092	95,5934	88,29732	100,724	92,34573	83,1021	73,53624
0.1	83,21597	100,3532	86,42148	70,72219	74,39675	95,10391	92,78216	76,80955	99,09443	83,91264	76,79851	69,84076
0.03	68,00917	74,37671	91,39893	71,88793	43,17081	84,01645	70,01394	41,52663	90,2836	59,81145	94,06014	94,18889
0.01	100	100	100	100	100	100	100	100	100	100	100	100

Table 7.9. Cell viability percentages of MOI values ranging from 0.01 to 30 for HSV-V17 in SKBR-3 cell lines.

SKBR-3	HSV-V17											
	24h			48h			120h			168h		
MOIs	Percentage of cell viability (n=3)			Percentage of cell viability (n=3)			Percentage of cell viability (n=3)			Percentage of cell viability (n=3)		
30	49,60229	30,53258	87,13154	48,55939	47,95739	37,01472	10,28919	12,51427	15,23472	2,44586	3,240328	4,048797
10	63,84997	87,39738	90,73886	70,62806	73,28426	71,51238	30,23105	38,52311	32,93667	8,913064	19,58247	22,54273
3	88,89578	80,59046	87,59409	85,65676	78,16278	92,71138	83,50514	79,01628	75,98183	54,49485	65,69313	78,17493
1	89,35812	92,37985	96,26342	89,67522	83,59744	82,27272	102,7598	89,10495	74,46668	97,4112	84,51972	87,84356
0.3	89,60319	97,08221	96,94475	88,18029	81,58485	75,71313	97,56708	91,50885	78,3477	91,24487	107,0693	95,63265
0.1	88,85436	97,96995	97,4095	85,66557	87,80112	68,84514	101,9058	95,06927	73,36416	84,21537	110,052	92,53984
0.03	88,79803	94,79301	69,59419	89,71672	90,96366	58,89859	99,1545	91,81421	67,18484	97,35265	101,8764	76,60179
0.01	100	100	100	100	100	100	100	100	100	100	100	100